UNIVERSITÀ DEGLI STUDI DI MILANO

PhD degree in Systems Medicine (Molecular Oncology curriculum)

European School of Molecular Medicine (SEMM)

University of Milan and University of Naples "Federico II"

A Cell Cycle Clock Regulates the Epigenetic Landscape of AML Cells and Determines Sensitivity to LSD1 Inhibition

Settore disciplinare: MED/04

Kourosh Hayatigolkhatmi

European Institute of Oncology (IEO), Milan, Italy

Matricola n. R12773

Tutor: Prof. Saverio Minucci

European Institute of Oncology (IEO), Milan, Italy

PhD Coordinator: Prof. Saverio Minucci

European Institute of Oncology (IEO), Milan, Italy

Anno Accademico: 2022-2023

Table of Contents

List of Abbreviations

2-OxoGlutarate: 2OG

4’,6-DiAmidino-2-PhenylIndole: DAPI

5-carboxylCytosine: 5caC

5-formylCytosine: 5fC

5-glucosylCytosine: 5gC

5-hydroxymethylCytosine: 5hmC

Absent, Small, or Homeotic 2: ASH2

Acute Myeloid Leukemia: AML

Acute Promyelocytic Leukemia: APL

Ada-Two-A-Containing: ATAC

ADP-RibosylHydrolase: ARH

All-Trans-Retinoic Acid: ATRA

allogenic Hematopoietic Stem Cell Transplantation: allo-HSCT

Amine Oxidase Domain: AOD

Anaphase Promoting Complex/Cyclosome: APC/C

Androgen Receptor: AR

Assay for Transposase-Accessible Chromatin with sequencing: ATAC-seq

Ataxia-Telangiectasia Mutated: ATM

Ataxia-Telangiectasia Mutated: ATM

ATM- and Rad3-related: ATR

Base Excision Repair: BER

BioSafety Level: BSL

Bone Marrow: BM

Bromodomain Adjacent to Zinc finger domain: BAZ

Bromodomain and ExtraTerminal domain: BET

BRomoDomain-containing protein: BRD

cAMP Response Element-Binding protein: CREB

CCCTC-binding Factor: CTCF

Chromatin ImmunoPrecipitation with sequencing: ChIP-seq

Chromodomain-Helicase-DNA-binding: CHD

ChromoDomain: CD

ChromoShadow Domain: CSD

Chromosomal INstability: CIN

Chronic Myeloid Leukemia: CML

Complete Remission: CR

COMplex of Proteins ASsociated with Set1: COMPASS

Cyclin-Dependent Kinase: CDK

Cysteine/Histidine-rich 1: CH1

Cysteine/Histidine-rich 3: CH3

Differentially Accessible Region: DAR

Differentially Expressed Gene: DEG

Disease-Free Survival: DFS

DNA Damage Response: DDR

DNA MethylTransferase: DNMT

DNA-dependent Protein Kinase: DNA-PK

DNMT inhibitors: DNMTi

DNMT3-Like: DNMT3L

double-stranded RNA: dsRNA

E1A binding protein p300: EP300

Embryonic Ectoderm Development: EED

Embryonic Stem Cell: ESC

Endogenous Retrovirus: ERV

Endothelial-to-Hematopoietic Transition: EHT

Enhancer of Zeste Homolog 2: EZH2

Epidermal Growth Factor: EGF

Epithelial-Mesenchymal Transition: EMT

Estrogen Receptor: ER

Estrogen-Related Receptor α: ERRα

Fibroblast Growth Factor: FGF

Flavin Adenine Dinucleotide: FAD

Flavin-containing Amine Oxidase domain-containing protein 2: AOF2

Fluorescent, Ubiquitination-based Cell Cycle Indicator, CUL4Ddb1 and APCCdh1 V.2: FUCCI(CA)2

French-American-British cooperative group: FAB

Gastric Cancer: GC

General Control Non-derepressible 5: GCN5

HDAC inhibitors: HDACi

Heat shock protein 90: Hsp90

Hematopoietic Stem Cell: HSC

Hematopoietic Stem and Progenitor Cells: HSPCs

Hepes-Buffered Solution: HBS

Heterochromatin Protein 1: HP1

High Sensitivity: HS

Histone AcetylTransferase: HAT

Histone DeACcetylates: HDAC

Histone MethylTransferase: HMT

histone Post-Translational Modification: hPTM

HypoMethylating Agent: HMA

Imitation SWItch: ISWI

Ingenuity Pathway Analysis: IPA

Insulin Growth Factor: IGF

Interferon-Stimulated Gene: ISG

Isocitrate DeHydrogenase 2: IDH2

Jumonji and AT-Rich Interaction Domain: JARID

JuMonJi C-domain-Containing: JMJC

Jumonji C: JmjC

Knock Down: KD

KnockOut: KO

Lactate DeHydrogenase A: LDHA

Lamina-Associated Domain: LAD

Leukemic Stem Cell: LSC

Loss-of-Function mutation: LoF

lung Squamous Cell Carcinoma: SCC

Lysine AcetylTransferase 2A: KAT2A

Lysine AcetylTransferase 2B: KAT2B

Lysine AcetylTransferase 5: KAT5

Lysine MethylTransferase 2: KMT2

Lysine-Specific Demethylase 1A: LSD1

Mass Spectrometry: MS

Melanoma Differentiation-Associated protein 5: MDA5

Metastasis Tumor Antigen: MTA

Mixed Lineage Leukemia: MLL

Moz, Ybf2/Sas3, sas2, and Tip60: MYST

Myocyte Enhancer Factor-2: MEF2

Neural Stem Cell: NSC

Non-Small Cell Lung Cancer: NSCLC

Nuclear Factor kappa-light-chain-enhancer of activated B cells: NF-κB

Nuclear receptor Co-Repressor: NCoR

Nucleosome Acetyltransferase of H4: NuA4

Nucleosome Remodeling Deacetylase: NuRD

O-linked N-acetylGlucosamine Transferase: OGT

OligoAdenylate Synthase-Like: OASL

OligoAdenylate Synthase: OAS

Overall Survival: OS

P300/CBP-Associated Factor: PCAF

Pattern Recognition Receptor: PRR

Peripheral Blood: PB

Plant HomeoDomain: PHD

Pluripotent Stem Cell: PSC

Poly(ADP-Ribose) Glycohydrolase: PARG

Poly(ADP-Ribose) Polymerase: PARP

Polycomb Group: PcG

Polycomb Repressive Complex 1: PRC1

Polycomb Repressive Complex 2: PRC2

PolyEthylene Glycol: PEG

Proliferating Cell Nuclear Antigen: PCNA

Protein Inhibitor of Activated STAT: PIAS

Protein Kinase R: PKR

Protein Phosphatase 1: PP1

Protein Phosphatase 2A: PP2A

Protein Phosphatase 2B: PP2B

REST Corepressor 1: CoREST

Results section

Retinoblastoma protein: Rb

RetinoBlastoma-Binding Protein 5: RBBP5

Retinoic acid-Inducible Gene I: RIG-I

Retinoic Acid: RA

RIG-I-Like Receptor: RLR

S-AdenosylMethionine: SAM

SENtrin-specific Protease: SENP

short hairpin RNA: shRNA

Short Interspersed Nuclear Element: SINE

Silencing Mediator of Retinoid and Thyroid hormone receptor: SMRT

Silent Information RegulaTor: SIRT

single-stranded RNA: ssRNA

SIRTuin: SIRT

small interfering RNA: siRNA

Small Ubiquitin-like MOdifier: SUMO

Specificity protein 1: Sp1

Spindle Assembly Checkpoint: SAC

Spt-Ada-Gcn5 Acetyltransferase: SAGA

SU(Var)3-9 Homolog 1: SUV39H1

Su(var)3-9, Enhancer-of-zeste, Trithorax: SET

Super Enhancer: SE

SUppressor of Zeste 12: SUZ12

SWI/SNF related Matrix Associated actin dependent Regulator of Chromatin, subfamily A: SMARCA

SWI3, ADA2, N-CoR, TFIIIB: SANT

Switch/Sucrose Non-Fermentable: SWI/SNF

T-cell LymphoBlastic Leukemia/lymphoma: T-LBL

Tat-Interactive Protein, 60 kDa: TIP60

Ten-Eleven Translocation: TET

Three-Dimensional: 3D

Thymine-DNA Glycosylase: TDG

Toll-Like Receptor: TLR

Topologically Associated Domain: TAD

Transcription Factor: TF

Transposable Element: TE

TranylCyPromine: TCP

TRIpartite Motif family: TRIM

Tumor Suppressor Gene: TSG

Tumor-Node-Metastasis: TNM

Ubiquitin-like, containing PHD and RING Finger domains 1: UHRF1

VRN2-EMF2-FIS2-SUZ12: VEFS

WD Repeat-containing protein 5: WDR5

Wild Type: WT

Wilms Tumor 1: WT1

World Health Organization: WHO

Table of Figures

Abstract

Acute Myeloid Leukemia (AML) remains a complicated challenge in oncology, characterized by a complex interplay of factors that contribute to poor survival rates and resistance to chemotherapy and targeted therapies. This study presents a novel approach to unravel the layers of AML biology and treatment, focusing on the epigenetic enzyme LSD1, which is regularly found overexpressed in AML, as a therapeutic target.

We revealed a crucial role for the cell cycle regulator p21 in determining sensitivity to LSD1 inhibition. Our findings further demonstrate that pharmacological prolongation of the cell cycle, specifically the G1 phase, can sensitize AML cells to LSD1 inhibitors. This is achieved through a novel combinatorial approach involving clinically approved CDK inhibitors, such as Palbociclib, with LSD1 inhibitors.

Moreover, the study investigates mechanistically the implications of cell cycle manipulation, focusing on modifications of the epigenome. Our ATAC-seq investigations show that extension of the G1 phase alters chromatin accessibility. The epigenomic remodeling is further characterized by ChIP-seq and mass spectrometry experiments on genomic distribution and quantities of functionally relevant histone post-translational modifications, respectively, suggesting that those changes prime AML cells for differentiation. Intriguingly, transcriptome analyses identify the activation of transposable elements as a possible mechanism potentially driving immune responses and mediating differentiation in the treated AML cells, which we intend to further explore.

The study offers the development and deciphers molecular mechanisms of a combination strategy, where use of a sub-optimal dose of a CDK inhibitor with a specific LSD1 inhibitor can be a promising treatment a for wide range of AML subtypes, and extending also to non hematopoietic tumors.

Introduction

1. Epigenetics

Human genome contains all the essential information for regulating the development and maintaining the necessary biological processes throughout the life of an individual. This information is encrypted within the sequence of 20,000-25,000 genes, comprising the coding compartment of the genome. However, the coding compartment builds up about 1-2% of the entire human genome. All the remaining regions of the genome are defined as non-coding regions, which do not code for known particular proteins, and their actual functions have been studied for several years. Up to this day, discovered functions of the non-coding compartment of the genome can be categorized as gene regulation, RNA production, chromatin structure and organization, genome stability and DNA repair, and contribution to genetic diversity and evolutionary processes. Apart from the evolutionary significance of the non-coding genome, all of its remaining known functions are directly or indirectly involved in preserving and fine-tuning the spatiotemporal expression of the genes. The versatile nature of such regulatory network requires a higher-level organization, which ought to be heritable and editable simultaneously. Such qualities can be clearly seen in the chromatin, the complex interplay of DNA and proteins within the cell nucleus. The chromatin can undergo dynamic structural and chemical modifications that would govern gene expression, fulfilling the aforementioned heritability and editability requirements. These modifications can be applied, read and modified on both DNA and protein compartments of the chromatin through a wide variety of enzymes and protein complexes. This dynamic regulation eventually affects the three-dimensional (3D) structure of the chromatin, enabling or limiting the physical interaction of particular genomic regions with

transcriptional machinery and regulatory proteins, thus intricately modulating gene activity. **Epigenetics investigates dynamic changes to chromatin that shape and maintain gene expression patterns, impacting physiological and pathological processes, and highlighting the interaction between genetics and the environment** (Bird, 2007; Cavalli and Heard, 2019).

1.1. Hierarchical organization of chromatin

Spatial organization of the chromatin is the biological hardware to govern and guarantee a coherent gene expression over time, customized for each single cell. This organization hires a complex network of proteins who will assist the DNA section of the chromatin to relax or get repressed at proper time points. This organization is set at several levels, relying on various factors, which will be discussed briefly in this section (Figure 1) (Felsenfeld and Groudine, 2003).

The first level chromatin organization starts with **DNA** itself (Figure 1). DNA is accessible to epigenetic enzymes for chemical modifications. In human genome, the most functionally studied modification is ***DNA methylation***. DNA methylation is the process of adding a methyl group to CG (**CpG**) dinucleotides, mediated by DNA methyltransferase (**DNMT**) enzymes. The methyl group can also be removed as a passive event or actively through epigenetic enzymes known as **demethylases**. Accumulation of DNA methylation in gene promoters can result in transcriptional repression of that gene. On the other hand, hypomethylation of gene locus can be associated to transcriptional activation of the gene. Other possible modifications of DNA are *hydroxymethylation*, *formylation*, *carboxylation*, *glucosylation*, and more. ***DNA hydroxymethylation*** is the process of adding a hydroxymethyl group to the 5-methylcytosine (**5mC**) in CpG dinucleotides, creating a 5-

hydroxymethylcytosine (**5hmC**). ***DNA formylation*** and ***carboxylation*** are further oxidative process on 5hmC, creating 5-formylcytosine (**5fC**), and 5-carboxylcytosine (**5caC**), respectively. ***DNA glucosylation*** is the addition of a glucose group to the cytosine in CpG dinucleotides, converting the 5caC to 5-glucosylcytosine (**5gC**). All the hydroxymethylation, formylation, carboxylation, and glucosylation processes are mediated by ten-eleven translocation (**TET**) enzymes. The outcome of all four steps is linked to active gene expression states. These modifications can be passively removed by getting diluted through replication or actively through a demethylation process mediated by the same TET enzymes (Svedružić, 2011; Yang, Rau and Goodell, 2015; Viner *et al.*, 2016; Gagliardi, Strazzullo and Matarazzo, 2018).

At *The second level* of chromatin organization, **nucleosomes** play the pivotal role (Figure 1). Nucleosomes are basal compacting units of chromatin. Each nucleosome is a 147 bp segment of DNA, wrapped around a histone octamer known as the nucleosome core (forming an approximate of 1.65 turns). The nucleosome core is made of two copies of each of histones **H2A**, **H2B**, **H3**, and **H4** (Figure 1). All these four histones are strictly conserved among different species, highlighting their fundamental role in controlling the chromatin compaction and hence accessibility to the underlying genetic information. Histones contain large proportions of amino acids lysine (**K**) and arginine (**R**), resulting in an overall positive electric charge of the histones at physiological pH. This will subsequently cause the binding of histones to the negatively charged phosphate groups throughout the DNA double helix. Histones can continuously undergo various chemical modifications on several amino acid residues, particularly on their N-terminal tails that extend outward from each histone of the nucleosome core (Figure 1). These modifications include *acetylation*, *methylation*, *phosphorylation*, *ubiquitination*, *sumoylation*, *ADP-ribosylation*, *lactylation*, etc. resulting in alterations of the electric charge and structure of histones, hence compaction and

decompaction of specific chromatin regions. ***Histone acetylation*** is a process of adding an acetyl group to the K residue of a histone tail, mediated by a histone acetyltransferase (**HAT**) enzyme. Addition of the acetyl group would oppose the positive charge of the histone, resulting in a weaker binding of the histone and DNA, hence a more relaxed chromatin state. This would consequently create a better accessibility of the chromatin region to particular transcription factors (TFs). The acetyl mark can be removed from the histone tail by histone deacetylates (**HDAC**) enzymes. ***Histone methylation(s)*** is the process of adding one, two or three methyl groups to the K or R residue of a histone tail, mediated by a histone methyltransferase (**HMT**) enzyme. Histone methylation can recruit various transcriptional regulating complexes to the methylated chromatin regions and drive different transcriptional effects, depending on the site of the methylation and the number of methyl groups. Methyl groups can be removed by a various number of specific **demethylases**. ***Histone phosphorylation*** is defined as the process in which a phosphate group is added to the serine (S) or threonine (T) residues of a histone tail, mediated by various **kinases**. The outcome of the histone phosphorylation can be a change of structure and hence transcriptional regulation, depending on the site of the phosphorylation and mainly in response to cellular processes such as DNA damage response (DDR) or cell cycle progression. Several different **phosphatase** enzymes, including protein phosphatase 1 (**PP1**), protein phosphatase 2A (**PP2A**), and protein phosphatase 2B (**PP2B**/**Calcineurin**) can remove the phosphate group from histone tails. ***Histone sumoylation*** is the addition of small ubiquitin-like modifier (SUMO) proteins to the K residue of a histone tail, mediated by SUMO **E3** and SUMO **E2 ligases** such as protein inhibitor of activated STAT (**PIAS**) family of proteins. Subsequently, SUMO marked K residues can attract other SUMO-modified proteins and chromatin associated complexes to interact with them and regulate gene expression. SUMO proteases also known as SUMO/Sentrin-specific protease (**SENP**) family

of enzymes (e.g., SENP1, SENP2, and SENP6), can catalyze the desumoylation process in which the SUMO proteins are removed from the target proteins. ***Histone ADP-ribosylation*** is the addition of ADP-ribose moieties to particular amino acid residues on histone tails, mediated by poly(ADP-ribose) polymerase (**PARP**) enzymes. The histone ADP-ribosylation yields activative or repressive transcriptional effects based on the modified amino acid residue and cellular context through impacting interactions with chromatin-remodeling complexes, TFs, and other chromatin-associated proteins. ADP-ribose chains can be removed from histone tails by catalytic activity of poly(ADP-ribose) glycohydrolase (**PARG**) or ADP-ribosylhydrolase (**ARH**) enzymes. Finally, ***histone lactylation*** is another recently discovered histone modification, which is the process of adding a lactyl group to K residues of a histone tail, mediated by lactate dehydrogenase A (**LDHA**) or **p300** enzymes. The impact of histone lactylation on chromatin structure and gene expression have been established in specific context like cancer and in particular cell types such as immune cells. However, its exact function is still unclear and needs further investigation. It has been shown that various HDACs (particularly **HDAC 1** and **3**) and silent information regulator1- 3 (**SIRT1-3**) can remove the lactyl from the K residue of a histone tail (Couture and Trievel, 2006; Sauer *et al.*, 2018; Zhou, Tang and Chen, 2018; Liu *et al.*, 2019; Zhang *et al.*, 2019; Xie *et al.*, 2022). All in all, the wide range of histone post-translational modifications (**hPTMs**) and DNA methylation deployed by epigenetic enzymes can be considered as the epigenetic alphabet of the cells, that can be written, erased and read depending on the biological and environmental needs (Couture and Trievel, 2006).

The third and the fourth levels of chromatin organization are beyond single nucleosomes and are referred to as the "higher order chromatin structure", mainly addressing the **3D structure of the chromatin** (Figure 1). At the third level, nucleosomes form **30 nanometer-wide fibers**, which eventually shape **solenoid-like structures** at the fourth level. These

levels of chromatin conformation employ various chromatin-associated proteins and epigenetic enzymes to maintain or reshape the 3D structure of the chromatin. If hPTMs and DNA methylation are considered letters of the epigenetic alphabet, "*histone codes*" are the words. ***Histone code*** is the cooccurrence of several specific hPTMs at particular chromatin regions, which can be read by and signal the recruitment of particular **chromatin-remodeling complexes** such as switch/sucrose non-fermentable (**SWI/SNF**) and imitation SWI (**ISWI**). Chromatin-remodeling complexes such as SWI/SNF and ISWI, can change the nucleosome positioning by consuming ATP. Histone codes with or without the help of chromatin-remodeling complexes, can induces structural alterations to the chromatin, resulting in increased/decreased accessibility to TFs and chromatin-associated proteins. The histone code can be inherited from mother cells to the daughter cells through cell division to maintain cellular memory and cell identity. Regulating the influence of histone code, requires cooperation of several regulators, including polycomb group (**PcG**) proteins and **TF**s. PcG proteins, including polycomb repressive complexes 1 and 2 (PRC1 and PRC2) establish repressive chromatin domains. PRC1 mediates chromatin compaction, while PRC2 deposits repressive hPTMs, such as H3K27me3. TFs can also mediate the recruitment of several chromatin-modifying complexes, hence contributing to the maintenance and genetically required reformations of the chromatin structure. The higher order chromatin structure is also functionally important to facilitate long-range interactions of chromatin regions, known as *topologically associated domain* (***TAD***) structures, which are important for enhancer-promoter connections and hence transcriptional regulation. Formation of TADs are mainly regulated through the interaction of two protein complexes, **cohesin** and CCCTC-binding factor (**CTCF**). Cohesin can actively propel DNA double strand through its ring-shaped structure by ATP hydrolysis (mediated by cohesin's ATPase subunit), until being anchored by CTCF at particular genomic loci, a process known as "**chromatin loop**

extrusion". Subsequently, the cohesin-CTCF complex forms loops in the chromatin, bringing distant genomic regions into spatial proximity and hence contributing to the formation of TADs (Li and Arnosti, 2010; Sanborn *et al.*, 2015; Cuartero, Innes and Merkenschlager, 2019; Heenan *et al.*, 2020; Oshita, 2022). While the higher order chromatin structure enables control over gene expression through regulating the physical interaction of distanced loci, it prepares the chromatin for the final level of organization inside a cell's nucleus.

The fifth level of chromatin organization is where the chromatin falls into its final folded form inside the nucleus of a cell. At this level of organization, during the interphase (part of the cell cycle where the cell is not actively dividing) the chromatin can form spatially distinctive territories, known as ***chromosome territories***. Chromosome territories are the spatial arrangement of individual chromosomes (densely packaged chromatin entity, pivotal for genetic inheritance and cellular processes) within the nucleus. This organization is shown to be non-random and influenced by various factors, including active gene density. Chromosome territories can be categorized as **compartment A** (**active**) or **compartment B** (**inactive**) territories. Compartment A is usually associated with **euchromatin**, a state of chromatin known to be enriched with actively transcribed genes, regulatory elements, and regions of the genome that require frequent access for gene expression. Euchromatin is essential for promoting transcription and facilitating the binding of transcriptional machinery and regulatory factors. Compartment B however, is associated with **heterochromatin**, a state of chromatin encompassing regions with silenced genes, repetitive DNA sequences, and chromosomal regions undergoing specific processes, such as X-chromosome inactivation in female cells. Heterochromatin is a key player in maintaining genome stability and preventing aberrant gene expression in specific genomic regions. Whilst the A compartments tend to localize towards the central nucleoplasm, B

compartments exhibit a predilection for the nuclear lamina, resulting in the formation of the lamina-associated domains (**LAD**s) (Matharu and Ahituv, 2015; Zheng and Xie, 2019).

All in all, the hierarchical organization of chromatin is a sophisticated regulatory system governing gene expression and cellular identity. Nucleosomal arrangement, hPTMs, and DNA compaction intricately collaborate to shape chromatin's landscape. The very central characteristic of this system, however, is its **dynamic nature**. Such attribute enables the epigenome to respond to the environmental changes and regulate birth, cellular identity, organ formation, growth, physiologic maintenance, and reproduction of an individual (Zhang and Pradhan, 2014). This dynamic nature is regulated by the correct function of **epigenetic modifiers** (Zhang and Pradhan, 2014; Han *et al.*, 2019).

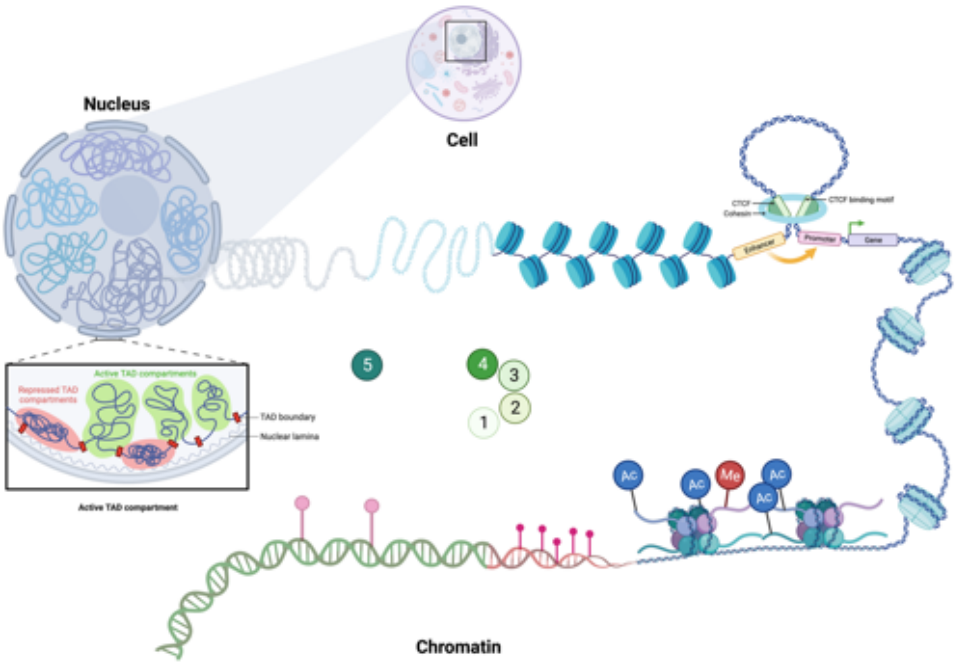

*Figure 1.**Hierarchical organization of chromatin**. First level of chromatin organization (1) starts with chemical modifications of the DNA, mainly methylations on CpG dinucleotides by DNMTs and their removal by demethylases. Second level of chromatin organization (2) relying mainly on nucleosome positioning, regulated by epigenetic enzymes and modifications of the histone tails. Third and fourth levels of chromatin organization (3) and (4) address the 3D structure of the chromatin, formed and reformed by various epigenetic regulating complexes, including CTCF and cohesin collaboration in forming chromatin loops and TADs. Fifth level of chromatin organization (5) is the highest level of chromatin organization, where chromosome territories are defined, LADs are formed and euchromatin can be distinguished from*

heterochromatin by cytogenetic staining techniques. Figure adapted from "Genomic Architecture (Layout)", "Chromosome Organization in Nucleus: TADs", and "Transcriptional Regulation by CTCF and Cohesin" by BioRender.com (2023). Retrieved from https://app.biorender.com/biorender-templates. Figure created with Biorender.com.

1.2. Epigenetic modifiers

Delving into the realm of epigenetic modifiers deepens our comprehension. These enzymatic orchestrators sculpt chromatin architecture and, consequently, gene accessibility. DNMTs and histone-modifying enzymes stand as architects of this dynamic system, their marks echoing across generations of cells. This intimate interplay between chromatin organization and epigenetic modifiers underscores the remarkable complexity of cellular regulation. Unraveling these mechanisms not only enriches our fundamental knowledge but also holds promising implications for therapeutic interventions and our grasp of biological intricacies. Epigenetic modifiers can be categorized into three main classes based on their primary function, identified as epigenetic **writers**, **readers**, and **erasers** (Figure 2) (Helin and Dhanak, 2013; Zhang and Pradhan, 2014; Han *et al.*, 2019).

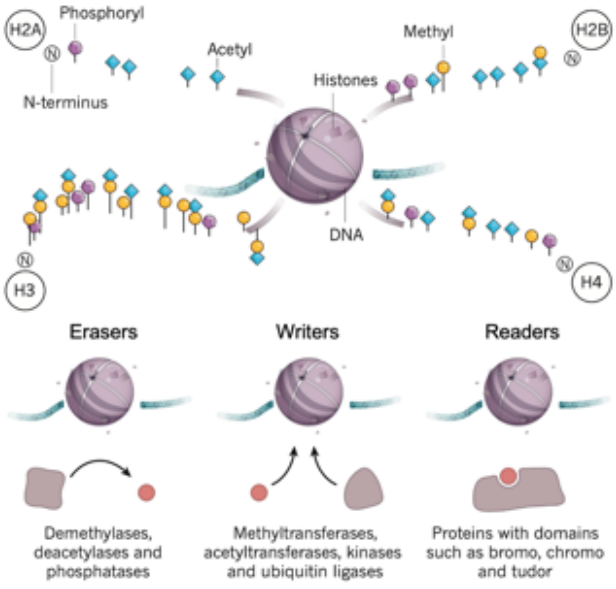

*Figure 2. **Epigenetic enzymes**. Writers add the hPTMs, while erasers remove them. Readers, interpret these PTMs and influence chromatin structure. Figure and legend adapted from Helin and Dhanak, 2013.*

Epigenetic writers are enzymes responsible for **covalent installation of chemical modifications on either DNA nucleobases or histone tail amino acid residues** (Couture and Trievel, 2006; Biswas and Rao, 2018). In this section, some important examples of epigenetic writers will be briefly discussed. However, there is a vast number of enzymes being recognized as epigenetic writers. Hence, a more comprehensive list of these enzymes is provided at the end of the section (Table 1). The main group of epigenetic writers, targeting the DNA, are ***DNMTs***. **DNMT1** is predominantly responsible for sustaining the DNA methylation pattern through DNA replication. During the S phase of the cell cycle, DNMT1 transports a methyl group from S-adenosylmethionine (SAM) to the carbon 5 position of the cytosine pyrimidine ring in the hemi-methylated DNA. DNMT1's basic structure includes a regulatory N-terminus region and a catalytic C-terminus region. The N-terminus region regulates DNMT1's interaction with other protein complexes and replication foci during the S phase. These protein complexes include ubiquitin-like, containing PHD and RING finger domains 1 (UHRF1), helping DNMT1 to identify hemi-methylated DNA regions. DNMT1 is one of the main guardians of transcriptional fine-tuning, X-chromosome inactivation, epigenomic imprinting, keeping transposable elements (TEs) silent, differentiation, senescence, and cell death (Svedružić, 2011; Zhou and Hu, 2016). **DNMT3A** is known to be mediating *de novo* DNA methylation during development. Similar to DNMT1, DNMT3A's N-terminus is responsible for interaction with other complexes and mainly binding to chromatin, with the C-terminus as the catalytic region. DNMT3A can add a methyl group directly on the C of a CpG dinucleotide without requiring the hemi-methylated pattern. DNMT3A builds up a heterotetrametric form with DNMT3-like (DNMT3L) for improved binding affinity to the DNA. It also interacts with several other regulators, such as HDACs, chromatin remodeling complexes and TFs. DNMT3A is crucial for development, particularly in epigenomic imprinting and subsequent regulation of lineage commitment and tissue-

specific gene regulations (Fatemi *et al.*, 2002; Yang, Rau and Goodell, 2015; Somasundaram *et al.*, 2018). **DNMT3B** is specifically involved in establishment de novo DNA methylation signatures in the process of embryogenesis and cellular differentiation. The structure of DNMT3B is very similar to DNMT3A, with the regulatory N-terminus and the catalytic C-terminus. DNMT3B as well as DNMT3A, acts on unmethylated CpG dinucleotides. However, DNMT3B has been shown to have distinct targets. DNMT3B has a pivotal role in establishing cellular identity and tissue-specific epigenetic imprinting (Gagliardi, Strazzullo and Matarazzo, 2018).

Arriving at epigenetic writers, which target histones, the first category to be discussed is the subset of ***HMTs***. Enhancer of zeste homolog 2 (**EZH2**) is known as the catalytic subunit of the PRC2 complex, responsible for tri-methylation of lysine 27 on the H3 tail, associated with epigenetic silencing of the genes. Su(var)3-9, enhancer-of-zeste, Trithorax (SET) domain of EZH2 is responsible for its methyltransferase activity, transferring a methyl group originating from SAM to the histone tail. SWI3, ADA2, N-CoR, TFIIIB (SANT) domain of EZH2 preserves its structural stability and PRC2-exclusive functionality. As a subunit of PRC2, EZH2 interacts with other subunits of PRC2, including suppressor of zeste 12 (SUZ12), embryonic ectoderm development (EED), and RbAp46/48. All together, these subunits maintain PRC2's stability and physiologic activity. As well as DNMTs, EZH2 is also involved in regulation of cellular differentiation, stem cell pluripotency, tissue-specific gene expression signatures, and X-chromosome inactivation (Oyama *et al.*, 2014; Kim and Roberts, 2016; Larrew *et al.*, 2021). As mentioned earlier, SUZ12, a core component of PRC2, acts as the scaffold for the PRC2-interacting protein complexes and chromatin. Hence, even though SUZ12 is not a classic epigenetic enzyme, it is crucial for the activity of PRC2. SUZ12's VRN2-EMF2-FIS2-SUZ12 (VEFS) domain mainly stabilizes it at the core of PRC2, sustaining the integrity of the entire complex. SUZ12 can also be the scaffold hosting cofactors and non-

coding RNAs, who modulate the methyltransferase activities of PRC2. SUZ12 as well as other PRC2 subunits, is involved in PRC2-mediated regulations of cell lineage commitment, X-chromosome inactivation and general developmental processes as named formerly (Chammas, Mocavini and Di Croce, 2020). Mixed lineage leukemia (**MLL**) family, also recognized as lysine methyltransferase 2 (KMT2) family, are a family of HMTs, who primarily mediate the addition of methyl groups to the lysine 4 of H3 tail. This process is eventually associated with activating gene promoters and hence is considered permissive for a transcriptional epigenetic regulatory effect. The family members are MLL1 (KMT2A), MLL2 (KMT2B), MLL3 (KMT2C), MLL4 (KMT2D), MLL5 (KMT2E), SETD1A (KMT2F), and SETD1B (KMT2G). The SET domain is mutually present in all the MLL family members, granting the methyltransferase activity. Other mutual domains, such as the plant homeodomain (PHD) fingers assist the MLL family members to interact with other complexes. The members of this family of proteins act as subunits of other complexes, conferring their epigenetic modifier activities. For example, MLL1 and MLL2 are parts of the complex of proteins associated with Set1 (COMPASS), cooperating with its other subunits, WD repeat-containing protein 5 (WDR5), retinoblastoma-binding protein 5 (RBBP5), and absent, small, or homeotic (ASH2) to conduct the methyltransferase activity on target substrates. MLL family of proteins, very similar to other methyltransferases, predominantly regulate gene expression patterns, essential for cellular differentiation and developmental processes (Ford and Dingwall, 2015; Rao and Dou, 2015; Sugeedha, Gautam and Tyagi, 2021). The last group of epigenetic writers to be discussed here, is another class of histone modifiers, known as ***HATs***. General control non-derepressible 5 (**GCN5**) is also known as lysine acetyltransferase 2A (KAT2A) is a (non-)histone acetyltransferase. Lysine 9 of H3 and lysine 14 of H3 are the primary targets for GCN5's acetyltransferase activity, eventually leading to activation of genes involved in various processes such as DDR and cell cycle progression.

The bromodomain of GCN5 assist its recruitment to specific lysine of the histone tail, while its acetyl-CoA binding domain enables its catalytic activity on the targeted sites. Spt-ada-gcn5 acetyltransferase (SAGA) and ada-two-A-containing (ATAC) complexes are the main hosts of GCN5, regulating specific acetylation processes on the chromatin. GCN5 is an important regulator for various biological processes, such as response to environmental changes, differentiation and apoptosis (Dyda, Klein and Hickman, 2000; Sela *et al.*, 2012). P300/CBP-associated factor (**PCAF**), also known as lysine acetyltransferase 2B (KAT2B) is the paralog of GCN5. PCAF primarily acetylates lysine 9 of H3. While the HAT domain of PCAF is the backbone for acetyl-CoA recruitment and hence PCAF's catalytic activity, its bromodomain helps the enzyme to interact with the substrate. Active interaction with CREB-binding protein (CBP) and p300 expands the functional range of PCAF's enzymatic activity. PCAF, as well as its paralog, GCN5, is a member of the ATAC complex. Transcending H3K9 acetylation impact of PCAF activity on gene regulation, this epigenetic writer is also important due to its ability to acetylate TFs and hence regulating their stability (Schiltz and Nakatani, 2000; Liang *et al.*, 2023). Tat-Interactive Protein, 60 kDa (**TIP60**) also known by the name lysine acetyltransferase 5 (KAT5), is a member of Moz, Ybf2/Sas3, Sas2, and Tip60 (MYST) family of HATs. Its three main domains are the catalytic domain, known as the MYST domain; the chromatin binding domain, chromodomain; and the protein binding domain, the zinc finger domain. Nucleosome acetyltransferase of H4 (NuA4) and ataxia-telangiectasia mutated (ATM) complexes both require TIP60, as the catalytic subunit and the functional facilitator, respectively. Being part of the ATM, highlights the crucial contribution of TIP60 to DDR and maintaining the genomic stability (Sapountzi, Logan and Robson, 2006; Nagasaka *et al.*, 2022; Kocpinar *et al.*, 2023). The final example of HAT family members to be mentioned here, is **p300** also known as E1A binding protein p300 (EP300). Various structural domains of p300, facilitate its activities. These domains include the HAT

domain, responsible for the catalytic activity; the bromodomain, responsible for interaction with acetylated lysine; cysteine/histidine-rich 1 (CH1) and cysteine/histidine-rich 3 (CH3) domains, responsible for its interactions with TFs and other proteins or DNA, respectively. CBP mainly interacts with p300, forming bigger complexes, which can mediate acetyltransferase activities on histones and other substrates. p300 is also a coactivator of several TFs, including p53, nuclear factor kappa-light-chain-enhancer of activated B cells (NF-κB), and cAMP response element-binding protein (CREB), therefore acting as a key regulator of transcriptional activities (Kalkhoven, 2004; Delvecchio *et al.*, 2013; Hytti *et al.*, 2015). Wide range of enzymatic and coactivator roles of p300, makes it a key gene regulator for various cellular processes and even systematic regulations, such as immune response. In summary, epigenetic writers like DNMTs, HMTs, and HATs serve as pivotal molecular architects in the regulation of genomic and epigenomic landscapes. These enzymes exhibit a complex yet highly orchestrated synergy in controlling cellular processes like transcription, differentiation, and DNA repair. The compartmentalized structure of these proteins—characterized by a regulatory N-terminus and a catalytic C-terminus—allows for multifaceted interactions with protein complexes, chromatin, and other epigenetic regulators. Understanding the functionalities of these epigenetic writers is crucial for advancing our comprehension of cellular identity and lineage commitment and opens up novel therapeutic avenues in cancer biology (Lessard and Sauvageau, 2003; Svedružić, 2011; Delvecchio *et al.*, 2013; Yang, Rau and Goodell, 2015; Gagliardi, Strazzullo and Matarazzo, 2018; Chammas, Mocavini and Di Croce, 2020).

Enzyme Name	Family/Class	Catalytic Activity	Partnering Complexes and Proteins	Structural Overview	Biological Relevance	Pathological Conditions Involved
EZH2	PRC2	H3K27me3	SUZ12, EED	SET domain	Gene silencing	Various cancers
EZH1	PRC2	H3K27me2	SUZ12, EED	SET domain	Gene silencing	Developmental disorders
DNMT1	DNA Methyltransferase	DNA methylation	UHRF1	CXXC domain	DNA replication	Cancer, imprinting disorders
DNMT3A	DNA Methyltransferase	DNA methylation	DNMT3L	CXXC domain	De novo methylation	Hematological malignancies
DNMT3B	DNA Methyltransferase	DNA methylation	DNMT3L	CXXC domain	De novo methylation	ICF syndrome, cancer
PRMT1	Protein Arginine Methyltransferase	Arginine methylation	N/A	Rossmann fold	RNA processing	Cancer, cardiovascular diseases
PRMT5	Protein Arginine Methyltransferase	Arginine methylation	MEP50	Rossmann fold	RNA splicing	Cancer, neurological disorders
SETD2	SET domain	H3K36me3	N/A	SET domain	Transcriptional elongation	Clear cell renal cell carcinoma
SETD7	SET domain	H3K4me1	N/A	SET domain	Gene activation	Cardiovascular diseases
MLL1	SET domain	H3K4me3	WDR5, RBBP5	SET domain	Gene activation	Leukemia
MLL2	SET domain	H3K4me3	WDR5, RBBP5	SET domain	Gene activation	Developmental disorders
MLL3	SET domain	H3K4me1	UTX, PTIP	SET domain	Gene activation	Cancer, developmental disorders
MLL4	SET domain	H3K4me1	UTX, PTIP	SET domain	Gene activation	Cancer, developmental disorders
NSD1	SET domain	H3K36me2	N/A	SET domain	Gene activation	Sotos syndrome, cancer
NSD2	SET domain	H3K36me2	N/A	SET domain	Gene activation	Multiple myeloma
NSD3	SET domain	H3K36me2	N/A	SET domain	Gene activation	Cancer
DOT1L	DOT1	H3K79me2	AF10, AF17	DOT1 domain	Transcriptional elongation	MLL-rearranged leukemia
SUV39H1	SUV39	H3K9me3	HP1	SET domain	Gene silencing	Cancer, heterochromatin formation
SUV39H2	SUV39	H3K9me3	HP1	SET domain	Gene silencing	Cancer, heterochromatin formation
G9a	SET domain	H3K9me1/2	GLP	SET domain	Gene silencing	Cancer, neurological disorders
GLP	SET domain	H3K9me1/2	G9a	SET domain	Gene silencing	Cancer, neurological disorders
CARM1	PRMT	Arginine methylation	N/A	Rossmann fold	Transcriptional regulation	Cancer, cardiovascular diseases
PRMT6	PRMT	Arginine methylation	N/A	Rossmann fold	Transcriptional regulation	Cancer, HIV latency
PRMT8	PRMT	Arginine methylation	N/A	Rossmann fold	Neuronal differentiation	Neurological disorders

SETDB1	SET domain	H3K9me3	TRIM28, MCAF1	SET domain	Gene silencing	Cancer, developmental disorders
SETDB2	SET domain	H3K9me3	TRIM28, MCAF1	SET domain	Gene silencing	Cancer, developmental disorders
ASH1L	SET domain	H3K36me2	N/A	SET domain	Gene activation	Cancer, developmental disorders
WHSC1	SET domain	H3K36me2	N/A	SET domain	Gene activation	Wolf-Hirschhorn syndrome, cancer
WHSC1L1	SET domain	H3K36me2	N/A	SET domain	Gene activation	Cancer
SETD1A	SET domain	H3K4me3	WDR5, RBBP5, ASH2L	SET domain	Gene activation	Neurodevelopmental disorders, cancer
GCN5	HAT	Histone acetylation	SAGA, ATAC	Bromodomain	Gene activation	Cancer, developmental disorders
p300	HAT	Histone acetylation	CBP	Bromodomain	Transcriptional regulation	Cancer, Rubinstein-Taybi syndrome
TIP60	HAT	Histone acetylation	NuA4	Chromodomain	DNA repair, apoptosis	Cancer, neurodegenerative diseases
PCAF	HAT	Histone acetylation	SAGA, ATAC	Bromodomain	Gene activation	Cancer, neurodegenerative diseases
MOF	HAT	Histone acetylation	MSL complex	Chromodomain	Gene activation	Cancer, developmental disorders
CBP	HAT	Histone acetylation	p300	Bromodomain	Transcriptional regulation	Cancer, Rubinstein-Taybi syndrome

*Table 1. **Epigenetic writers**. This table provides a comprehensive list of epigenetic "writers," enzymes responsible for adding epigenetic marks to chromatin. Epigenetic Role: Categorizes the enzyme as an epigenetic writer, reader, or eraser. Enzyme Name: The name of the epigenetic enzyme. Family/Class: The family or class to which the enzyme belongs. Catalytic Activity: The specific histone or DNA modification catalyzed by the enzyme. Partnering Complexes and Proteins: Proteins or complexes that interact with the enzyme to facilitate its function. Structural Overview: Key structural domains relevant to the enzyme's function. Biological Relevance: The biological processes in which the enzyme plays a role. Pathological Conditions Involved: Diseases or conditions where the enzyme is implicated. Data extracted from reactome.org and ncbi.nlm.nih.gov (Gillespie* et al.*, 2022).*

Epigenetic readers are the second subcategory of epigenetic modifiers to be briefly discussed here. This class of modifiers consist of several families of enzymes, able to **read and interpret the histone code**. This reading happens in the form of interaction with the particular histone, leading to the recruitment of other proteins such as chromatin remodelers and/or TFs, eventually being interpreted to transcriptional fine-tuning (Couture

and Trievel, 2006; Biswas and Rao, 2018). Various proteins fall into the category of epigenetic readers, which most studied ones are summarized in (Table 2). Bromodomain-containing proteins (***BRDs***) are a class of several epigenetic reader enzymes, which contain bromodomains, enabling them to recognize and mount on acetylated lysine residues on histones. Subsequently, they act as scaffolds for other protein complexes to be recruited to the acetylated histone sites and induce structural and/or transcriptional changes. The bromodomains among different members of the BRD family, usually share the 100 amino acid backbone, while slight differences in their structure gives them different specificity for different lysine acetylation marks. BRD family hosts the bromodomain and extraterminal domain (**BET**) (including **BRD2**, **BRD3**, **BRD4**, **BRDT**), **CBP/p300**, Bromodomain adjacent to zinc finger domain (**BAZ**) (including **BAZ1A** and **BAZ1B**), SWI/SNF Related Matrix Associated Actin Dependent Regulator of Chromatin, Subfamily A (**SMARCA**) (including **SMARCA2**/BRM and **SMARCA4**/BRG1), tripartite motif family (**TRIM**) (including **TRIM24**, **TRIM28**, **TRIM33**, etc.) subfamilies. The spectrum of molecular and cellular processes that BRD family can impact ranges from transcriptional elongation to differentiation, DDR, cell cycle progression, and more (Dawson *et al.*, 2014; Braun and Gardin, 2017; Fujisawa and Filippakopoulos, 2017; Jevtic *et al.*, 2022). The next class of epigenetic readers are chromodomain proteins, mainly consisting of the two families of heterochromatin protein 1 (***HP1***) and chromodomain-helicase-DNA-binding (***CHD***). HP1 family of readers contain a N-terminus chromodomain (CD) and a c-terminus chromoshadow domain (CSD). Whilst the CD facilitates recognition of methylation marks on lysine residues of H3, CSD mediates HP1 family members' interaction with other protein complexes. **HP1α** (CBX5), **HP1β** (CBX1), and **HP1γ** (CBX3) are the three members of the HP1 family. HP1 proteins interact with nucleosome remodeling deacetylase (NuRD) complex and the HMT Su(Var)3-9 homolog 1 (SUV39H1), participating in epigenetic repression of euchromatic genes' expression,

expansion of heterochromatic regions, and regulation of telomere length (Schoelz and Riddle, 2022). CHD family of epigenetic readers contain tandem chromodomains at their n-terminus and a SNF2-like helicase/ATPase domain at the center of their structure. The chromodomain helps them to recognize the methylated histones and the helicase domain is responsible for nucleosome repositioning. **CHD1 to CHD9** are family members of the CHD family. **CHD3** and **CHD4** are subunits of the NuRD complex, involved in active chromatin remodeling and transcriptional fine-tuning. The main functions of the CHD family address transcriptional activation and repression, DDR, cellular lineage commitment, and chromosome organization (Hall and Georgel, 2007; Mills, 2017). In conclusion, epigenetic readers like BRD and CHD family members serve as critical interpreters of the histone code, recruiting other molecular players for transcriptional modulation and chromatin remodeling. These proteins exhibit specific domain architectures for precise recognition of acetylated or methylated histone marks and influence diverse cellular processes, from gene expression to DNA damage response. Their complex interactions with chromatin remodelers and TFs underline their pivotal role in the dynamic regulation of the epigenome (Hall and Georgel, 2007; Mills, 2017; Schoelz and Riddle, 2022).

Enzyme Name	Family/Class	Catalytic Activity	Partnering Complexes and Proteins	Structural Overview	Biological Relevance	Pathological Conditions Involved
BRD4	BET	Reader	P-TEFb	Bromodomains	Transcriptional regulation	AML, NMC
BRD2	BET	Reader	N/A	Bromodomains	Cell cycle regulation	Cancer
BRD3	BET	Reader	N/A	Bromodomains	Transcriptional regulation	Cancer
BRDT	BET	Reader	N/A	Bromodomains	Spermatogenesis	Infertility
PHF9/PHF19	PHD finger	Reader	PRC2	PHD domain	Gene silencing	Cancer
CHD1	CHD	Reader	N/A	Chromodomains	Chromatin remodeling	Cancer
CHD2	CHD	Reader	N/A	Chromodomains	Chromatin remodeling	Neurodevelopmental disorders
CHD3	CHD	Reader	NuRD complex	Chromodomains	Chromatin remodeling	Cancer, developmental disorders

CHD4	CHD	Reader	NuRD complex	Chromodomains	Chromatin remodeling	Cancer, developmental disorders
CHD5	CHD	Reader	NuRD complex	Chromodomains	Chromatin remodeling	Cancer, developmental disorders
CHD6	CHD	Reader	N/A	Chromodomains	Chromatin remodeling	Developmental disorders
CHD7	CHD	Reader	N/A	Chromodomains	Chromatin remodeling	CHARGE syndrome
CHD8	CHD	Reader	N/A	Chromodomains	Chromatin remodeling	Autism spectrum disorders, cancer
CHD9	CHD	Reader	N/A	Chromodomains	Chromatin remodeling	Developmental disorders, cancer
BAZ1A	BAZ	Reader	ACF1	Bromodomains	Chromatin remodeling	Cancer, developmental disorders
BAZ1B	BAZ	Reader	ACF1	Bromodomains	Chromatin remodeling	Williams-Beuren syndrome, cancer
CBP/p300	KAT3	Reader	N/A	Bromodomains	Transcriptional regulation	Cancer, Rubinstein-Taybi syndrome
SMARCA2	SWI/SNF	Reader	BRG1	Bromodomains	Chromatin remodeling	Nicolaides-Baraitser syndrome
SMARCA4	SWI/SNF	Reader	BRM	Bromodomains	Chromatin remodeling	Cancer, Coffin-Siris syndrome
TRIM family	TRIM	Reader	N/A	Bromodomains	Ubiquitination	Various diseases
HP1 family	HP1	Reader	SUV39H1, SUV39H2	Chromodomains	Gene silencing	Heterochromatin formation, cancer

*Table 2. **Epigenetic readers**. This table enumerates epigenetic "readers," proteins that recognize and interpret epigenetic marks on chromatin. Epigenetic Role: Categorizes the enzyme as an epigenetic writer, reader, or eraser. Enzyme Name: The name of the epigenetic enzyme. Family/Class: The family or class to which the enzyme belongs. Catalytic Activity: The specific histone or DNA modification catalyzed by the enzyme. Partnering Complexes and Proteins: Proteins or complexes that interact with the enzyme to facilitate its function. Structural Overview: Key structural domains relevant to the enzyme's function. Biological Relevance: The biological processes in which the enzyme plays a role. Pathological Conditions Involved: Diseases or conditions where the enzyme is implicated. Data extracted from reactome.org and ncbi.nlm.nih.gov (Gillespie* et al.*, 2022).*

Epigenetic erasers complete the definition of dynamism in epigenetics. These enzymes are complementary to the functions of epigenetic writers. They can **actively remove the chemical modifications formerly installed by epigenetic writers**, therefore enabling the organism to adapt and signal necessary molecular changes in response to real-time endogenous or exogenous requirements. List of epigenetic erasers is a very long list of enzymes, and the most studied ones are mentioned in Table 3. These acts of erasure take

place both on DNA and histones. The family of epigenetic erasers, targeting the DNA directly, are the family of ***TET*** enzymes, which were briefly discussed before. This group of enzymes are considered more as mediators of epigenetic changes rather than a group of classic epigenetic enzymes. This is because these enzymes – including **TET1**, **TET2**, and **TET3** – mediate the oxidation process of 5mC to 5hmC, 5fC, and 5caC. While the methylated cytosine is at one of these oxidized forms, it can eventually get unmethylated either by an active or passive mechanism. The active process can be done through other enzymes such as thymine-DNA glycosylase (TDG), which is able to recognize 5fC and 5caC and remove the methylation mark through base excision repair (BER). The passive process is simply the result of lack of hemi-methylated cytosine pattern during DNA replication and hence dilution of the mark throughout generations of cells. The catalytic domains of TET enzymes are located at their c-terminus, containing the Fe(II)- and α-ketoglutarate-dependent dioxygenase activity, required for oxidation of 5mC. HDACs, PRC2, O-linked N-acetylglucosamine transferase (OGT), and Wilms tumor 1 (WT1) are all shown to be interacting with TET enzymes, directing their target specificity, and enhancing their enzymatic activity outcomes. TET activities can cause both gene activation and maintenance of silenced genes, contributing to various processes such as embryogenesis, differentiation, DDR, cell cycle regulation and more (Tan and Manley, 2009; Cimmino *et al.*, 2017). Next to be discussed, is a large family of epigenetic erasers, acting on histones, known as ***HDAC****s*. HDACs can be classified into four main classes, based on their structure and function. **Class I HDACs** include **HDAC1**, **HDAC2**, **HDAC3**, and **HDAC8**. These HDACs are **restricted to the nucleus**. They share a catalytic domain and zinc-dependent deacetylase activity. HDAC1 and HDAC2 are components of both NuRD and Sin3 complexes, involved in transcriptional repression. HDAC1 and HDAC2 are subsequently involved in the regulation of cell cycle (in cooperation with retinoblastoma and E2F TFs) and deacetylation of proteins

involved in DDR. HDAC1 is also a regulator of hematopoiesis. HDAC3 is a component of nuclear receptor co-repressor (NCoR) and silencing mediator of retinoid and thyroid hormone receptor (SMRT) co-repressors' complex, involved in transcriptional repression during biological processes such as embryogenesis. HDAC3 is involved in cell cycle (G1 to S) progression control and cell differentiation. HDAC8 mainly interacts with cohesin and TP53, regulating cell cycle and apoptosis as well as playing roles in DDR and differentiation through gene silencing (Hayakawa and Nakayama, 2010; Chakrabarti *et al.*, 2015; Zhou, Tang and Chen, 2018; Planques *et al.*, 2020; Lee *et al.*, 2021; Yang *et al.*, 2021; Hess *et al.*, 2022). **Class II HDACs** include **HDAC4**, **HDAC5**, **HDAC7**, and **HDAC9** (**subclass a**); and **HDAC6** and **HDAC10** (**subclass b**). Class II HDACs also have zinc-dependent deacetylase activity similar to class I HDACs. However, they also possess a longer N-terminal domain, which makes them able to **shuttle between the nucleus and the cytoplasm**. Class IIa HDACs have a weaker catalytic potency and rely on interactions with class I HDACs for enhanced enzymatic activities. However, class IIb HDACs have more potent and more specific catalytic activities, such as polyamine deacetylation by HDAC10. HDAC4 and HDAC5 cooperate with myocyte enhancer factor-2 (MEF2) TFs in regulation of muscle cell differentiation. HDAC6 controls deacetylation of heat shock protein 90 (Hsp90) and α-tubulin, therefore regulating maturation and stability of various proteins, including kinases and hormone receptors. Class IIa HDACs are mainly involved in differentiation processes in contexts ranging from muscular cells to T-cells. HDAC6 is involved in cell motility and stress response. HDAC10 is thought to be involved in cell cycle regulation and apoptosis (Verdin, Dequiedt and Kasler, 2003; Zhang *et al.*, 2012; Parra, 2015; Herbst-Gervasoni *et al.*, 2020). **Class III HDACs** are also known as sirtuins (**SIRTs**) and include **SIRT1 to SIRT7**. SIRTs include a core catalytic domain and unlike the other HDAC classes, their catalytic activity relies on NAD^+ instead of zinc, implying that they are **functionally linked with cellular metabolism**. SIRT1 deacetylates histones and

several TFs, such as p53, FOXO, and NF-κB, regulating cell cycle progression, apoptosis, stress response, DDR and more. SIRT6 deacetylates H3K9 and H3K56 and interacts with DNA-dependent protein kinase (DNA-PK), leading to transcriptional repression and contribution to DDR, respectively. SIRT1 and SIRT6 are also mutually involved in glucose homeostasis. SIRT3, SIRT4, and SIRT5 are factors in regulation of oxidative metabolism. Moreover, SIRT3 also interacts with isocitrate dehydrogenase 2 (IDH2) fine-tuning the redox state. SIRT7 regulates ribosome biogenesis and cellular stress responses (Zhou, Tang and Chen, 2018; Wu *et al.*, 2022). **Class IV HDAC** is the final class of HDACs to be mentioned here and includes solely **HDAC11**. HDAC11 is the smallest HDAC (only 347 amino acids-long) and incorporates the same deacetylase domain of HDACs classes I and II. It has been suggested that HDAC11 interacts with specificity protein 1 (Sp1) TF and REST corepressor 1 (CoREST), and probably other repressive complexes, hence modulating gene expression patterns. The result of such gene expression regulating behaviors are particularly evident in modulating T-cell tolerance through HDAC11's activity (Villagra *et al.*, 2009; Liu *et al.*, 2020). The last group of epigenetic erasers to be stated here are ***HDMs***. The first family is Jumonji C-domain-containing (**JMJC**) family of HDMS. The Jumonji C (JmjC) domain is shared between JMJC family members and is responsible for HDM catalytic activities of these enzymes. Their catalytic activity relies on presence of Fe(II) and 2-oxoglutarate (2OG) as co-factors. The range of HDM activities of the JMJC family members covers mono-, di-, and tri-methylated lysine residues. These family members have differences in specificity and structure, hence stratified and mainly annotated as Jumonji and AT-Rich Interaction Domain (JARID) enzymes, KDM2/7, KDM3, KDM4, KDM5, and KDM6. Different JMJC family members interact with different complexes. For example, KDM6A partners with PRC2 and confers repressive genetic activities. SWI/SNF complex interacts with KDM5B, or MLL family incorporating JMJC enzymes like KDM2B and hence regulating differentiation and

chromatin structure (Chen *et al.*, 2006; Tsukada *et al.*, 2006; Vicioso-Mantis, Aguirre and Martínez-Balbás, 2022). Next HDM to be discussed in more details is **lysine-specific demethylase 1A** (**LSD1**) also referred to as flavin-containing amine oxidase domain-containing protein 2 (AOF2) is a HDM encoded by the *KDM1A* gene on chromosome 1 in homo sapiens (Binda *et al.*, 2010; Helin and Dhanak, 2013; Kim *et al.*, 2020).

Enzyme Name	Family/Class	Catalytic Activity	Partnering Complexes and Proteins	Structural Overview	Biological Relevance	Pathological Conditions Involved
HDAC1	HDAC	Histone deacetylation	Sin3, NuRD	Deacetylase domain	Gene repression	Cancer, neurodegenerative diseases
HDAC2	HDAC	Histone deacetylation	Sin3, NuRD	Deacetylase domain	Gene repression	Cancer, neurodegenerative diseases
HDAC3	HDAC	Histone deacetylation	NCoR, SMRT	Deacetylase domain	Gene repression	Cancer, metabolic disorders
HDAC4	HDAC	Histone deacetylation	MEF2	Deacetylase domain	Muscle differentiation	Muscular disorders, cancer
HDAC5	HDAC	Histone deacetylation	MEF2	Deacetylase domain	Muscle differentiation	Muscular disorders, cancer
HDAC6	HDAC	Histone deacetylation	HSP90	Deacetylase domain	Cellular stress response	Cancer, neurodegenerative diseases
HDAC7	HDAC	Histone deacetylation	MEF2	Deacetylase domain	Immune regulation	Autoimmune diseases, cancer
HDAC8	HDAC	Histone deacetylation	N/A	Deacetylase domain	X-linked disorders	Cornelia de Lange syndrome
HDAC9	HDAC	Histone deacetylation	MEF2	Deacetylase domain	Immune regulation	Autoimmune diseases, cancer
HDAC10	HDAC	Histone deacetylation	N/A	Deacetylase domain	Autophagy	Cancer
HDAC11	HDAC	Histone deacetylation	N/A	Deacetylase domain	Immune regulation	Autoimmune diseases, cancer
SIRT1	Sirtuin	Histone deacetylation	N/A	Sirtuin domain	Cellular metabolism	Aging, cancer
SIRT2	Sirtuin	Histone deacetylation	N/A	Sirtuin domain	Cell cycle	Cancer, neurodegenerative diseases
SIRT3	Sirtuin	Histone deacetylation	N/A	Sirtuin domain	Mitochondrial function	Metabolic disorders, cancer
SIRT4	Sirtuin	ADP-ribosylation	N/A	Sirtuin domain	Mitochondrial function	Metabolic disorders, cancer

SIRT5	Sirtuin	Histone deacetylation	N/A	Sirtuin domain	Mitochondrial function	Metabolic disorders, cancer
TET1	TET	5mC to 5hmC	OGT, TDG	CXXC domain	DNA demethylation	Cancer, developmental disorders
TET2	TET	5mC to 5hmC	OGT, TDG	CXXC domain	DNA demethylation	Hematological malignancies, clonal hematopoiesis
TET3	TET	5mC to 5hmC	OGT, TDG	CXXC domain	DNA demethylation	Developmental disorders, cancer
LSD1/KDM1A	KDM	H3K4me1/2, H3K9me1/2 demethylase	CoREST, NuRD, HDACs	AOD domain	Gene silencing/activation	Neurological disorders, cancer
KDM2A/FBXL11	Jumonji	H3K36me2 demethylase	N/A	JmjC domain	Gene silencing	Cancer, developmental disorders
KDM2B/FBXL10	Jumonji	H3K4me3 demethylase	N/A	JmjC domain	Gene activation	Cancer, developmental disorders
KDM3A/JMJD1A	Jumonji	H3K9me1/2 demethylase	N/A	JmjC domain	Gene activation	Cancer, metabolic disorders
KDM3B/JMJD1B	Jumonji	H3K9me1/2 demethylase	N/A	JmjC domain	Gene activation	Cancer, metabolic disorders
KDM4A/JMJD2A	Jumonji	H3K9me3, H3K36me3 demethylase	N/A	JmjC domain	Gene activation	Cancer, metabolic disorders
KDM4B/JMJD2B	Jumonji	H3K9me3, H3K36me3 demethylase	N/A	JmjC domain	Gene activation	Cancer, metabolic disorders
KDM4C/JMJD2C	Jumonji	H3K9me3, H3K36me3 demethylase	N/A	JmjC domain	Gene activation	Cancer, metabolic disorders
KDM4D/JMJD2D	Jumonji	H3K9me3, H3K36me3 demethylase	N/A	JmjC domain	Gene activation	Cancer, metabolic disorders
KDM5A/JARID1A	Jumonji	H3K4me3 demethylase	N/A	JmjC domain	Gene silencing	Cancer, developmental disorders
KDM5B/JARID1B	Jumonji	H3K4me3 demethylase	N/A	JmjC domain	Gene silencing	Cancer, developmental disorders
KDM5C/JARID1C	Jumonji	H3K4me3 demethylase	N/A	JmjC domain	Gene silencing	X-linked mental retardation
KDM5D/JARID1D	Jumonji	H3K4me3 demethylase	N/A	JmjC domain	Gene silencing	Cancer, developmental disorders
KDM6A/UTX	Jumonji	H3K27me3 demethylase	N/A	JmjC domain	Gene activation	Kabuki syndrome, cancer
KDM6B/JMJD3	Jumonji	H3K27me3 demethylase	N/A	JmjC domain	Gene activation	Inflammation, cancer
KDM7A	Jumonji	H3K9me1, H3K27me1 demethylase	N/A	JmjC domain	Gene activation	Developmental disorders, cancer

PHF8	PHD finger	H3K9me1/2 demethylase	N/A	PHD domain	Gene activation, cell cycle progression, DDR	Cancer, developmental disorders
NO66	Jumonji	H3K4me3, H3K36me3	N/A	JmjC domain	Gene silencing	Cancer, developmental disorders

Table 3. ***Epigenetic erasers****. This table compiles a list of epigenetic "erasers," enzymes that remove epigenetic marks from chromatin. Epigenetic Role: Categorizes the enzyme as an epigenetic writer, reader, or eraser. Enzyme Name: The name of the epigenetic enzyme. Family/Class: The family or class to which the enzyme belongs. Catalytic Activity: The specific histone or DNA modification catalyzed by the enzyme. Partnering Complexes and Proteins: Proteins or complexes that interact with the enzyme to facilitate its function. Structural Overview: Key structural domains relevant to the enzyme's function. Biological Relevance: The biological processes in which the enzyme plays a role. Pathological Conditions Involved: Diseases or conditions where the enzyme is implicated. Data extracted from reactome.org and ncbi.nlm.nih.gov (Gillespie* et al.*, 2022).*

Navigating the complex landscape of epigenetic writers, readers, and erasers reveals the fine-tuned mechanisms governing cellular identity and function. In this context, the triad serves as key regulators of chromatin architecture and gene expression. These molecules are responsible for the addition, recognition, and removal of epigenetic marks, respectively. Their coordinated activities are essential for cellular differentiation, homeostasis, and the cellular response to environmental stimuli. Importantly, dysregulation in any of these categories has been implicated in a range of pathologies, including oncological conditions.

LSD1 is a notable example of an "eraser" that has been extensively studied. LSD1 is responsible for the demethylation of histone H3 at lysine 4 and lysine 9, thereby serving a dual role in both gene activation and repression. Aberrant activity of LSD1 has been associated with the pathogenesis of various types of leukemia as well as solid tumors. A deeper understanding of the mechanistic roles of LSD1 could offer new avenues for targeted therapies in cancer treatment (Wade, Pruss and Wolffe, 1997; Binda *et al.*, 2010; Helin and Minucci, 2017; Kim *et al.*, 2020; Kunadis *et al.*, 2021).

1.3. LSD1 in health and cancer

LSD1 is a flavin adenine dinucleotide (**FAD**)-**dependent enzyme** with a central role in epigenetic regulation. It is a key player in regulating epigenetic marks, impacting gene expression, DNA repair, and cell differentiation. Under normal conditions, LSD1 helps maintain the structure and function of chromatin, which is essential for cell stability. It mainly removes methyl groups from histone H3 at lysine 4 (**H3K4**) and lysine 9 (**H3K9**), marks that are generally linked to **gene activation and silencing**, respectively (Wang *et al.*, 2007; Carnesecchi *et al.*, 2017; Chen *et al.*, 2017; Kim *et al.*, 2020). In the context of cancer, however, LSD1 takes on a more complex role. It's often **found at elevated levels in various cancers**, including leukemia and solid tumors, where it promotes disease progression. The enzyme's altered activity can lead to the deregulation of tumor suppressor genes (TSGs) or promote tumor growth, contributing to increased cell proliferation, metastases, and drug resistance (Lynch, Harris and Somervaille, 2012; Hosseini and Minucci, 2017). Recent research in cancer biology and experimental oncology is focusing on the potential of LSD1 inhibitors as a treatment option. These drugs aim to specifically inhibit LSD1's enzymatic or scaffolding functions, with the goal of restoring a balanced epigenetic and genetic states in cancer cells, thereby offering a new approach for cancer therapy (Sheng *et al.*, 2018; Fang, Liao and Yu, 2019; Ravasio *et al.*, 2020; Nicosia *et al.*, 2022).

LSD1 structure is organized into an **N-terminal SWIRM domain** and a **C-terminal amine oxidase domain** (**AOD**). The SWIRM domain is primarily involved in protein-protein interactions and potentially in substrate recognition. The AOD is the catalytic core responsible for the enzyme's demethylase activity. The AOD is further characterized by a unique helical insert, known as the "**tower domain**," which is formed by two long α-helices, TαA and TαB. These helices pack against each other without coiling and are connected by

a short, disordered loop. The tower domain is directly connected to the catalytic center and is speculated to be a binding platform for members of the CoREST complex or other histone-modification complexes. It may also allosterically regulate the catalytic activity of LSD1 (Figure 3) (Stavropoulos, Blobel and Hoelz, 2006; Janardhan *et al.*, 2018). LSD1 exhibits a specialized affinity for histone H3 lysine 4 (H3K4). The enzyme's active site is inherently designed to snugly fit its target substrate, histone H3. Upon binding, the H3 peptide undergoes a unique conformational change, allowing its N-terminal end to engage with a negatively charged pocket within LSD1. This positions H3K4 in close proximity to the FAD cofactor, facilitating the demethylation process (Yang *et al.*, 2007).

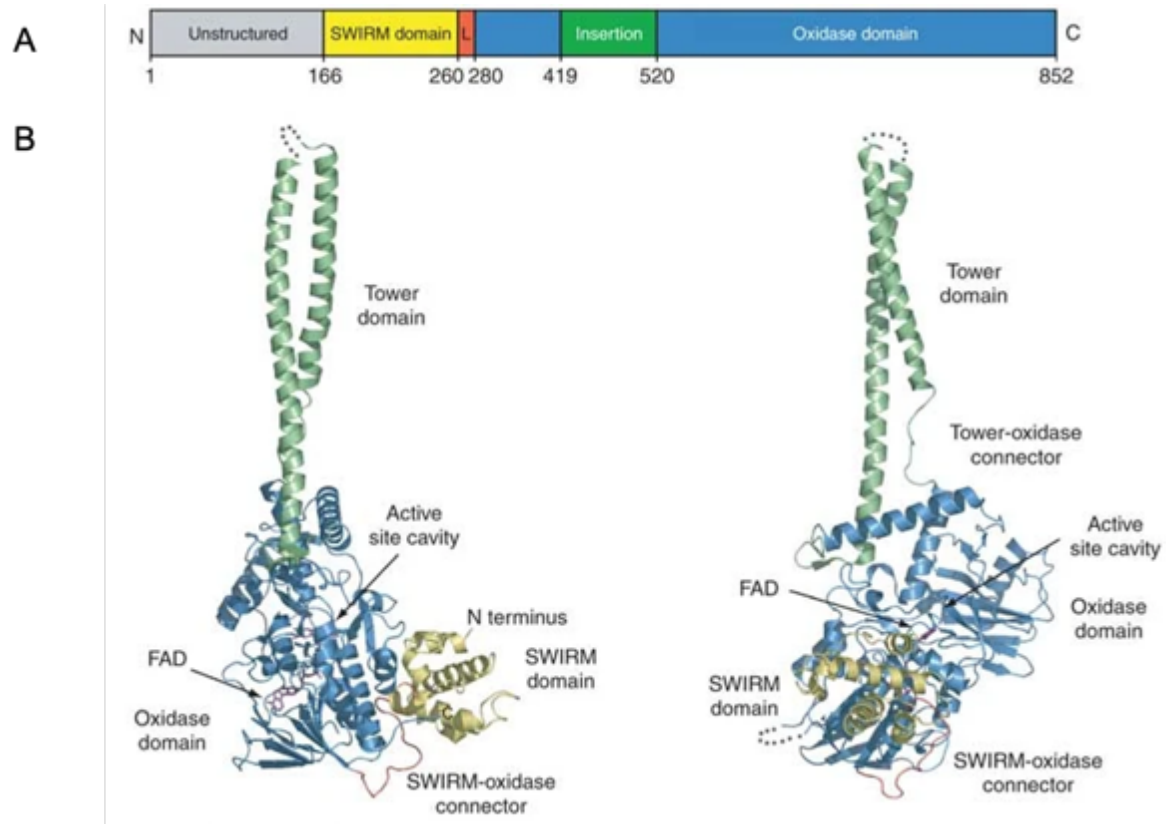

Figure 3. ***Structure of LSD1****. (A) Structure of LSD1 domains. Unstructured N-terminal region: Gray; SWIRM domain: Yellow; SWIRM-oxidase connector: Red; Oxidase domain: Blue; Helical insertion: Green. (B) Structure of LSD1 in ribbon representation, colored as in "A". Right panel shows a 90°-rotated view. Figure and legend adapted from Stavropoulos, Blobel and Hoelz, 2006.*

LSD1's enzymatic function employs an **FAD-dependent oxidation mechanism**. It selectively removes **mono-** and **di-methyl** groups from **H3K4** through a series of reactions involving the transient reduction of FAD to $FADH_2$. This reduced form of FAD oxidizes the methylated lysine, forming an imine intermediate that is hydrolyzed to yield formaldehyde and a demethylated lysine residue. The $FADH_2$ is then reoxidized, completing the catalytic cycle (Figure 4) (Stavropoulos, Blobel and Hoelz, 2006; Zheng, Yu, *et al.*, 2016). LSD1's enzymatic repertoire extends beyond H3K4 to include demethylation of **H3K9**, a substrate specificity that has significant implications in cancer biology and androgen receptor- (AR-)mediated gene expression. LSD1 and JMJD2C collaborate to focus on AR-regulated genes, removing methyl groups from H3K9 mono- and di-methyl to trigger gene activation. This combined action of demethylation isn't just a minor biochemical occurrence; it has crucial implications for cancers that respond to androgens (Wissmann *et al.*, 2007). Additionally, LSD1's interaction with estrogen-related receptor α (ERRα) has been shown to induce the enzyme to demethylate H3K9 *in vitro*, adding another layer of complexity to its role in epigenetic regulation (Carnesecchi *et al.*, 2017). LSD1 has key roles in various cancer progressions through demethylation of both H3K4me1/2 and H3K9me1/2, underscoring its potential as a therapeutic target (Zheng, Yu, *et al.*, 2016). The dual transcriptional regulating role of LSD1 is evident also looking at its partnering complexes and proteins or even different isoforms. Where LSD1 teams up with CoREST or NuRD complexes, conferring its H3K4 demethylating activities, it is a classic gene repressor (Figure 5A) (Hakimi *et al.*, 2003; Yang *et al.*, 2006; Wang *et al.*, 2009). On the other hand, when LSD1 is interacting with AR/estrogen receptor (ER) or its alternate splicing variant, LSD1+8a is present, it can change its substrate affinity towards H3K9 and hence induce transcriptional activation (Figure 5B & C) (Garcia-Bassets *et al.*, 2007; Wissmann *et al.*, 2007; Helin and Dhanak, 2013; Laurent *et al.*, 2015; Carnesecchi *et al.*, 2017).

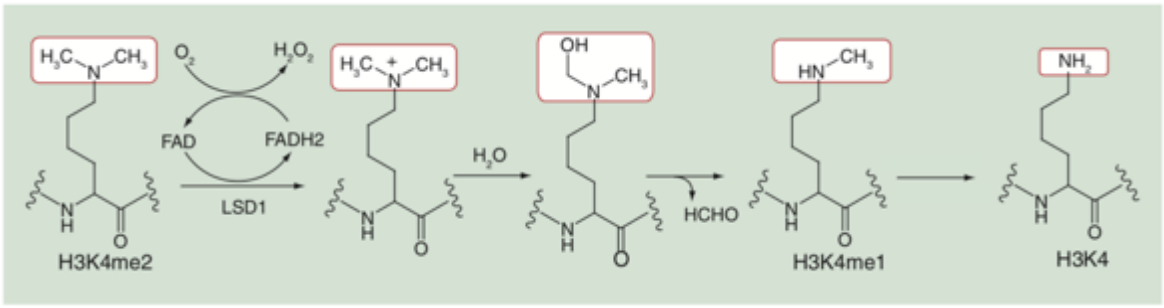

Figure 4. ***Catalytic process of LSD1's activity****. The process selectively eliminates one and two methyl groups from H3K4. This is done through a chain of reactions that temporarily turn FAD into its reduced form, $FADH_2$. This reduced FAD oxidizes the methylated lysine, creating an imine intermediate that eventually breaks down into formaldehyde and a demethylated lysine. The cycle concludes by reoxidizing $FADH_2$. Figure and legend adapted from Zheng et al., 2016.*

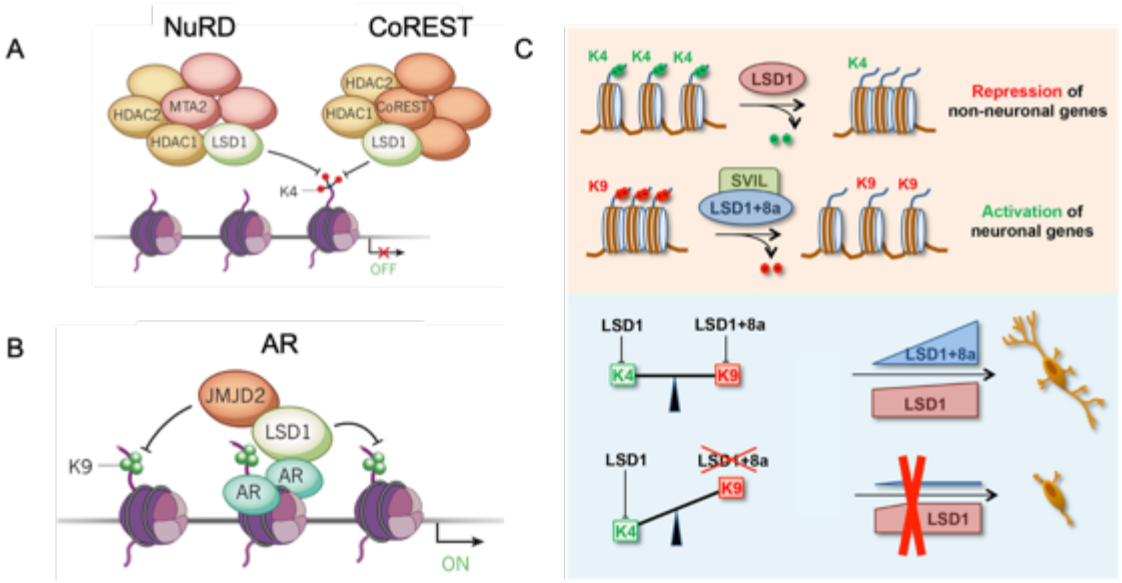

Figure 5. ***LSD1 can confer different transcriptional effects****. (A) LSD1 in cooperation with repressive complexes, NuRD and CoREST, causes gene silencing. Figure and legend adapted from Helin and Dhanak, 2013. (B) LSD1 in cooperation with AR or JMJD2, directs gene expression. Figure and legend adapted from Helin and Dhanak, 2013. (C) LSD1's isoform, LSD1+8a preferentially demethylates H3K9 and causes gene activation. Figure and legend adapted from Laurent et al., 2015.*

Biological functions of LSD1 include a wide spectrum of biological processes from cell cycle regulation and fate determination, to DDR in a variety of cell types, including embryonic stem cell (ESC), to neuron neural stem cell (NSC), and hematopoietic stem cell (HSC). For example, in **trophoblast stem cells**, LSD1's role extends beyond minimal gene regulation; it

acts as a metabolic gatekeeper. Castex *et al*. (2017) show that when LSD1 is deactivated, the activity of the mitochondrial protein Sirt4 increases, disrupting the redox balance and mitochondrial function. This leads to cellular senescence, indicating that LSD1 is essential for maintaining metabolic flexibility (Castex *et al.*, 2017). LSD1 shows a dynamic association with chromatin in embryonic stem cells (**ESCs**). It doesn't remain in chromatin consistently but is brought in during specific phases of the cell cycle, namely G1, S, and G2, then removed during mitosis. This transient interaction allows LSD1 to regulate pluripotency markers like Oct4 and Sox2. By controlling when it associates with chromatin, LSD1 orchestrates quick changes in gene transcription, playing a critical role in maintaining the unique properties of stem cells (Nair *et al.*, 2012). LSD1 plays a central role in the differentiation of ESCs, as highlighted by multiple studies. Research led by Whyte underlined LSD1's significance in regulating gene expression, particularly through its role in deactivating enhancers. They observed that inhibiting LSD1 caused a partial repression of key ESC genes during differentiation. Notably, the study revealed that when LSD1 was active, the NuRD complex was primarily found at enhancers instead of CoREST, suggesting that LSD1 collaborates with specific chromatin-remodeling complexes to control gene activation and deactivation, thereby guiding the differentiation of stem cells (Whyte *et al.*, 2012).

LSD1 is a crucial epigenetic regulator in hematopoiesis, playing a significant role in modifying chromatin structure through its demethylase activity. This function doesn't operate in isolation; instead, LSD1 collaborates with other proteins to shape gene expression. For example, LSD1 interacts with Gfi1b, Hoxa9, and Meis1, which allows it to impact a complex network of genes essential for hematopoietic differentiation (Sprüssel *et al.*, 2012). LSD1's connection with GFI1B is crucial in directing **erythroid and myeloid lineage commitment**. GFI1B is a key TF in these differentiation pathways, and its

partnership with LSD1 acts as a regulatory mechanism. This interaction controls the expression of specific genes, affecting how hematopoietic stem cells commit to erythroid or myeloid lineages (Saleque *et al.*, 2007; Ravasio *et al.*, 2020). LSD1 is also involved in suppressing erythroid differentiation by interacting with the TF GATA1, which is crucial for erythroid lineage commitment. When LSD1 and GATA1 cooperate, they repress genes responsible for promoting erythroid differentiation, demonstrating higher complexity of LSD1's function in hematopoiesis. This interaction reveals how LSD1 can influence the balance between promoting and suppressing erythroid differentiation (Kerenyi *et al.*, 2013). On the other hand, LSD1 has been shown to have evolutionarily conserved roles in hematopoietic development. Recent studies indicate that LSD1 plays a role in the **endothelial-to-hematopoietic transition** (**EHT**) during zebrafish development. This process involves the movement of hematopoietic stem and progenitor cells (HSPCs) from the endothelial lining into the bloodstream. Interestingly, LSD1's function in this context seems to operate independently of Etv2-Etsrp, a TF known for its role in primitive hematopoiesis. There's also evidence suggesting that LSD1 may collaborate with Gfi1b to suppress endothelial gene expression, thereby supporting the shift to definitive hematopoiesis (Tamaoki *et al.*, 2023). The enzyme's role is further complicated by its ability to form complexes with other proteins. For example, LSD1 interacts with CoREST, a corepressor, to modulate the expression of target genes, adding another dimension to its influence on **HSC differentiation**. Furthermore, LSD1's interaction with SNAG-domain-containing TFs is crucial for LSD1's role in regulating gene expression during primitive hematopoiesis. The SNAG domains of proteins like Gfi1 and Snail recruit LSD1 to specific genomic locations, where it acts as a scaffold to form chromatin-modifying complexes (e.g., CoREST). This scaffolding function is essential for the repression of early developmental programs, including primitive hematopoiesis. Interestingly, **LSD1's scaffolding function has been**

proposed to be more critical for its role in gene regulation than its demethylase activity. Moreover, a negative feedback loop was suggested where LSD1 recruitment through SNAG, downregulates the expression of the very same SNAG-containing genes, thereby controlling developmental gene expression (T. Lin *et al.*, 2010; Y. Lin *et al.*, 2010; Casey *et al.*, 2023). **The interaction between LSD1 and GFI1, a transcriptional repressor, serves to fine-tune the expression of genes that are critical for hematopoietic differentiation**. This interaction is not merely a passive one but actively modulates the expression of target genes, thereby influencing the differentiation pathways of HSCs (Chen, Odenike and Rowley, 2010; Thambyrajah *et al.*, 2016). In summary, LSD1 emerges as a multifunctional regulator in hematopoiesis, influencing the differentiation of HSCs into various lineages through its enzymatic activity and its interactions with a range of TFs.

LSD1's altered function in cancer as well as its biological functions, cover a wide spectrum of affected mechanisms in various tumor cell types, ranging from lung cancer, digestive tract cancers, bladder cancer, retinoblastoma, prostate cancer, and breast cancer to hematological malignancies. Among solid tumors, In **non-small cell lung cancer (NSCLC)**, LSD1 is expressed at higher levels compared to normal lung tissues. This increase is noticeable in both protein and mRNA measurements. Elevated LSD1 levels correlate with a lower overall survival (OS) rate for NSCLC patients, regardless of other clinical factors. Experimentally, when LSD1 is inhibited in A549 and H460 cells, their ability to multiply and invade is significantly reduced (Lv *et al.*, 2012). **Human bladder cancer** tissues also show significantly higher LSD1 levels compared to non-cancerous bladder tissues. Moreover, reducing LSD1 expression leads to slowed cell growth in various bladder and lung cancer cell lines. An excess of LSD1 has been associated with speeding up the cell cycle in human embryonic kidney fibroblasts. Importantly, LSD1 plays a role in gene expression changes tied to chromatin structure, affecting processes like centromeric chromatin reorganization,

heterochromatin formation, and chromatin assembly (Hayami *et al.*, 2011). Research indicates that AR, along with LSD1 and JMJD2A, plays an important role in both early-stage and advanced bladder cancer in humans. LSD1 showed higher expression in cancerous samples compared to non-cancerous tissue (Kauffman *et al.*, 2011). In **gastric cancer** (**GC**), LSD1 has been shown to significantly influence the tumor immune microenvironment. There is a negative association between LSD1 expression and the presence of CD8+ T-cells, while a positive association exists with PD-L1 expression in GC tissues. Notably, removing LSD1 results in a substantial reduction of exosomal PD-L1, restoring the function of T-cells. This effect was observed in studies involving mouse forestomach carcinoma cells, where LSD1 knockout (KO) caused a more pronounced slowing of tumor growth in mice with intact immune systems compared to those lacking T-cells. These findings shed light on the possiblity of targeting LSD1 as a potential combinatorial immunotherapy approach for GC patients (Shen *et al.*, 2022). LSD1 has also been identified as a significant player in the growth and spread of **colon cancer**. High levels of LSD1 were detected in colon cancer tissues, with a strong correlation to advanced tumor-node-metastasis (TNM) stages and metastasis. When LSD1 was inhibited, colon cancer cells exhibited reduced proliferation and invasiveness, and an increase in apoptosis in *in vitro* experiments. In terms of mechanism, LSD1 was found to bind to the promoter region of CDH-1 (E-cadherin), resulting in less demethylation of H3K4 in this area. This epigenetic change reduced CDH-1 expression, thereby promoting the invasiveness of colon cancer cells (Ding *et al.*, 2013). In addition to its role in proliferation of cancer cells, LSD1 is also implicated in **epithelial-mesenchymal transition** (**EMT**), a process crucial for cancer metastasis. LSD1 was shown to regulate EMT by modulating the expression levels of CDH-1 and CDH-2 (N-cadherin). Specifically, inhibition of LSD1 led to upregulation of CDH-1 and downregulation of CDH-2, thereby affecting the invasive capabilities of colon cancer cells as discussed formerly (Ding

et al., 2013; Lamouille, Xu and Derynck, 2014). LSD1 is recognized as an essential part of the NuRD complex, which broadens the complex's chromatin remodeling abilities to encompass ATPase, HDAC, and HDM functions. The LSD1-NuRD complexes are implicated in controlling various cellular signaling pathways, including TGFβ1, which plays a crucial role particularly in EMT (Wang *et al.*, 2009). Regarding **breast cancer**, LSD1 has been shown to reduce the invasiveness of breast cancer cells. A negative correlation was identified between the expression levels of LSD1 and TGFβ1 in breast carcinomas, indicating that LSD1 might play a part in regulating TGFβ1 signaling (Wang *et al.*, 2009). Moreover, LSD1 was discovered to interact directly with metastasis tumor antigen (MTA) proteins, which are part of the NuRD complex. This interaction occurs at the tower domain of LSD1 and is crucial for LSD1's ability to demethylate nucleosomal substrates (Wang *et al.*, 2009). Furthermore, it has been elucidated that the deubiquitinase USP28 plays a pivotal role in stabilizing LSD1, thereby contributing to the **cancer stem cell-like properties in breast cancer**. USP28 was identified as a deubiquitinase of LSD1 through a comprehensive small interfering RNA (siRNA) screening. Intriguingly, the protein levels of USP28 and LSD1 were found to be positively correlated in multiple cancer cell lines and breast tumor samples, although no such correlation was observed at the mRNA level. This suggests that USP28 primarily controls LSD1 stability at the post-translational level. The interaction between USP28 and LSD1 was mapped to the AO domain of LSD1 and the N-terminal region of USP28 were required for their interaction. Moreover, it is demonstrated that the KD of USP28 led to the rapid degradation of LSD1, confirming the role of USP28 in stabilizing LSD1. This stabilization was shown to be mediated through a deubiquitination event, as evidenced by the restoration of LSD1 levels following treatment with the proteasome inhibitor MG132 (Wu *et al.*, 2013). LSD1 is notably overexpressed in **lung squamous cell carcinomas** (**SCCs**) that also express *Sox2*. This heightened expression isn't just a mere observation—it has practical

consequences. Specifically, LSD1-targeted inhibitors specifically hamper the growth of lung SCCs with *Sox2* expression, while having almost no effect on cells lacking Sox2. Inhibiting LSD1 leads to a decrease in Sox2 levels, triggers G1 cell-cycle arrest, thus encouraging the cells to differentiate. These outcomes are suggested to be influenced by the specific regulation of the methylation levels on H3K4 and H3K9 (Zhang *et al.*, 2013). LSD1 has further been reported to regulate epidermal differentiation in **cutaneous SCC**. It achieves this by suppressing key epithelial TFs that drive differentiation, such as *GRHL1*, *GRHL3*, *NOTCH3*, and *KLF4*. Upon inhibition, there is a meaningful elevation of H3K4me and expression of these key TFs, causing an early epidermal differentiation (Egolf *et al.*, 2019). The same research revealed that LSD1 is elevated in epithelial cancers like SCC, suggesting that targeting LSD1 could be a therapeutic strategy. The study also demonstrated that inhibiting LSD1 caused a significant rise in the expression of well-known differentiation-related genes, including *DSG1*, *SPRR1B*, *PI3*, *KLK13*, *KRT1*, and *CDSN* (Egolf *et al.*, 2019). These observations were extended to additional cancer cell types, including **breast and ovarian carcinoma** cells. Researchers found that cells expressing Sox2 showed a high sensitivity to LSD1 inhibition, while those lacking Sox2 did not. This sensitivity was not exclusive to lung carcinoma cells; various breast and ovarian carcinoma cells also responded strongly to LSD1 inhibitors. The study revealed a notable correlation between Sox2 and LSD1 expression across a diverse range of human cancers (Zhang *et al.*, 2013).

In the context of hematological malignancies, it has been established that overexpression of LSD1 is instrumental in the onset of **T-cell lymphoblastic leukemia/lymphoma** (**T-LBL**). While LSD1 is poorly expressed in normal HSCs, its levels are significantly increased in leukemic cells, particularly those originating from T-cells. The amplification of the shortest LSD1 isoform enhances the self-renewal capabilities of HSCs, primarily through the activation of the *HoxA* gene cluster. This elevated expression acts as an initial event in T-LBL

leukemogenesis as evidenced by *in vivo* studies (Wada *et al.*, 2015). Moreover, transgenic mice models, designed to overexpress a particular LSD1 isoform in HSCs, were utilized to explore its role in the malignant transformation of HSPCs. These mice were as well susceptible to T-LBL after gamma-irradiation (Wada *et al.*, 2015). Additionally, the same study elucidated the distinct functionalities of various LSD1 isoforms. For example, the shortest isoform was found to be more efficient in demethylating histone H3K9 compared to the longer isoforms, and is selectively inhibited in dormant HSCs. These observations underscore the potential of LSD1 alternate expression as a foundational aberration in T-LBL (Wada *et al.*, 2015). LSD1 is crucial in hematopoiesis and plays a role in regulating **super-enhancers** (**SEs**). The LSD1 inhibitor NCD38 specifically breaks the interaction between LSD1 and GFI1B, without impacting its connections with other partners such as RUNX1, HDAC1, and HDAC2. This specific disruption leads to the activation of particular differentiation regulating SEs. The same research shows that GFI1B binds specifically to the ERG SE, likely suppressing its activity. When treated with NCD38, the binding of LSD1 and CoREST to the ERG SE decreases, while GFI1B's occupancy remains consistent. This implies that NCD38's approach involves specifically breaking the connection between GFI1B and the LSD1-CoREST complex, thereby releasing the ERG SE from suppression (Yamamoto *et al.*, 2018). In the realm of **AML** treatment, it has been demonstrated that inhibiting LSD1 can reactivate the all-trans-retinoic acid (ATRA) differentiation pathway, especially in (non-)acute promyelocytic leukemia (APL) subtypes of AML. Tranylcypromine (TCP), an LSD1 inhibitor, has been employed to test this effect, showing that it does not lead to a genomewide increase in H3K4me2. However, it does boost H3K4me2 levels and the expression of genes linked to myeloid differentiation. The engraftment of primary human AML blasts in NOD-SCID mice models were significantly less succesfull upon the combinatorial administration of ATRA and TCP. This suggests that such combination is

effectively targeting leukemia-initiating cells (Schenk *et al.*, 2012). Additionally, inhibiting LSD1, when combined with ATRA, induces apoptosis in 55% of TEX cells (cells derived from primitive human cord blood that resemble primary AML). This indicates that the combination of ATRA with LSD1 inhibitors may be an effective anti-leukemic approach (Schenk *et al.*, 2012). Furthermore in (non-)APL AML we have also demonstrated that inhibiting LSD1 makes AML cells more sensitive to low concentrations of retinoic acid (RA), impacting cell viability and myeloid differentiation phenotype. This increased sensitivity occurs without affecting the stability of the PML-RARα oncogene, a fusion protein that is characteristic of APL. Our research indicates that LSD1's non-enzymatic functions are key to preventing differentiation, and that using LSD1 inhibitors along with RA triggers a differentiation gene expression pattern that doesn't rely solely on alterations in histone H3K4 methylation (Ravasio *et al.*, 2020). Furthermore, our work demonstrates that LSD1 inhibition allows AML cell differentiation without affecting the oncogenic function of PML-RARα. LSD1 and PML-RARα share most of their binding sites, but LSD1 is not recruited by PML-RARα. The combined treatment with LSD1 inhibitors and low doses of RA allows differentiation and growth arrest of AML cells without affecting PML-RARα stability and its recruitment on chromatin (Ravasio *et al.*, 2020). Additionally, the study explored the genome-wide distribution of LSD1 and how it influences chromatin structure. LSD1 tends to attach to regulatory regions of genes linked to hematopoiesis and cellular differentiation. Inhibition of LSD1, especially in combination with low doses of RA, results in significant reorganization of chromatin, including the activation of new SEs. However, the observed increase in H3K4me2 at LSD1-bound regulatory sites does not necessarily correlate with active gene transcription (Ravasio *et al.*, 2020).

LSD1 inhibitors in AML, have shown promise in clinical trials, with compounds such as TCP, ORY-1001, GSK2879552, and IMG-7289 being particularly noteworthy. These inhibitors not

only serve as scaffolds for designing new LSD1 inhibitors but also offer potential in combination therapies for AML (Fang, Liao and Yu, 2019; Zhang *et al.*, 2021). In the context of AML, LSD1 inhibitors have been shown to block the interaction between LSD1 and chromatin transcription factors like GFI1b. This inhibition prevents GFI1-mediated suppression of SPI1 (PU.1) target genes, thereby inducing AML differentiation. Moreover, pharmacological inhibition of LSD1 has led to the complete elimination of tumor growth in AML xenograft models containing runx1-runx1t1 translocations. The development of novel LSD1 inhibitors, especially those based on TCP derivatives, is actively underway, and these compounds are entering clinical trials with promising prospects for AML treatment (Zhang *et al.*, 2021). In general, the main classes of LSD1 inhibitors can be classified as ***TCPs***, ***polyamine-based Inhibitors***, ***natural compounds***, and ***peptidic inhibitors*** (Table 4) (Fang, Liao and Yu, 2019). **TCPs** are irreversible inhibitors of LSD1 through formation of a covalent adduct with FAD. The examples include ORY-1001, GSK690 and more, which many have been proceeded to clinical trials as single or in combinatorial treatment regimens (please refer to Table 4) (Zheng, Yu, *et al.*, 2016; Pandey and Wang, 2019; Dai *et al.*, 2020; Sacilotto *et al.*, 2021). Pharmaceutical and research groups have been working on increasing the specificity of TCPs over the years as this is the main property of drugs potential for translation to a clinical intervention. This has resulted in development of various TCPs with higher efficacy and less off-target effects, such as GSK2879552 (Schober *et al.*, 2019). **Polyamine-based inhibitors** act through interfering with the substrate binding motif of LSD1, hence benefiting from a higher specificity. They have not yet emerged into clinical trials as common as TCPs despite their positive experimental outcomes. The examples include SP-2509, and NCL-1 (Table 4) (Huang *et al.*, 2007, 2009; Przespolewski and Wang, 2016). Various **natural compounds** have also shown competitive inhibition potential towards LSD1. The examples include Sinefungin and Baicalin, and some have already

proceeded to pre-clinical evaluations (Table 4) (Gauthier *et al.*, 2012; Zheng, Shen, *et al.*, 2016; Fang *et al.*, 2021). Lastly are **peptidic inhibitors** of LSD1, which are basically structural mimetics of histone and are still under evaluation for their potential therapeutic advantages (Fu, Li and Yu, 2021).

Therapeutic targeting of LSD1 can be challenging at translational level. LSD1 deficiency has been associated with a severe increase in immune response and expansion of a harmful subpopulation of HSCs, particularly when administered in hematological malignancies. A study by Wang et al. revealed that a lack of LSD1 can lead to a condition resembling septic shock, marked by a dramatic rise in a morbid group of myeloid progenitors in the bone marrow (BM). These cells are characterized by their increased proliferation and inflammatory responses. This abnormal expansion correlated with a spike in cytokine levels, known as a "cytokine storm," can potentially lead to sudden mortality (Wang *et al.*, 2018).

Name of Inhibitor	Type of Inhibitor	IC50	Cancers Tested On	Alternate Names	Clinical Trial Phase	Solubility in Water
Tranylcypromine	TCP	2 µM	Various	Parnate	Phase 2	Moderate
RN-1	TCP	70 nM	Various	N/A	Preclinical	Moderate
Pargyline	TCP	5 µM	Various	N/A	Preclinical	Moderate
Phenelzine	TCP	N/A	N/A	Nardil	Unknown	Unknown
GSK-LSD1	TCP	2 nM	AML	N/A	Phase 1	Good
ORY-1001	TCP	18 nM	AML, SCLC	RG6016	Phase 2	Good
GSK2879552	TCP	1.7 nM	SCLC	N/A	Phase 1	Good
INCB059872	TCP	0.02 µM	Various	N/A	Phase 2	Good
MC2580	TCP	0.129 µM	Various	14e	Unknown	Unknown
DDP-38003	TCP	0.084 µM	Various	N/A	Preclinical	Good
Namoline	Polyamine-Based Inhibitor	31 nM	Various	N/A	Preclinical	Good
SP-2509	Polyamine-Based Inhibitor	13 nM	Various	N/A	Preclinical	Moderate
OG-L002	Polyamine-Based Inhibitor	20 nM	Various	N/A	Preclinical	Moderate
S2101	Polyamine-Based Inhibitor	0.2 µM	Various	N/A	Preclinical	Moderate
HCI2509	Polyamine-Based Inhibitor	13 nM	Various	N/A	Preclinical	Moderate
T-3775440	Polyamine-Based Inhibitor	2.5 nM	Various	N/A	Preclinical	Good
Seclidemstat	Polyamine-Based Inhibitor	6.6 nM	Ewing Sarcoma	N/A	Phase 1	Good

NCL-1	Natural Compound	49 nM	Leukemia	N/A	Preclinical	Poor
Curcumin	Natural Compound	3 µM	Various	N/A	Preclinical	Poor
Sinefungin	Natural Compound	N/A	N/A	N/A	Unknown	Unknown
Baicalin	Natural Compound	N/A	N/A	N/A	Unknown	Unknown
Resveratrol	Natural Compound	N/A	N/A	N/A	Unknown	Unknown
Geranylgeranoic Acid	Natural Compound	N/A	N/A	N/A	Unknown	Unknown

Table 4. ***LSD1 inhibitors with potential therapeutic advantages****. Name of Inhibitor: This column lists the names of the LSD1 inhibitors. Type of Inhibitor: This column categorizes the inhibitors based on their chemical structure or mechanism of action. TCP refers to Tranylcypromine-based inhibitors, Polyamine-Based Inhibitors are derived from polyamine structures, and Natural Compounds are naturally occurring substances with LSD1 inhibitory activity. Protein-protein interaction inhibitors disrupt LSD1's interaction with other proteins. IC50: This column provides the half-maximal inhibitory concentration (IC50) values for each inhibitor, indicating the concentration at which the compound inhibits 50% of the enzyme's activity. The unit is generally in nM (nanomolar) or µM (micromolar). Cancers Tested On: This column lists the types of cancer on which the inhibitor has been tested, either in preclinical models or clinical trials. Alternate Names: This column provides any alternate names or identifiers for the inhibitors. Clinical Trial Phase: This column indicates the current phase of clinical trials for each inhibitor, if applicable. Phases range from preclinical studies to Phase 1, 2, or 3 clinical trials. Solubility in Water: This column provides information on the solubility of each inhibitor in water, categorized as "Good," "Moderate," or "Poor." Data extracted from Wishart* et al.*, 2018; Fang, Liao and Yu, 2019; Ravasio* et al.*, 2020; Fang* et al.*, 2021; Fu, Li and Yu, 2021; Nicosia* et al.*, 2022; Noce* et al.*, 2023.*

2. Cell Cycle

Growth and **reproduction** are the two fundamental aspects defining what can be considered a living entity (Hoffman and Rosenkrantz, 1998). Eukaryotic cell perfected the biological pattern to grow, multiply, form an organism, and eventually bring an offspring to life. **The biological framework that controls the process of cellular growth and metabolism, correct replication of the DNA, balanced chromosomal segregation, and cell division is defined as the cell cycle** (Hochegger, Takeda and Hunt, 2008; Matthews, Bertoli and de Bruin, 2022). This framework is divided into two main stages, the ***interphase,*** and cell ***division***. **Interphase** is the period when the cell is growing, replicating its DNA and organelles, and gets ready for an upcoming division. Interphase itself is divided into three stages known as **G1** for cell growth and nutrient production, **S** for replication of the DNA, **G2** for further growth and protein synthesis. **Division** which can be mitotic (somatic cells) or meiotic (germ cells) is where the mother cell equally distributes its genetic material between two or four daughter cells, respectively (Hochegger, Takeda and Hunt, 2008). The process of **mitosis** (**M** phase) is also partitioned into **prophase** for chromosome condensation and nuclear envelope disassembly, **metaphase** for chromosome alignment and spindle apparatus assembly, **anaphase** for sister chromatids segregation, **telophase** for nuclear envelope reformation and chromosomal decondensation, and **cytokinesis** for cytoplasmic division. **Meiosis**, which exclusively takes place in germ cells, can be simplified as a two-step mitosis, giving birth to genetically shuffled and haploid sperms or eggs (Hochegger, Takeda and Hunt, 2008; Matthews, Bertoli and de Bruin, 2022). However, not all cells are obliged to follow this framework. In particular conditions and settings, a cell can exit the cell cycle and enter a ***quiescent*** or a ***senescent*** state (Imai *et al.*, 2014). **Quiescence** is a reversible state of cell cycle quitting, also referred to as the **G0** phase. Once quiescent,

a cell keeps its metabolic machinery on and poised to restart the cell cycle (Zou *et al.*, 2011; Terzi, Izmirli and Gogebakan, 2016). **Senescence**, on the other hand, is an irreversible state of cell cycle quitting, in which the cell is also metabolically active, but unable to re-enter the cell cycle (Terzi, Izmirli and Gogebakan, 2016; Stallaert *et al.*, 2022).

2.1. Cell cycle regulation in health and cancer

Cells regulate their cell cycle progression employing a range of molecular tools, including protein complexes, TFs and most importantly ***cyclins*** and ***cyclin-dependent kinases*** (***CDKs***), in a precisely scheduled fashion. In mammals particularly, a precise and complex cell cycle regulation is essential for tissue homeostasis, fate decision making and preventing pathological conditions such as cancer (Pauklin and Vallier, 2013; Matthews, Bertoli and de Bruin, 2022). The basic framework of the cell cycle is defined by consecutive four main phases of G1-S-G2-M, and checkpoints controlling the transition from one to the next (Figure 6) (Hochegger, Takeda and Hunt, 2008; Wagener, Stocking and Müller, 2017; Matthews, Bertoli and de Bruin, 2022). Cyclins and CDKs serve as key regulators in controlling the cell cycle progression, with each having a specific role in different phases. **Cyclins**, whose levels oscillate throughout the cell cycle (Figure 7), act as activators of **CDKs**, which are serine/threonine kinases. For example, Cyclin D collaborates with CDK4 and CDK6 (CDK4/6) during the G1 phase, and Cyclin B works with CDK1 during mitosis. The activity of CDKs is further fine-tuned by phosphorylation and interactions with CDK inhibitors such as p21 and p27. When cyclins bind to CDKs, they induce a structural change that activates the kinase's catalytic function, allowing it to phosphorylate various substrates. This interaction is crucial for the operation of cell cycle checkpoints. Disruptions in this regulatory network are commonly associated with tumorigenesis (Hochegger, Takeda and Hunt, 2008;

Malumbres, 2014; Wagener, Stocking and Müller, 2017; Matthews, Bertoli and de Bruin, 2022).

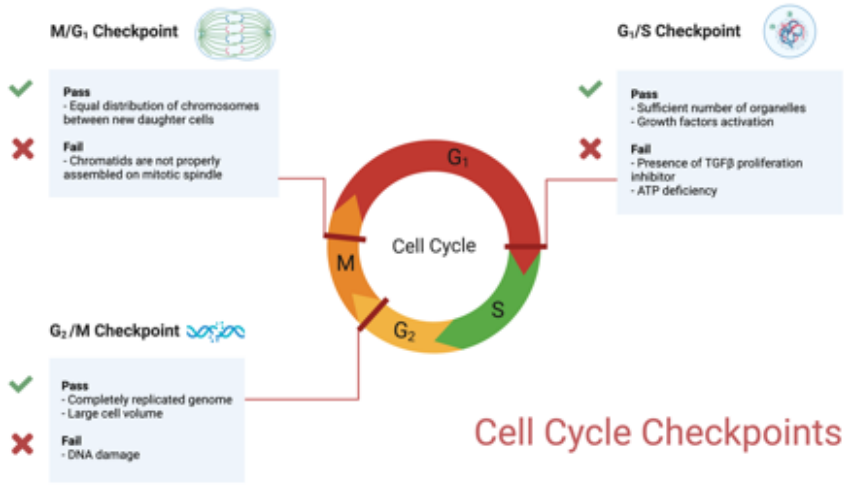

Figure 6. ***Cell cycle checkpoint****. The main three checkpoints of a normal cell cycle are presented. Requirements to pass or to fail each checkpoint are mentioned in brief. Figure adapted from "Cell Cycle Checkpoints Callout", by BioRender.com (2023). Retrieved from https://app.biorender.com/biorender-templates and modified from Hochegger, Takeda and Hunt, 2008; Wagener, Stocking and Müller, 2017. Figure created with Biorender.com.*

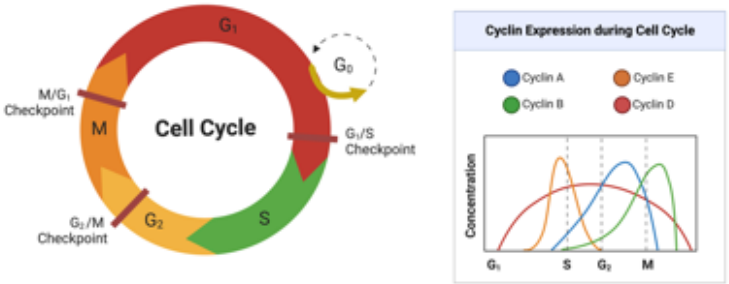

Figure 7. ***Oscillation of cyclins throughout the cell cycle****. Figure adapted from "Cyclins: Cell Cycle Regulators", by BioRender.com (2023). Retrieved from https://app.biorender.com/biorender-templates and modified from Hochegger, Takeda and Hunt, 2008; Wagener, Stocking and Müller, 2017. Figure created with Biorender.com.*

G1 phase is where a newly born cell prepares for entry to the S phase, and ultimately decides its fate. Various groups have challenged the classic understanding of G1 to S phase progression, during the past years. There is a mutual agreement around the involvement of ***CDK4/6-cyclin D***, ***CDK2-cyclin E***, ***p21*** and ***p27***, ***Rb***, and ***E2F*** TFs directing this process (Narasimha *et al.*, 2014; Chung *et al.*, 2019; Rubin, Sage and Skotheim, 2020). It is evident that for a cell to pass from the G1 to S phase, **Rb needs to be hyperphosphorylated** and hence **release a subset of E2F TFs**, possibly causing a transcriptional switch, leading to the **expression of the cyclin and DNA replication licensing genes**, that will in turn **allow the transition**. Hyperphosphorylation of Rb relies on the activities of **CDK4/6-cyclin D** and **CDK2-cyclin E** complexes. It is still unclear if the activities of the two complexes on the Rb are in reality a linear process where CDK4/6s' activities are pre-requirements for CDK2's function as stated by the classic model; a parallel of serial events where CDK4/6 also regulate CDK2 activities simultaneously through p21 and p27; or a linear process where CDK2's role is simply maintaining the kinase activities of CDK4/6 throughout the S phase. All three possible models are summarized in Figure 8 (Hu *et al.*, 2018; Rubin, Sage and Skotheim, 2020).

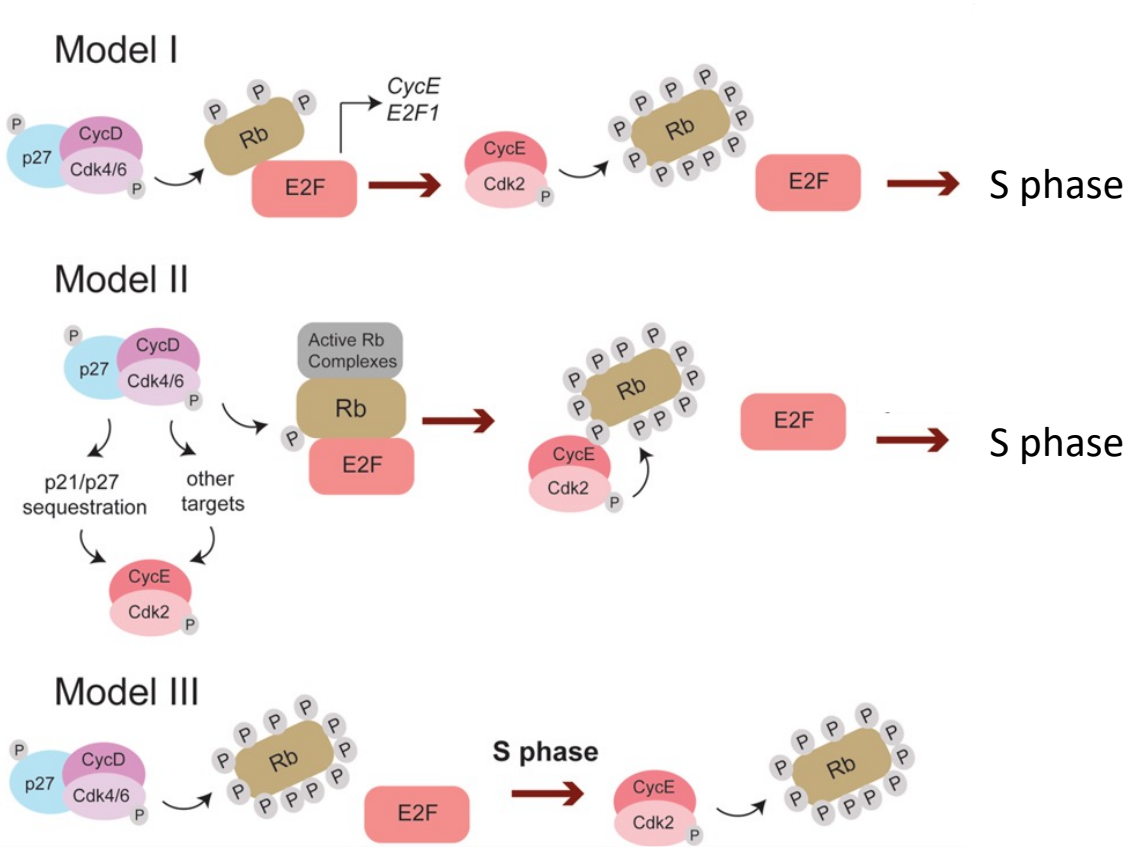

Figure 8. ***G1 to S transition suggested models****. In the first model, CDK4/6 partially phosphorylates Rb, activating E2F and triggering the transcription of genes like cyclin E. This, in turn, fully activates CDK2, which then hyperphosphorylates Rb, allowing the cell to enter the S phase. In the second model, CDK4/6 monophosphorylates Rb, creating different active Rb forms that suppress E2F and aid in forming protein complexes during G1. CDK4/6 also activates CDK2 through processes such as p21/p27 sequestration, leading to CDK2 hyperphosphorylation of Rb, which deactivates it and prompts the transition to the S phase. The third model has CDK4/6 solely responsible for Rb hyperphosphorylation during G1, deactivating Rb and initiating the S phase. Here, CDK2's role is to maintain the hyperphosphorylation of Rb throughout the S phase. Figure and legend adapted from Rubin, Sage and Skotheim, 2020.*

Nevertheless, it is clear that the G1 to S transition relies on CDK4/6 and CDK2 activities, in a way that most possibly CDK4/6 commences and CDK2 joins the process subsequently (Rubin, Sage and Skotheim, 2020). Mammalian cells have gained the ability to control CDK4/6 and CDK2 activities using a **complex network of inhibitors and activators**, each in response to various internal and environmental factors (Figure 9) (Donjerkovic and Scott, 2000; Pelengaris and Khan, 2013; Hume, Dianov and Ramadan, 2020). ***Mitogens*** such as

epidermal, fibroblast, and insulin growth factors (**EGF**, **FGF**, and **IGF**) activate pathways that upregulate cyclin D, thereby activating CDK4/6 complexes. Concurrently, CDK2 complexes are regulated by cyclin E, whose expression is influenced by **E2F** TFs. These CDK complexes are also subject to inhibition by an array of molecules. **$p21^{Cip1}$**, **$p27^{Kip1}$**, and **$p57^{Kip2}$** serve as universal inhibitors, with their expression often being upregulated by **p53** in response to **DNA damage**. Specificity towards CDK4/6 is exhibited by **$p16^{INK4a}$** and **$p15^{INK4b}$**. The role of p53 is further modulated by its regulation through **MDM2**, an E3 ubiquitin ligase, and by phosphorylation via Ataxia-Telangiectasia mutated (**ATM**) and ATM- and Rad3-related (**ATR**) in response to DNA damage, which also activates **CHK2**. Moreover, **$p19^{ARF}$**, a component of the ARF-MDM2-p53 pathway, stabilizes p53 by inhibiting MDM2. **APC^{CDH1}** targets cyclins for degradation, adding another layer of control. **GSK3β** modulates cyclin D stability, while **$CUL4^{DDB1}$** ubiquitin ligase complex targets CDK inhibitors like p21 for degradation. **SMAD3/4**, often activated by **TGF-β** signaling, can induce p21 and p15, thereby inhibiting CDK4/6 and CDK2. Furthermore, Rb mediated recruitment of epigenetic regulators such as **class I HDACs** and **SWI/SNF** complex at the promoters of E2F target genes is speculated (simple scheme in Figure 9) (Donjerkovic and Scott, 2000; Harbour and Dean, 2000; Pelengaris and Khan, 2013; Hume, Dianov and Ramadan, 2020). Eventually, the balance between mitogens and cell cycle inhibitors would decide for the cell to whether stay longer in the G1 phase or proceed immediately to the S phase, or exit the cell cycle and become a senescent or quiescent cell, or even activate apoptosis (Hume, Dianov and Ramadan, 2020; Rubin, Sage and Skotheim, 2020). The ***longer time a cell spends in the G1 phase***, the better chances it has to **accumulate lineage-specific TFs**, **shape a particular epigenetic landscape** through regulating its epigenetic modifiers, subsequently activate or poise those TFs through the newly acquired epigenetic landscape, **repair possible genetic lesions**, and **switch its metabolic programing**, hence **determining its fate towards differentiation**

(Lange and Calegari, 2010; Pauklin and Vallier, 2013; Singh *et al.*, 2013, 2015; Ahuja *et al.*, 2016; Michowski *et al.*, 2020). The elongation of the G1 phase significantly influences the transcriptional variability within human PSC populations. This prolonged G1 phase leads to increased expression of key developmental genes, contributing to the variability in gene expression in human ESCs. Furthermore, changes in global levels of 5-hmC have been linked to the cell cycle, with specific peaks observed in late G1. This cell-cycle-based regulation of development-related TFs appears to continue through lineage specification. These discoveries provide insights into the underlying causes of transcriptional variability in human ESCs and offer a theoretical framework for "lineage priming," especially during the extended G1 phase (Singh *et al.*, 2013). In another study, Michowski and colleagues presented a comprehensive role for Cdk1 in the orchestration of the epigenetic landscape in ESCs. Interestingly, Cdk1 was found to phosphorylate a broad spectrum of epigenetic regulators, including writers and erasers of major hPTMs. The high activity of Cdk1 in ESCs, as mentioned, implies a potential role in cell cycle regulation, which could indirectly influence epigenetic modifications during the G1 phase. These findings collectively suggested that Cdk1 is instrumental in maintaining the epigenetic identity of ESCs (Michowski *et al.*, 2020). Moreover, in mouse ESCs when the G1 to S phase transition in ESCs is delayed, there is a noticeable reduction in replication stress markers, suggesting that the the G1 length, is a key factor in regulating the replication stress (Ahuja *et al.*, 2016). Conclusively it has been established that the length of the G1 phase in the cell cycle is intimately connected to the differentiation of stem cells. Specifically, a lengthening of the G1 phase was found to be a precursor of differentiation. This lengthening allows for the accumulation of factors necessary for differentiation, while a short G1 phase maintains self-renewal and pluripotency. Cdks and cyclins were identified as the core molecular machinery governing this process. For instance, pharmacological inhibition of Cdk2 was shown to

lengthen the G1 phase and induce differentiation in embryonic stem cells. Similarly, deletion of cyclin D2 led to a 30% increase in G1 length in neural stem cells, resulting in premature neurogenesis. **These findings highlight the fundamental role of G1 length, regulated by Cdk/cyclin complexes, in stem cell differentiation and potentially in tissue homeostasis and repair** (Lange and Calegari, 2010). In cells different from stem cells, however, the role of G1 length has not been widely studied.

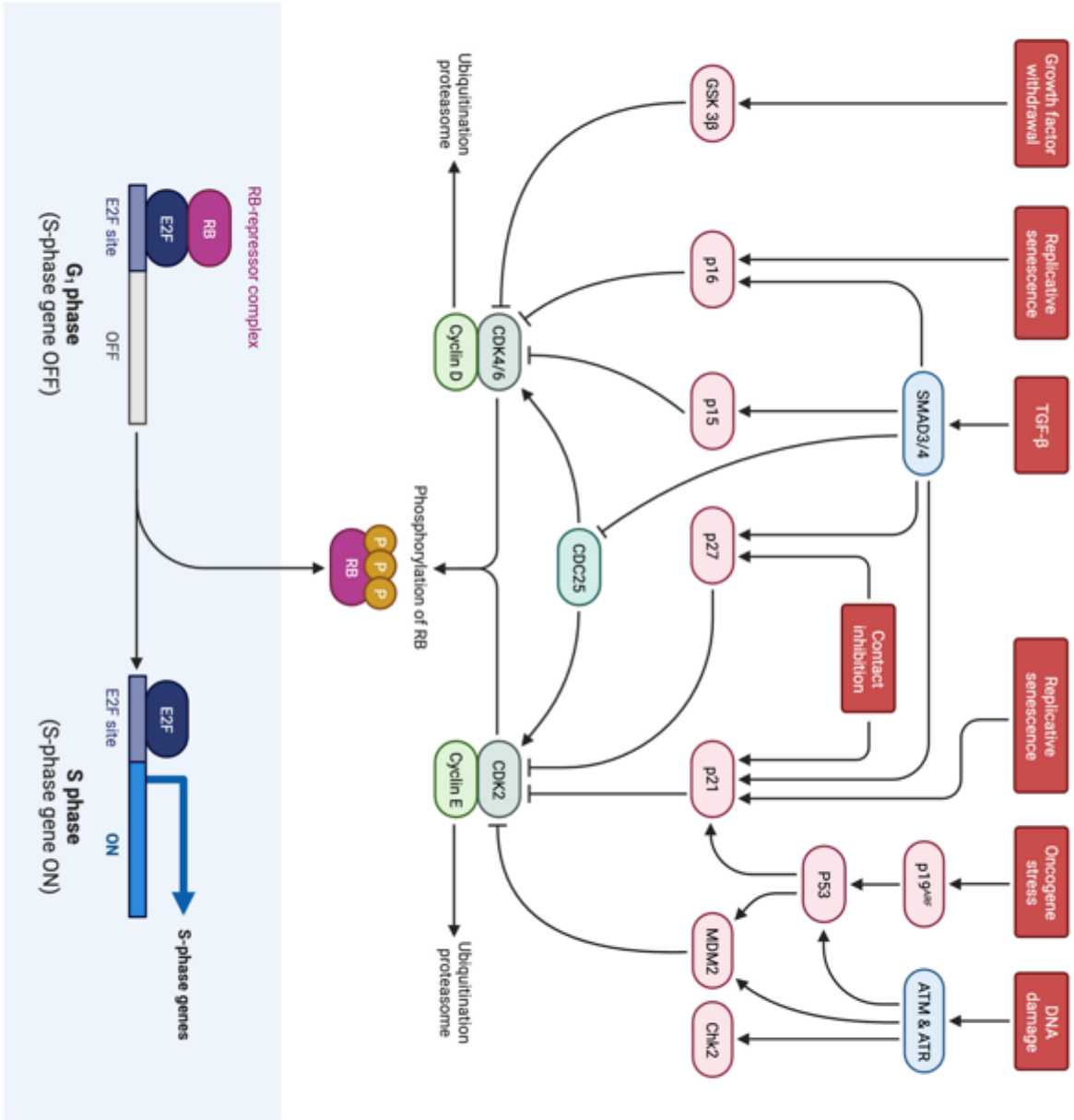

Figure 9. ***G1 to S molecular regulatory network****. Figure adapted from "G1/S Checkpoint", by BioRender.com (2023). Retrieved from https://app.biorender.com/biorender-templates and modified from Donjerkovic and Scott, 2000; Hume, Dianov and Ramadan, 2020; Pelengaris and Khan, 2013. Figure created with Biorender.com.*

S and G2 phases are the two phases were a cell replicates its genetic material and confirm its integrity before proceeding to mitosis. Hence, the activity of the machineries watching over the genome integrity, like ***ATM*** and ***ATR*** are crucial for progression through these two phases to cell division (Ronco *et al.*, 2017). The activity of **CDK2-cyclin E** complex reaches its peak upon S phase entry and through the S phase, **cyclin A** would substitute cyclin E as it is required for DNA replication (Figure 7). The final checkpoint before entering mitosis is permitted through the activation of **CDK1** by **cyclin B** at the end of the G2 phase (Figure 8). CDK1 however is kept inactive through kinase activities of **WEE1** and **MYT1**. This can be opposed by the phosphatase function of **CDC25**. WEE1, MYT1 and CDC25 functions are affected by ATM and ATR. Other regulators of DNA replication and cell cycle progression such as proliferating cell nuclear antigen (PCNA), p53, and p21 are in a real-time crosstalk with each other as well as with ATM and ATR (Figure 10). **This whole process is employed to ensure the genome integrity before initiation of mitosis** (Figure 11) (Hustedt and Durocher, 2017; Ronco *et al.*, 2017). Interestingly, the classic understanding of cell cycle regulation that the commitment to cell division is irreversible at the restriction point (where a cell is committed to proliferation independent of mitogens), has been recently challenged as it has been demonstrated that such decision is subject to a temporal competition between mitosis and cell cycle exit (Cornwell *et al.*, 2023). This process is orchestrated by CDK2-cyclin A activity, which relies on CDK4/6 signaling during the cell cycle progression. It was revealed that cells can exit the cell cycle even in S/G2 phases if mitogen signaling is lost, thereby challenging the long-standing belief that cells are committed to mitosis post-restriction point. The same study also disproves the idea that CDK2 activity is self-sustaining, showing that all cells contain a cell cycle exit clock and cannot sustain CDK2 activity without CDK4/6 signaling (Cornwell *et al.*, 2023).

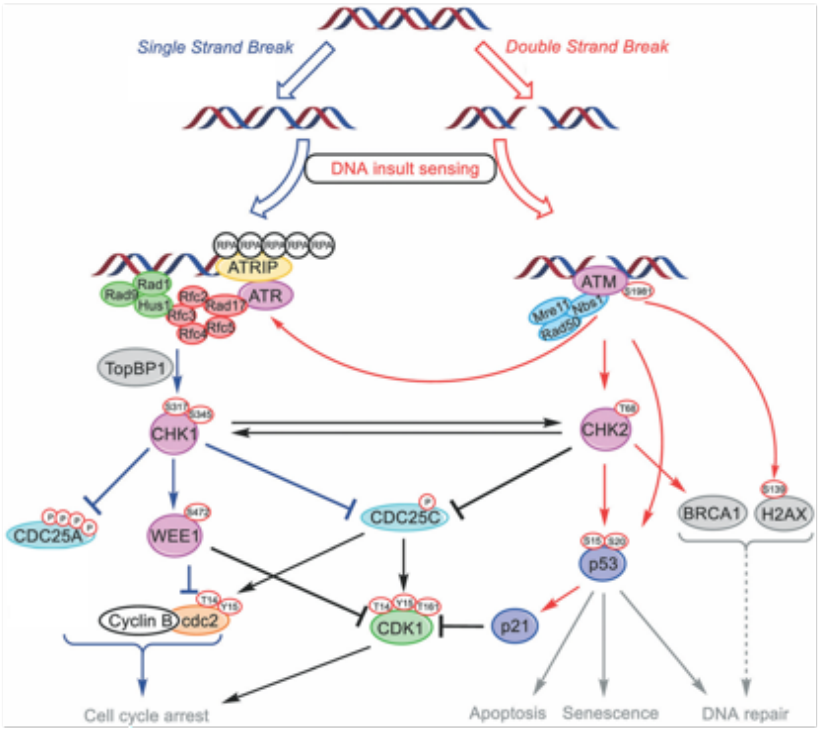

Figure 10. ***ATM and ATR ensure correct DNA replication in S and G2 phase****. Figure and legend adapted from Ronco et al., 2017.*

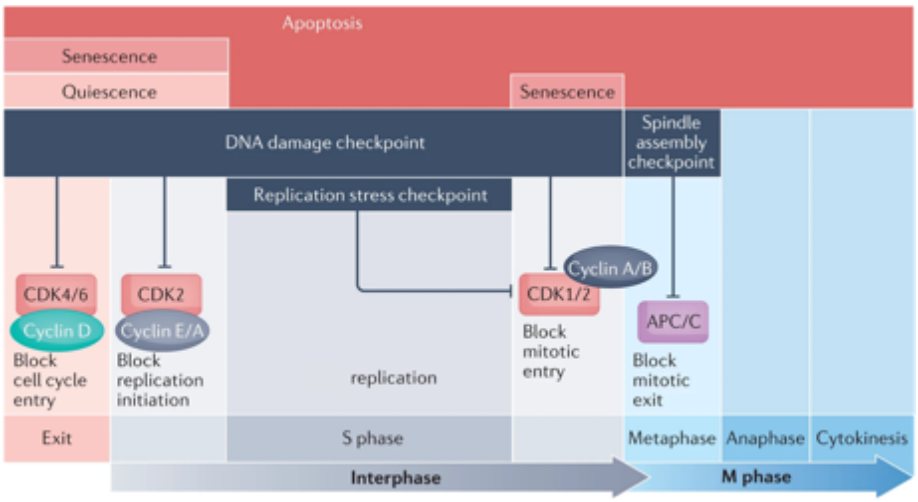

Figure 11. ***Monitoring genome integrity throughout cell cycle****. Checkpoints that monitor replication stress stop cells from entering mitosis during the S phase by inhibiting CDK1/2-cyclin A/B activity. The spindle assembly checkpoint, active during the M phase, can prevent cells from exiting mitosis by blocking APC/C activation. The DNA damage checkpoint operates throughout interphase, affecting the cell cycle in various ways depending on the phase. For example, the DNA damage checkpoint can stop cells from entering mitosis during and after the S phase by reducing CDK2-cyclin E/A activity. It can also delay the cell cycle after mitosis or at late G1 by lowering CDK4/6-cyclin D activity, leading to a temporary pause known as quiescence. If DNA damage is severe, this checkpoint can permanently halt the cell cycle, causing cells to undergo senescence or die through apoptosis. Figure and legend adapted from Matthews, Bertoli and de Bruin, 2022.*

Mitosis is where a mother cell is divided into two daughter cells, each carrying an identical diploid genetic material to their sister cell. Once a specific level of **CDK1** activity is reached, cells perform a series of phosphorylation activities on several CDK1 targets, which in turn initiates the mitosis. In *prophase*, heightened CDK1 activity in the cytoplasm causes the cell to round up and initiates centrosome division. The translocation of CDK1 into the nucleus leads to the activation of the anaphase-promoting complex/cyclosome (**APC/C**), chromosome condensation, and disassembly of the nucleolus. These structural changes set the stage for the formation of the mitotic spindle. As cells progress to *metaphase*, the alignment of chromosomes is strictly monitored by the spindle assembly checkpoint (**SAC**). This quality control mechanism delays the start of *anaphase* and ensures proper chromosome separation by inhibiting the APC/C^{CDC20} complex until all **kinetochores** are correctly attached. Extended activation of the SAC can cause the cell to be stuck in mitosis, potentially leading to cell death or an abnormal exit from mitosis, often triggering additional cellular responses such as **p53** activation (Figure 11). Finally, the process of *exiting mitosis* is managed by the APC/C^{CDC20} complex, which marks cyclins for destruction. This action facilitates a series of events that result in the *division of the cell* through an actomyosin contractile ring. Concurrently, protein phosphatases undo the phosphorylation actions of CDK1, effectively resetting the cell cycle in the newly formed daughter cells (Matthews, Bertoli and de Bruin, 2022).

Cell cycle in cancer is classically defined as uncontrolled proliferation of a cell in which TSGs are dysfunctional and oncogenes are active (Carnero, 2002; Williams and Stoeber, 2012). Even though this is correct, it will be more accurate to **define the tumorigenesis process as the state of inability of cancer cells to exit the cell cycle**. This is especially obvious when looking at CDKs, which are frequently overactive in cancer cells. Increased CDK activity not only pushes the cell cycle forward but also inhibits the APC/C, a crucial ubiquitin ligase

complex for exiting mitosis (Figure 11). The persistent growth signaling in cancer is mainly a result of mutations that inhibit apoptosis and disrupt the normal exit from the cell cycle. These mutations are commonly found in pathways that either push the cell toward S phase entry or initiate the process of cell cycle termination. Interestingly, mutations that obstruct entry into or exit from mitosis are relatively rare, indicating that particular cell cycle checkpoints are still operational in cancer cells. **This situation makes cancer cells particularly dependent on certain cell cycle regulatory mechanisms, making them susceptible to targeted therapeutic interventions** (Figures 12 and 13) (Matthews, Bertoli and de Bruin, 2022; Bansal, Pandey and Ruwali, 2023).

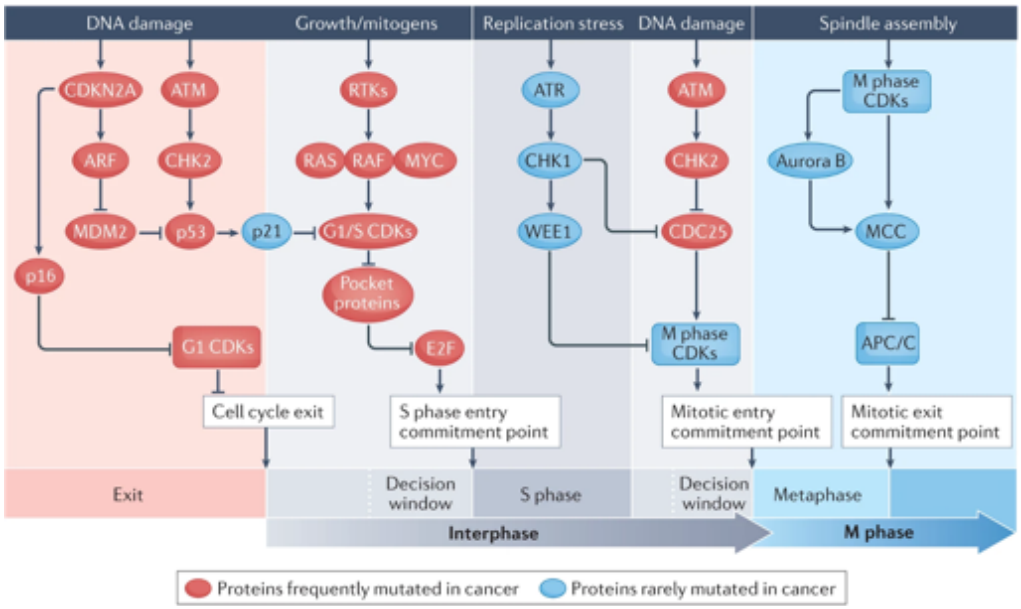

Figure 12. ***Abundant vs non-abundant mutations in cell cycle regulatory proteins****. Cancer cells often maintain continuous cell cycle progression due to mutations or disruptions in cell cycle control proteins. These mutations, primarily affecting late G1, are usually linked to DNA damage responses and growth signals, leading to S phase entry and preventing cell cycle exit. Such mutations, highlighted in red, are common in cancer cells. Conversely, mutations affecting responses to replication stress or incomplete spindle assembly, shown in blue, are rare in cancer. Key regulators of the cell cycle include pocket proteins like RB, p107, and p130, along with activating E2Fs (E2F1–E2F3). The G1/S CDKs consist of CDK4/6-cyclin D and CDK2-cyclin E, while the M phase CDKs are CDK1/2-cyclin A/B. Other notable components include the APC/C, ATM, ATR, and the mitotic checkpoint complex (MCC), which comprises BUB3 with MAD2 and MAD3 bound to CDC20. Receptor tyrosine kinases are also involved in these pathways. Figure and legend adapted from Matthews, Bertoli and de Bruin, 2022.*

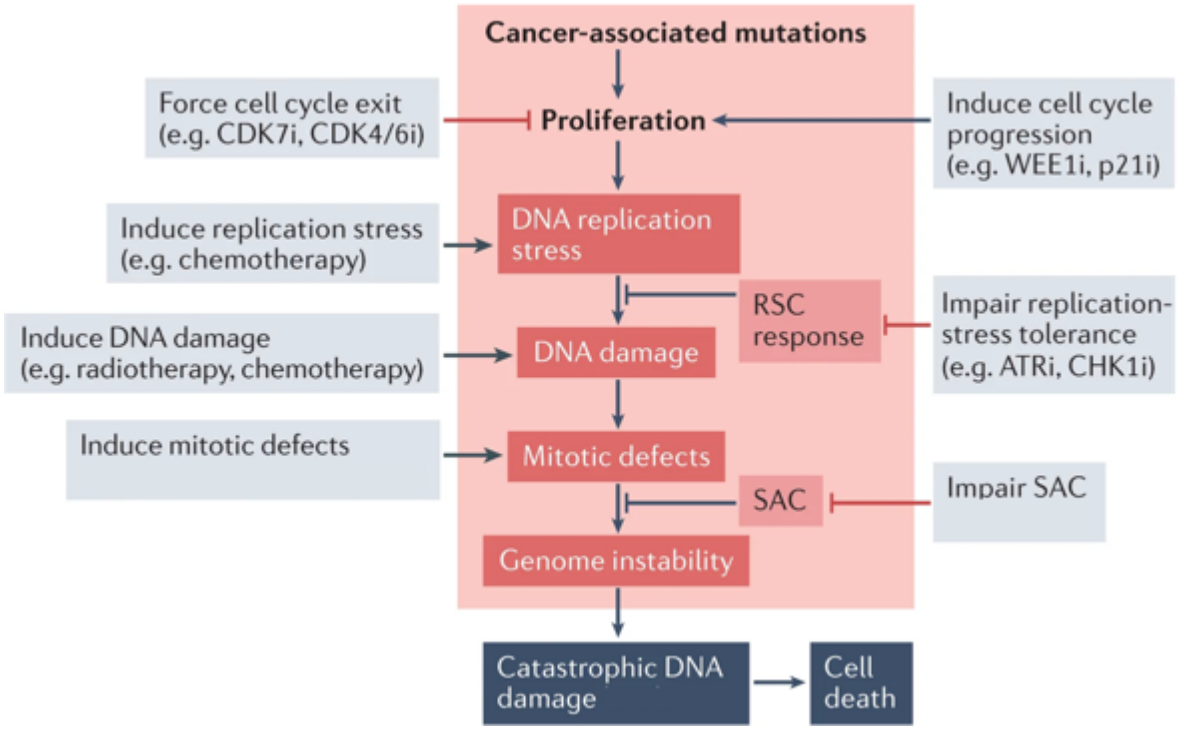

Figure 13. ***The persistent growth of cancer cells offers multiple avenues for therapeutic intervention****. Cancer is driven by DNA mutations that allow cells to divide uncontrollably. This means all cancers rely on continuous cell division, but also on cell cycle checkpoints to avoid severe genomic instability and cell death. The mutations that support ongoing cell growth, along with the mechanisms that reduce genomic instability, are crucial in cancer development. Understanding the balance between unchecked cell growth and the cellular mechanisms that prevent chaos is key to creating effective therapies. Cancer treatments aim to disrupt this balance by targeting cell cycle regulators and components involved in replication stress and spindle assembly checkpoints. These approaches use inhibitors to block the pathways that cancer cells rely on, offering potential strategies for combating cancer's progression. Figure and legend adapted from Matthews, Bertoli and de Bruin, 2022.*

In the **G1 phase**, CDK activity levels is a tool for the cell to decide on DNA replication vs cell cycle exit or G1 extension. This decision-making juncture is frequently impaired in cancer cells. The Rb is often either mutated or non-functional in a range of cancers. Furthermore, mutations in oncogenes or TSGs, linked to E2F TF transcriptional activity is highly frequent in tumor cells. When Rb is inactivated or E2F secondary regulators are dysfunctional, it results in unrestrained E2F TF activity, which in turn contributes to the unregulated progression of the cell cycle, a hallmark of cancer (Matthews, Bertoli and de Bruin, 2022).

Moreover, regulating DNA replication in the **S phase** is crucial for avoiding re-initiation at origins where replication has already taken place. In cancer cells, this regulatory mechanism frequently breaks down, resulting in re-replication and losing genomic instability. CDK activity serves two functions in this context: it authorizes the origins for replication and triggers the replication process from these licensed points. Any disruption in this phase, as **oncogene-induced replication stress** can add to the cancer-forming capabilities of the cells, illustrating the relationship between various cell cycle regulatory systems in cancer. In such a situation, it is vital for the cancer cell not to exceed the tumorigenic chromosomal instability (CIN), and reach a catastrophically lethal level of DNA damage. To prevent this, a cancer cell usually relies on **replication stress checkpoints** and **SAC**, which the components are usually found overexpressed in various cancers (Figures 12 and 13) (Matthews, Bertoli and de Bruin, 2022). The **G2 phase** following replication serves as an additional critical juncture, which is frequently disrupted in cancer. Once again, CDK activity is pivotal in this decision-making stage, dictating whether the cell should advance to mitosis or go through DNA repair. In cancer cells, faulty CDK activity may push the cell into premature mitosis, often skipping essential DDR mechanisms. Such actions can lead to further genomic instability, a characteristic frequently linked with cancerous conditions (Matthews, Bertoli and de Bruin, 2022). The idea of targeting cell cycle regulatory pathways in cancer carries therapeutic significance. The prevailing notion is that cancer cells are highly dependent on the remaining functional cell cycle control mechanisms to prevent severe genomic instability (Matthews, Bertoli and de Bruin, 2022). Hence, one possibility would be to **push them towards cell cycle arrest or exit**. For this purpose, CDK inhibitors, especially CDK4/6 inhibitors such as Palbociclib, Ribociclib, and Abemaciclib, have demonstrated noteworthy clinical advantages. These inhibitors are believed to compel cancer cells to leave the cell cycle, resulting in outcomes like senescence, apoptosis, quiescence, gain of sensitivity to

secondary treatments, or even differentiation depending on the specific type of cancer (Table 5) (Beaver *et al.*, 2015; Goel *et al.*, 2018). CDK7 inhibitors are also in use, given their ability to target key cell cycle-associated CDKs while being well-tolerated in normal cells (Table 5) (Sava *et al.*, 2020). A second approach would be perturbing the activity of CDK inhibitors, such as WEE1 and p21, based on the idea to **push the cancer cells with unrepaired genetic lesions towards further uncontrolled mitosis** until they reach a catastrophic level of DNA damage. In this context WEE1 inhibitor, Adavosertib, have shown to be particularly advantageous for patients with TP53-mutated, platinum-sensitive ovarian cancer, head and neck SCS, pancreatic cancer, and more (Table 5) (Cuneo *et al.*, 2019; Oza *et al.*, 2020; Chera *et al.*, 2021). Third possibility would be to **disable the replication stress response mechanisms**, which a cancer cell depends on for survival, such as ATR. This strategy would also result in accumulation of DNA damage and eventual death of the cancerous cell (Hall *et al.*, 2014; Daud *et al.*, 2015; King *et al.*, 2015; Matthews, Bertoli and de Bruin, 2022). The fourth possible therapeutic intervention based on cell cycle control in cancer is the **disruption of chromosomal segregation during the M phase**. This can be achieved by directly targeting SAC or perturbing the mitotic spindle performance during the chromosome segregation (Table 5) (Jordan, Thrower and Wilson, 1991; Mortlock *et al.*, 2007; McGrogan *et al.*, 2008; Matthews, Bertoli and de Bruin, 2022).

In conclusion, the dysregulation of the cell cycle in cancer is not simply a matter of uncontrolled proliferation but rather an interplay of failed exit mechanisms and checkpoints accompanied by hyperactivity of replication stress response machineries. Targeting these specific vulnerabilities with CDK inhibitors and other agents has shown promise, but the heterogeneity of cancer cells necessitates a multilayered approach. The future of cancer therapy likely lies in the strategic combination of agents that force cell cycle exit, induce DNA damage, exploit the cancer cell's own dependencies on certain cell cycle control

mechanisms, and affect fate decision making of them. This combinatorial approach could potentially lead to more durable responses and overcome the adaptive resistance often seen in targeted cancer therapies (Goel *et al.*, 2018; Matthews, Bertoli and de Bruin, 2022).

Medication Name	Target Molecule	Clinical Applications	Biological Consequence
Palbociclib	CDK4/6	ER+ and HER2- advanced breast tumors	Inducing Cell Cycle Arrest (G1)
Ribociclib	CDK4/6	ER+ and HER2- advanced breast tumors	Inducing Cell Cycle Arrest (G1)
Abemaciclib	CDK4/6	ER+ and HER2- advanced breast tumors	Inducing Cell Cycle Arrest (G1)
PF-06873600	CDK2/4/6	Breast, Ovarian Cancer	Inducing Cell Cycle Arrest (G1)
Milciclib	CDK2/6, mTOR	Ovarian Cancer	Inhibition of invasion and proliferation (G1)
ICEC0942 (CT7001)	CDK7	Phase I/II for ER+ breast cancer and AML	Inducing Cell Cycle Arrest
Adavosertib (AZD1775)	WEE1	Phase II for various cancers incl. relapsed SCLC and ovarian cancer	Promoting Cell Cycle Progression
VX-970	ATR	Phase II for recurrent ovarian and urothelial carcinoma	Hindering Tolerance to Replication Stress
LY2606368	CHK1	Phase II for various cancers incl. SCLC and BRCA1/BRCA2-mutated cancers	Hindering Tolerance to Replication Stress
MK-8776	CHK1	Phase II for relapsed AML	Hindering Tolerance to Replication Stress
Taxanes	Mitotic Spindle	Broad spectrum of cancers	Triggering Catastrophic Genome Instability
Vinca alkaloids	Mitotic Spindle	Broad spectrum of cancers	Triggering Catastrophic Genome Instability
MPS inhibitors	SAC	Broad spectrum of cancers	Triggering Catastrophic Genome Instability
Aurora B inhibitors	SAC	Phase II for various cancers incl. AML and multiple myeloma	Triggering Catastrophic Genome Instability

Table 5. ***Cell cycle manipulating drugs for oncological settings****. Medication Name: This column lists the names of medications that are designed to interact with the target molecules. These are usually small-molecule inhibitors or other forms of therapeutic agents. Target Molecule: This column identifies the specific molecular target that the medication aims to inhibit or modulate. These targets are usually proteins or enzymes involved in cell cycle regulation or other cellular processes relevant to cancer biology. Clinical Applications: This column describes the clinical settings in which these medications are commonly used. This could range from specific types of cancer to other diseases where cell cycle regulation is implicated. Biological Consequence: This column outlines the expected biological outcomes upon medication administration. This could include forcing the cell to exit the cell cycle, inducing apoptosis, or other relevant cellular responses. Table adapted and data extracted from Freeman-Cook* et al.*, 2021; Matthews, Bertoli and de Bruin, 2022; Lengyel, 2023.*

3. Acute Myeloid Leukemia

A defective hematopoietic system can lead to a spectrum of hematological malignancies, the specific type of which is determined by the initiating genetic alteration and the originating cell type. AML is one of these malignant disorders in which myeloid-lineage hematopoietic differentiation is mainly malfunctional, resulting in the domination of BM by the undifferentiated myeloid blast population and eventual flow of the blasts in the patients' peripheral blood (PB). AML stands out as one of the most medically demanding among these hematological disorders. AML continues to be a significant clinical challenge, accounting for a considerable proportion of leukemia cases in both adults (31%) and children (17%). Its five-year survival rates are alarmingly poor, standing at 27% for adults and 69% for children. The disease's inherent complexity has challenged the effectiveness of existing treatments in achieving lasting disease-free survival. Even with the discovery of new therapeutic interventions, the recurrence of drug-resistant forms of the disease is a common issue. Consequently, induction chemotherapy continues to be the primary treatment strategy for most AML patients, highlighting the urgent need for more effective long-term treatment options (Hayatigolkhatmi *et al.*, manuscript in preparation; Döhner *et al.*, 2010; Papaemmanuil *et al.*, 2016).

Occurrence and co-occurrence of various genetic lesions can initiate the process of AML leukemogenesis. These mutations range from TFs, to regulators of signaling networks, and epigenetic regulators both at molecular and cytogenetic levels. Moreover, additional (non-)mutational genetic and epigenetic alterations take place during the process of clonal expansion. This process will ultimately give rise to a highly heterogenous tumor with varying phenotypic outcomes and therapeutic needs (Hayatigolkhatmi *et al.*, manuscript in preparation; Papaemmanuil *et al.*, 2016; Cai and Levine, 2019). Such complicated level of

heterogeneity creates challenges both for **classification** and **treatment** (Hayatigolkhatmi *et al.*, manuscript in preparation; Di Nardo and Cortes, 2016; Papaemmanuil *et al.*, 2016; Ngai *et al.*, 2021).

AML classification have classically been relying on the morphologic determinants decided by the French-American-British (**FAB**) cooperative group on hematological disorders in 1976 (Bennett *et al.*, 1976). There are eight main FAB classes determined for AML diagnosis and classification (Please refer to Table 6 and Figure 14) (Bennett *et al.*, 1976; Krause and Etten, 2007; Cheuk and Guinn, 2008; Quessada *et al.*, 2021). However, with the advancement of diagnostic tools, particularly in the fields of molecular genetics and cytogenetics, various leukemia initiating mutations and prognostic markers were integrated in classifications of AML subtypes (Papaemmanuil *et al.*, 2016). Hence the world health organization (WHO) offered new principles, integrating these advancements into the AML stratification systems used in the clinics (Table 7) (Cheuk and Guinn, 2008; Walter *et al.*, 2013; Swerdlow *et al.*, 2017).

Subtype	MPO	Morphology	Surface Markers	Morphological Findings in Wright-Giemsa Staining
M0	-	Undifferentiated Myeloblasts	CD13+, CD33+, CD34+	High N/C ratio, fine chromatin
M1	+/-	Myeloblasts	CD13+, CD33+, CD34+/-	High N/C ratio, fine chromatin, few granules
M2	++	Myeloblasts	CD13+, CD15+, CD33+, CD34+/-	Regular nuclear shape, clumped chromatin, Auer rods
M3	+++	Promyelocytes	CD13+, CD15+, CD33+	Folded/indented nucleus, clumped chromatin, Auer rods
M3v	+++	Variant Promyelocytes	CD13+, CD15+, CD33+	Folded/indented nucleus, clumped chromatin
M4	+	Myelomonocytic	CD13+, CD15+, CD33+, CD14+, CD11b+	Regular nuclear shape, clumped chromatin
M4Eo	+	Myelomonocytic/Eosinophilia	CD13+, CD33+, CD14+, CD14+, CD11b+	Regular nuclear shape, clumped chromatin
M5a	+/-	Monoblasts	CD13+/-, CD15+, CD33+, CD14+/-, CD11b+	High N/C ratio, fine chromatin
M5b	+/-	Promonocytes	CD13+/-, CD15+, CD33+, CD14+/-, CD11b+	High N/C ratio, fine chromatin
M6	+/-	Erythroblasts	CD33+, CD36+	Erythroblasts
M7	-	Megakaryoblasts	CD41+, CD61+	High N/C ratio, fine chromatin

Table 6. ***FAB classification of AML****. Subtype: This column lists the FAB (French-American-British) classification categories for Acute Myeloid Leukemia, ranging from M0 to M7. Each class represents a specific subtype of AML based on morphological and cytochemical criteria. MPO (Myeloperoxidase): This column indicates the presence (+), absence (-), or variable presence (+/-) of Myeloperoxidase activity in the leukemia cells. Myeloperoxidase is an enzyme commonly used to identify myeloid cells. Morphology: This column describes the morphological characteristics of the leukemia cells, such as cell size, granulation, and the presence of Auer rods. Surface Markers: This column is divided into sub-columns for specific surface markers (CD13, CD14, CD15, CD33, CD34, CD11b, CD36, CD41, CD61). It indicates the presence (+) or variable presence (+/-) of these markers on the leukemia cells. Morphological Findings in Wright-Giemsa Staining: This column provides additional morphological details that can be observed under Wright-Giemsa staining, such as nuclear shape, chromatin condensation, and the ratio of nuclei to cytoplasm volume. "+" indicates the presence of the marker, while "-" indicates its absence. Morphological findings include nuclear shape, chromatin condensation, and nuclei/cytoplasm volume where applicable. Auer rods are present in M1, M2, and M3 subtypes. Table modified from Mak and Saunders, 2006.*

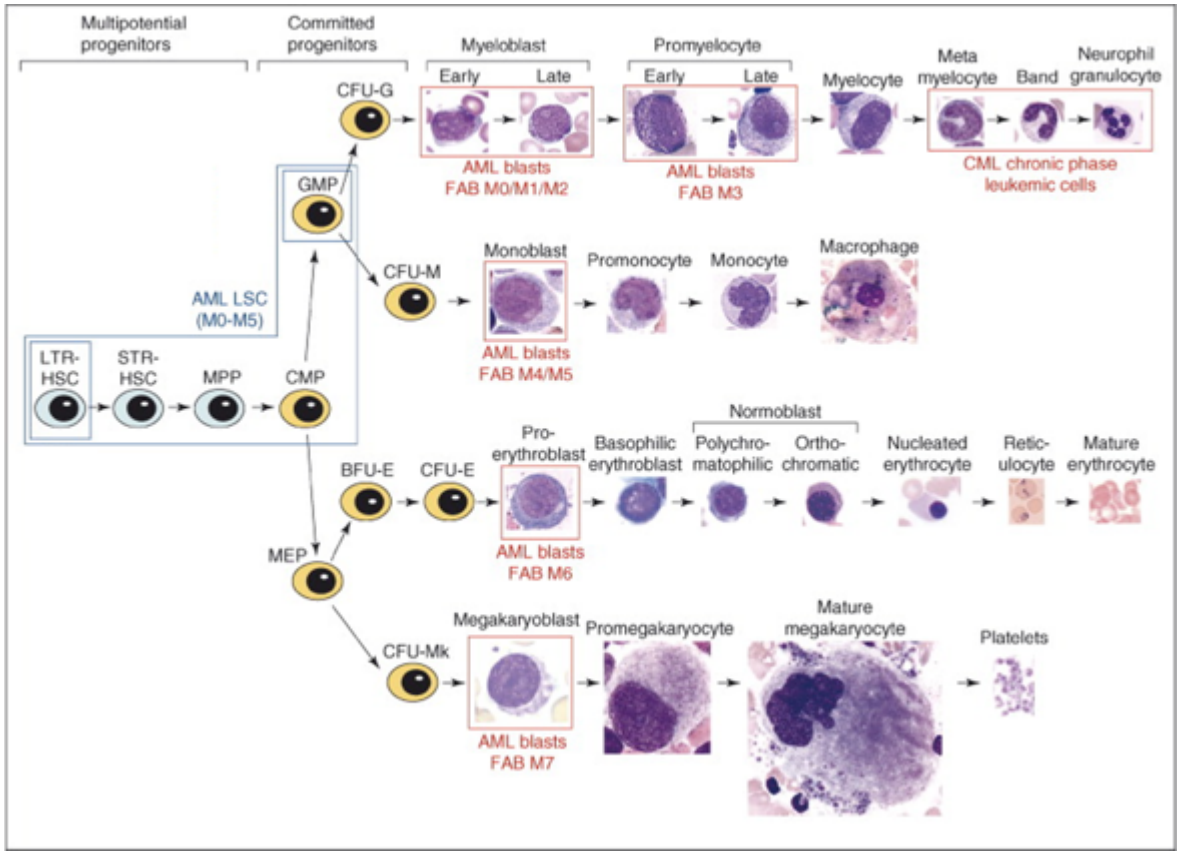

Figure 14. ***AML FAB classes and their origin in hematopoietic hierarchy****. The diagram outlines the typical development of myeloid cells and its connection to leukemic stem cells (LSCs). On the left, shown in blue, are different stem and progenitor cells, including long-term repopulating (LTR) and short-term repopulating (STR) stem cells, as well as multipotential progenitors (MPPs). The middle section, features specialized progenitors like common myeloid progenitors (CMPs),*

granulocyte-macrophage progenitors (GMPs), and megakaryocyte-erythroid progenitors (MEPs). It also includes colony-forming units for specific cells such as granulocytes (CFU-Gs), macrophages (CFU-Ms), erythroid cells (CFU-E), and megakaryocytes (CFU-Mks). On the right side, differentiated myeloid cells are shown with their distinct characteristics. Leukemic cells and LSCs in both acute and chronic myeloid leukemia are highlighted in red. In AML, leukemic blasts from various subtypes (M0 to M7) typically correspond to their respective normal cell lineages. Meanwhile, cells in the chronic phase of Chronic Myeloid Leukemia (CML) resemble fully matured granulocytes. LSCs in these leukemias are found in a limited range of multipotential and specialized progenitors, which are indicated by the blue boxes. Figure and legend adapted from Krause and Etten, 2007.

Category	Subtype	Cytogenetic Abnormality	Molecular Features	Clinical Features	Prognosis
AML with recurrent genetic abnormalities	AML with t(8;21)(q22;q22.1); RUNX1-RUNX1T1	t(8;21)(q22;q22.1)	Presence of RUNX1-RUNX1T1 fusion gene	Often presents in younger adults; associated with granulocytic sarcomas	Generally favorable
	AML with inv(16)(p13.1q22) or t(16;16)(p13.1;q22); CBFB-MYH11	inv(16)(p13.1q22) or t(16;16)(p13.1;q22)	Presence of CBFB-MYH11 fusion gene	Frequently associated with abnormal BM eosinophils	Generally favorable
	Acute promyelocytic leukemia (APL) with PML-RARA	t(15;17)(q22;q21)	Presence of PML-RARA fusion gene	Often presents with coagulopathy; high risk of early death	Favorable with ATRA and arsenic trioxide treatment
	AML with t(9;11)	t(9;11)(p22;q23)	MLLT3-MLL	Often presents with high WBC count	Intermediate
	AML with t(6;9)	t(6;9)(p23;q34)	DEK-NUP214	Often presents with FLT3-ITD mutations	Poor
	AML with inv(3) or t(3;3)	inv(3)(q21q26.2) or t(3;3)(q21;q26.2)	RPN1-EVI1	Often presents with high platelet count	Poor
	AML (megakaryoblastic) with t(1;22)	t(1;22)(p13;q13)	RBM15-MKL1	Common in infants; associated with Down syndrome	Poor
	AML with mutated NPM1	N/A	NPM1 mutations	Often presents with normal karyotype	Favorable if FLT3-ITD negative
	AML with biallelic mutations of CEBPA	N/A	Biallelic CEBPA mutations	Often presents with normal karyotype	Favorable
	AML with BCR-ABL1	t(9;22)(q34.1;q11.2)	Presence of BCR-ABL1 fusion gene	Often resistant to standard AML therapies	Poor; often treated like CML
AML with myelodysplasia-related changes	N/A	N/A	History of MDS or MDS/MPN; multilineage dysplasia	Older adults; often resistant to therapy	Poor
Therapy-related myeloid neoplasms	Therapy-related AML	Various	Variable	History of cytotoxic therapy	Poor

	Therapy-related MDS	Various	Variable	History of cytotoxic therapy	Poor
AML, not otherwise specified	AML with minimal differentiation	N/A	Lack of lineage-specific markers	Variable	Intermediate
	AML without maturation	N/A	Myeloperoxidase positivity in <3% blasts	Variable	Intermediate
	AML with maturation	N/A	Myeloperoxidase positivity in ≥3% blasts	Variable	Intermediate
	Acute myelomonocytic leukemia	N/A	Both myeloid and monocytic differentiation	Variable	Intermediate
	Acute monoblastic/monocytic leukemia	N/A	≥80% monoblasts and promonocytes	Variable	Intermediate
	Acute erythroid leukemia	N/A	≥50% erythroid precursors	Variable	Poor
	Acute megakaryoblastic leukemia	N/A	≥50% megakaryoblasts	Variable	Poor
	Acute basophilic leukemia	N/A	≥40% basophils	Variable	Poor
	Acute panmyelosis with myelofibrosis	N/A	Myelofibrosis	Variable	Very poor
Myeloid Sarcoma	N/A	Various	Variable	Extramedullary tumor of myeloid blasts	Depends on associated leukemia, if present
Myeloid Proliferations Related to Down Syndrome	Transient abnormal myelopoiesis (TAM)	N/A	GATA1 mutations	Occurs in newborns with Down syndrome; usually self-limited	Generally good
	Myeloid leukemia associated with Down syndrome	N/A	GATA1 mutations	Occurs in children with Down syndrome and history of TAM	Intermediate to poor
Blastic Plasmacytoid Dendritic Cell Neoplasm	N/A	Complex karyotype	CD4+, CD56+, CD123+	Skin lesions, lymphadenopathy, leukemia	Poor

Table 7. ***Updated WHO classification of AML****. Category: This column outlines the primary divisions within the WHO classification, such as AML with recurrent genetic abnormalities, AML with myelodysplasia-related changes, and so on. Subtype: This column specifies the subcategories within each primary division. For example, under the category "AML with recurrent genetic abnormalities," subtypes like AML with t(8;21)(q22;q22.1); RUNX1-RUNX1T1 are listed. Cytogenetic abnormality: This column provides information on the commonly found karyotypic changes in each particular subtype. Molecular features: This column describes additional cytogenetic or molecular characteristics that are commonly found in each subtype. Clinical Features: This column offers a brief overview of the clinical manifestations commonly associated with each subtype, such as age group most affected or common symptoms. Prognosis: This column gives an indication of the expected clinical course for each subtype, categorized as favorable, intermediate, or adverse, based on available clinical data. Table and legend adapted from Walter* et al.*, 2013; Swerdlow* et al.*, 2017.*

AML treatment has gone through a roller coaster of newly discovered interventions and failures in pre-clinical or clinical settings. Hence, the primary line of care remains the induction chemotherapy scheduled as a cycle of 7 days of cytarabine and 3 days of anthracycline (7+3 regimen), followed by allogenic hematopoietic stem cell transplantation (allo-HSCT) in case complete remission (CR) is achieved. However, there have been major improvements throughout years and recently been improving with much increased pace (Hayatigolkhatmi *et al.*, manuscript in preparation; Dombret and Itzykson, 2017; Canaani, 2019; Dzama *et al.*, 2020). For example, the utilization of ATRA stands out as a particularly effective strategy for managing APL, achieving CR rates that surpass 85%. Beyond ATRA, the therapeutic landscape for AML includes targeted treatments against distinct genetic or epigenetic drivers of the disease. Allo-HSCT, CAR T-cell interventions, assorted immunotherapy options, and conventional chemotherapy agents also form part of the broader treatment arsenal. In particular the emergence of epigenetic therapies have opened a window of opportunity for enhanced differentiation inducing and cytotoxic combinatorial therapeutic strategies (Hayatigolkhatmi *et al.*, manuscript in preparation; Dombret and Itzykson, 2017; Canaani, 2019; Fiorentini *et al.*, 2020; Heuser *et al.*, 2021; Yan *et al.*, 2022).

3.1. Epigenetics of AML

Epigenetic modulation serves as a cornerstone in the pathogenesis of AML, **influencing both coding and non-coding genomic regions**. This modulation aims to enhance the stem-like qualities of leukemic stem cells (**LSCs**) by optimizing the epigenetic environment for the **expression of self-renewal regulating genes and leukemia-promoting TFs**, and **suppressing genes related to normal hematopoietic differentiation** (Hayatigolkhatmi *et al.*, manuscript

in preparation; Mehdipour, Santoro and Minucci, 2015; Glass *et al.*, 2017; Ueda and Steidl, 2021). The orchestration of this complex regulation involves various chromosomal translocations with a core of epigenetic regulators. Writers like DNMT3A and MLL have been implicated in AML, as have erasers such as KDMs and HDACs, and readers like CBX family proteins (Figure 15) (Hayatigolkhatmi *et al.*, manuscript in preparation; Di Croce *et al.*, 2004; Ueda and Steidl, 2021). It is noteworthy that such epigenomic dysregulation extends its impact beyond genomic to include intergenic regions, impacting elements like TEs (Hayatigolkhatmi *et al.*, manuscript in preparation; Jones *et al.*, 2019). Understanding these epigenetic alterations can offer new avenues for therapeutic intervention. Modulating the epigenetic landscape not only can enhance the efficacy of existing treatments but also counteract therapy resistance and immune evasion mechanisms (Hayatigolkhatmi *et al.*, manuscript in preparation; Bewersdorf *et al.*, 2019; Majchrzak-Celinska, Warych and Szoszkiewicz, 2021).

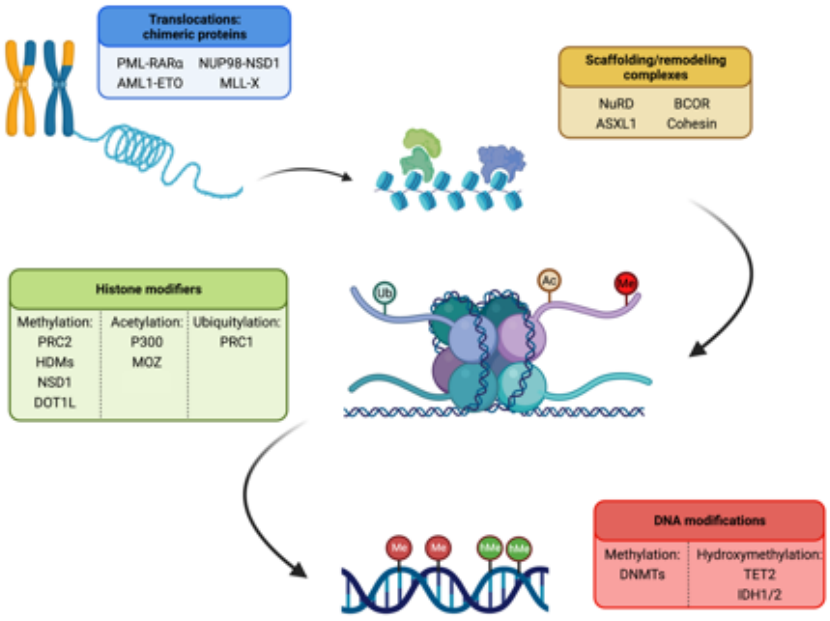

Figure 15. ***Cytogenetic and genetic alterations contributing to AML pathogenesis through induction of epigenetic changes****. Figure and legend adapted from Hayatigolkhatmi et al., manuscript in preparation. Figure created with Biorender.com.*

Understanding the impact of epigenetic alterations in gain of ***stemness and self-renewal*** abilities in LSCs have been studied for years by different research groups. Aberrations in key histone modifiers as well as cytogenetic abnormalities, have been implicated through this epigenomic dysregulation (Hayatigolkhatmi *et al.*, manuscript in preparation; Bewersdorf *et al.*, 2019; Shukla *et al.*, 2021; Arnold *et al.*, 2022). **BMI1**, a subunit of **PRC1**, is often overexpressed in AML and enhances self-renewal and blast expansion. Deminishing BMI1 leads to reduced self-renewal and increased apoptosis (Rizo *et al.*, 2009). **PRC2**, another histone modifier, modulate *HOX* genes, which are crucial for hematopoietic processes and are aberrantly expressed in AML (Asada *et al.*, 2019). **DOT1L**, a HMT, is also implicated in the regulation of *HOX* genes and is a point of convergence for various genetic drivers in AML (Chen and Armstrong, 2015). HDMs like **JMJD3** have been shown to impact AML cell growth by altering cell cycle regulators and repressing *HOX* genes (Li *et al.*, 2018). Additionally, fusion proteins like **NUP98-NSD1** and **MLL-translocations** have been identified as key drivers of epigenomic changes related to *HOX* gene expression (Gough, Slape and Aplan, 2011; Thol *et al.*, 2012). Targeting these epigenetic regulators could be a promising therapeutic strategy, especially in the relapsed stage of AML where stemness properties are often observed (Hayatigolkhatmi *et al.*, manuscript in preparation; Short, Rytting and Cortes, 2018; Liu, 2021; Ueda and Steidl, 2021).

In parallel to gaining self-renewal potential, leukemia initiating cells need to **deny their normal hematopoietic differentiation fate**. Here again, epigenetic changes occur to set the stage for such an atypical route (Hayatigolkhatmi *et al.*, manuscript in preparation). DNA methylation is a key epigenetic process, with DNMTs like **DNMT3A** being especially relevant in AML. Mutations in DNMT3A are found in a significant proportion of AML patients with normal karyotypes and are linked to poor prognosis (Russler-Germain *et al.*, 2014). Non-epigenetic enzymes like **IDH1/2** can also influence DNA methylation. Mutations in these

enzymes lead to the accumulation of 2-HG, which inhibits TET2 and other α-KG-dependent enzymes, affecting DNA and histone methylation (Im *et al.*, 2014). Histone methylation patterns are often altered in AML, sometimes due to loss-of-function mutations (LoF) in epigenetic regulators like **UTX** (Zheng *et al.*, 2018; Chang, Yim and Park, 2019). **LSD1** is another key player in hematopoietic differentiation, and its inhibition has been proposed as a therapeutic strategy for AML (Schenk *et al.*, 2012; Ravasio *et al.*, 2020; Zhang *et al.*, 2021; Nicosia *et al.*, 2022). Histone acetylation, often altered by mutations or translocations in HATs like **MYST3**, can also lead to differentiation impairment (Rozman *et al.*, 2004). Scaffolding proteins like **ASXL-1** are involved in AML, and mutations in these proteins can disrupt their interaction with histone-modifying complexes, leading to global changes in histone methylation (Asada *et al.*, 2019). TFs affected by chromosomal translocations, such as **PML-RARα** and **AML1-ETO**, can also induce epigenetic changes that impair differentiation (Hayatigolkhatmi *et al.*, manuscript in preparation; Mehdipour, Santoro and Minucci, 2015; Fiorentini *et al.*, 2020). The epigenetic landscape in AML is a critical determinant in the disease's onset and progression, influencing both *stem-like properties of LSCs* and their *hematopoietic differentiation blockade*. Key epigenetic regulators and chromosomal translocations, such as DNMT3A, PRCs, DOT1L, and MLL translocations, play pivotal roles in these processes. However, the list of epigenetic regulators involved in AML initiation, maintenance and relapse goes beyond the ones mentioned so far (Table 8) (Hayatigolkhatmi *et al.*, manuscript in preparation; Mehdipour, Santoro and Minucci, 2015; Sun, Chen and Deshpande, 2018; Ueda and Steidl, 2021). Focused studies on these epigenetic determinants can lead to more effective combinatorial therapeutic regimens (Hayatigolkhatmi *et al.*, manuscript in preparation; Ueda and Steidl, 2021).

Genetic translocations	Frequency	Mutation/Alteration	Description	References
PML-RARα	95% of APL	t(15;17) translocation	Fusion of PML gene on chromosome 15 and RARα gene on chromosome 17. RARα acts as a repressive transcription factor, while the fusion with PML grants the protein a broader spectrum of targets.	(Roussel and Lanotte, 2001)
AML1-ETO	5-10% of all AML (10-20% in paediatric AML)	t(8; 21) translocation	The fusion protein maintains AML1 DNA binding capability, but the fusion with corepressor domain of ETO results in gene silencing.	(Bruserud *et al.*, 2011)
MLL translocations	10 % in all AML (70% in paediatric AML)	Translocations at 11q23	MLL is a H3K4 methyltransferase. The different onco-fusion proteins lack the SET domain, but they can impair the activation of HOXA genes.	(Daser and Rabbitts, 2004)
NUP98-NSD1	2% of adult CN-AML (16% of paediatric CN-AML)	t(5;11)(q35;p15.5)	This fusion protein activates HOXA genes by an aberrant NSD1-dependent methylation of H3K36	(Thol *et al.*, 2012)
HATs	<1% of AML	t(8;16)(p11;q13)	The MOZ-CBP fusion protein favors the mistargeting of specific HAT activity.	(Sun, Chen and Deshpande, 2018)
Histone modifiers	**Frequency**	**Mutation/Alteration**	**Description**	**References**
MLL-PTD	3-5% of AML patients	Partial Tandem Duplications (PTD) at 11q23	Partial duplications of this lysine methyltransferase increase the binding to unmethylated CpG and repression of critical genes, altering differentiation.	(Sun, Chen and Deshpande, 2018)
Polycomb complexes (EZH2 and BMI1)	BMI1: increased expression in ~45-50% of AML; EZH2: 1-2% of AML patients	BMI1 Overexpression/amplification and EZH2 Deletion/mutation	BMI1 overexpression favors the PRC1-dependent self-renewal capacity. Loss of EZH2 activity reduces the level of H3K27 methylation, altering the epigenetic silencing capability.	(Lessard and Sauvageau, 2003; Kim and Roberts, 2016)
Histone demethylases (KDM6A and KDM6B)	<1% of AML, increasing at relapse	LoF mutations	UTX loss causes the increased expression of PU.1. JMJD3 inhibition reduces cell cycle regulators, repressing HOX genes expression.	(Li *et al.*, 2018; Zheng *et al.*, 2018; Chang, Yim and Park, 2019)
ASXL1	11% of AML patients	Frameshift and stop mutations	Mutations in ASXL1 lead to a reduced function of its scaffolding role. For example, it reduces PRC2 activity favoring HOXA genes upregulation.	(Kakosaiou *et al.*, 2018; Asada *et al.*, 2019)

DNA modification	Frequency	Mutation/Alteration	Description	References
DNMT3a	30-35% of normal karyotype AML patients	Point mutations (60%), and nonsense/frameshift/splice-site	The loss of DNMT3A activity leads to aberrant patterns of de novo DNA methylation facilitating oncogenes' activation.	(Russler-Germain *et al.*, 2014)
IDH1/2	20% of AML patients	Point mutations (gain-of-function)	The mutant IDH1/2 enzymes catalyze the production of 2-HG. This oncometabolite acts as an inhibitor of α-KG-dependent enzymes such as TET2, important in the DNA demethylation process.	(Chen *et al.*, 2013; Im *et al.*, 2014; Chaturvedi *et al.*, 2016)
TET2	7-23% of AML patients	Loss-of-function and deletions (67% of the cases)	Similarly, to IDH1/2 mutations, the loss of TET2 function impairs DNA demethylation, impairing the proper differentiation process.	(Cimmino *et al.*, 2017)
Other chromatin interacting proteins	**Frequency**	**Mutation/Alteration**	**Description**	**References**
Cohesin complex	13% of adult de novo AML	Truncation, exon skipping, or missense mutations (depending on the gene)	The precise role of cohesin complex alterations is still poorly clear, but it seems to be related to the chromatin architecture-dependent transcriptional regulation.	(Cuartero, Innes and Merkenschlager, 2019)
NPM1	50% to 60% of adult AML-NK	Mutant NPM1 (namely NPM1c) changes its localization to the cytoplasm	The aberrant protein NPM1c relocalization favors the expression of the HOX gene cluster.	(Dawson *et al.*, 2014; Brunetti *et al.*, 2018; Oka *et al.*, 2019)
BCOR	3-4% of AML	Mutations introducing premature stop codons	The mutant protein interacts with HDACs, PRC proteins, and FBXL10, but its precise mechanism of action is poorly understood.	(Grossmann *et al.*, 2011; Honda *et al.*, 2021)

Table 8. ***Epigenetic alterations contributing to AML leukemogenesis****. Genetic Translocations: Lists the chromosomal translocations commonly associated with AML, such as t(8;21), and t(15;17). Histone Modifiers: Enumerates the histone-modifying enzymes implicated in AML, such as EZH2, DOT1L, and HDACs. DNA Modification: Describes the types of DNA modifications involved, such as DNA methylation and hydroxymethylation, and the enzymes responsible for these modifications like DNMT3A. Other Chromatin Interacting Proteins: Lists other proteins that interact with chromatin and contribute to AML pathogenesis, such as cohesin. Frequency: Indicates the prevalence of each epigenetic alteration in AML patient cohorts, expressed as a percentage. Mutation/Alteration: Specifies the type of mutation or alteration observed, such as point mutations, deletions, or amplifications. Description: Provides a brief overview of how each listed epigenetic alteration contributes to AML leukemogenesis, including its role in gene expression, cellular differentiation, and other*

relevant cellular processes. References: Cites the primary literature, reviews, or clinical studies that provide evidence for each epigenetic alteration's role in AML. Table and legend adapted from Hayatigolkhatmi et al., manuscript in preparation.

To devise an effective treatment approach for AML, it's crucial to account for the intricate networks within and between leukemic cells. These networks sustain the blockage of hematopoietic differentiation, preserve LSC properties, and disrupt immune responses (Hayatigolkhatmi *et al.*, manuscript in preparation; Madan and Koeffler, 2021; Stubbins and Karsan, 2021). The epigenomic landscape in AML is highly variable and plastic, facilitating transcriptional imbalances that allow LSCs to evade targeted therapies and relapse (Hayatigolkhatmi *et al.*, manuscript in preparation; Papaemmanuil *et al.*, 2016; Silva *et al.*, 2017; Molica *et al.*, 2019). *Epigenetic therapies in AML* offer a promising opportunity to alter this landscape, steering LSCs toward differentiation and immune activation (Pfister and Ashworth, 2017; Fennell, Bell and Dawson, 2019). However, monotherapies with epigenetic drugs have limitations. At low doses, their effects can be counterbalanced by other epigenetic modifiers, while high doses can disrupt normal cellular functions (Hayatigolkhatmi *et al.*, manuscript in preparation; Fennell, Bell and Dawson, 2019; Stomper *et al.*, 2021). Therefore, a combinatorial approach is needed, combining various therapies to target multiple leukemogenic processes while minimizing harm to normal cells (Hayatigolkhatmi *et al.*, manuscript in preparation; Molica et al., 2019; Noguera et al., 2019; Fiorentini et al., 2020b; Ngai et al., 2021).

DNMT inhibitors (**DNMTi**) and HDAC inhibitors (**HDACi**), also known as hypomethylating agents (**HMAs**), have long been employed in epigenetic therapies for various malignancies (Hayatigolkhatmi *et al.*, manuscript in preparation; Stomper *et al.*, 2021). Combining DNMT with HDAC inhibitors has shown promise in pre-clinical settings, affecting various cellular pathways like oncogene downregulation, cell cycle modulation, and DNA damage (Hayatigolkhatmi *et al.*, manuscript in preparation; Blagitko-Dorfs *et al.*, 2019; Stomper *et*

al., 2021). Therapeutic targeting of other epigenetic targets are also being explored in combination with HMAs (Hayatigolkhatmi *et al.*, manuscript in preparation; Fiskus *et al.*, 2009; Kim and Roberts, 2016; Montesinos *et al.*, 2022; Watts *et al.*, 2023). HMAs can also be used as "primers" for chemotherapy, making the chromatin more accessible to DNA-damaging agents (Hayatigolkhatmi *et al.*, manuscript in preparation; Majchrzak-Celinska, Warych and Szoszkiewicz, 2021; Stomper *et al.*, 2021). They can also synergize with targeted therapies, including tyrosine kinase inhibitors (TKIs), although the mechanisms require further exploration (Hayatigolkhatmi *et al.*, manuscript in preparation; Fennell, Bell and Dawson, 2019; Majchrzak-Celinska, Warych and Szoszkiewicz, 2021). The only definitive cure for most AML patients remains allo-HSCT. HMAs can play roles at various stages of this process, including pre-transplant conditioning, enhancing graft-versus-leukemia effects, and post-transplant maintenance (Hayatigolkhatmi *et al.*, manuscript in preparation; Flotho, Sommer and Lübbert, 2018; Kalin *et al.*, 2020; Yan *et al.*, 2022). In summary, HMAs offer a range of options for AML treatment, in combinatorial and multi-modal treatment regimens (Figure 16).

Beyond the well-known HMAs, a new generation of epigenetic therapies has demonstrated considerable efficacy in halting cell growth, inducing apoptosis, and promoting differentiation in AML. These epigenetic therapies would target one **specific epigenetic modifier** and shown therapeutic advantages particularly when being used in combinatorial interventions (Figure 16) (Hayatigolkhatmi *et al.*, manuscript in preparation; Fennell, Bell and Dawson, 2019; Majchrzak-Celinska, Warych and Szoszkiewicz, 2021). For example, targeting **EZH2 degradation** pathways has shown promise in sensitizing AML cells to chemotherapy (Göllner *et al.*, 2016). Moreover, recent studies suggest that EZH2 inhibitors can be effectively combined with BCL-2 inhibitors, modulating pathways like PI3K/AKT/mTOR and downregulating stemness markers such as c-KIT (Yang *et al.*, 2022). In

another attempt, combining the **DOT1L inhibitor** "Pinometostat" with multi-kinase inhibitor Sorafenib has been shown to induce differentiation in AML cells, possibly through the epigenetic modulation of key genes like *MEIS1*, *FLT3*, and *BRAF* (Lonetti *et al.*, 2020). Another study demonstrated the synergistic effects of DOT1L inhibition with menin inhibitors, mediated by the regulation of key MLL complex genes (Dafflon *et al.*, 2016). Furthermore, DOT1Li has been shown to sensitize AML cells to various chemotherapeutic agents (Liu *et al.*, 2014).

LSD1 inhibitors have also shown compatibility with a broad array of combination strategies in AML (Hayatigolkhatmi *et al.*, manuscript in preparation; Schenk *et al.*, 2012; Cusan *et al.*, 2018; Ravasio *et al.*, 2020; Majchrzak-Celinska, Warych and Szoszkiewicz, 2021). For instance, Ravasio *et al*., 2020 illustrated that combining LSD1 inhibitors "MC2580" and "DDP38003" with low-dose ATRA led to the differentiation and growth inhibition of AML cells. The underlying mechanism was traced back to the disruption of LSD1's interaction with the TF GFI1, thereby enhancing ATRA-induced differentiation (Ravasio *et al.*, 2020). Similarly, Ishikawa *et al*., 2017 reported synergistic effects of LSD1 inhibitor "T-3775440" with NAE inhibitor "Pevonedistat," suggesting that the mechanism involves altered interactions between GFI1 and LSD1, along with changes in the regulation of key transcription factors like GATA1 and PU.1 (SPI1) (Ishikawa *et al.*, 2017). Another study by Deb *et al*., 2019 found that the treatment of an mTOR inhibitor "Rapamycin" amplified the differentiation-inducing effects of LSD1 inhibition in AML cells. While the exact synergistic mechanism between LSD1 inhibitors and Rapamycin remains to be fully elucidated, it is hypothesized to involve NF-kB-mediated immune response regulation, hence stimulation of myeloid lineage differentiation (Hayatigolkhatmi *et al.*, manuscript in preparation; Deb *et al.*, 2019; Abdel-Aziz *et al.*, 2020). These findings highlight the crucial roles of epigenetic regulators like LSD1, which extend beyond their epigenetic modification functions. They

also highlight the need for a comprehensive approach in therapeutic design, where differentiation induction, blast eradication, and prevention of the relapse are foreseen in a multi-step and combinatorial strategy with the least side effects for the patient (Hayatigolkhatmi *et al.*, manuscript in preparation).

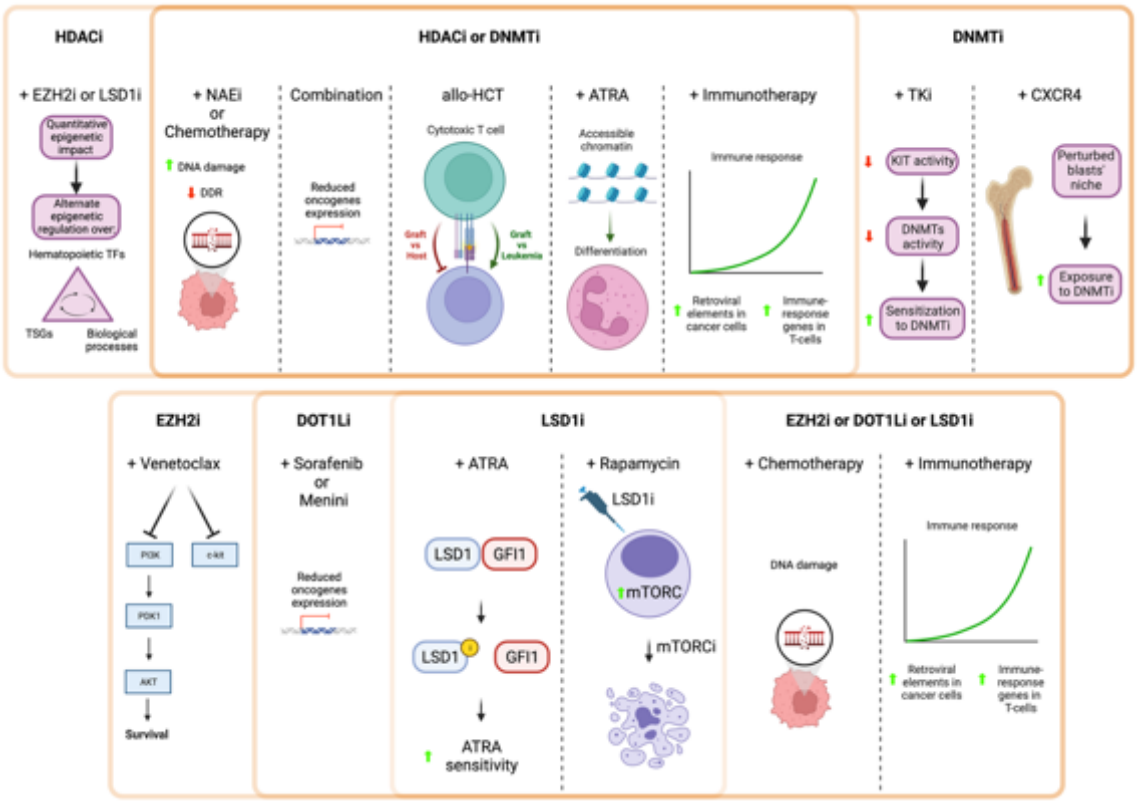

Figure 16. ***Combinatorial therapeutic strategies using at least one epidrug in AML****. Figure and legend adapted from Hayatigolkhatmi et al., manuscript in preparation. Figure created with Biorender.com.*

Aim of the project

The ultimate aim of this comprehensive study is to dive into the complex nature of AML, a hematologic malignancy that has proven difficult to treat despite extensive research. One of the key challenges in AML treatment is the disease's resistance to targeted therapies, often due to the complex interplay of genetic and epigenetic factors. Given that AML has one of the lowest five-year survival rates among leukemias, there is an urgent clinical need for more effective therapeutic strategies. To address this, the study focuses on the potential of epigenetic therapy, specifically inhibitors of the epigenetic enzyme LSD1, to serve as a novel treatment avenue. LSD1 has been a subject of interest in the realm of epigenetic therapy for AML and other malignancies. The study aims to explore the efficacy of LSD1 inhibition across a range of AML subtypes.

The research is designed to be translational, meaning it aims to **bridge the gap between laboratory findings and clinical application**. The goal is **to develop an effective and well-tolerated treatment regimen that could be applied to a diverse AML patient population**. To achieve this, the study plans to investigate a novel combinatorial approach that integrates LSD1 inhibition with other pharmacological strategies, such as cell cycle manipulation, to enhance the drug's efficacy and overcome resistance.

In summary, **the study aims to deepen our understanding of AML's complex biology and treatment resistance, with a particular focus on the role of LSD1 inhibition and its link with the cell cycle regulation**. It seeks to **extend the applicability of LSD1 inhibitors to a wide range of AML subtypes and to develop a multi-targeted therapeutic approach that can be more effective in treating this challenging disease**.

Results

1. Cell cycle speed governs LSD1 inhibition sensitivity

The heterogeneity of AML has created serious obstacles for the available therapies to achieve sustainable levels of disease-free survival rates (Döhner *et al.*, 2010; Creutzig *et al.*, 2012; Molica *et al.*, 2019). Even in cases of promising preliminary effects of novel therapeutic options, relapse of the drug resistant phenotype stands as a frequent concern (Heuser *et al.*, 2021; Ngai *et al.*, 2021). Considering the fundamental role of epigenetic dysregulation in leukemogenesis of AML, several epigenetic regulator targeting agents have proceeded to clinical trials during the past years (Naoe and Kiyoi, 2013; Fennell, Bell and Dawson, 2019). Among the potential epi-targets, inhibiting LSD1 has been highly promising in promoting AML differentiation and is being evaluated through several clinical trials (Fang, Liao and Yu, 2019). However, it has been demonstrated that **in several cases AML patients show resistance to LSD1 inhibitors, as shown also for other epi-drugs** (Fennell, Bell and Dawson, 2019; Ravasio *et al.*, 2020). Thus, the first step of the project was ***to study the cause of dissimilar responses to LSD1 inhibition in AML***.

1.1. AML cell lines from the same clinical subtype respond oppositely to LSD1 inhibition

Examining a panel of AML cell lines, we noted contrasting responses to LSD1 inhibition in various AML cell lines, reflecting clinical observations (*Study Record | ClinicalTrials.gov*, no date a; *Study Record | ClinicalTrials.gov*, no date b). In particular, two APL cell lines – UF-1 and NB4 – with the same t(15;17)(q24;q21) leukemogenic translocation (producing the

PML-RARα fusion oncoprotein), show opposite responses to LSD1 inhibition. Different responses to the LSD1 inhibitor, MC2580, were observed at both proliferative and morphologic levels of the two cell lines (Figure 17). NB4 cells demonstrated resistance to LSD1 inhibition, whereas MC2580 significantly impeded UF-1 cell proliferation. Both of these cell lines represent the FAB3 classification of AML, from the morphologic point of view. However, treatment with MC2580 induced UF-1 cells to exhibit a more differentiated phenotype compared to NB4 cells after one week of treatment, appreciated from the appearance of differentiation morphologic markers at the nucleus and cytoplasm of the UF-1 cells (Figure 17). To provide additional validation for the targeted mechanism of action of MC2580, we treated both cell lines with an alternate LSD1 inhibitor, DDP38003. DDP38003 displayed a dose and time-dependent inhibition of UF-1 cell proliferation, notably, this effect was not observed in NB4 cells (Figure 18).

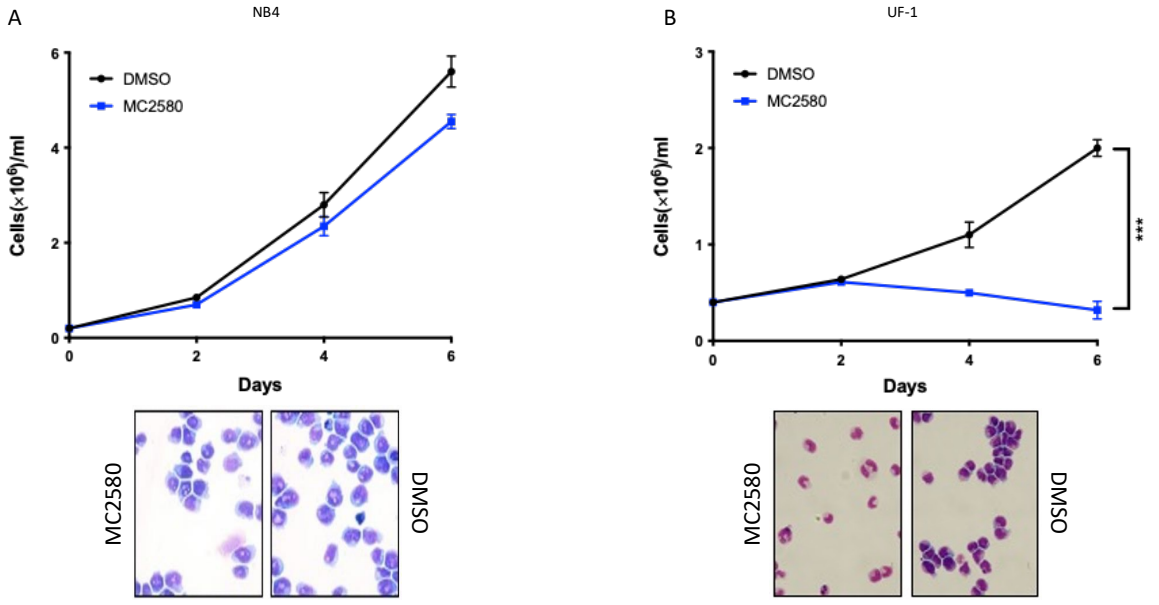

Figure 17. ***Different response to LSD1 inhibition between two APL cell lines, NB4 and UF-1****. Growth curve and representative Wright-Giemsa staining images of NB4 cells (A) and UF-1 cells (B) treated with vehicle (DMSO) or 2μM MC2580. Data are presented as mean of triplicates ± SD. Data are presented as mean of triplicates ± SD. Data were statically analyzed using Bonferroni two-way ANOVA. P value < 0.05 (✱), P < 0.01 (✱ ✱) and P <0.001 (✱ ✱ ✱).*

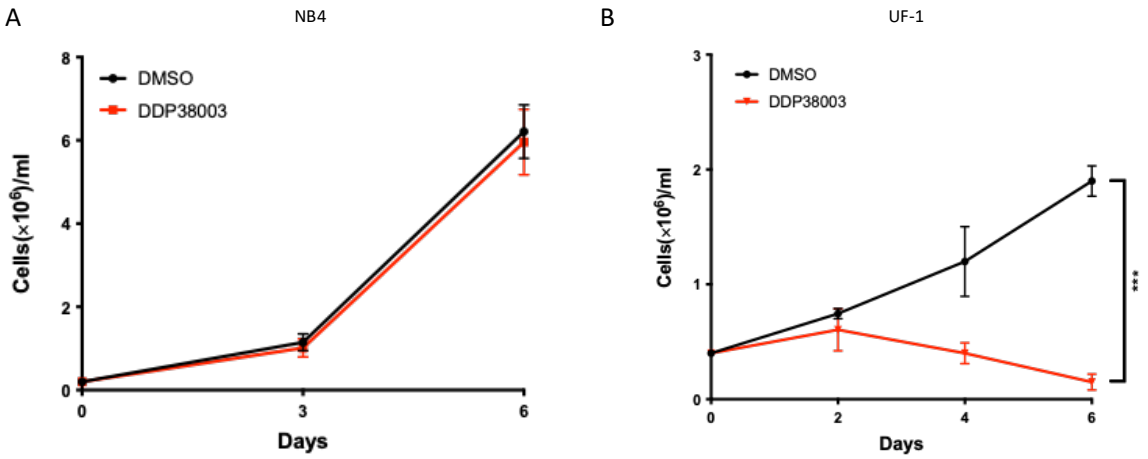

Figure 18. ***Different response to alternate LSD1 inhibitor between the two APL cell lines, NB4 and UF-1****. Growth curve and representative Wright-Giemsa staining images of NB4 cells (A) and UF-1 cells (B) treated with vehicle (DMSO) or 1μM DDP38003. Data are presented as mean of triplicates ± SD. Data are presented as mean of triplicates ± SD. Data were statically analyzed using Bonferroni two-way ANOVA. P value < 0.05 (✱), P < 0.01 (✱ ✱) and P <0.001 (✱ ✱ ✱).*

We subsequently investigated whether the difference in responsiveness of AML cells correlates with their basal levels of LSD1 expression. To address this, we conducted a western blot analysis for LSD1. The comparable levels of LSD1 in both NB4 and UF-1 cells dismissed the notion that sensitivity to LSD1 inhibitors is dependent on LSD1 basal expression levels (Figure 19A). Subsequently, we evaluated the impact of LSD1 inhibition on global levels of H3K4me2 and direct repressive targets of LSD1, *GFI1b* and *CD86*, in both cell lines (Lynch *et al.*, 2013; Speranzini *et al.*, 2016). Regardless of sensitivity to LSD1 inhibition, we observed in both cell lines an increase in global H3K4me2 and upregulation of *GFI1b* and *CD86*. Altogether, these findings indicate that the sensitivity or resistance to LSD1 inhibitor is not due to the basal levels of LSD1 and approve the efficacy of MC2580 in targeting LSD1 (Figure 19B & C).

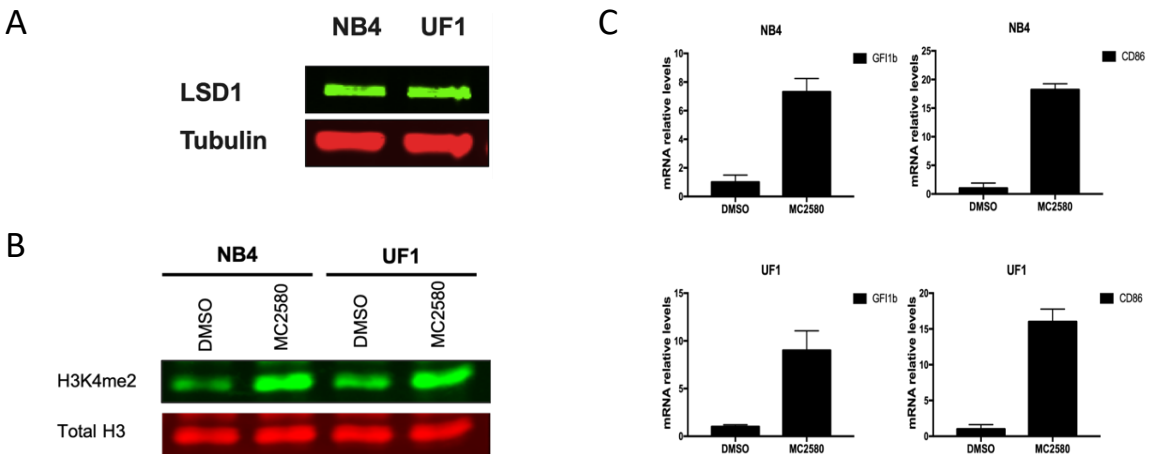

Figure 19. ***LSD1 basal levels are comparable between NB4 and UF-1 cells and can be efficiently targeted by MC2580****. (A) Western blot analysis of LSD1 levels in UF1 and NB4 cells. Tubulin was used as the loading control. (B) Western blot analysis of H3K4me2 level in UF1 and NB4 cells treated with vehicle (DMSO) or 2μM MC2580. Total H3 was used as a loading control. (C) Analysis of GFI1b and CD86 mRNA relative levels in NB4 and UF1 cells treated with vehicle (DMSO) or 2μM MC2580. Values were normalized to GAPDH and referred to DMSO treated.*

These two cell lines provided a valuable model to investigate the reasons behind the distinct responses to LSD1 inhibition in AML. Their nearly identical gene expression profiles made them particularly suitable for this study (Figure 20).

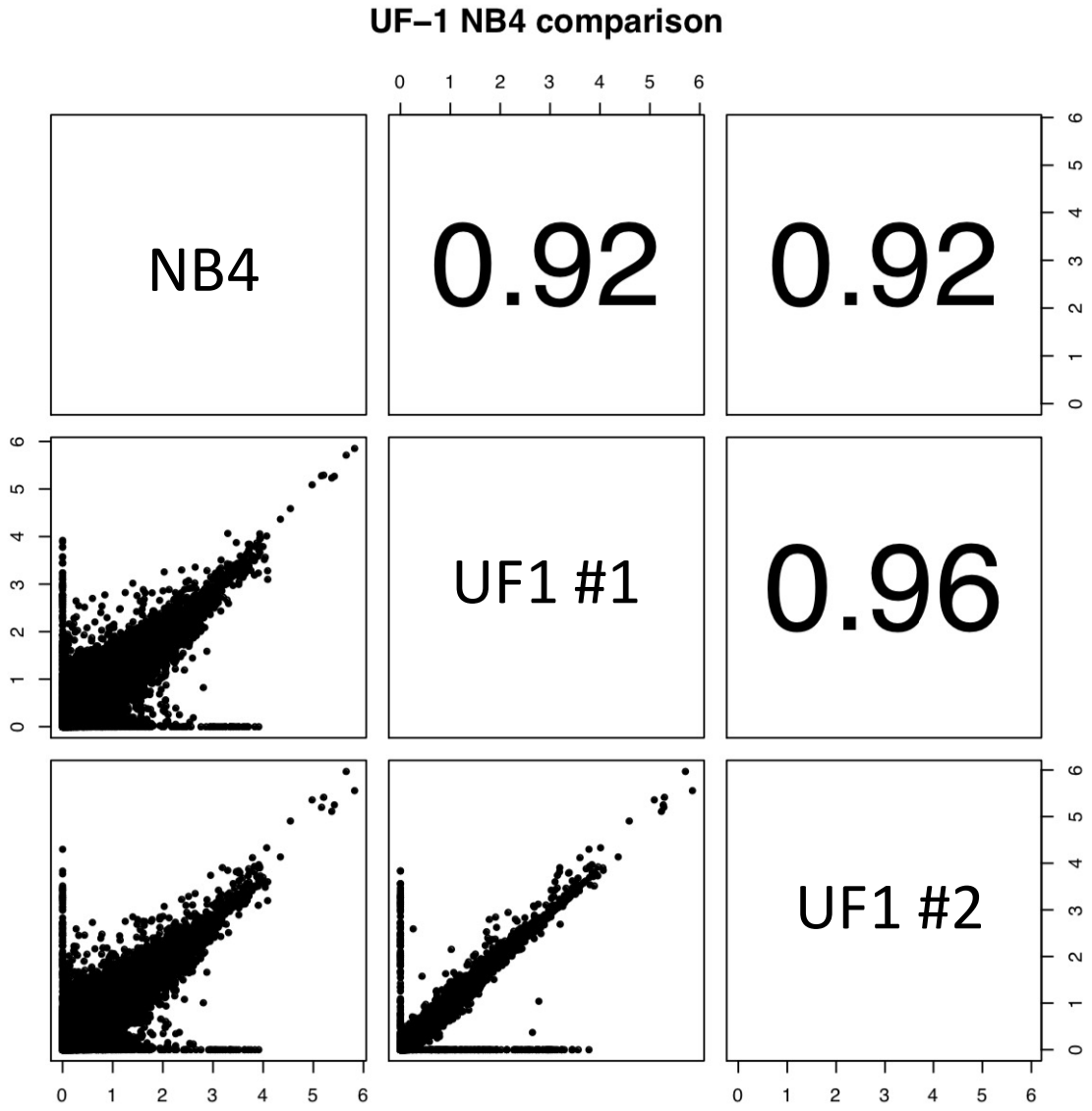

Figure 20. ***NB4 and UF-1 cells have high transcriptomic correlation****. Dot-plot analysis of the correlation in basal gene expression profiles between NB4 and UF-1 cells.*

1.2. CDKN1A (p21) expression levels determine the response to LSD1 inhibition

Despite the high correlation of transcriptomic profile of NB4 and UF-1 cells, we found a handful of differentially expressed genes (DEGs) between the two cell lines (Figure 21A). Manually inspecting the list, we noticed a significantly higher basal expression levels of *CDKN1A* (coding p21, a CDK inhibitor) in UF-1 compared to NB4 cells (Figure 21B). This was in line with the naturally slower proliferation of UF-1 cells compared to NB4 cells (higher

than 48 hours and less than 24 hours, respectively). Interestingly, *CDKN1A* expression was further increased after treatment with MC2580 (Figure 22).

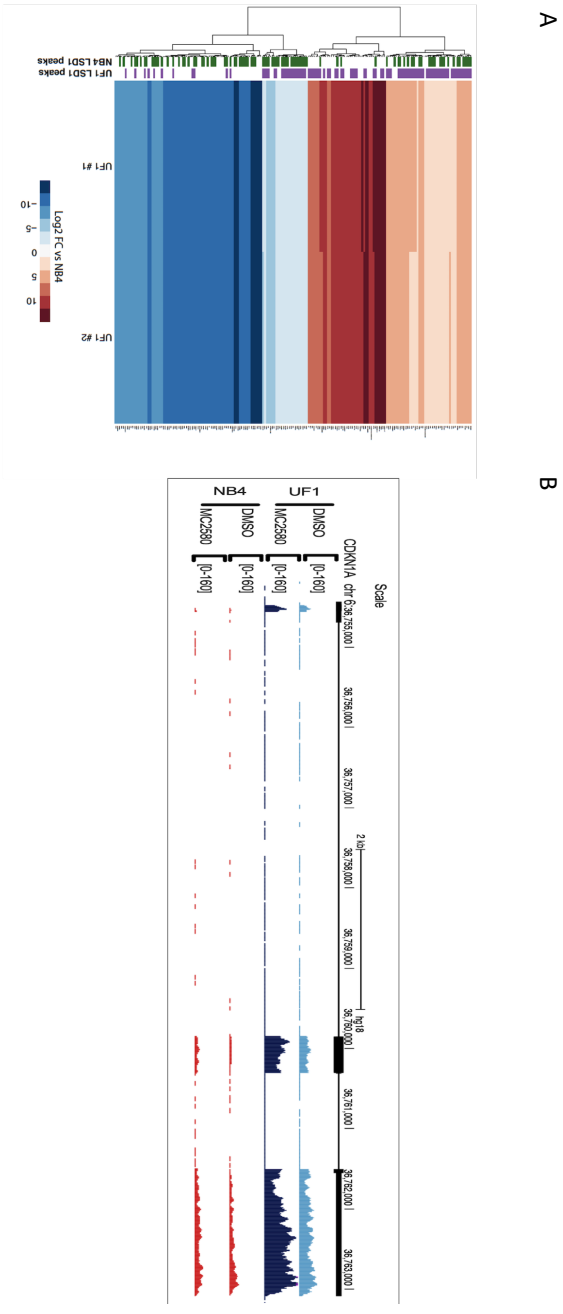

Figure 21. ***CDKN1A (p21 coding gene) expression is higher in LSD1 inhibition responsive cell line, UF-1, relative to its unresponsive counterpart, NB4****. (A) Heatmap representation of gene expression in UF-1(2 replicates) compared with NB4 cells. The data are presented as the average log2 fold change. The magnitude of the changes is indicated by a color scale, with shades of red indicating increase and shades of blue indicating decrease in expression. (B) Genome browser representation of RNA-seq in UF-1 and NB4 cells treated with vehicle (DMSO) or 2μM MC2580 for 24h on CDKN1A (p21) genomic locus.*

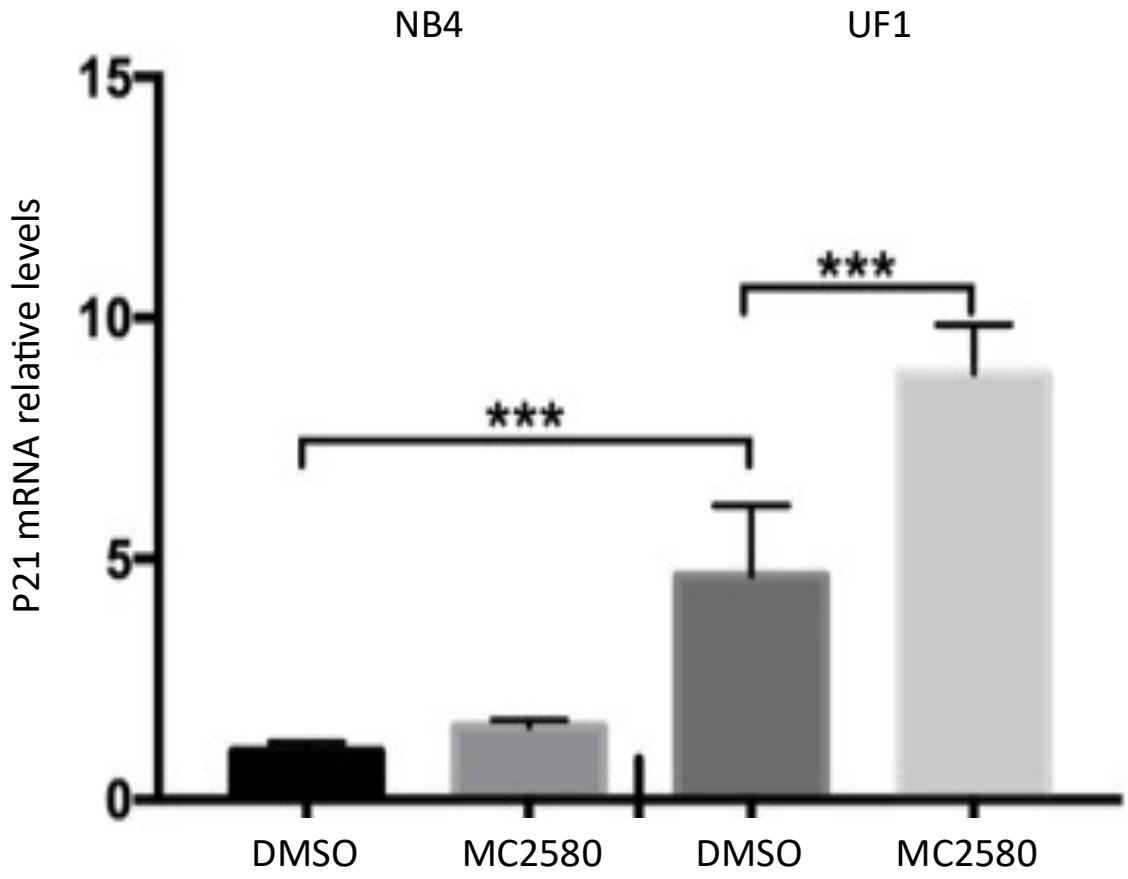

Figure 22. ***CDKN1A (p21 coding gene) expression increases upon LSD1 inhibition****. Analysis of p21 mRNA relative levels in NB4 and UF-1 cells treated with vehicle (DMSO) or MC2580. Values were normalized against GAPDH.*

We hypothesized that the differential expression and subsequent induction of p21 following LSD1 inhibition could potentially explain their distinct sensitivity to LSD1 inhibition. To address this, we employed two specific short hairpin RNA (shRNA) constructs to KD p21 expression (Figure 23A). In p21-KD UF-1 cells, the p21 induction noted upon LSD1 inhibition could be fully countered by p21 KD (Figure 23B). Consequently, the cell growth arrest and the induction of differentiation mediated by MC2580 were abolished (Figure 23C & D).

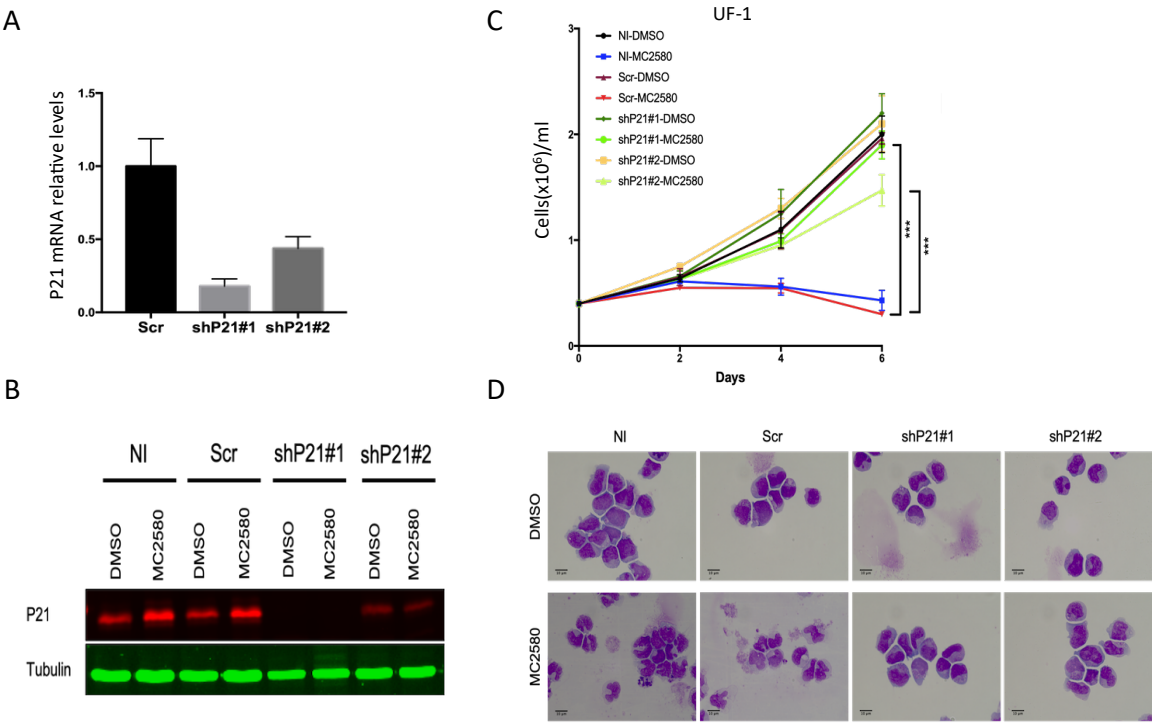

Figure 23. ***Knock down of p21 abolishes sensitivity to LSD1 inhibition in UF-1 cells****. (A) Analysis of p21 mRNA relative levels in UF-1 cells transduced with the indicated lentiviral vectors. Values were normalized against GAPDH and referred to Scr. (B) Western blot analysis of p21 protein in cell lysates from UF-1 cells transduced with the indicated lentiviral vectors or left not infected (NI), and following treatment with vehicle (DMSO) or 2μM MC2580. Tubulin was used as a loading control. (C) Growth curves of UF-1 cells stably transduced with the indicated vectors or left not infected (NI), following treatment with vehicle (DMSO) or 2μM MC2580. Data are presented as mean of triplicates ± SD. (D) Representative images of UF-1 cells as in (H) and stained by Wright-Giemsa. Data were statically analyzed using Bonferroni two-way ANOVA. P value < 0.05 (✱), P < 0.01 (✱ ✱) and P <0.001 (✱ ✱ ✱).*

Conversely, in NB4 cells that were naturally resistant to LSD1 inhibition, we aimed to moderately overexpress p21. Although moderate p21 overexpression in NB4 cells decelerated their growth, it did not induce morphological alterations, and cellular proliferation continued. Notably, the introduction of p21 expression sensitized NB4 cells to the LSD1 inhibitor. This transformation was marked by distinct morphological changes, and growth arrest (Figure 24A & B).

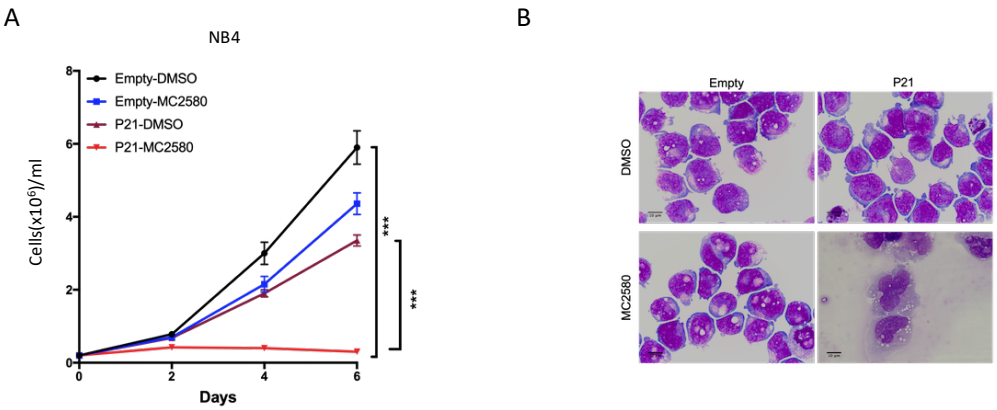

Figure 24. ***Mild overexpression of p21 provokes sensitivity to LSD1 inhibition in NB4 cells****. (A) Growth curves of NB4 cells stably transduced with p21-expressing viral vector or control (Empty), and following treatment with vehicle (DMSO) or 2μM MC2580. Data are presented as mean of triplicates ± SD. (B) Representative images of NB4 cells as in (B) and stained by Wright-Giemsa. Data were statically analyzed using Bonferroni two-way ANOVA. P value < 0.05 (✱), P < 0.01 (✱ ✱) and P <0.001 (✱ ✱ ✱).*

Expanding our observations beyond APL cells to other AML subtypes, we examined Kasumi-1 cells (representing FAB M2 subtype), which, similar to UF-1 cells, exhibit sensitivity to LSD1 inhibition. Remarkably, p21 expression in Kasumi-1 cells parallels that of UF-1 cells, and this expression is further elevated upon LSD1 inhibition. Through p21 KD, its expression and induction by MC2580 were effectively reduced (Figure 25A). Notably, this KD consistently hindered the growth arrest and differentiation induction observed in control cells treated with the LSD1 inhibitor (Figure 25B).

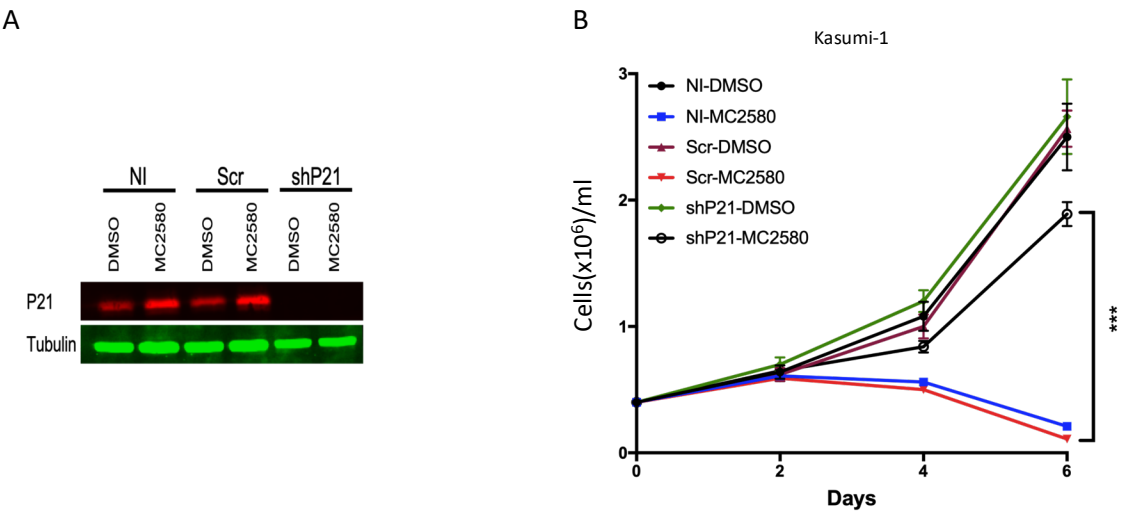

Figure 25. ***Knock down of p21 abolishes sensitivity to LSD1 inhibition in Kasumi-1 cells****. (A) Growth curves of Kasumi-1 cells stably transduced with either control shRNA (Scr) or shRNA targeting p21, or left not infected (NI), and following treatment with vehicle (DMSO) or 2µM MC2580. Data are presented as mean of triplicates ± SD. (B) Western blot analysis of p21 protein in cell lysates from Kasumi-1 cells as in (A). Tubulin was used as a loading control. Data were statically analyzed using Bonferroni two-way ANOVA. P value < 0.05 (✱), P < 0.01 (✱ ✱) and P <0.001 (✱ ✱ ✱).*

These observations unveiled the pivotal role of p21 in modulating the distinct responses of AML cells to LSD1 inhibition, enabling us to further question the mechanism behind.

1.3. Regulation of cell cycle by p21-CDK axis is crucial for response to LSD1 inhibition

The involvement of p21 in regulation of the cell cycle (mainly G1 to S entry) through inhibition of CDKs and in DNA replication and repair through interaction with PCNA is well characterized (Waga *et al.*, 1994; Abbas and Dutta, 2009; Rubin, Sage and Skotheim, 2020). Given the precise mapping of p21's interaction with CDKs and PCNA, we conducted further investigations utilizing NB4 cells expressing wild-type (WT) p21 or variants with specific point mutations preventing association with either CDKs (CDKm) or PCNA (PCNAm) (Figure 26A). Notably, while the expression of both wild-type and PCNA-interaction-deficient

mutated p21 sensitized NB4 cells to LSD1 inhibition, the CDK-interaction-deficient mutant failed to emulate the effects of WT p21 and did not enhance sensitivity to MC2580 treatment (Figure 26B & C). These findings decisively establish a direct link between p21's role in sensitizing cells to LSD1 inhibition and its capacity to regulate the cell cycle, mainly the G1 to S transition (Rubin, Sage and Skotheim, 2020).

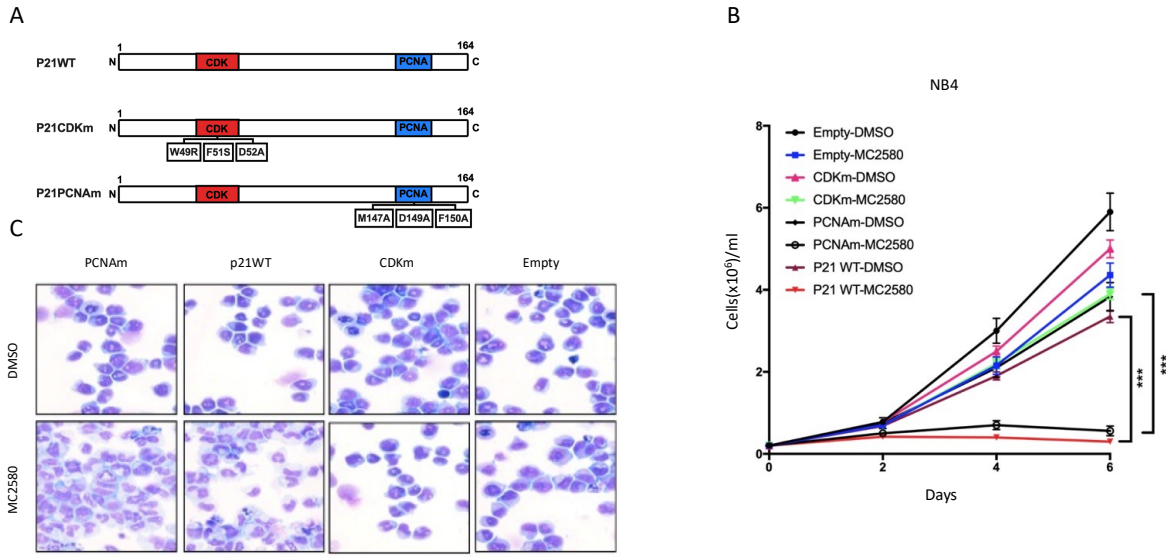

Figure 26. ***Cell cycle regulating function of p21 determines respond to LSD1 inhibition****. (A) Scheme of the p21 expression constructs used in (B). p21 CDKm, unable to associate with CDKs, is impaired in its ability to arrest cell cycle, while p21-PCNAm is defective in binding to PCNA. (B) Growth curves and (C) representative Wright-Giemsa staining images of NB4 cells stably transduced with the indicated p21 expressing viral vectors or control (Empty), and following treatment with vehicle (DMSO) or 2μM MC2580. Data are presented as mean of triplicates ± SD. Data were statically analyzed using Bonferroni two-way ANOVA. P value < 0.05 (✱), P < 0.01 (✱ ✱) and P <0.001 (✱ ✱ ✱).*

1.4. Pharmacologic manipulation of cell cycle can lengthen the G1 phase without entering a quiescent state

Having demonstrated p21's role in exerting its impact via cell cycle modulation, we hypothesized that its function could be replaced by treatment with drugs able to inhibit CDKs. Such approach would enable us to approve the importance of G1 length in

determining response to LSD1 inhibition and to better translate our findings to a possible clinical intervention for AML patients. Palbociclib is a clinically approved selective inhibitor of CDK4/6, crucial for G1 to S transition, used for treating HR-positive breast cancer patients (Beaver *et al.*, 2015). We postulated that given its action Palbociclib could substitute p21's function (Goel *et al.*, 2018; Rubin, Sage and Skotheim, 2020).

The first step was to make sure, that we identified an optimal dosing for Palbociclib. At standard doses, Palbociclib treatment leads to arrest in G1: while the study of G1 arrested cells in the context of our observations is potentially of interest, this is not the focus of our current study, where we would like Palbociclib-treated cells to have a **prolonged** G1 phase without majorly impacting other phases; and, that they **won't enter quiescence** and continue their proliferation. We also needed to be able to compare their cell cycle profile to the naturally slow-cycling AML cells and conduct biological studies. In this regard, we permanently transduced our target cell lines with the fluorescent, ubiquitination-based cell cycle indicator, $CUL4^{Ddb1}$ and APC^{Cdh1} V.2 (**FUCCI(CA)2**) lentiviral vector, a technology to follow the cell cycle progression of the cells. Precise discrimination of all phases of the cell cycle is possible by the FUCCI(CA)2 technology, based on the phase-exclusive emissions of its two fluorescent probes, mCherry and mVenus (Sakaue-Sawano *et al.*, 2017). We initially validated its feasibility by comparing its compatibility with an alternate cell cycle profiling method, using DAPI staining. We assessed NB4 cells treated with either DMSO or a nanomolar dose of Palbociclib, employing both approaches (Figure 27). The two techniques effectively identified an increased proportion of G1 cells due to Palbociclib treatment, and there was concurrence in the cell phases detected by each approach (Figure 27). Furthermore, FUCCI(CA)2 was able to better distinguish a group of cells in the G2/M phases, which were less easily identified by DAPI profiling (Figure 27).

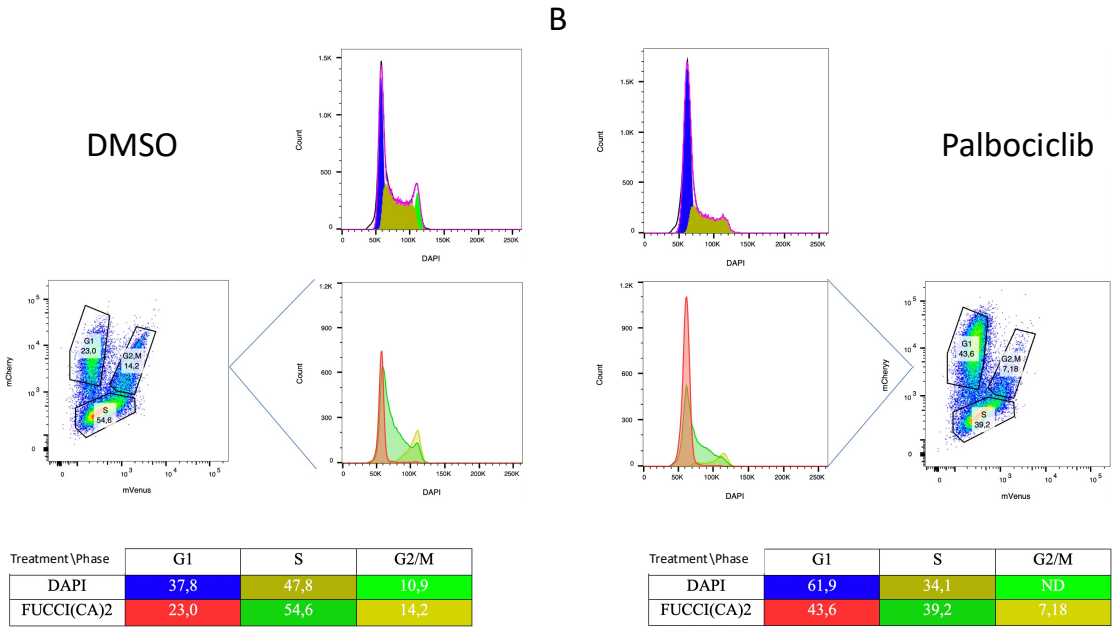

Treatment\Phase	G1	S	G2/M
DAPI	37,8	47,8	10,9
FUCCI(CA)2	23,0	54,6	14,2

Treatment\Phase	G1	S	G2/M
DAPI	61,9	34,1	ND
FUCCI(CA)2	43,6	39,2	7,18

Figure 27. ***Cell cycle profiling findings using FUCCI(CA)2 correlates with and excels the accuracy of classic methods.*** *(A) 24-hours vehicle (DMSO) treated and (B) 24-hours Palbociclib treated FUCCI(CA)2 expressing NB4 cells, stained with DAPI. Upper histograms are indicative of DAPI cell cycle analysis; navy blue: G1, mustard: S, light green: G2. Dot plots are indicative of mCherry vs mVenus emission in tFUCCI(CA)2 lentiviral infected NB4 cells. Correlating DAPI staining for the cell cycle phase-based populations distinguished by FUCCI(CA)2 FACS analysis, have been shown in the lower histograms; red: G1, green: S, yellow: G2/M. Summarized ratios of cell populations in each cell cycle phase, have been shown in the indicative table at the bottom with interrelated colors in each cell population.*

Upon the validation of FUCCI(CA)2, we aimed to understand the impact of Palbociclib on the real-time cell cycle status of the treated NB4 cells. This was to discover the correct doses of Palbociclib, to imitate a slow-cycling behavior, without entering quiescence. Thus, we employed our FUCCI(CA)2-NB4 and FUCCI(CA)2-Kasumi-1 cell lines for a live-cell imaging study. This study was conducted utilizing an in-house developed method, which enabled us to automatically track AML cells at single-cell level for at least 72 hours, quantifying the length of each phase of the cell cycle and measuring the viability of the cells (shown in brief in Figure 28: Hayatigolkhatmi, Soriani, Soda, *et al*., manuscript submitted in attachment). NB4 cells were treated with either DMSO or sub-optimal doses of Palbociclib, and Kasumi-1 cells were cultivated in normal growth conditions without any treatment. Consequently,

we observed administration of 10-50nM Palbociclib, can successfully cause NB4 cells to mimic the proliferative profile of slow-cycling cells (Figure 29). Our live-cell imaging experiments illustrated, that for the majority of the cells to complete at least one full cell cycle in presence of 50nM Palbociclib, they need 24 hours (Figure 30A). The live-cell imaging outcomes depicted that using a sub-optimal dose of Palbociclib, can successfully direct a high proportion of NB4 cells into mimicking the proliferative profile of slow-cycling AML cells, within one day and without impacting their viabilities.

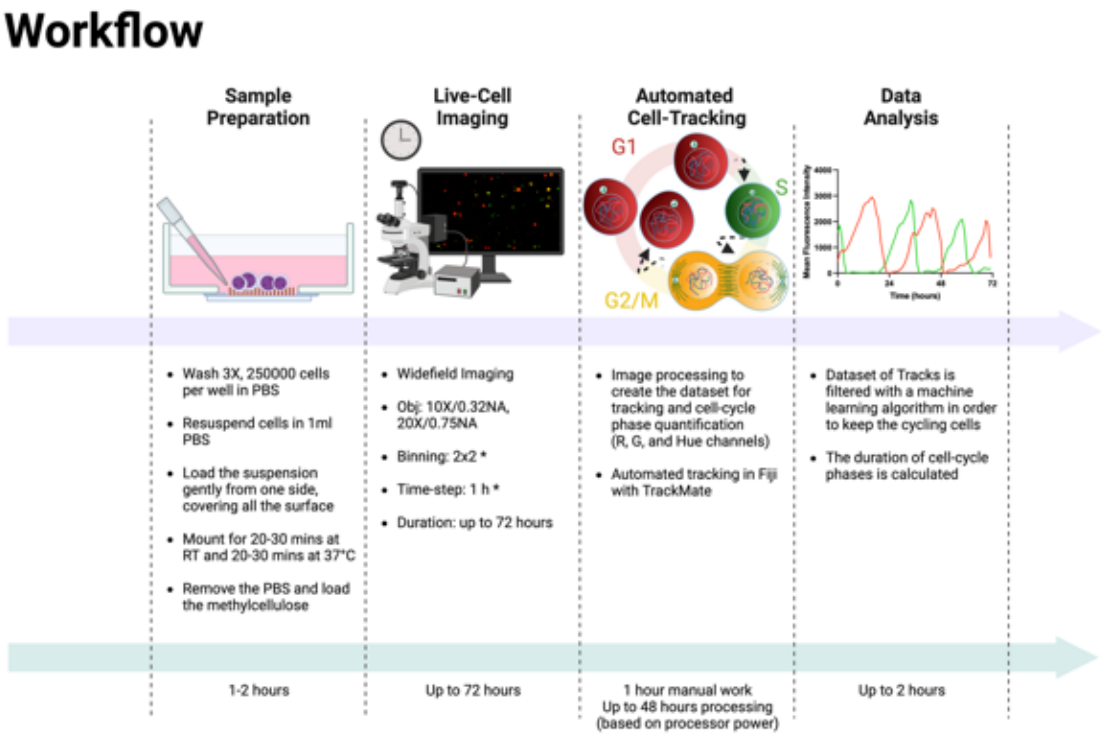

Figure 28. ***Novel devised protocol can effectively follow single cells and quantify their cell cycle progression automatically for long periods****. Experimental and analysis workflow of the in-house developed method for live-cell imaging and cell cycle quantification of in-suspension and adherent cells used in this study. Asterisks in the "Live Cell Imaging" section mean optional settings. Figure and legend adapted from Hayatigolkhatmi, Soriani, Soda, et al., manuscript submitted in attachment. Figure created with Biorender.com.*

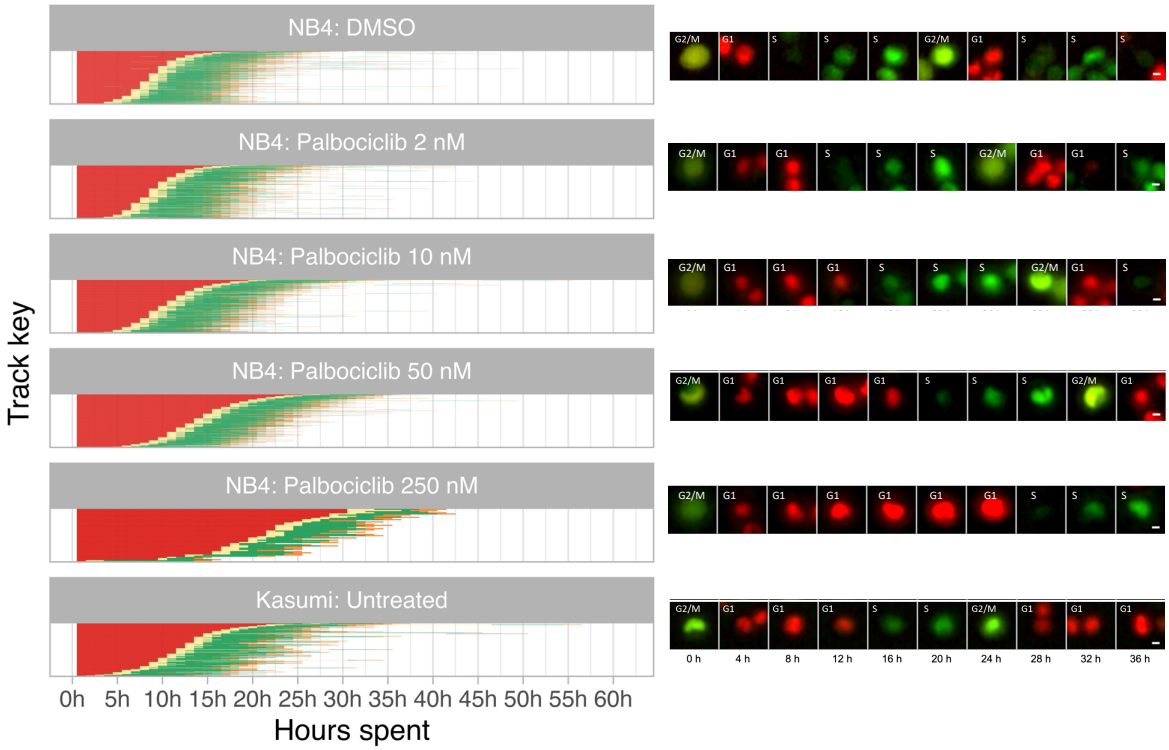

Figure 29. ***Sub-optimal doses of Palbociclib can extend the G1 phase in the fast-cycling AML cells, making them similar to the slow-cycling counterparts, without affecting other phases of the cell cycle****. Waterfall graph (left), represents single cells' cell cycle phase quantification representation of live-cell imaging analysis of FUCCI(CA)2-NB4 cells treated with vehicle (DMSO) or Palbociclib at increasing nanomolar concentrations, and untreated FUCCI(CA)2-Kasumi-1 cells, tracked automatically by the in-house developed method for 72 hours. G1: Red; G1-S transition: Yellow; S: Green; G2/M: Orange. Image series (right) captured through live-cell imaging shows actual footage of a single cell proceeding through one full cell cycle, correlating to the condition at their left side. Cell cycle phase is annotated at top left of each image. Time (in hours) indicated at the bottom of the last series and is similar for all other footages. Figure and legend adapted from Hayatigolkhatmi, Soriani, Soda, et al., manuscript submitted in attachment.*

1.5. Pharmacologic lengthening of G1 bypasses p21 effect and sensitizes cells to LSD1 inhibition

Based on our observations, we designed a treatment schedule, where we treat NB4 cells (infected with vectors coding for either scramble or shRNA for p21) with 50nM Palbociclib, 24 hours prior to treatment with the LSD1 inhibitor (Figure 30B). Notably, the combination of MC2580 and Palbociclib significantly diminished cell growth, and induced differentiation

(Figure 30C & D). In this context, the absence of any impact from p21, confirms the substitutive role of the CDK inhibitor. The same effect was observed, using two alternate CDK inhibitors, PF-06873600 and Milciclib with different affinities for CDK2/4/6, in combination with MC2580 (Figure 31A & B) (Besse *et al.*, 2018; Freeman-Cook *et al.*, 2021). This observation further confirmed the importance of G1 to S transition control in determining sensitivity to LSD1 inhibition, rather than targeting a single cyclin-CDK complex. Concurrently, we could observe the same effect in another fast-cycling and LSD1 inhibition-resistant AML cell line, PL-21 (Figure 32A & B). These experiments confirmed the feasibility of our approach, in which, pre-treatment with a sub-optimal dose of Palbociclib can successfully lengthen the G1 phase of the fast-cycling AML cells and sensitize them to LSD1 inhibition. Upon inhibiting LSD1 at such conditions, cells will show decreased proliferative rates and exhibit morphologic signs of differentiation.

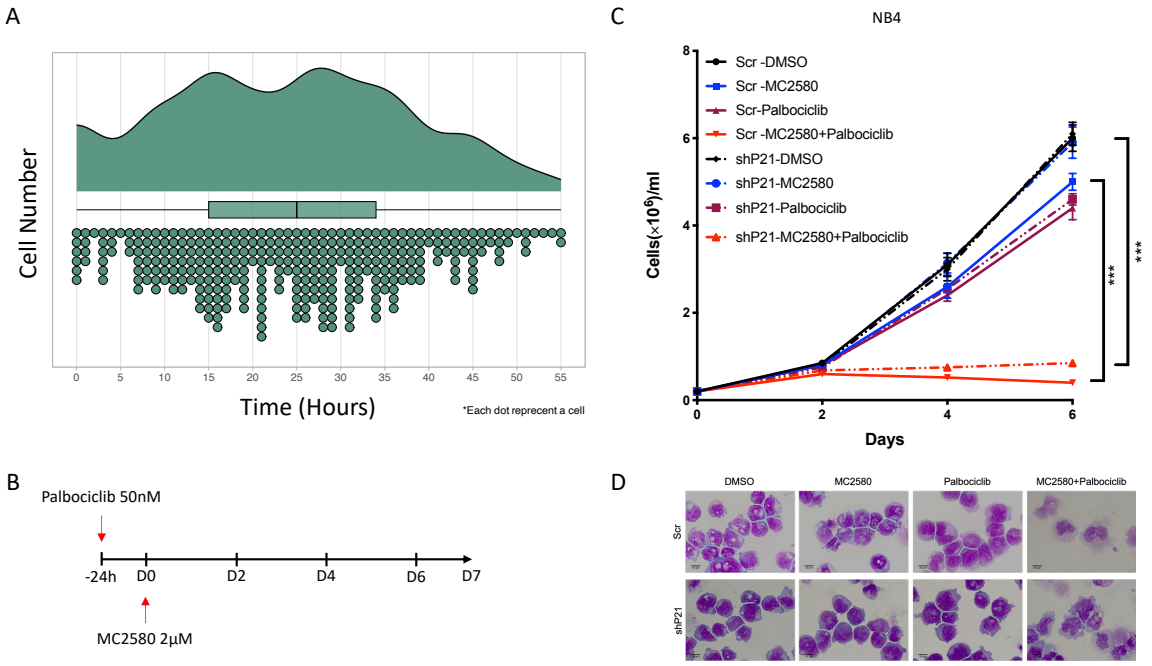

Figure 30. ***Prolongation of the G1 phase of the cell cycle by Palbociclib bypasses p21 effect and effectively sensitizes NB4 cells to LSD1 inhibition****. (A) Rain-cloud plot, representing 100 single NB4 cells, which have undergone a full cell cycle in presence of 50nM Palbociclib. (B) Schematic representation of co-treatment of Palbociclib with LSD1 inhibitor in NB4 cells. (C) Growth curves and (D) representative Wright-Giemsa staining images of NB4 cells stably transduced with shRNA for*

p21 or Scr by viral vector, and following treatment with vehicle (DMSO) or 2μM MC2580 or 50nM Palbociclib or combination of 2μM MC2580 + 50nM Palbociclib. Data are presented as mean of triplicates ± SD. Data were statically analyzed using Bonferroni two-way ANOVA. P value < 0.05 (✱), P < 0.01 (✱ ✱) and P <0.001 (✱ ✱ ✱).

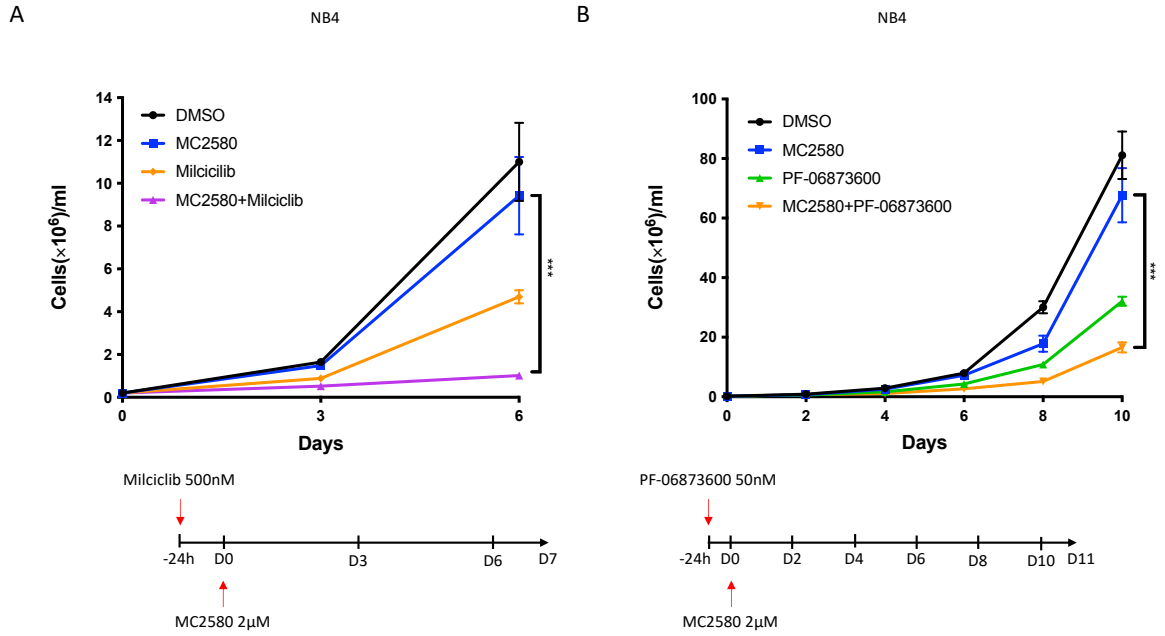

Figure 31. ***Prolongation of the G1 phase of the cell cycle by PF-06873600 and Milciclib effectively sensitizes NB4 cells to LSD1 inhibition****. (A) Schematic representation of co-treatment of 500nM Milciclib and (B) 50nM PF-06873600 with 2μM MC2580 in NB4 cells and its growth curves. Data are presented as mean of triplicates ± SD. Data were statically analyzed using Bonferroni two-way ANOVA. P value < 0.05 (✱), P < 0.01 (✱ ✱) and P <0.001 (✱ ✱ ✱).*

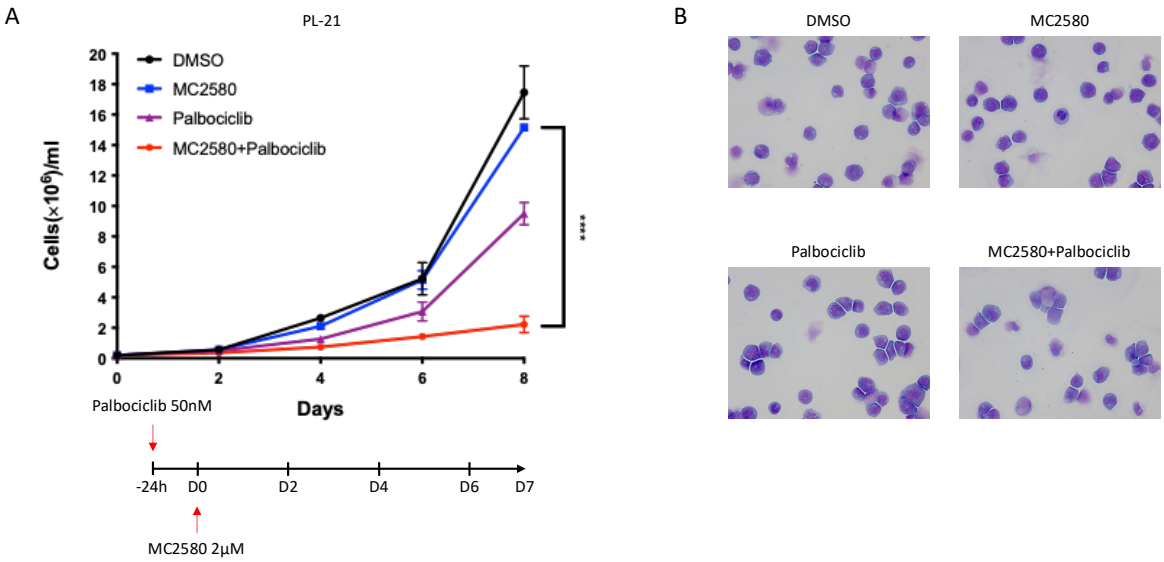

Figure 32. ***Prolongation of the G1 phase of the cell cycle by Palbociclib effectively sensitizes PL-21 cells to LSD1 inhibition****. (A) Schematic representation of co-treatment and growth curves and (B) representative Wright-Giemsa staining images of PL-21 cells treated with vehicle (DMSO) or 2µM MC2580 or 40nM Palbociclib or combination of 2µM MC2580 + 40nM Palbociclib. Data are presented as mean of triplicates ± SD. Data were statically analyzed using Bonferroni two-way ANOVA. P value < 0.05 (✱), P < 0.01 (✱ ✱) and P <0.001 (✱ ✱ ✱).*

2. G1 lengthening alters the epigenetic landscape of AML cells

Our observations compelled us to hypothesize that **AML cells with relatively longer G1 might have a specific chromatin state (e.g., higher accessibility to hematopoiesis regulating TFs, enriched enhancer-promoter proximity for hematopoietic genes, etc.), which poises them towards differentiation induction by an epigenetic therapy**. This idea draws inspiration from the established connection between prompting differentiation in AML through the inhibition of LSD1 and the subsequent control it exerts over TFs like GFI1b and SPI1 (Ravasio *et al.*, 2020). Furthermore, it builds upon the less well explored concept that CDKs may modulate directly epigenetic enzymes depending on their activity state, as mainly observed in ES cells (Michowski *et al.*, 2020). To test our hypothesis, we devised an experimental plan involving multiple steps to examine the chromatin state of AML cells

under various G1 length conditions, both in the presence and absence of an LSD1 inhibitor. In essentially all cases, we built upon the availability of the FUCCI system to be able to sort cells in the G1 phase of the cell cycle, or in other phases: this way, we eliminate the possibility that the observed results were biased by the different distribution of cells in the various phases of cell cycle, depending on treatment/cell type. The aim was to ***assess possible changes in chromatin accessibility, enhancer and super-enhancer distribution, and epigenetic landscape of the cells, promptly resulting from the length of the G1 phase***.

2.1. Chromatin accessibility is altered upon G1 lengthening

To investigate whether extending the G1 phase alone could modify fundamental chromatin characteristics, we opted to replicate the previous treatment regimen with NB4 cells (Figure 30B). We then evaluated their chromatin accessibility during the midpoint of this regimen within the cells at their G1 phase using the assay for transposase-accessible chromatin with sequencing (ATAC-seq). Notably, we could observe around six thousand unique ATAC-seq peaks appearing only in standalone Palbociclib treated cells (Figure 33). Further analysis showed 196 differentially accessible regions (DARs) in Palbociclib treated cells in comparison to DMSO, which was higher than the impact of MC2580 standalone treatment (96 DARs) and less than the combination of both treatments (823 DARs) (Figure 34). Collectively, these observations demonstrate that extending the G1 phase by itself can initiate alterations in chromatin accessibility. This finding could provide valuable insights into the mechanism responsible for the effectiveness of LSD1 inhibition in promoting differentiation among AML cells with slow cell cycle progression.

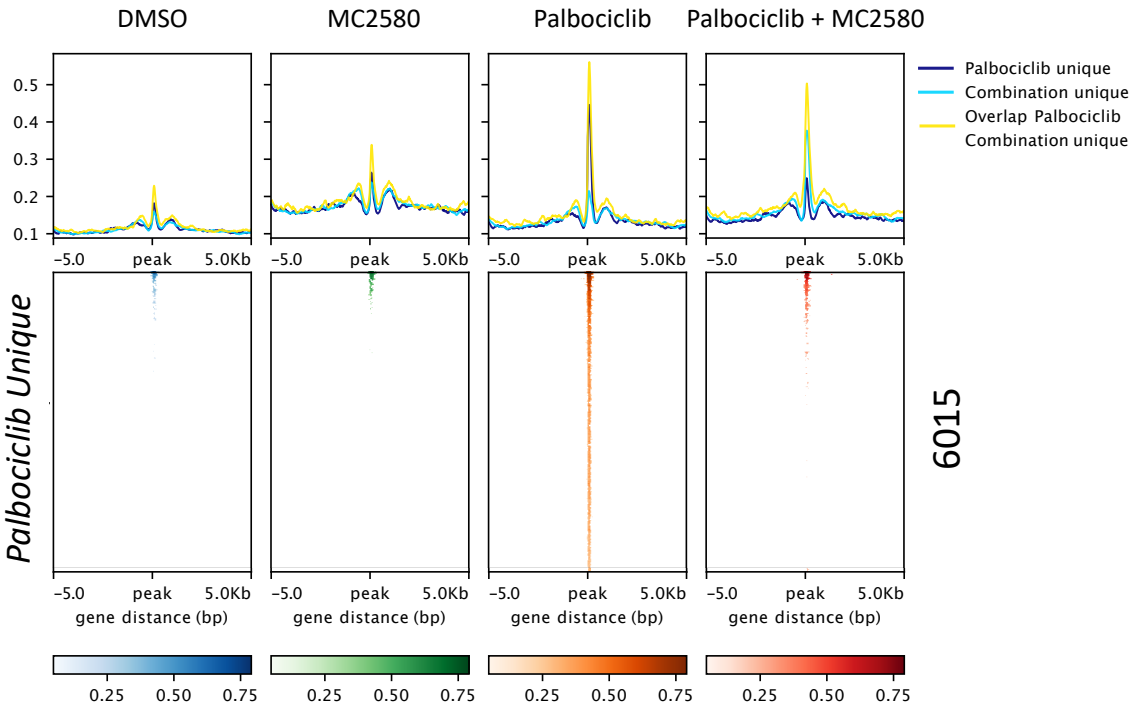

Figure 33. ***Prolongation of the G1 phase of the cell cycle leads to unique chromatin openings****. Heatmaps, representative of unique ATAC peaks in NB4 cells to 50nM Palbociclib based on ATAC-seq analysis. Cells are in their G1 phase and treated with vehicle (DMSO) or 2µM MC2580 or 50nM Palbociclib or combination of 2µM MC2580 + 50nM Palbociclib, 72 hours post LSD1 inhibition.*

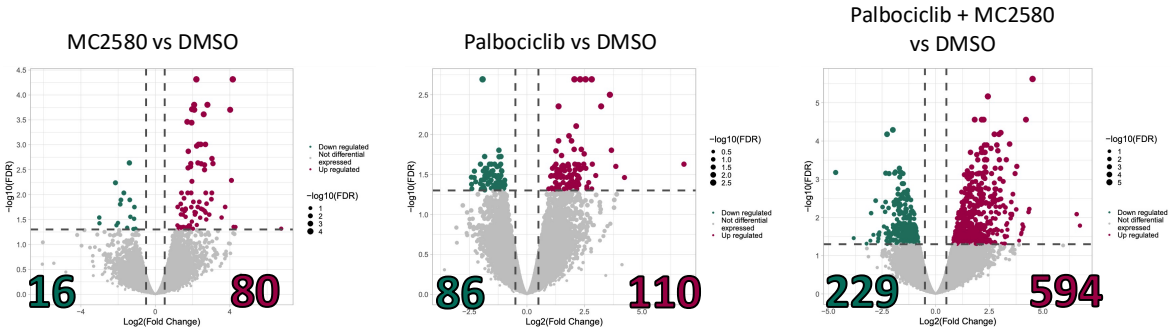

Figure 34. ***Prolongation of the G1 phase of the cell cycle leads to amplified accessible regions in presence of LSD1 inhibitor****. Volcano plots, representing DARs (vs DMSO) based on the ATAC-seq results in NB4 cells in their G1 phase, 72 hours post LSD1 inhibition with the same treatment conditions as in Figure 33.*

2.2. Enhancer and super enhancer landscape is altered upon G1 lengthening

Following our hypothesis, the second point to investigate was to assess if the actual enhancer landscape of AML cells changes upon lengthening of the G1 phase. To achieve this, we examined the presence of H3K27ac, a marker for enhancers, under the same previous experimental conditions using chromatin immunoprecipitation with sequencing (ChIP-seq). Initially, we could observe nearly five thousand unique H3K27ac ChIP-seq peaks appearing exclusively with Palbociclib singular treatment (Figure 35). Considering the functional relevance of SEs in regulating the differentiation process, we decided to quantify them for each treatment (Hnisz *et al.*, 2013; Jia, Chng and Zhou, 2019). This analysis revealed the effectiveness of Palbociclib singular treatment in changing the total number of SEs and enhancing the effect of MC2580, when combined together (Figure 36). Our ChIP-seq findings, further supported chromatin accessibility studies, showing that prolonging the G1 phase can be enough to change the enhancer and SE landscape of AML cells. This can also be an initial point towards the possibly facilitated enhancer-promoter interactions for differentiation-inducing genes, necessary for LSD1 inhibitor impact.

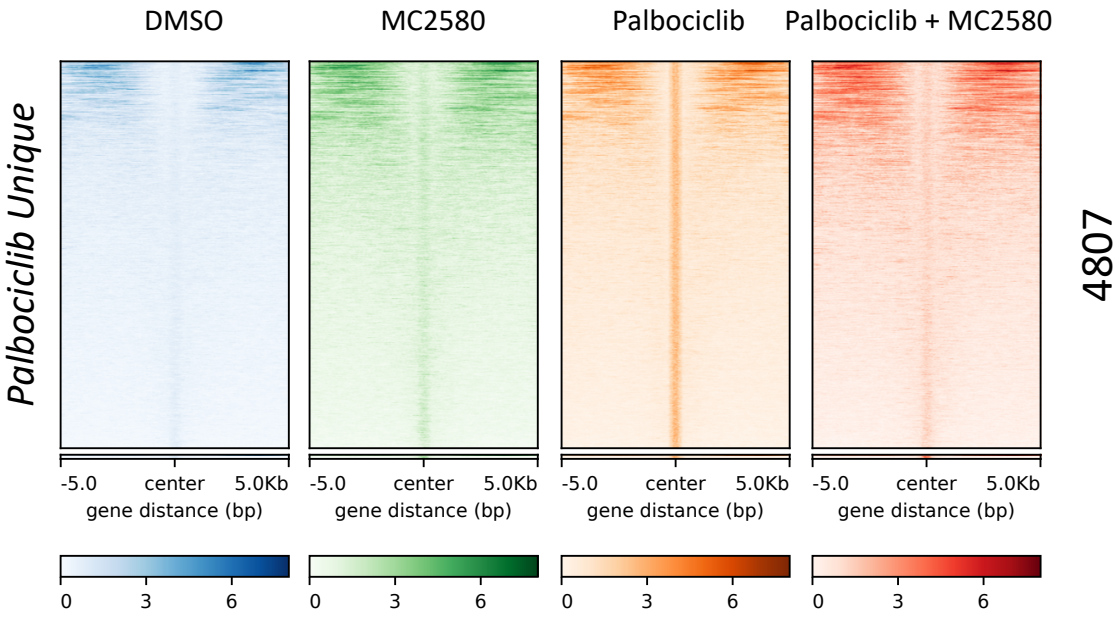

Figure 35. ***Prolongation of the G1 phase of the cell cycle leads to unique H3K27ac enrichment****. Heatmaps, representative of unique H3K27ac peaks in NB4 cells to 50nM Palbociclib based on ChIP-seq analysis. Cells are in their G1 phase and treated with vehicle (DMSO) or 2µM MC2580 or 50nM Palbociclib or combination of 2µM MC2580 + 50nM Palbociclib, 72 hours post LSD1 inhibition.*

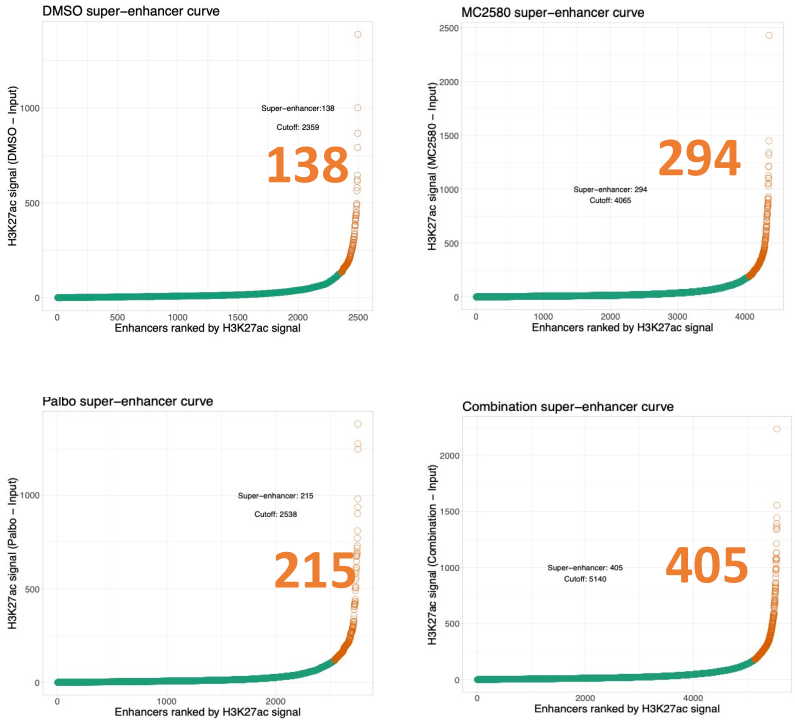

Figure 36. ***Prolongation of the G1 phase of the cell cycle leads to amplified super enhancer formation in presence of LSD1 inhibitor****. Enhancers plot based on increasing background-subtracted peak intensity based on the H3K27ac ChIP-seq of NB4 cells in their G1 phase, in the same treatment conditions as in Figure 35. Peaks with signals above the uniquely-calculated inflection points are defined as SE.*

2.3. Epigenetic landscape of AML cells changes upon G1 lengthening

Observing how extending the G1 phase affects chromatin accessibility and the distribution of H3K27Ac indicated the possibility of a broader, systemic epigenetic transformation. To investigate this possibility, we decided to quantify a comprehensive list of hPTMs in a bulk population of NB4 cells, being treated with either DMSO or Palbociclib, using an unbiased mass spectrometry (MS) approach (Noberini *et al.*, 2020). This investigation revealed a global change in the epigenetic landscape of NB4 cells in response to G1-lengthening, which for the majority of hPTMs shown to be highly stable over time (Figure 37). This observation led us to speculate whether this change is specific to a particular phase of the cell cycle. Consequently, we refined our analysis, applying the same approach at a phase-specific level. As a result, we could immediately notice, that the formerly discovered changes in hPTM quantities are highly stable throughout all phases of the cell cycle (Figure 38). Taken together, these investigations made clear that extending the G1 phase in AML cells can bring about a comprehensive alteration in their epigenetic profile, notably impacting all cell cycle phases.

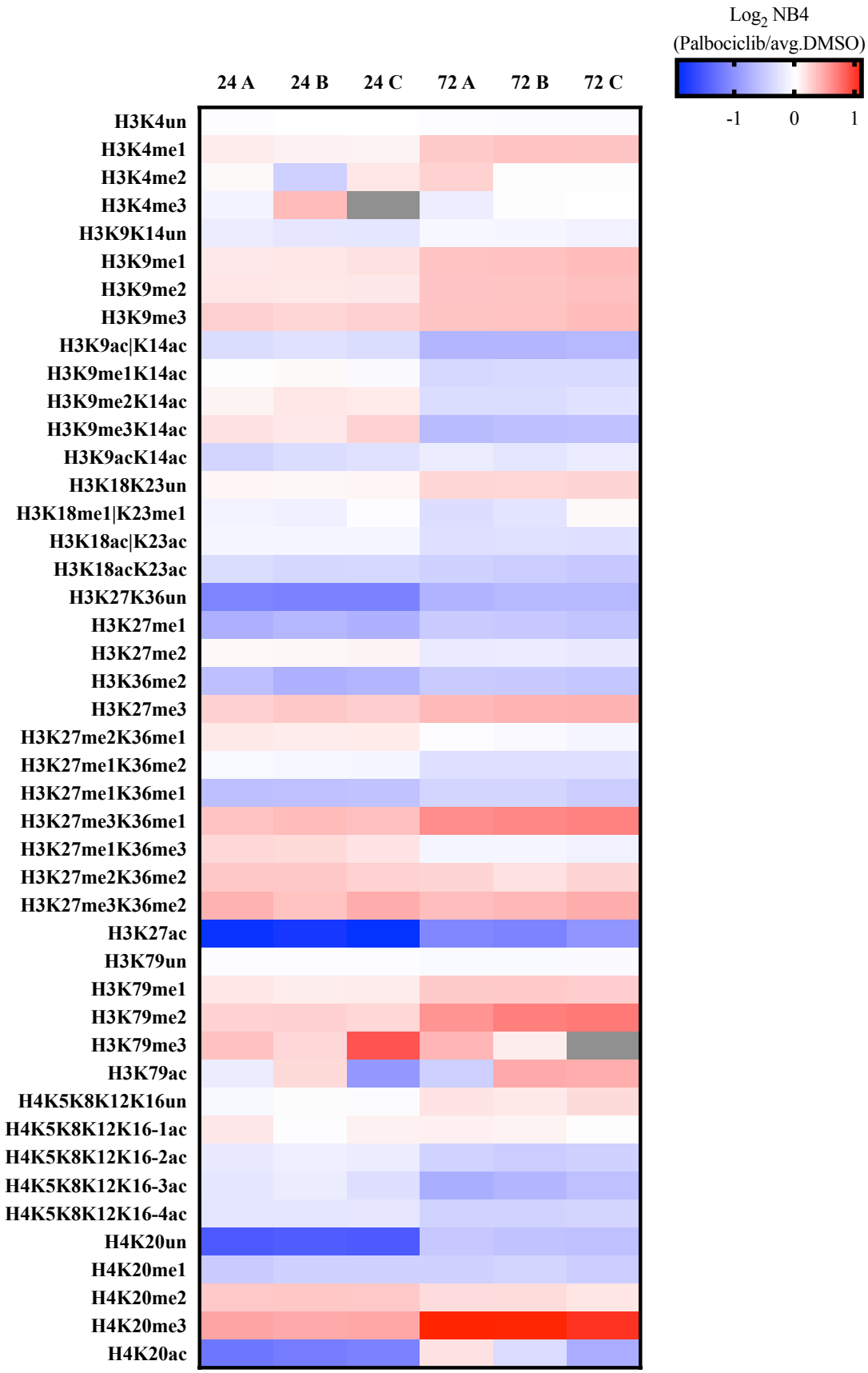

Figure 37. ***Epigenetic profile of NB4 cells change upon G1-prolongation****. Heatmap, representing quantification of hPTMs by MS in triplicates (indicated as A-C) for two time points of 24hrs and 72hrs (indicated as 24 and 72, respectively) of NB4 cells treated with 50nM Palbociclib normalized over corresponding controls treated with vehicle (DMSO) in the same time-course. Red and Blue shades present increase or decrease of each indicated mark, respectively.*

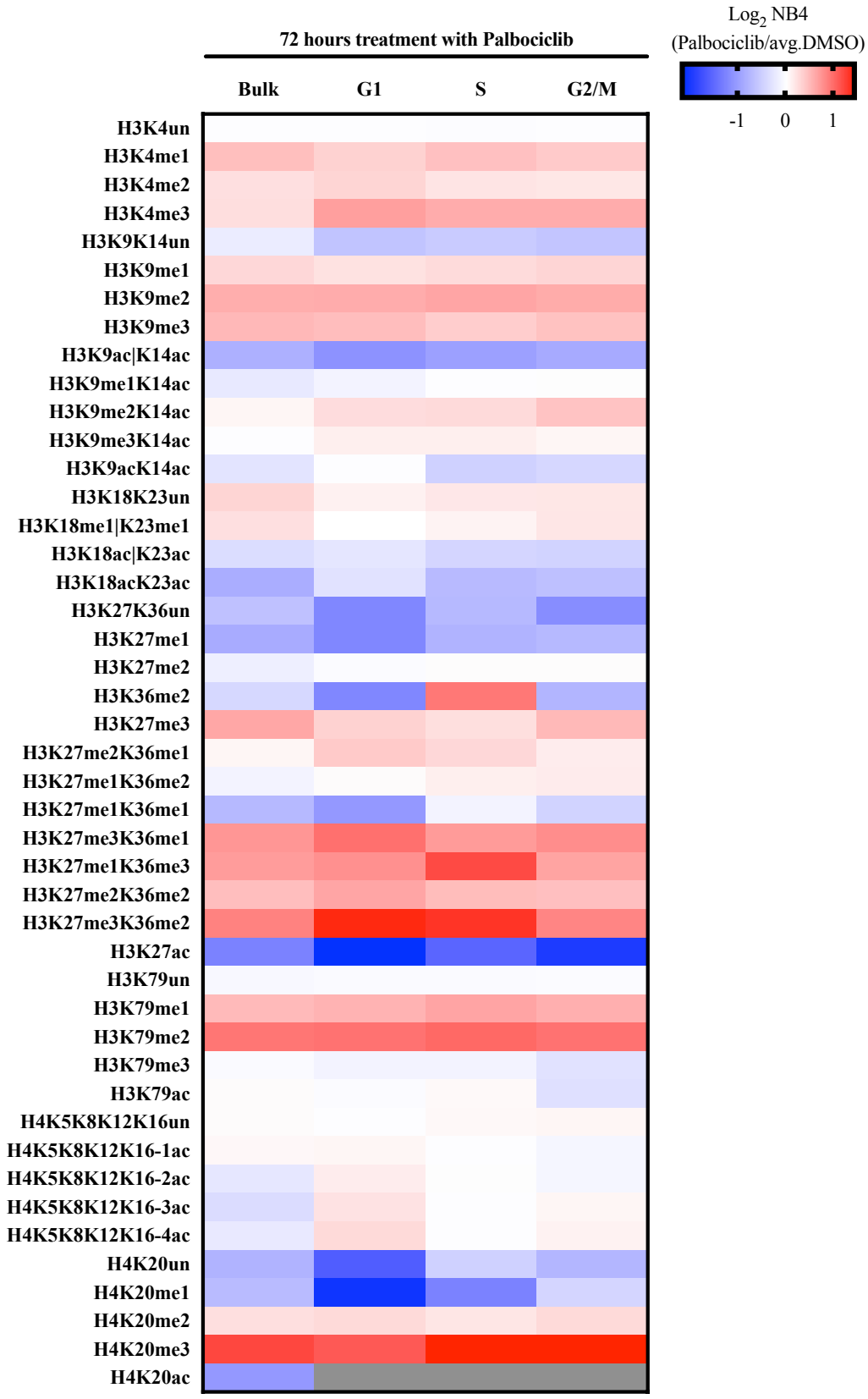

Figure 38. ***The change in the epigenetic profile of G1-extended NB4 cells does not depend on the different distribution of cells in the various phases of the cell cycle****. Heatmap, representing quantification of hPTMs at bulk population or separated by cell cycle phases, by MS as average of triplicates for 72hrs of NB4 cells treated with 50nM Palbociclib normalized over corresponding controls treated with vehicle (DMSO) in the same time-course and cell population. Data is presented in logarithmic scale. Red and Blue shades present increase or decrease of each indicated mark, respectively.*

2.4. Epigenetic landscape of fast-cycling AML cells become more similar to slow-cycling counterparts upon G1 lengthening

To explore the connection between the observed alterations in the epigenetic profile of G1-extended NB4 cells and their heightened sensitivity to LSD1 inhibition, we needed to determine whether the epigenetic landscape of NB4 cells differs from that of naturally slow-cycling AML cell lines. If we identified substantial differences, our next step was to investigate whether G1-lengthening was actually causing the typically fast-cycling NB4 cells to resemble the naturally slow-cycling cell lines. To address the first question, we performed MS analysis on basal hPTM levels of NB4 cells in comparison to UF-1 and Kasumi-1 cells (representing the slow-cycling phenotype). Our investigation clearly demonstrated that the slow-cycling cell lines, UF-1 and Kasumi-1, share a highly similar epigenetic profile, which significantly differs from that of NB4 cells (Figure 39). Subsequently, we assessed whether the changes in hPTM quantities induced by extending the G1 phase in NB4 cells were aligning them more closely with the baseline levels found in naturally slow-cycling cells. This comparative analysis unveiled specific hPTM levels in the slow-cycling cells, which were consistently replicated by the NB4 cells treated with Palbociclib (Figure 40).

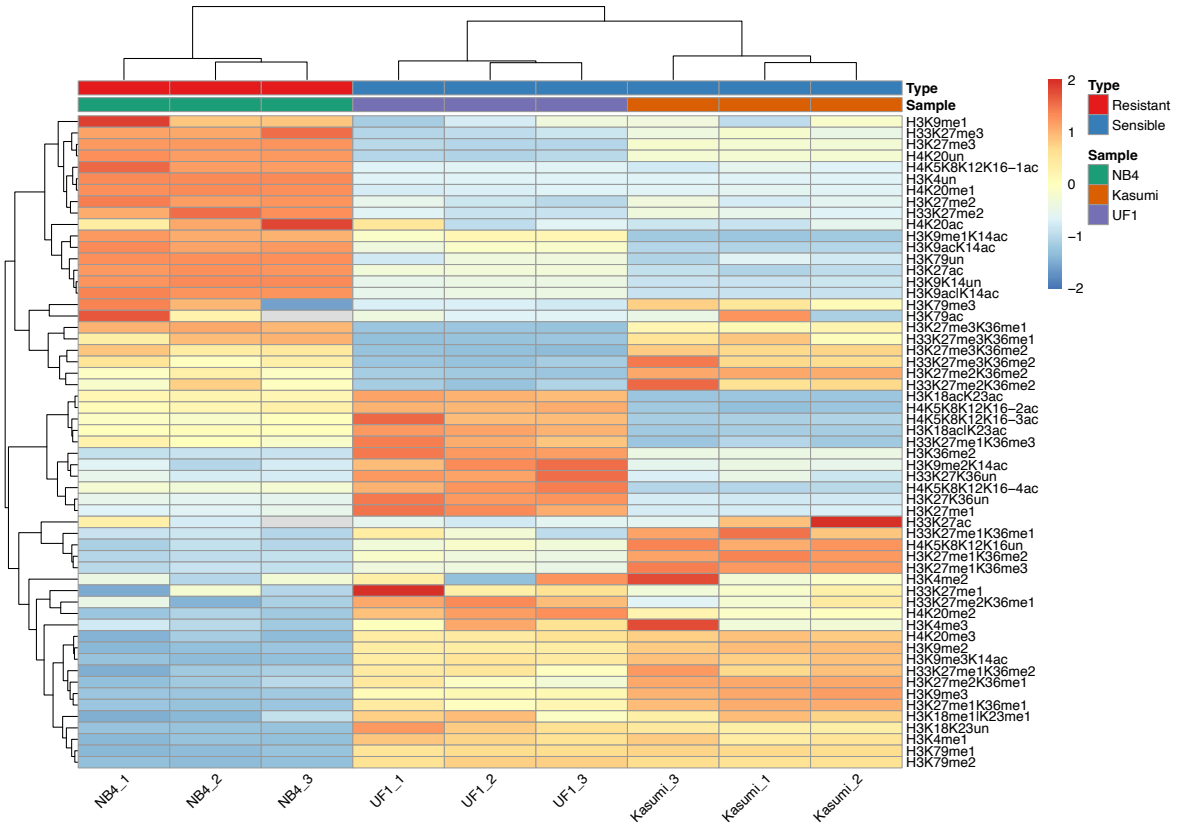

Figure 39. ***Epigenetic profile of slow-cycling AML cells is similar to each other, and differ to that of the fast-cycling AML cells****. Clustered heatmaps, representing quantification of basal hPTMs in triplicates of NB4, UF-1 and Kasumi-1 cell lines. Sensitivity and resistance to MC2580 is being indicated as red and blue boxes at the top of heatmaps, respectively.*

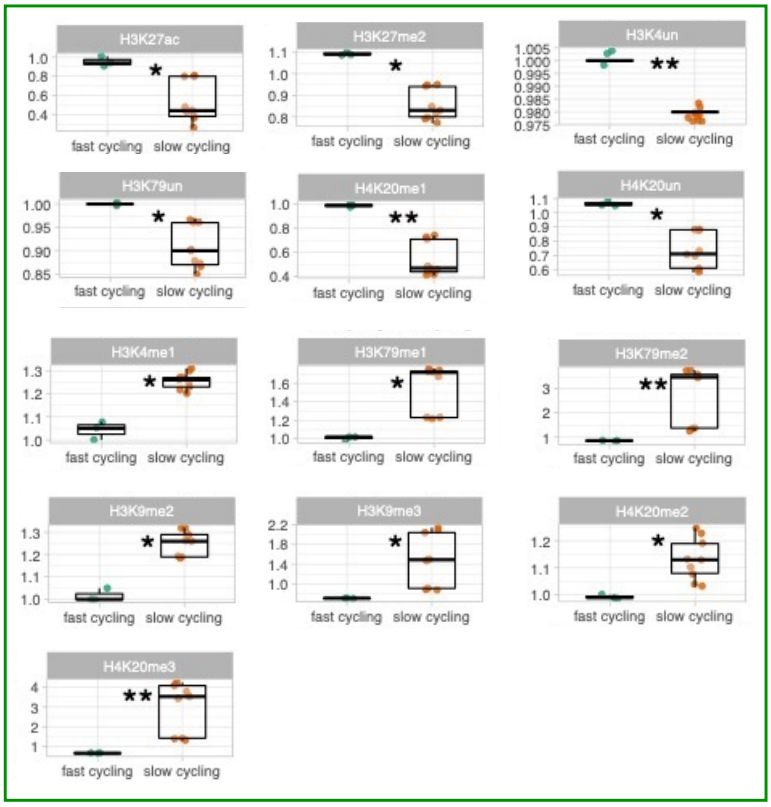

Figure 40. ***G1-extended and naturally slow-cycling AML cells have several comparable hPTM levels, compared to that of the fast-cycling AML cells****. Upper panel shows box-plots representing quantification of hPTMs in triplicates by MS analysis of 72hrs vehicle (DMSO) treated NB4 cells (labeled as fast-cycling); and 72hrs 50nM Palbociclib treated NB4 cells, and untreated UF-1 and Kasumi-1 cells (labeled as slow-cycling). Green boxes highlight single hPTMs, which have the same trend of difference in the slow-cycling vs fast-cycling AML cells, and present statistically significant state of difference. The selected hPTMs are represented in the lower panel separately. Data were statically analyzed using Wilcoxon test. P value < 0.05 (✱) and P < 0.001 (✱ ✱).*

Next, we selected these single hPTMs and performed a principal component analysis (PCA), based on the quantities of these marks in NB4 cells treated with either DMSO or Palbociclib, both at bulk and cell cycle phase-separated levels, compared to the UF-1 and Kasumi-1 cells. This investigation unveiled that G1-lengthening not only induces NB4 cells to more closely resemble the epigenetic profile of slow-cycling AML cells but also that these changes occur consistently across all phases of the cell cycle (Figure 41). Consequently, the observed epigenetic transformation we've described cannot be attributed solely to a higher proportion of cells being in the G1 phase of the cell cycle.

Building on our initial findings that highlight the crucial role of cell cycle speed in shaping AML cell responsiveness to LSD1 inhibitors, we've pinpointed the G1 phase as the key temporal window in this mechanism. Using a pharmacological method, we successfully extended the duration of the G1 phase, without hindering overall cell proliferation or affecting other cell cycle phases. This targeted manipulation led to significant alterations in the chromatin attributes of NB4 cells, including changes in chromatin accessibility, enhancer and SE architecture, and the overall hPTM profile. Remarkably, these shifts made the naturally fast-cycling NB4 cells more similar to slower-cycling lines, UF-1 and Kasumi-1. Thus, we conclude that pharmacologically induced elongation of the G1 phase in AML cells is an effective strategy for epigenomic remodeling, concurrently heightening their susceptibility to LSD1 inhibition.

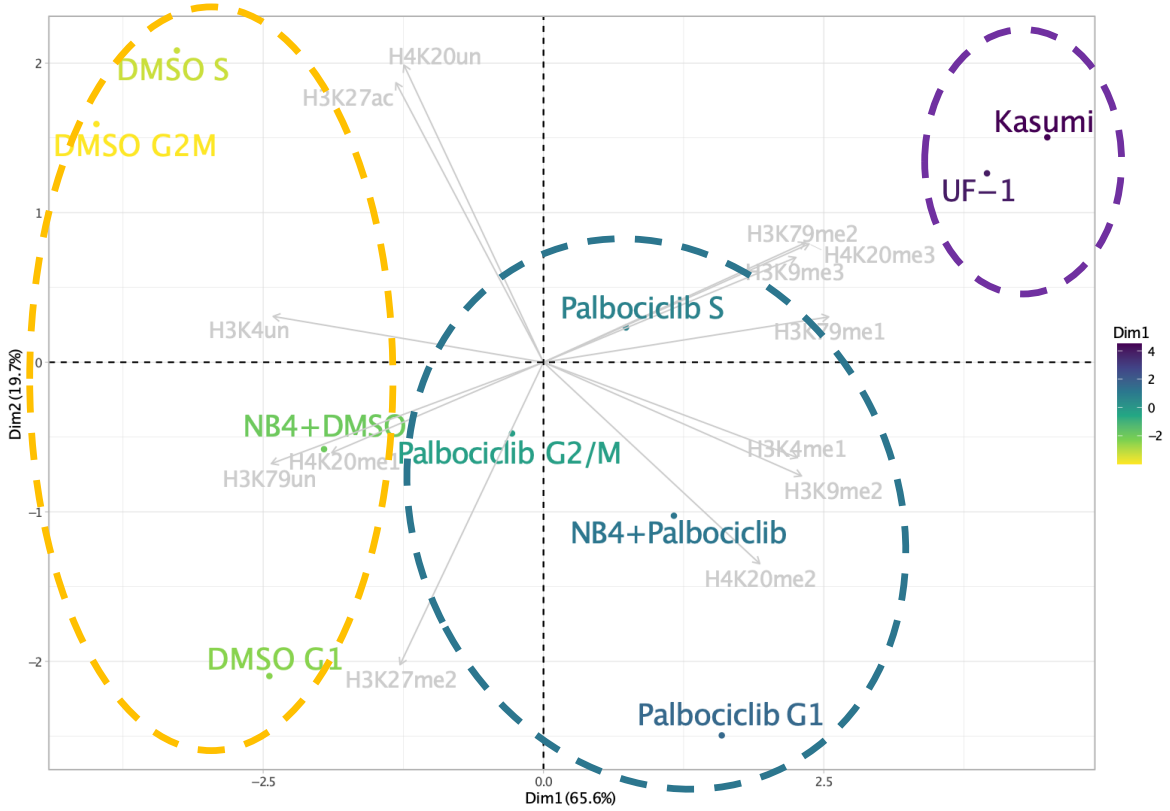

Figure 41. ***G1-prolongation makes the epigenetic profile of NB4 cells more similar to slow-cycling UF-1 and Kasumi-1 cells, in a non-cell-cycle dependent manner****. PCA of hPTMs mentioned formerly for UF-1, Kasumi-1 and NB4 treated with vehicle (DMSO) or 50nM Palbociclib for 72 hours. Dimension 1 (X axis) and dimension 2 (Y axis) explain nearly 90% of the variability present in the data. Gray arrows indicate original directions: Same directions are positively correlated hPTMs; orthogonal directions are uncorrelated hPTMs; opposite directions are negatively correlated hPTMs.*

3. Epigenetic landscape of G1-extended AML cells favors differentiation

Arriving at this stage of our study, the main question was **how the epigenetic landscape correlating with the longer G1 phase in AML cells, contribute to differentiation induction through LSD1 inhibition**. To answer such question, we had to evaluate the newly acquired qualities of the chromatin upon G1-prolongation and try to find a possible mechanistic link to differentiation induction in AML. Considering the dependency of hematopoietic differentiation on the activity of particular TFs, we evaluated whether this new state of chromatin is actually favoring the binding of those TFs. The aim was to look at the events

initiating the differentiation process. So, we had to focus on the outset of the co-treatment to conduct our investigations. With these considerations in mind, ***we investigated accessibility vs repression of the chromatin of the fast-cycling AML cells upon G1 elongation, in presence or absence of LSD1 inhibitor at early treatment time-point***.

3.1. Key hematopoietic TFs have increased accessibility to chromatin in G1-extended AML cells

In order to discover the changes of chromatin accessibility during the initiation of differentiation, we conducted the same former treatment regimen in NB4 cells (Figure 30B). Next, we performed ATAC-seq investigations 24 hours through the co-treatment within the cells in their G1 phase. Our first observation was the appearance of unique ATAC-seq peaks for each treatment and mutually between separate treatments, and we focused on the exclusive peaks for Palbociclib, Palbociclib + MC2580 and their mutual impact (Figure 42A). We could visualize these unique signal peaks as 11060 peaks for Palbociclib, 13853 for Palbociclib + MC2580, and 6951 mutual among the two conditions (Figure 42B).

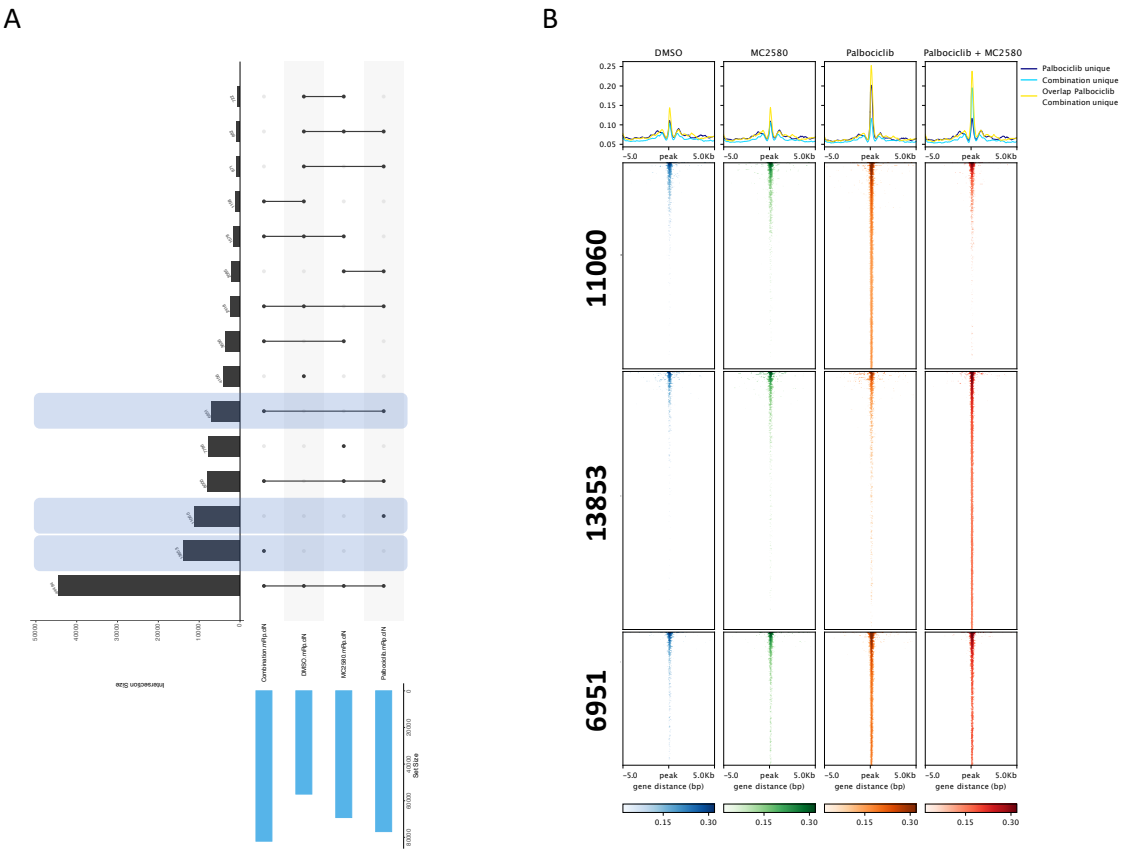

Figure 42. ***Early exclusive and mutual chromatin openings in NB4 cells upon G1-extension and LSD1 inhibition****. (A) Bar charts representing unique and mutual ATAC-seq peaks in NB4 cells to different treatments. Cells are in their G1 phase and treated with vehicle (DMSO) or 2μM MC2580 or 50nM Palbociclib or combination of 2μM MC2580 + 50nM Palbociclib, 24 hours post LSD1 inhibition. (B) Heatmaps representing unique ATAC-seq peaks in NB4 cells to Palbociclib (up) and Palbociclib+MC2580 (middle) and mutual between the two treatments (down). Similar treatment conditions as in (A).*

For the succeeding step, we assessed the DARs upon each therapy compared to DMSO and discovered the majority of changes upon the combination of Palbociclib + MC2580, followed by singular Palbociclib, and MC2580 treatments (Figure 43). Next, we performed TF footprinting analysis on these data and noticed appearance of several binding motifs for specialized hematopoietic TFs, including SPI1, GFI1(b), C\EBP family of TFs, RUNX1, etc. upon G1-prolongation, and more pronounced upon combination with LSD1 inhibitor (Figure 44) (Bentsen *et al.*, 2020). This was initial evidence defining, that TFs required for differentiation induction by LSD1 inhibition, indeed have increased access to their binding sites in the G1-extended NB4 cells.

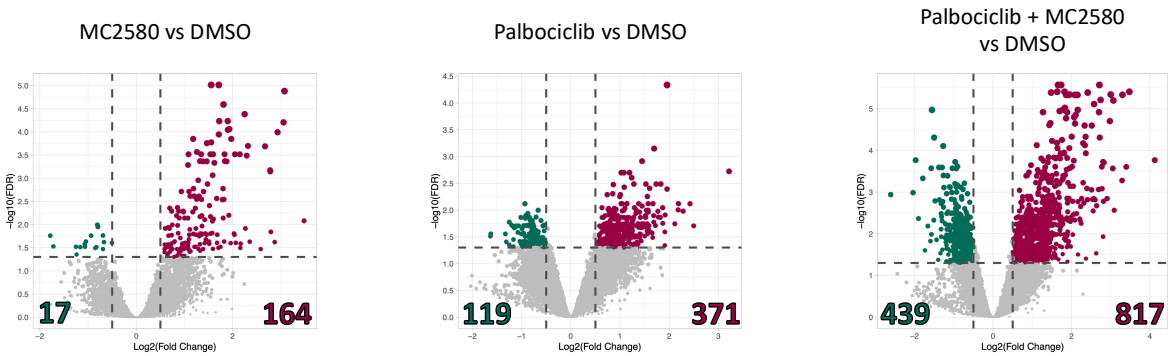

Figure 43. ***Early changes in differentially accessible chromatin regions of NB4 cells upon G1-extension and LSD1 inhibition****. DARs vs DMSO in NB4 cells treated with vehicle (DMSO) or 2µM MC2580 or 50nM Palbociclib or combination of 2µM MC2580 + 50nM Palbociclib, 24 hours post LSD1 inhibition.*

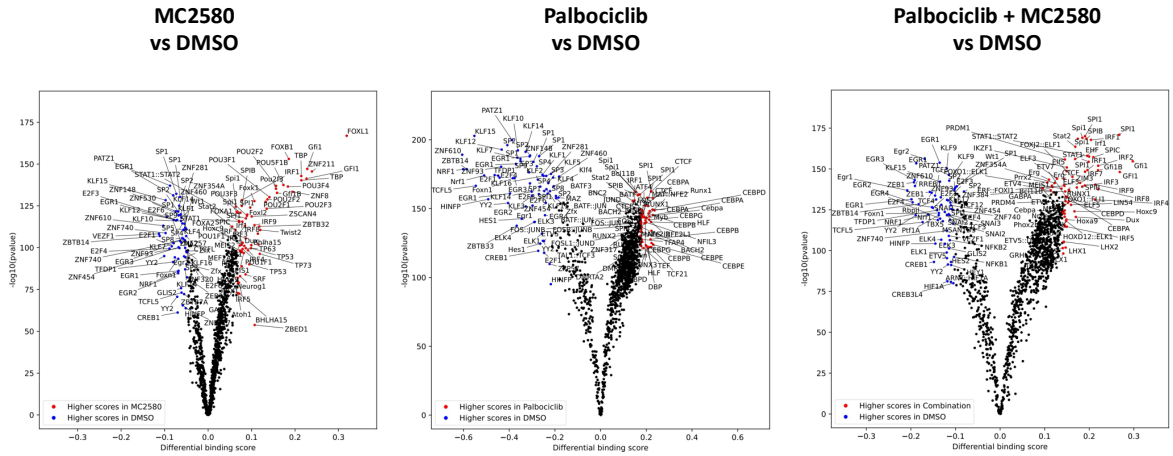

Figure 44. ***Early changes in TF activity in NB4 cells upon G1-extension and LSD1 inhibition****. Pairwise comparison of TF activity between treatments vs DMSO in NB4 cells treated with vehicle (DMSO) or 2µM MC2580 or 50nM Palbociclib or combination of 2µM MC2580 + 50nM Palbociclib, 24 hours post LSD1 inhibition. Red and Blue dots indicate significantly higher and lower binding scores (BS) for the annotated TFs, respectively, upon each treatment vs DMSO.*

3.2. Key hematopoietic TFs have decreased chromatin repression at their binding sites in G1-extended AML cells

In conjunction with our studies of accessible chromatin, we sought to investigate its counterpart, repressed chromatin. Our goal was to determine whether regions that become more accessible during the extended G1 phase, also experience a concurrent reduction in H3K27me3, a key repressive mark. Thus, we performed ChIP-seq investigations 24 hours through the co-treatment, following the previous treatment regimen (Figure 30B) within the NB4 cells in their G1 phase. First, looking at the chromatin regions with increased or decreased differential accessibilities (from the ATAC-seq data), we confirmed the reverse-correlation of such ATAC-seq peaks with the H3K27me3 enrichment ChIP-seq signals (Figure 45). Meaning that the two datasets represent reverse images of one another.

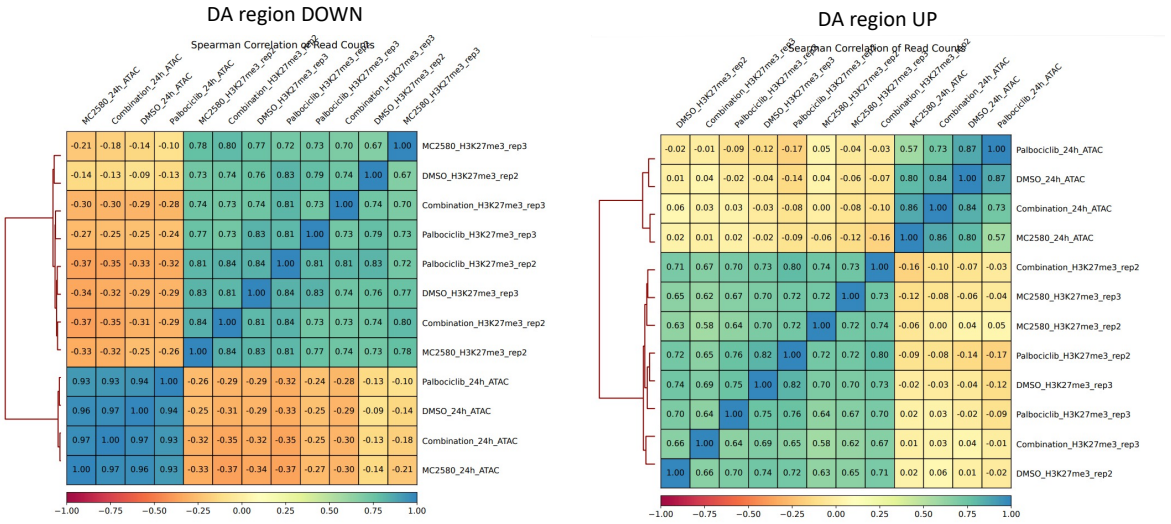

Figure 45. ***ATAC-seq detected chromatin regions with increased accessibility reverse-correlate with ChIP-seq detected H3K27me3-enriched regions****. Correlation plot, representing H3K27me3 enrichment and ATAC signal in genomic regions discovered to lose (left panel) or gain more (right panel) accessibility upon similar experimental conditions. Cells are in their G1 phase and treated with vehicle (DMSO) or 2μM MC2580 or 50nM Palbociclib or combination of 2μM MC2580 + 50nM Palbociclib, 24 hours post LSD1 inhibition.*

Consequently, we identified the facultative heterochromatin regions, by looking at H3K27me3-rich regions and performed TF motif discovery among these regions (Cai *et al.*, 2021). Initially, we could observe motifs belonging to the key TFs, to exhibit high intensity of H3K27me3 enrichment upon standalone MC2580 treatment (Figure 46). Interestingly, Palbociclib standalone treatment maintained or decreased those H3K27me3-enrichment zones, and once combined with MC2580, such repressive domains completely disappeared (Figure 46). Cross-interpretation of the ATAC-seq and H3K27me3 ChIP-seq studies suggest that extending the G1 phase gives higher chromatin accessibility to a spectrum of hematopoietic master regulators. Thus, we conclude that the epigenomic remodeling caused by the G1 lengthening can ultimately lead to a chromatin state, which evidently favors differentiation induction by an epigenetic therapy such as LSD1 inhibition. The direct demonstration of binding of the candidate TFs, however, is missing at this stage (see Discussion).

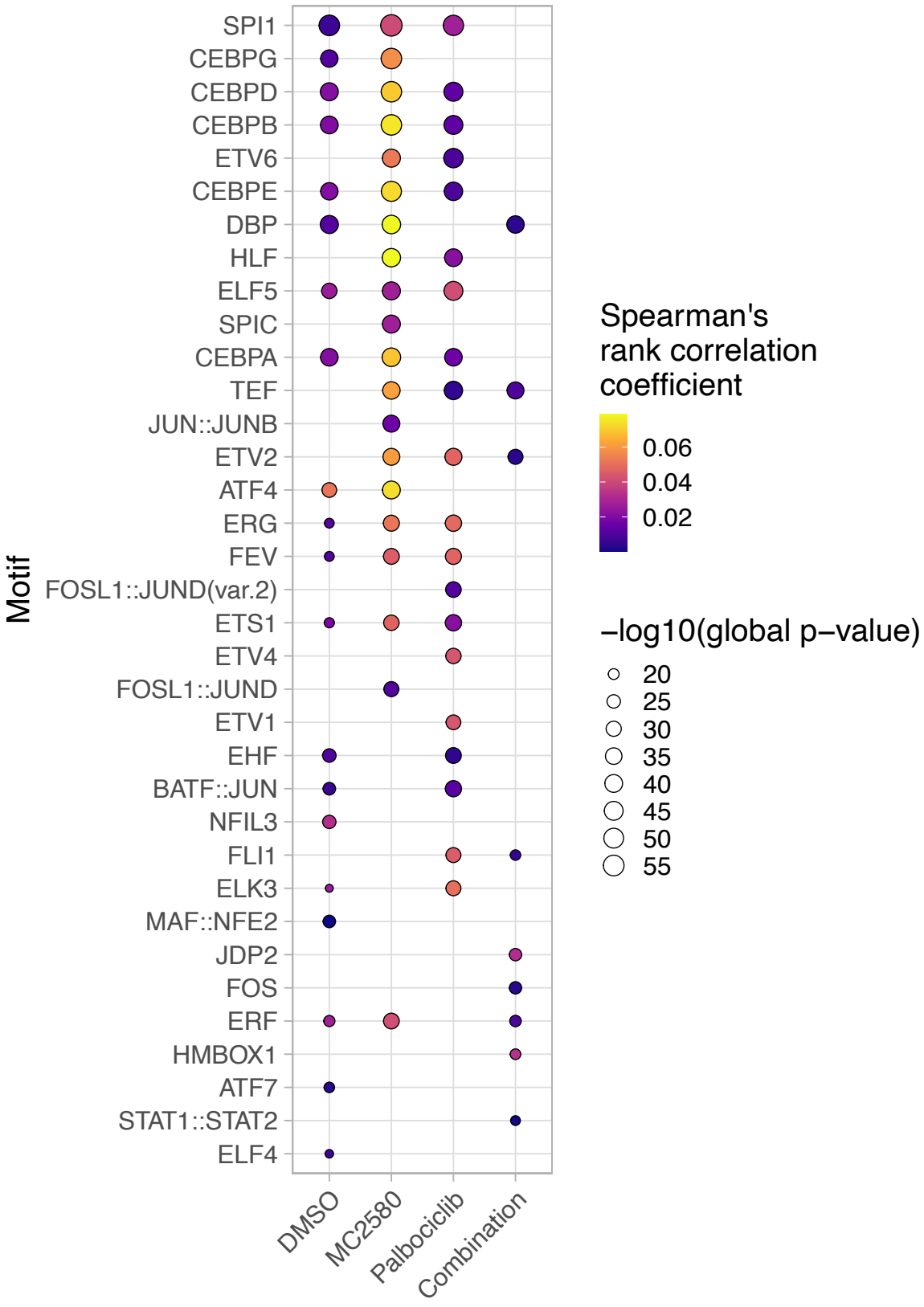

Figure 46. ***Early changes in repressed chromatin domains, covering TF motifs in NB4 cells upon G1-extension and LSD1 inhibition****. Bubble plot, representing H3K27me3-enriched TF motifs in NB4 cells treated with vehicle (DMSO) or 2µM MC2580 or 50nM Palbociclib or combination of 2µM MC2580 + 50nM Palbociclib, 24 hours post LSD1 inhibition.*

4. LSD1 inhibition induces differentiation, activating transposable elements in slow-cycling AML cells

Our research has shown that G1-prolongation leads to a broad range of epigenetic changes. Such a broad change, can lead to a very different orchestration of hPTMs, constructing a distinctive chromatin with newly accessible and repressed sites as formerly observed. In the context of inducing differentiation, such changes could impact a diverse array of pathways in presence of the relevant stimuli. This was deduced from examining the spectrum of the formerly discovered TF binding sites. Many of these TFs regulate hematopoiesis either through canonical or non-canonical mechanisms. We have formerly shown the involvement of the LSD1-GFI1b-SPI1 axis in differentiation induction through LSD1 inhibition in APL (Ravasio *et al.*, 2020). Furthermore, formerly discovered TFs in this study, including C\EBP family of TFs and RUNX1 are well-known to be regulating myeloid differentiation (Tenen, 2001; Puig-Kröger *et al.*, 2003; Alberich-Jordà *et al.*, 2012). However, we see the process of differentiation induction in AML as a complex rewiring happening in successive layers (Gruszka, Valli and Alcalay, 2017, 2017; Dhall *et al.*, 2019). Thus, it was interesting and crucial to **discover more comprehensively the underlying origins of differentiation induction by an epigenetic therapy like LSD1 inhibition in a broader spectrum of AML cells**, happening at such a widely poised epigenomic environment. To address this question, we decided to ***study the transcriptional changes happening prior to morphologic differentiation in the fast-cycling and slow-cycling AML cells***.

4.1. LSD1 inhibition in slow-cycling AML cells activates transcriptional differentiation cascades

As the first step in investigating the transcriptional changes in AML cells upon LSD1 inhibition at early time-points, we aimed to confirm that such changes are actually directed towards differentiation induction. Hence, we performed RNA-seq investigations in the fast-cycling (NB4 and PL-21) and slow-cycling (Kasumi-1) AML cell lines, following the classic treatment regimen we have been using so far, 24- and 72-hours post LSD1 inhibition. Then, we used these data to look at a spectrum of gene signatures associated with normal hematopoietic function. It immediately became evident that the combination of Palbociclib + MC2580 in NB4 and PL-21 cells, and MC2580 in Kasumi-1 cells causes a global increase in the enrichment of the majority of the relevant gene sets (Figure 47). This initial analysis made us realize that the transcriptional impact of LSD1 inhibition in AML cells with longer G1 is indeed aimed towards differentiation, regardless of the cell line. It also showed us that we chose the correct time-window to study the primary transcriptional events prior to differentiation, since the majority of the changes took place particularly in the first 24-hours. Hence, we could further study this time-window, aiming to decipher the origins of differentiation initiation upon LSD1 inhibition in AML cells.

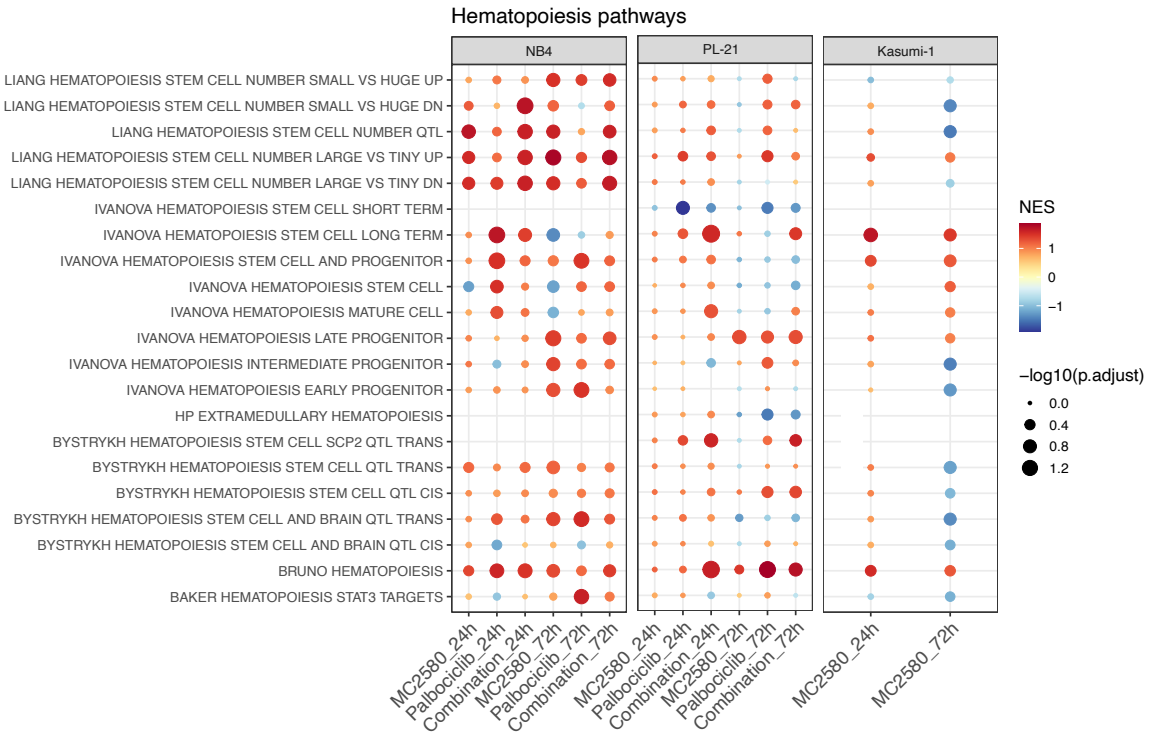

Figure 47. ***Increased enrichment of gene signatures correlating to normal hematopoiesis upon LSD1 inhibition in G1-extended NB4 cells.*** *Bubble plots representing selected gene sets evaluating normal hematopoietic transcriptional activity based on treatments vs DMSO, in NB4, PL-21, and Kasumi-1 cells treated with vehicle (DMSO) or 2µM MC2580 or 50nM Palbociclib or combination of 2µM MC2580 + 50nM Palbociclib, 24- and 72-hours post LSD1 inhibition. NES: normalized enrichment scores.*

4.2. LSD1 inhibition in slow-cycling AML cells upregulates spectrum of immune response genes

Next, we wanted to gain insights on the general transcriptomic changes in the fast-cycling and slow-cycling AML cells upon LSD1 inhibition. Hence, we looked through the RNA-seq data, aiming to discover the significant DEGs and subsequently the most significantly affected pathways. Among the NB4 cells, we observed most of the significant DEGs when Palbociclib combined with MC2580, and the highest upregulations in the first 24 hours compared to the most downregulation taking place after 72 hours of the co-treatment (Figure 48). Within the PL-21 cells, most of the significant DEGs detected similarly when

Palbociclib combined with MC2580, and the highest upregulations in the first 24 hours compared to the most downregulation taking place after 72 hours of the co-treatment (Figure 49). Lastly, MC2580 treatment in Kasumi-1 cells induced most of the significant DEGs 72 hours post-treatment (Figure 50). Overall evaluation of the DEGs confirm that the combination therapy in the fast-cycling and the LSD1 inhibition in the slow-cycling cells induce sufficient DEGs, potent to activate differentiation regulating pathways genes.

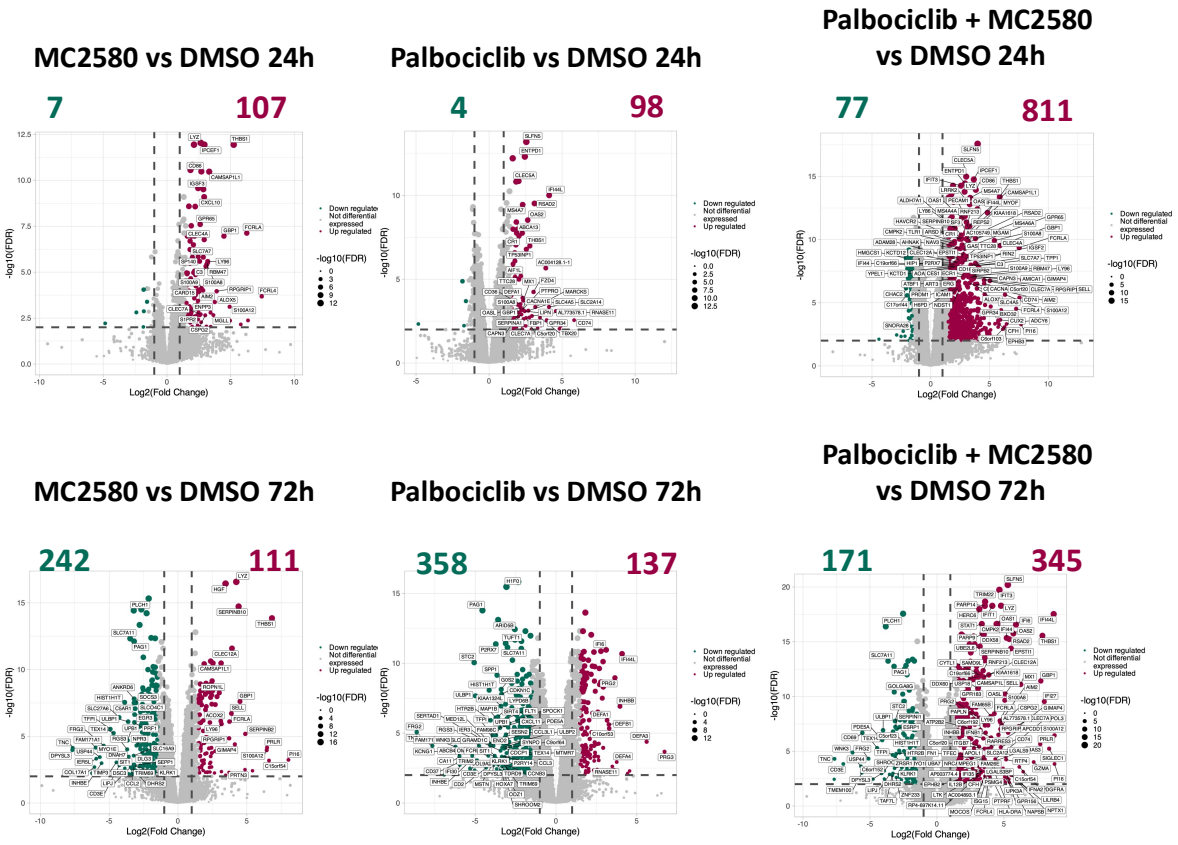

Figure 48. ***Amplified transcriptional impact of LSD1 inhibition in G1-extended NB4 cells.*** *Volcano plots, representing DEGs (treatment vs DMSO) in NB4 cells treated with vehicle (DMSO) or 2μM MC2580 or 50nM Palbociclib or combination of 2μM MC2580 + 50nM Palbociclib, 24- and 72-hours post LSD1 inhibition. Abs(logFC) > 1.5 and -logadjPval > 2.*

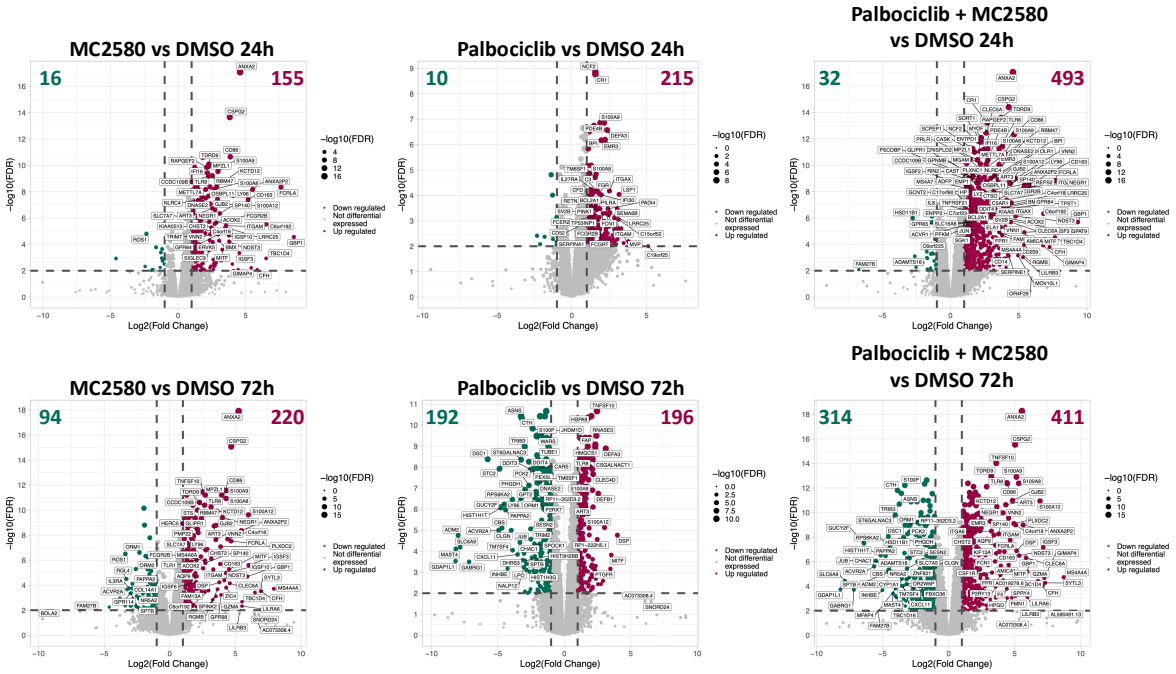

Figure 49. ***Amplified transcriptional impact of LSD1 inhibition in G1-extended PL-21 cells****. Volcano plots, representing DEGs (treatment vs DMSO) in PL-21 cells treated with vehicle (DMSO) or 2µM MC2580 or 50nM Palbociclib or combination of 2µM MC2580 + 50nM Palbociclib, 24- and 72-hours post LSD1 inhibition. Abs(logFC) > 1 and -logadjPval > 2.*

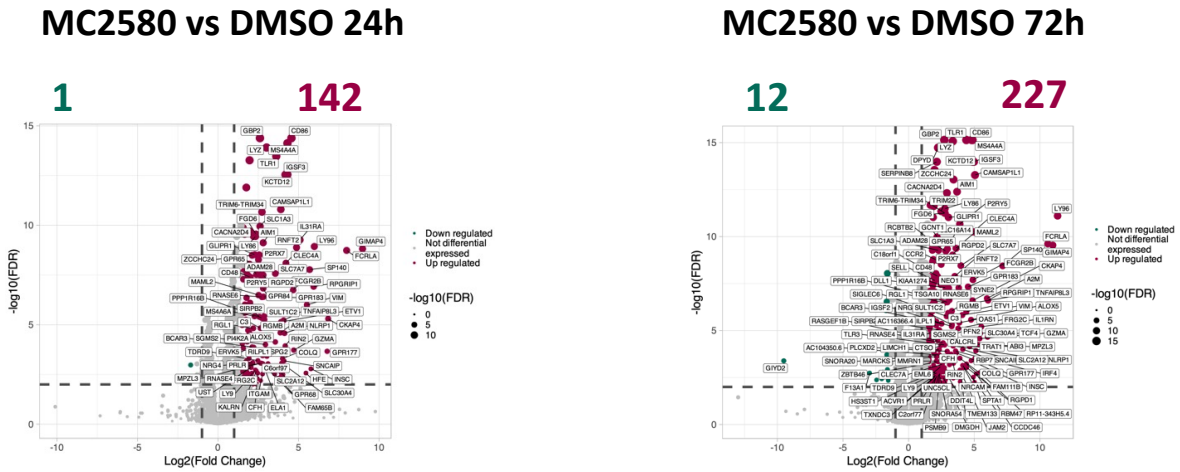

Figure 50. ***Transcriptional impact of LSD1 inhibition in Kasumi-1 cells****. Volcano plots, representing DEGs (treatment vs DMSO) in Kasumi-1 cells treated with vehicle (DMSO) or 2µM MC2580, 24- and 72-hours post LSD1 inhibition. Abs(logFC) > 1.5 and -logadjPval > 2.*

Ingenuity pathway analysis (IPA) and search for the mutually influenced pathways and regulators among the three cell lines upon different treatments identified the top 30 enriched pathways and the predicted upstream regulators, separately for each cell line (Figure 51-Figure 53). The data clearly indicates that in all three cell lines undergoing differentiation-inducing treatments, the predominant upregulated pathways are those related to microbial infection sensing, immune signaling, and subsequent immune response. We repeatedly encountered keywords indicating pathogen sensing, including pattern recognition receptors (PRRs), toll-like receptors (TLRs), NOD1/2, RIG-I-like receptors (RLRs), etc. This observation was followed by an overrepresentation of terms concerning immune response at large scale, such as interferon signaling, cytokine storm, etc. Finally, immune response activation keywords were enriched, for example macrophage activation, phagosome formation, immunogenic cell death signaling, etc. Additionally, evaluation of the upstream regulators among all the conditions further confirmed the pathway analysis, by showing a clear enrichment for immune response-regulators. Taken together, these observations hint to the possible involvement of an immune activating phenomenon to play a role in the initiating phases of differentiation induction through LSD1 inhibition in AML.

A

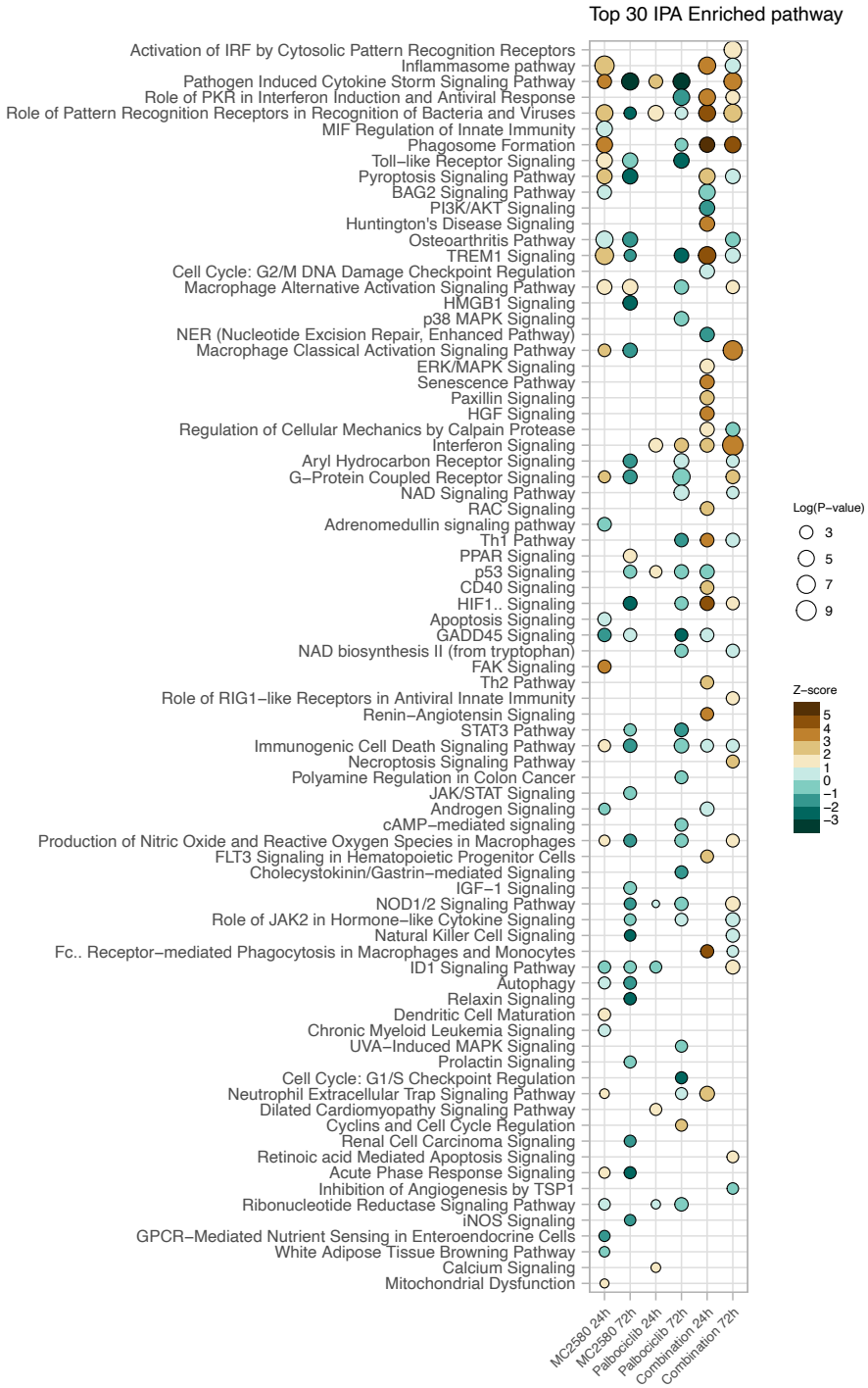
Top 30 IPA Enriched pathway
Activation of IRF by Cytosolic Pattern Recognition Receptors
Inflammasome pathway
Pathogen Induced Cytokine Storm Signaling Pathway
Role of PKR in Interferon Induction and Antiviral Response
Role of Pattern Recognition Receptors in Recognition of Bacteria and Viruses
MIF Regulation of Innate Immunity
Phagosome Formation
Toll–like Receptor Signaling
Pyroptosis Signaling Pathway
BAG2 Signaling Pathway
PI3K/AKT Signaling
Huntington's Disease Signaling
Osteoarthritis Pathway
TREM1 Signaling
Cell Cycle: G2/M DNA Damage Checkpoint Regulation
Macrophage Alternative Activation Signaling Pathway
HMGB1 Signaling
p38 MAPK Signaling
NER (Nucleotide Excision Repair, Enhanced Pathway)
Macrophage Classical Activation Signaling Pathway
ERK/MAPK Signaling
Senescence Pathway
Paxillin Signaling
HGF Signaling
Regulation of Cellular Mechanics by Calpain Protease
Interferon Signaling
Aryl Hydrocarbon Receptor Signaling
G–Protein Coupled Receptor Signaling
NAD Signaling Pathway
RAC Signaling
Adrenomedullin signaling pathway
Th1 Pathway
PPAR Signaling
p53 Signaling
CD40 Signaling
HIF1.. Signaling
Apoptosis Signaling
GADD45 Signaling
NAD biosynthesis II (from tryptophan)
FAK Signaling
Th2 Pathway
Role of RIG1–like Receptors in Antiviral Innate Immunity
Renin–Angiotensin Signaling
STAT3 Pathway
Immunogenic Cell Death Signaling Pathway
Necroptosis Signaling Pathway
Polyamine Regulation in Colon Cancer
JAK/STAT Signaling
Androgen Signaling
cAMP–mediated signaling
Production of Nitric Oxide and Reactive Oxygen Species in Macrophages
FLT3 Signaling in Hematopoietic Progenitor Cells
Cholecystokinin/Gastrin–mediated Signaling
IGF–1 Signaling
NOD1/2 Signaling Pathway
Role of JAK2 in Hormone–like Cytokine Signaling
Natural Killer Cell Signaling
Fc.. Receptor–mediated Phagocytosis in Macrophages and Monocytes
ID1 Signaling Pathway
Autophagy
Relaxin Signaling
Dendritic Cell Maturation
Chronic Myeloid Leukemia Signaling
UVA–Induced MAPK Signaling
Prolactin Signaling
Cell Cycle: G1/S Checkpoint Regulation
Neutrophil Extracellular Trap Signaling Pathway
Dilated Cardiomyopathy Signaling Pathway
Cyclins and Cell Cycle Regulation
Renal Cell Carcinoma Signaling
Retinoic acid Mediated Apoptosis Signaling
Acute Phase Response Signaling
Inhibition of Angiogenesis by TSP1
Ribonucleotide Reductase Signaling Pathway
iNOS Signaling
GPCR–Mediated Nutrient Sensing in Enteroendocrine Cells
White Adipose Tissue Browning Pathway
Calcium Signaling
Mitochondrial Dysfunction
MC2580 24h
MC2580 72h
Palbociclib 24h
Palbociclib 72h
Combination 24h
Combination 72h
Log(P–value)
3
5
7
9
Z–score
5
4
3
2
1
0
−1
−2
−3

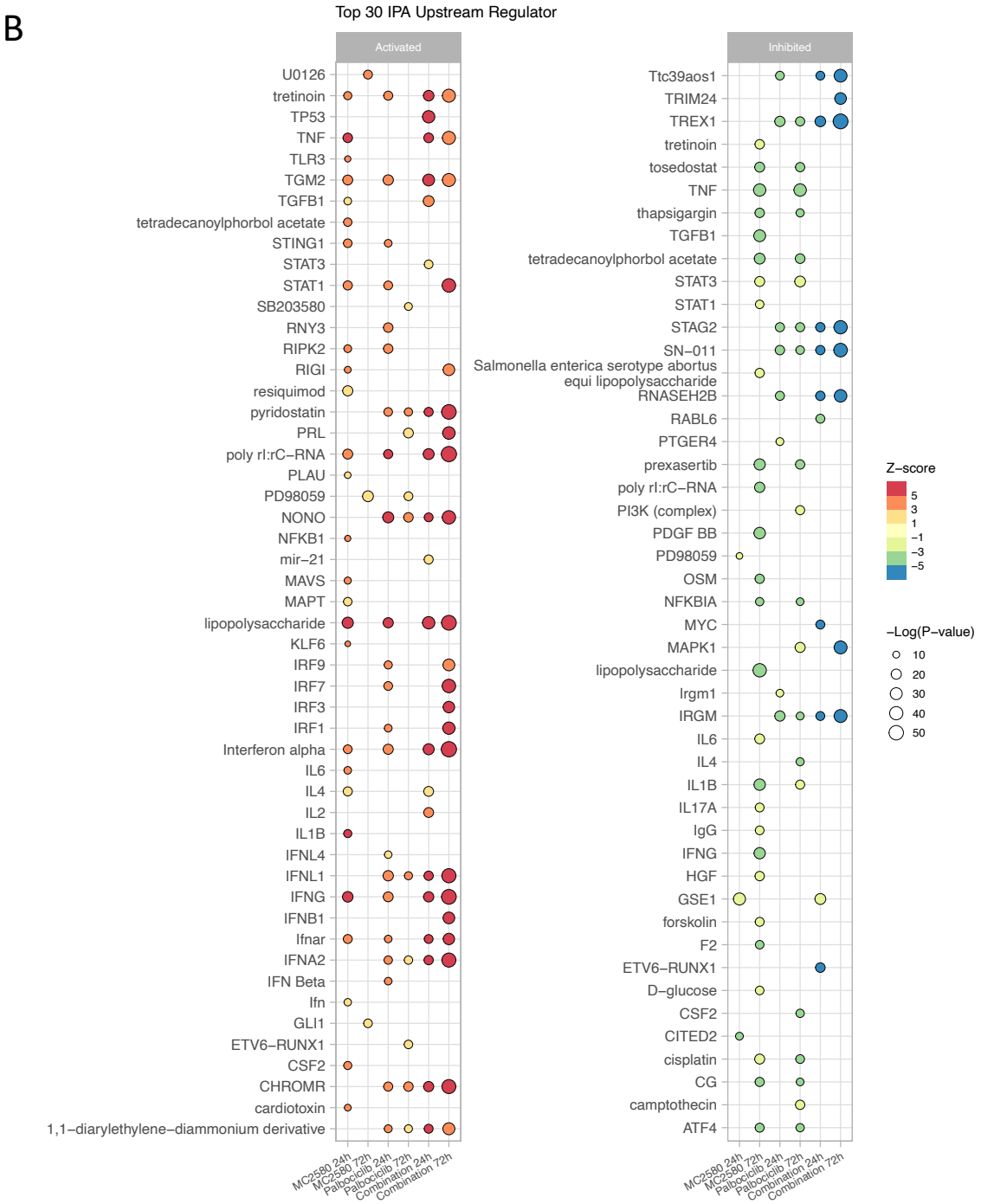

Figure 51. ***Top 30 enriched pathways and upstream regulators upon G1-prolongation and LSD1 inhibition in NB4 cells.*** *(A) IPA top 30 enriched pathways in NB4 cells treated with 2μM MC2580 or 50nM Palbociclib or combination of 2μM MC2580 + 50nM Palbociclib vs vehicle (DMSO), 24- and 72-hours post LSD1 inhibition. (B) Top 30 upstream regulators correlating to (A).*

A


Top 30 IPA Enriched pathway
NAD Signaling Pathway
Cholesterol Biosynthesis III (via Desmosterol)
Cholesterol Biosynthesis II (via 24,25–dihydrolanosterol)
Cholesterol Biosynthesis I
tRNA Charging
TREM1 Signaling
Zymosterol Biosynthesis
Phagosome Formation
Ferroptosis Signaling Pathway
Pyroptosis Signaling Pathway
S100 Family Signaling Pathway
Role of Pattern Recognition Receptors in Recognition of Bacteria and Viruses
Neutrophil Extracellular Trap Signaling Pathway
Macrophage Classical Activation Signaling Pathway
Inflammasome pathway
Superpathway of Cholesterol Biosynthesis
Complement System
LXR/RXR Activation
Mevalonate Pathway I
RAC Signaling
Immunogenic Cell Death Signaling Pathway
IL–8 Signaling
Toll–like Receptor Signaling
Pathogen Induced Cytokine Storm Signaling Pathway
CLEAR Signaling Pathway
Superpathway of Geranylgeranyldiphosphate Biosynthesis I (via Mevalonate)
IL–10 Signaling
Macrophage Alternative Activation Signaling Pathway
Leukocyte Extravasation Signaling
RAR Activation
IL–12 Signaling and Production in Macrophages
HMGB1 Signaling
DHCR24 Signaling Pathway
Dermatan Sulfate Biosynthesis
LPS/IL–1 Mediated Inhibition of RXR Function
HIF1.. Signaling
NOD1/2 Signaling Pathway
Adrenomedullin signaling pathway
G–Protein Coupled Receptor Signaling
Dermatan Sulfate Biosynthesis (Late Stages)
UVB–Induced MAPK Signaling
GNRH Signaling
Integrin Signaling
Apelin Endothelial Signaling Pathway
Prolactin Signaling
HGF Signaling
Signaling by Rho Family GTPases
Th1 Pathway
ID1 Signaling Pathway
Chondroitin Sulfate Biosynthesis (Late Stages)
Oxytocin In Brain Signaling Pathway
Regulation of Cellular Mechanics by Calpain Protease
Tumor Microenvironment Pathway
fMLP Signaling in Neutrophils
Inhibition of Angiogenesis by TSP1
FAK Signaling
IL–33 Signaling Pathway
CXCR4 Signaling
p38 MAPK Signaling
Growth Hormone Signaling
GPCR–Mediated Nutrient Sensing in Enteroendocrine Cells
eNOS Signaling
Th2 Pathway
Fc.. Receptor–mediated Phagocytosis in Macrophages and Monocytes
Wound Healing Signaling Pathway
Macropinocytosis Signaling
NF–..B Activation by Viruses
G Beta Gamma Signaling
Corticotropin Releasing Hormone Signaling
Role of PKR in Interferon Induction and Antiviral Response
Role of Tissue Factor in Cancer
cAMP–mediated signaling
Insulin Secretion Signaling Pathway
Activin Inhibin Signaling Pathway
Crosstalk between Dendritic Cells and Natural Killer Cells
ABRA Signaling Pathway
Myelination Signaling Pathway
Renin–Angiotensin Signaling
MSP–RON Signaling In Cancer Cells Pathway
Protein Kinase A Signaling
MC2580 24h
MC2580 72h
Palbociclib 24h
Palbociclib 72h
Combination 24h
Combination 72h
Log(P–value)
3
5
7
9
Z–score
5
4
3
2
1
0
−1
−2

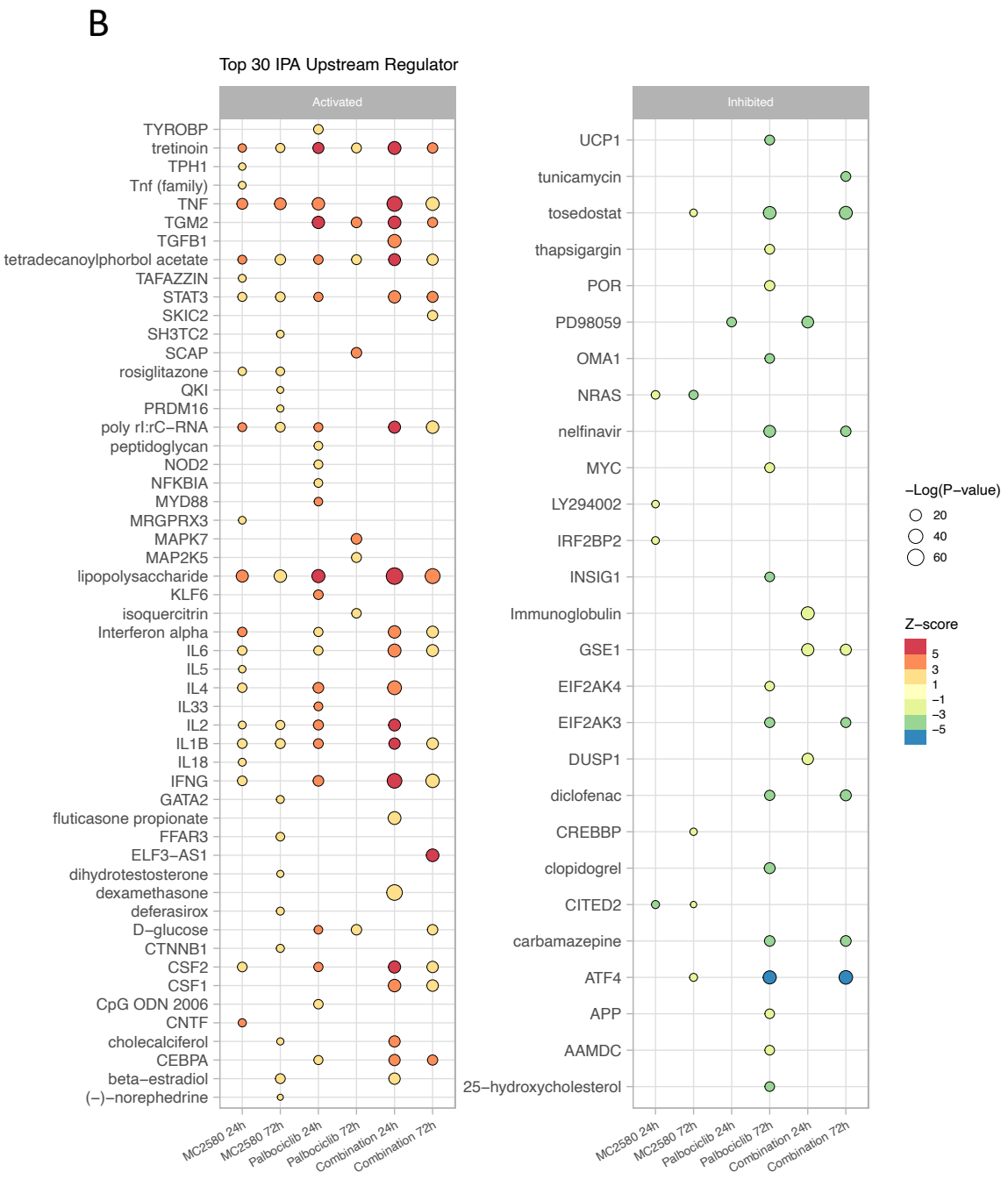

Figure 52. ***Top 30 enriched pathways and upstream regulators upon G1-prolongation and LSD1 inhibition in PL-21 cells****. (A) IPA top 30 enriched pathways in PL-21 cells treated with 2µM MC2580 or 50nM Palbociclib or combination of 2µM MC2580 + 50nM Palbociclib vs vehicle (DMSO), 24- and 72-hours post LSD1 inhibition. (B) Top 30 upstream regulators correlating to (A).*

A

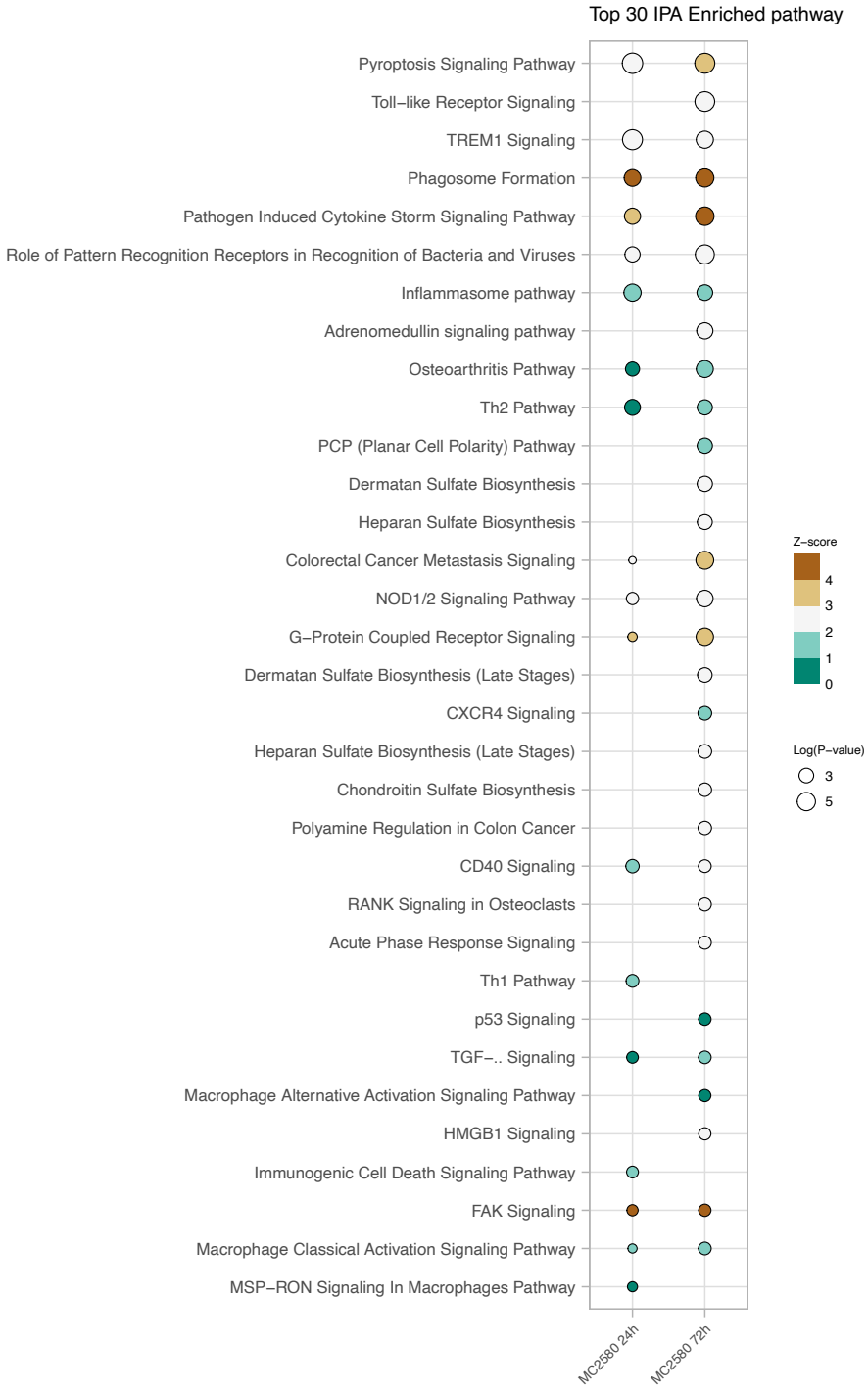
Top 30 IPA Enriched pathway
Pyroptosis Signaling Pathway
Toll–like Receptor Signaling
TREM1 Signaling
Phagosome Formation
Pathogen Induced Cytokine Storm Signaling Pathway
Role of Pattern Recognition Receptors in Recognition of Bacteria and Viruses
Inflammasome pathway
Adrenomedullin signaling pathway
Osteoarthritis Pathway
Th2 Pathway
PCP (Planar Cell Polarity) Pathway
Dermatan Sulfate Biosynthesis
Heparan Sulfate Biosynthesis
Colorectal Cancer Metastasis Signaling
NOD1/2 Signaling Pathway
G–Protein Coupled Receptor Signaling
Dermatan Sulfate Biosynthesis (Late Stages)
CXCR4 Signaling
Heparan Sulfate Biosynthesis (Late Stages)
Chondroitin Sulfate Biosynthesis
Polyamine Regulation in Colon Cancer
CD40 Signaling
RANK Signaling in Osteoclasts
Acute Phase Response Signaling
Th1 Pathway
p53 Signaling
TGF–.. Signaling
Macrophage Alternative Activation Signaling Pathway
HMGB1 Signaling
Immunogenic Cell Death Signaling Pathway
FAK Signaling
Macrophage Classical Activation Signaling Pathway
MSP–RON Signaling In Macrophages Pathway
MC2580 24h
MC2580 72h
Z–score
4
3
2
1
0
Log(P–value)
3
5

B

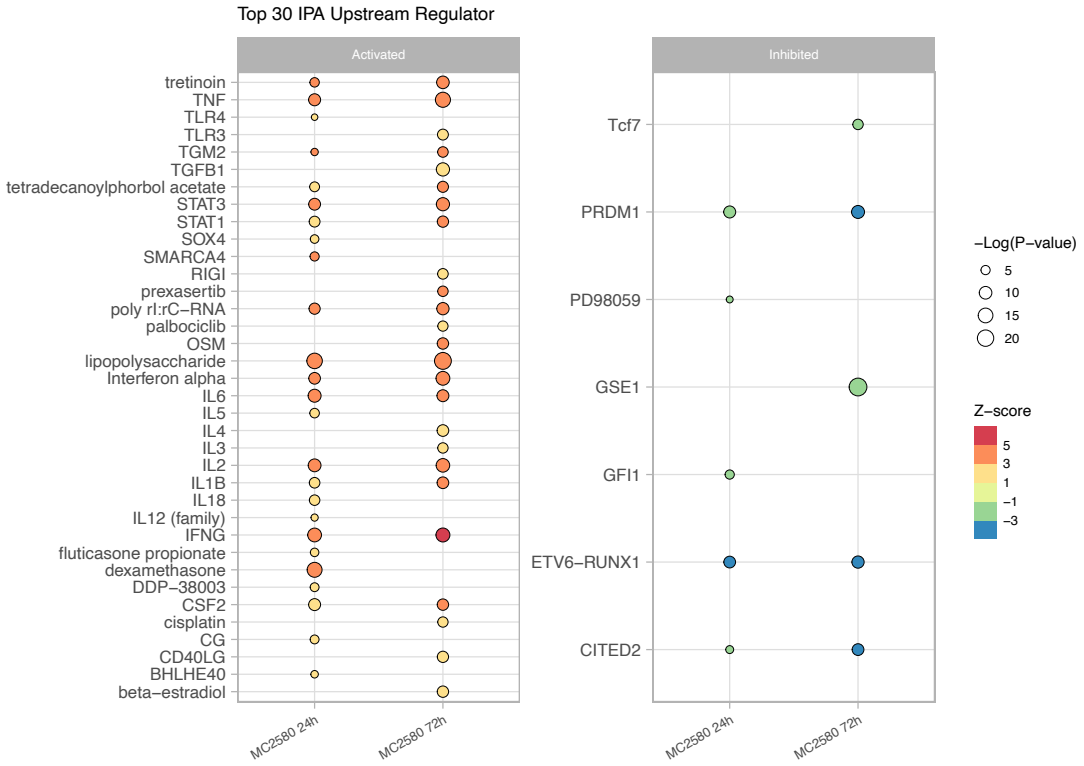

Figure 53. ***Top 30 enriched pathways and upstream regulators upon G1-prolongation and LSD1 inhibition in Kasumi-1 cells****. (A) IPA top 30 enriched pathways in Kasumi-1 cells treated with 2µM MC2580 vs vehicle (DMSO), 24- and 72-hours post LSD1 inhibition. (B) Top 30 upstream regulators correlating to (A).*

4.3. Transcriptional footprint of G1-extended AML cells overlaps with their slow-cycling counterparts upon LSD1 inhibition

To investigate whether the suspected transcriptional changes, thought to drive the differentiation, yield a consistent gene expression pattern across our model systems, we elected to selectively monitor these transcriptional activities under all experimental conditions in NB4, PL-21, and Kasumi-1 cell lines. Hence, we selected the top 50 significant DEGs of Palbociclib + MC2580 in NB4 and PL-21, and MC2580 in Kasumi-1 cells at both 24-

and 72-hours post treatments and merged them in a panel (Figure 54). Next, we performed PCA analysis among all treatments of the two time-points with the three cell lines, based on this gene panel (Figure 55). The findings notably revealed that slow-cycling Kasumi-1 cells treated with DMSO have a similar gene transcription profile to that of fast-cycling NB4 and PL-21 cells treated with Palbociclib, for this specific set of genes examined (Figure 55). This illustrates how G1-prolongation is directly poising the fast-cycling AML cells towards differentiation induction by making them more similar to the slow-cycling counterparts. The next observation was how Kasumi-1 cells + MC2580 cluster close with NB4 and PL-21 cells + Palbociclib combined with MC2580 (Figure 55). This highlights that AML cells with extended G1 follow very closely the same transcriptional axes towards differentiation, that the naturally slow-cycling cells would take upon LSD1 inhibition. This observation is in line with our former discovery on the similarity of the activated pathways prior to differentiation induction among our models.

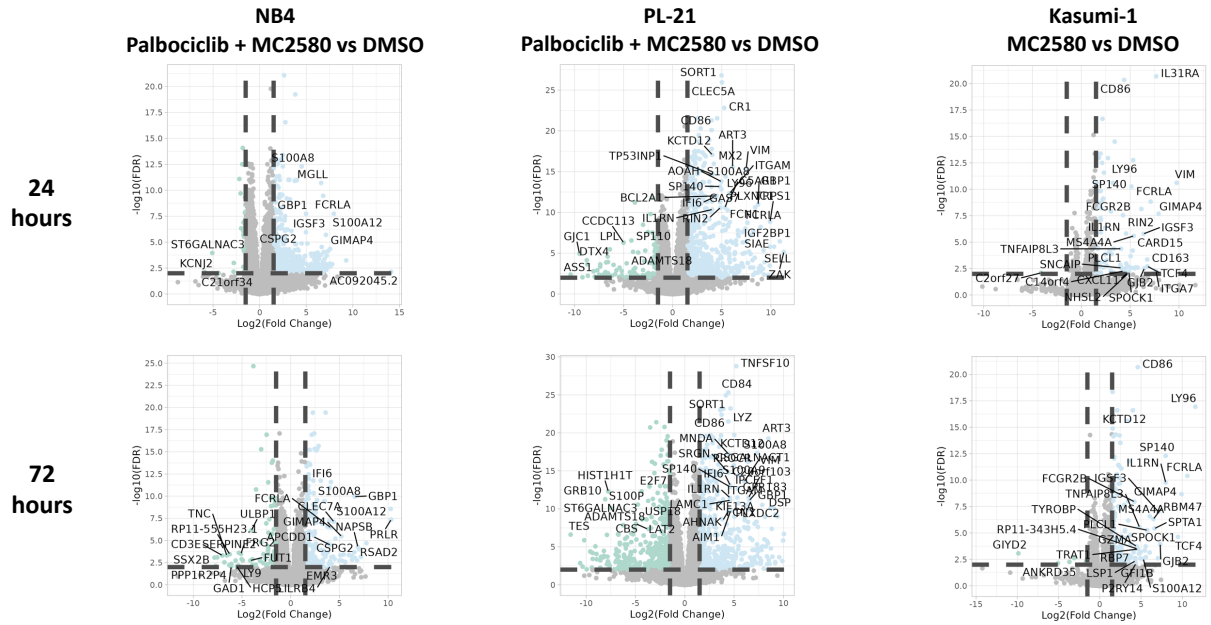

Figure 54. ***Top 50 DEGs upon differentiation induction therapy in NB4, PL-21, and Kasumi-1 cells, 24- and 72-hours post LSD1 inhibition.***.

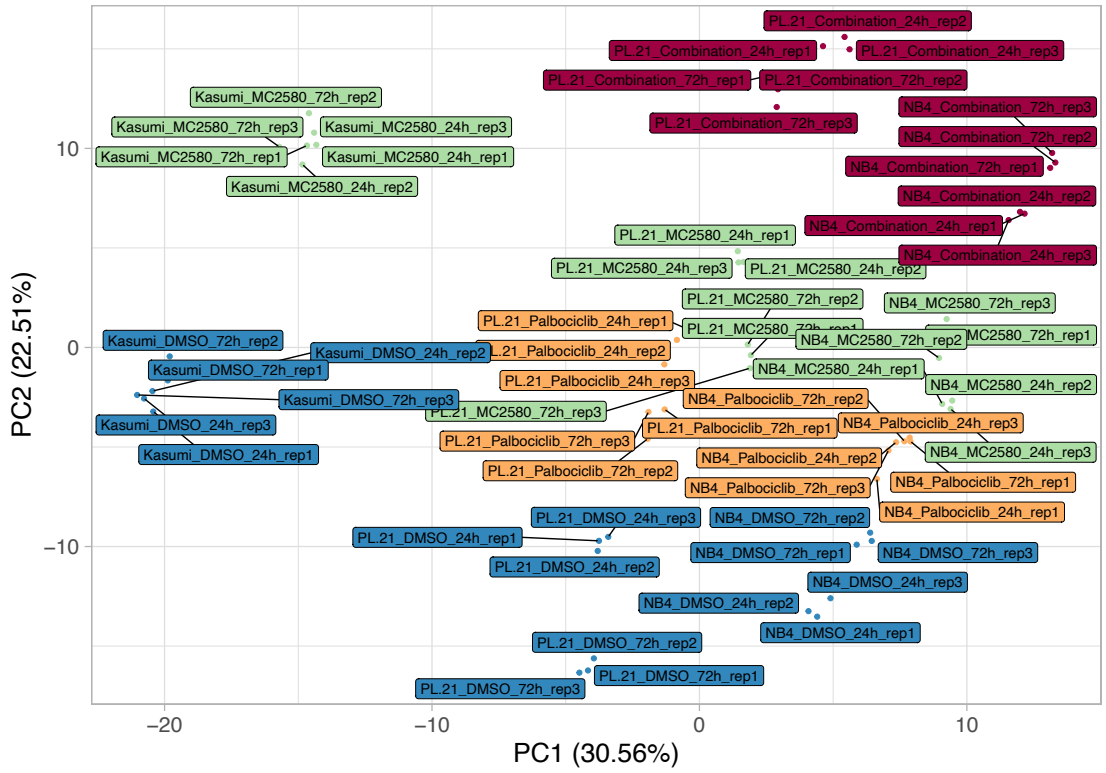

Figure 55. ***Transcriptional alterations prior to differentiation induction is highly similar among G1-extended and naturally slow-cycling AML cells upon LSD1 inhibition****. PCA analysis performed based on 333 top DEGs in response to differentiation inducing therapy among the three cell lines of NB4, PL-21, and Kasumi-1. Name of the cell lines and the time-points (post LSD1 inhibition) indicated in the annotations. Blue: DMSO; Orange: 50nM Palbociclib; Green: 2µM MC2580; Red: 2µM MC2580 + 50nM Palbociclib.*

Furthermore, looking at the genes found impacting in both PC1 and PC2, we can observe a high proportion of immune-regulating genes contributing to stablished immune-response pathways (Figure 56). In conclusion, we can confirm that LSD1 inhibition-mediated differentiation in G1 extended AML cells and the naturally slow-cycling AML cells is similar and is based on the induction of immune-response regulatory pathways.

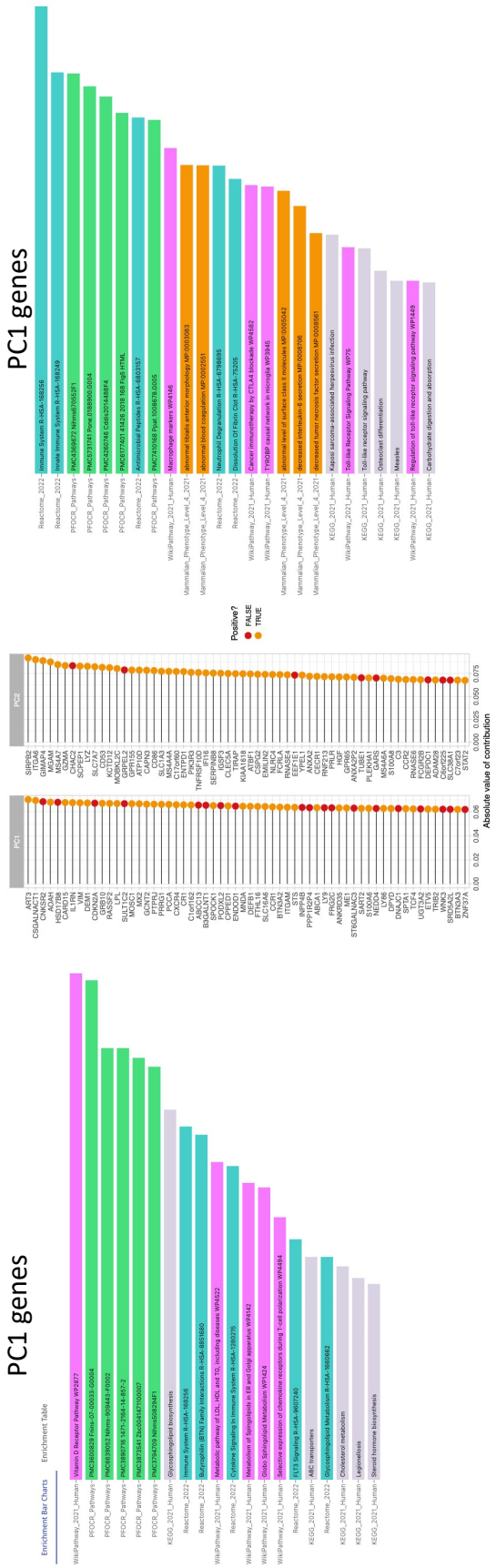

Figure 56. ***Mutually determinative genes upon LSD1 inhibition among slow- and fast-cycling AML cells mainly contribute to immune response regulating pathways****. Genes constructing the PC1 and PC2 of the PCA analysis in figure 36, listed based on contribution (top to bottom) and analyzed for their corresponding pathways (shown as bars with annotations). Colors represent different online referenced databases.*

4.4. Exclusive upregulation of transposable elements' expression is observed upon LSD1 inhibition in slow-cycling AML cells

Discovering the dominance of immune response pathways among the differentiation initiative pathways directed us towards questioning its origin. We knew from the work of colleagues in recent years, the strong link between administration of epigenetic drugs (including LSD1 inhibitors) and activation of endogenous retroviruses (ERVs) and non-ERV transposable elements (TEs) (Sheng *et al.*, 2018; Gambacorta *et al.*, 2019; Jones *et al.*, 2019; Pallavi, Mazzarella and Pelicci, 2019). This would have been relevant considering the upregulation of several PRRs, and type I and type II interferon signatures (Figure 57-Figure 59). Interestingly, we could observe that G1-prolongation in the fast-cycling AML cells can enhance these signatures more than LSD1 inhibition alone, but once combined with LSD1 inhibition the effect gets more pronounced. On the other hand, sole LSD1 inhibition in the slow-cycling AML cells was enough to significantly enrich such interferon response signatures.

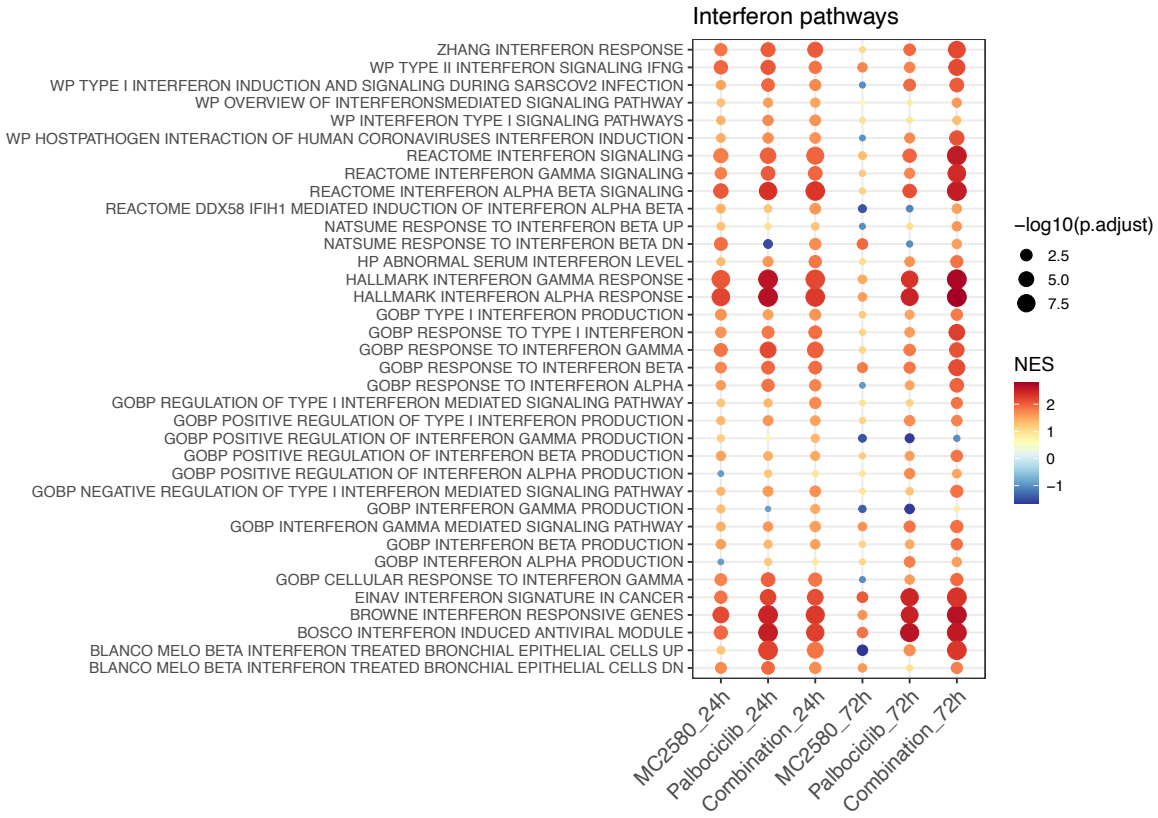

Figure 57. ***Increased enrichment of gene signatures correlating to interferon production and response upon LSD1 inhibition in G1-extended NB4 cells.*** *Bubble plots representing selected gene sets containing the keyword "Interferon" based on treatment vs DMSO, in NB4 cells treated with vehicle (DMSO) or 2μM MC2580 or 50nM Palbociclib or combination of 2μM MC2580 + 50nM Palbociclib, 24- and 72-hours post LSD1 inhibition. NES: normalized enrichment scores.*

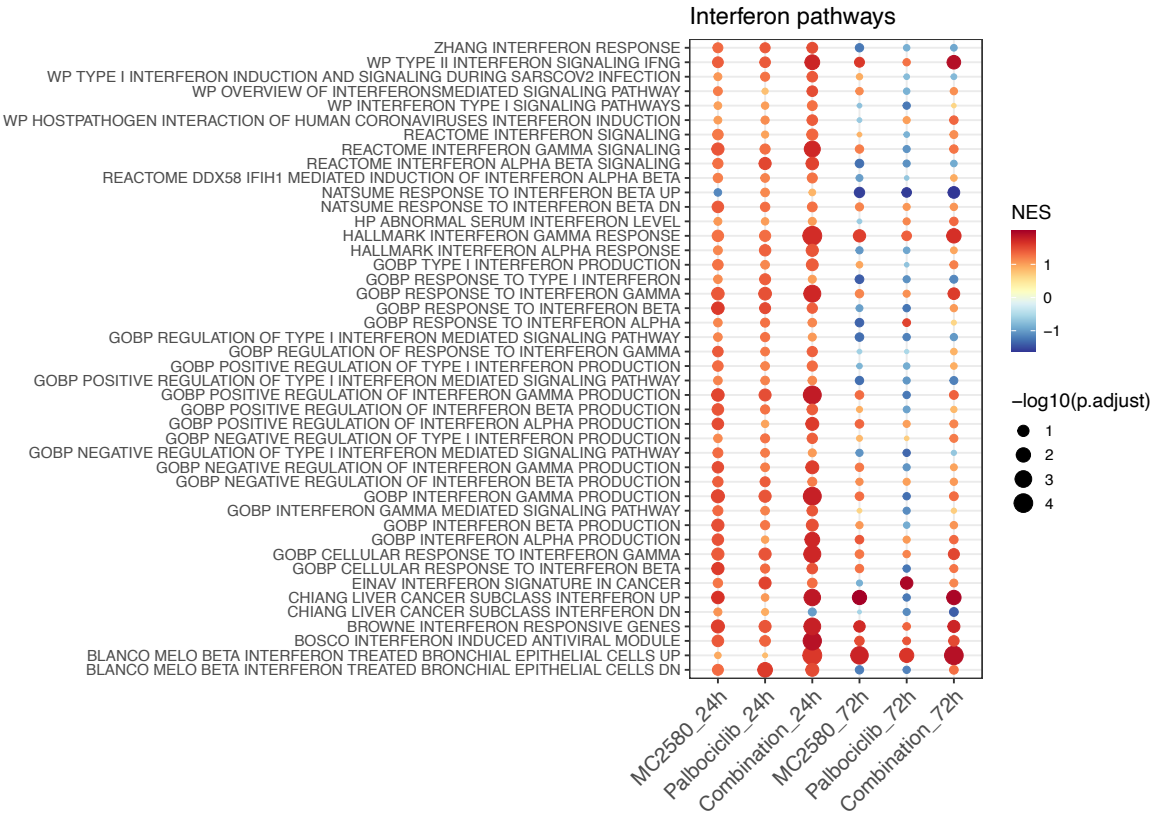

Figure 58. ***Increased enrichment of gene signatures correlating to interferon production and response upon LSD1 inhibition in G1-extended PL-21 cells****. Bubble plots representing selected gene sets containing the keyword "Interferon" based on treatment vs DMSO, in PL-21 cells treated with vehicle (DMSO) or 2µM MC2580 or 50nM Palbociclib or combination of 2µM MC2580 + 50nM Palbociclib, 24- and 72-hours post LSD1 inhibition. NES: normalized enrichment scores.*

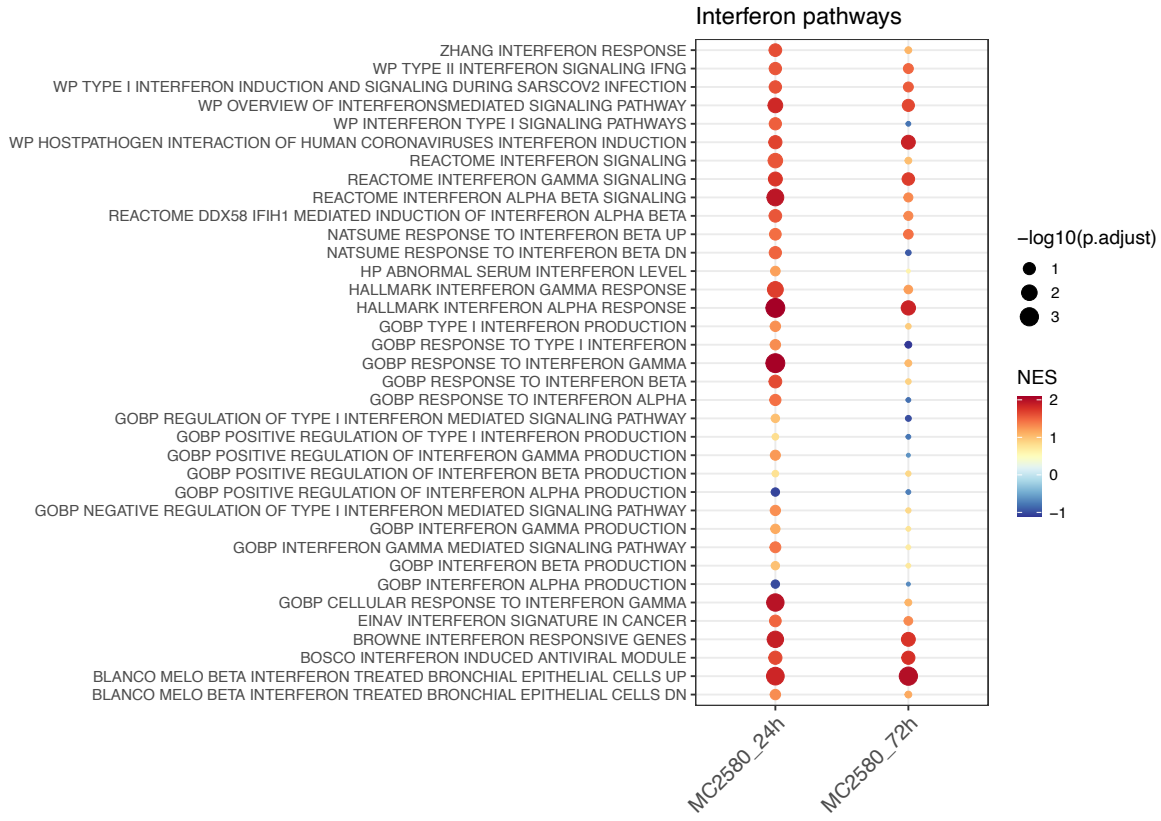

Figure 59. ***Increased enrichment of gene signatures correlating to interferon production and response upon LSD1 inhibition in G1-extended Kasumi-1 cells****. Bubble plots representing selected gene sets containing the keyword "Interferon" based on treatment vs DMSO, in Kasumi-1 cells treated with vehicle (DMSO) or 2µM MC2580, 24- and 72-hours post LSD1 inhibition. NES: normalized enrichment scores.*

Thus, if the expression of TEs was indeed the driver of such immune response signatures, we should have been able to discover the same pattern of upregulation of TEs looking among our slow- and fast-cycling models. Hence, we started to collaborate with Beatrice Bodega's group, actively involved in the study of TEs in ES cells (Marasca *et al.*, 2022). we performed an optimized RNA-seq in NB4 and Kasumi-1 cells, at 24- and 72-hours post LSD1 inhibition, which enables us to quantify the expression levels of repetitive elements with higher accuracy (Marasca *et al.*, 2022). Initially, we had a global visualization of TE families and non-TE repetitive elements among our different conditions to assess if there is any consistent change (Figure 60). Strikingly, we observed a very consistent global increase in TEs happening only upon G1-prolongation +/- LSD1 inhibition in NB4 cells and LSD1

inhibition in Kasumi-1 cells. This was particularly interesting since the LSD1 inhibition alone, could not cause such an upregulation in the fast-cycling NB4 cells (Figure 60). The interpretation also appeared reliable due to the random expression pattern of short interspersed nuclear elements (SINEs), like Alu, and non-TE repetitive elements, like satellite repeats across the experimental conditions (Figure 60).

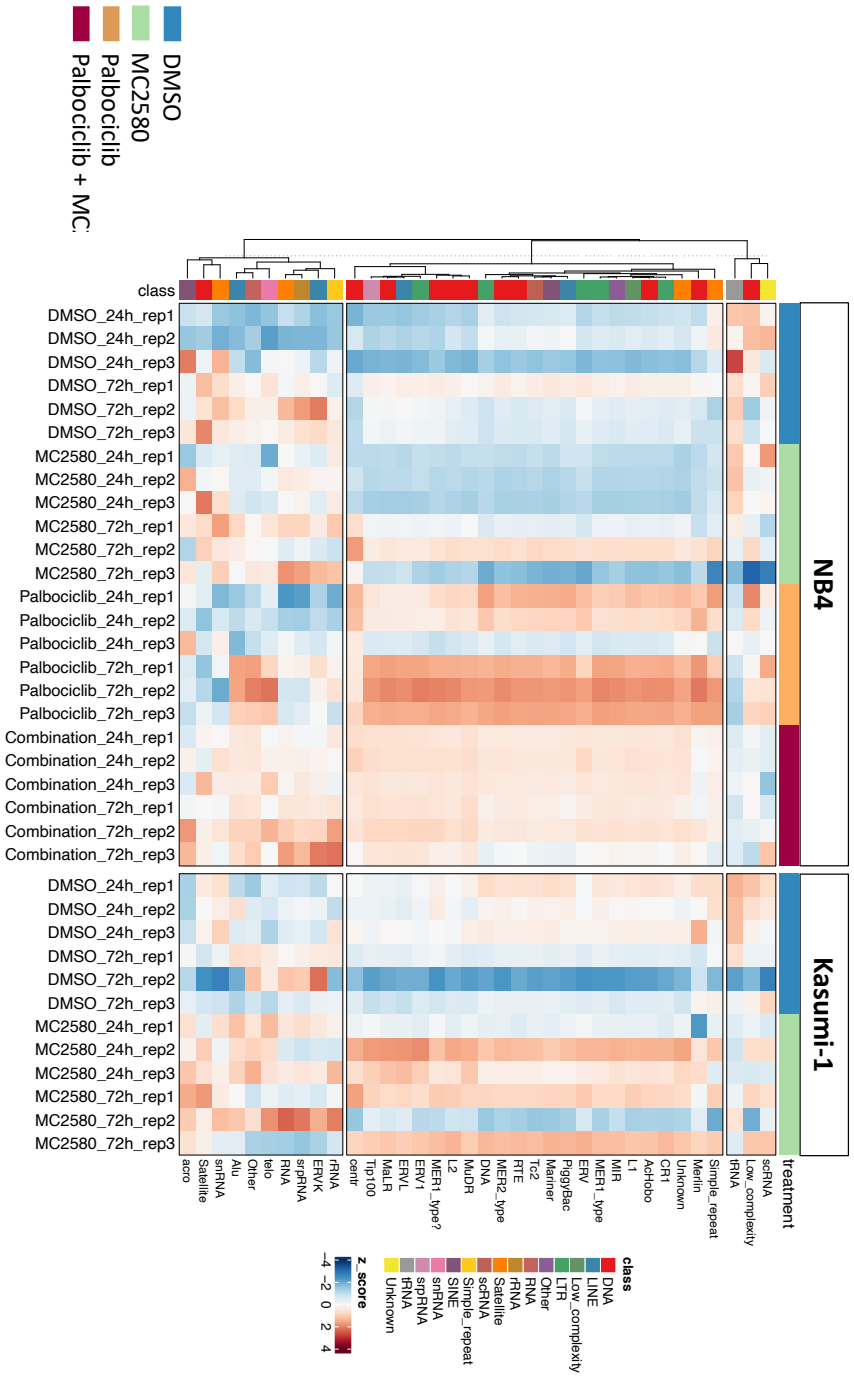

Figure 60. ***LSD1 inhibition in G1-extended or naturally slow-cycling AML cells is accompanied by increase in transcriptional activity of TEs****. Heatmap, representing quantification of TEs' transcripts in a clustered fashion in NB4 cells*

treated with vehicle (DMSO) or 2µM MC2580 or 50nM Palbociclib or combination of 2µM MC2580 + 50nM Palbociclib, and Kasumi-1 cells treated with vehicle (DMSO) or 2µM MC2580, 24- and 72-hours post LSD1 inhibition. Class of the TE is indicated by color boxes shown at the right side of the graph. Each row represents the annotated TE. Each column represents one experimental replicate of the mentioned condition and time-point.

Next question was to see if at the level of subfamily, some elements are driving the increased TE expression observed at the large scale. Thus, we performed differential expression analysis at the levels of superfamilies, families, and subfamilies, in the same experimental conditions as before. As a result, we could detect major involvement of HERV and occasionally L1 subfamilies in differentiation inducing treatments in both fast-cycling and slow-cycling AML cells (Figure 61). Taken together, these observations indicate that G1 extension and subsequent LSD1 inhibition in AML cells can induce an upregulation of TEs' expression levels, mainly driven by HERV1 subfamily. These observations were in-line with the prior pattern of immune response activation among the same AML cell lines. Hence, we could conclude that alternate expression of ERVs in slow-cycling AML cells is perhaps the triggering event prior to activation of immune response regulating genes, which we observed formerly upon LSD1 inhibition in these cells. This might finally lead us to deciphering the origins of differentiation induction in AML cells through an epigenetic therapy such as LSD1 inhibition. The experimental validation of this hypothesis, however, is at present missing (see Discussion).

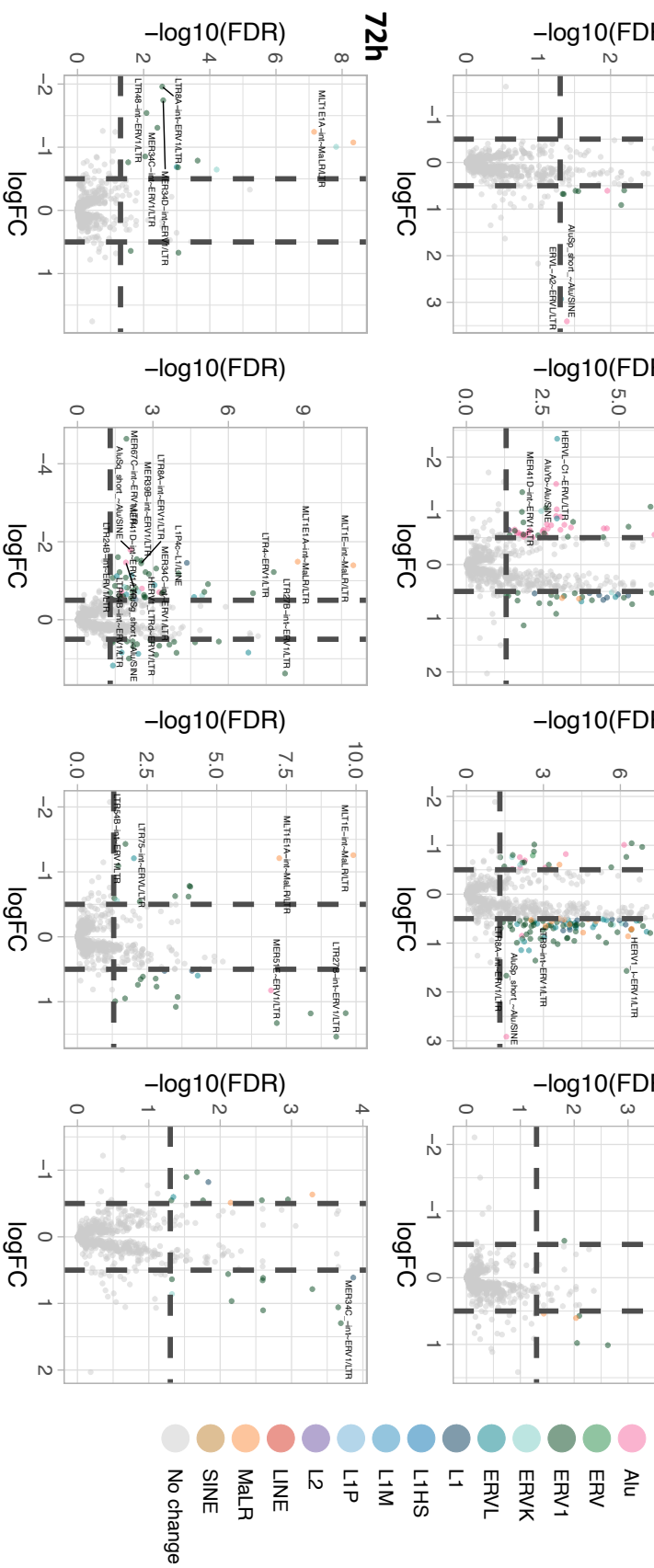

Figure 61. ***Distinct upregulation of HERV1 subfamilies is observed upon LSD1 inhibition in G1-extended NB4 and naturally slow-cycling Kasumi-1 cells****. Volcano plots, representing differential transcript counts of TE families and subfamilies in NB4 cells treated with vehicle (DMSO) or 2μM MC2580 or 50nM Palbociclib or combination of 2μM MC2580*

+ 50nM Palbociclib, and Kasumi-1 cells treated with vehicle (DMSO) or 2μM MC2580, 24- and 72-hours post LSD1 inhibition. TE families and subfamilies are indicated by color shades as indicated at the right side of the panel. Abs(logFC) > 0.5 and -logadjPval > 1.3.

4.5. Several dsRNA sensors show increased transcription upon G1 lengthening and LSD1 inhibition

For the ERVs to trigger an immune response to the extent we observed formerly, there should be a double-stranded or 5'-triphosphorylated single-stranded RNA (dsRNA/5'-triphosphorylated ssRNA) production and sensing process. This, in turn, activates various cascades, including interferon secretion, regulation of interferon-stimulated genes (ISGs), production of antiviral signaling proteins, and so on as those of we formerly observed (Weber *et al.*, 2013; Chiappinelli *et al.*, 2015). Therefore, we had to study any possible increased transcription of specific dsRNA sensors in conditions where we observed TEs' amplification and differentiation initiation. So, we evaluated manually genomic loci of the most relevant dsRNA sensors, looking at the H3K27ac enrichment over their first exons and RNA transcription of the genes within the same treatment and time-point conditions we had been using so far. Notably, we found increased H3K27ac enrichment and expression levels of several dsRNA sensors, including retinoic acid-inducible gene I (RIG-I), protein kinase R (PKR), melanoma differentiation-associated protein 5 (MDA5), oligoadenylate synthase1-3 (OAS1-3), and OAS-like (OASL) upon G1-lengthening alone and subsequent LSD1 inhibition (Figure 62-Figure 68). Our data illustrate that upon LSD1 inhibition, HERV and L1 subfamilies are activated in G1-extended or naturally slow-cycling AML cells. This activation is closely followed by elevated expression of dsRNA sensors, sensors for their principal activity product. Conclusively, these findings are complementary with the previously seen production of type I and II interferons, activation of ISGs, cytokine storm,

induction of immunogenic cell death signaling, coupled with further decreased proliferation and cell cycle control and eventually differentiation.

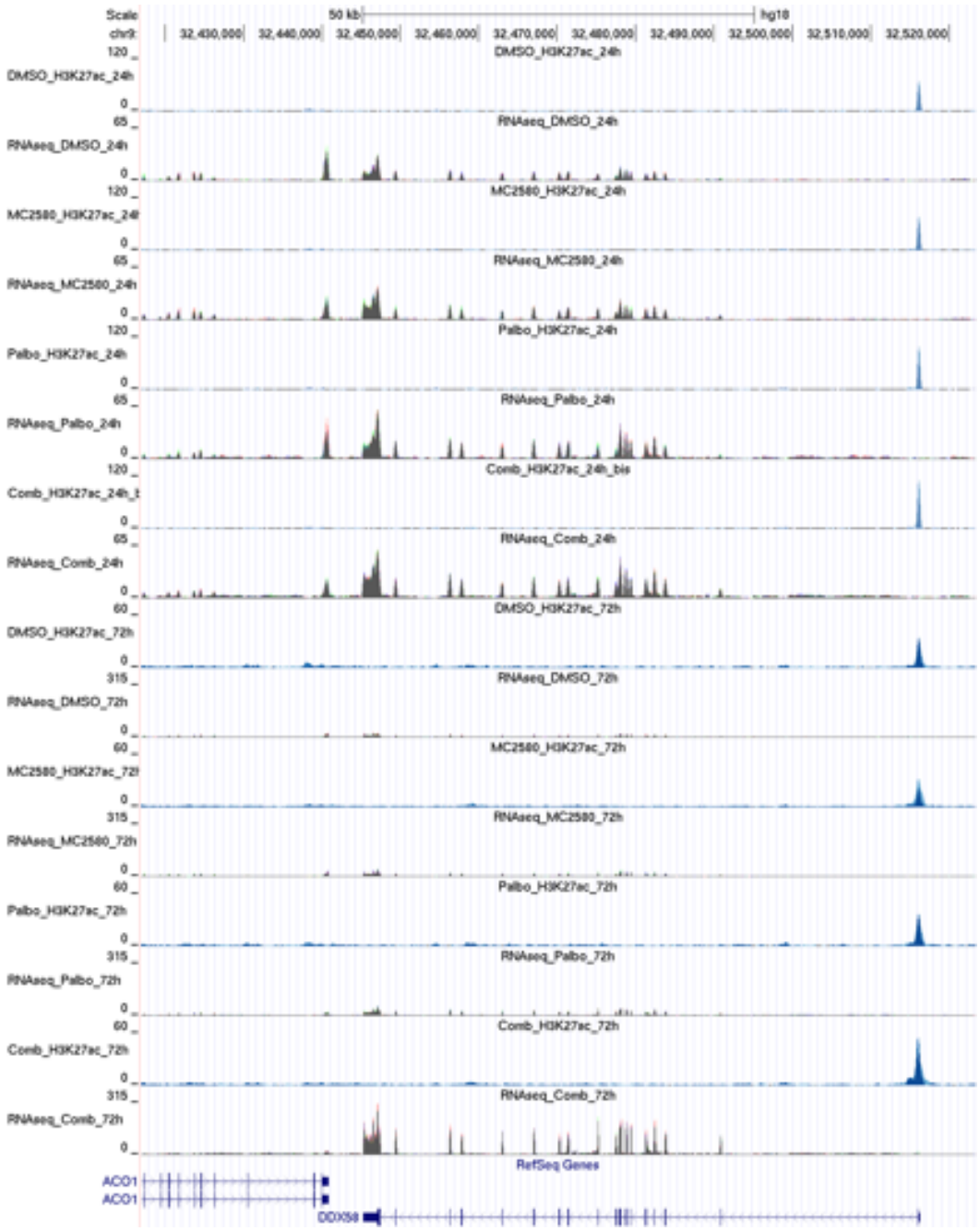

Figure 62. ***Increased epigenetic and genetic regulation of RIG-I transcription upon LSD1 inhibition in G1-extended NB4 cells****. Snapshot of the DDX58 (AKA RIG-I) genomic locus, representing H3K27ac and RNA levels in NB4 cells treated with vehicle (DMSO) or 2µM MC2580 or 50nM Palbociclib or combination of 2µM MC2580 + 50nM Palbociclib, 24- and 72-hours post LSD1 inhibition. Each track is annotated at the top, mentioning the treatment, time point, and correspondence to H3K27ac or RNA. Tracks are scaled equally for each experiment and time-point. The order from top to bottom is H3K27ac-24hrs followed by RNA-seq track-24hrs for DMSO, MC2580, Palbociclib, and MC2580+Palbociclib; then H3K27ac-72hrs followed by RNA-seq track-72hrs for DMSO, MC2580, Palbociclib, and MC2580+Palbociclib.*

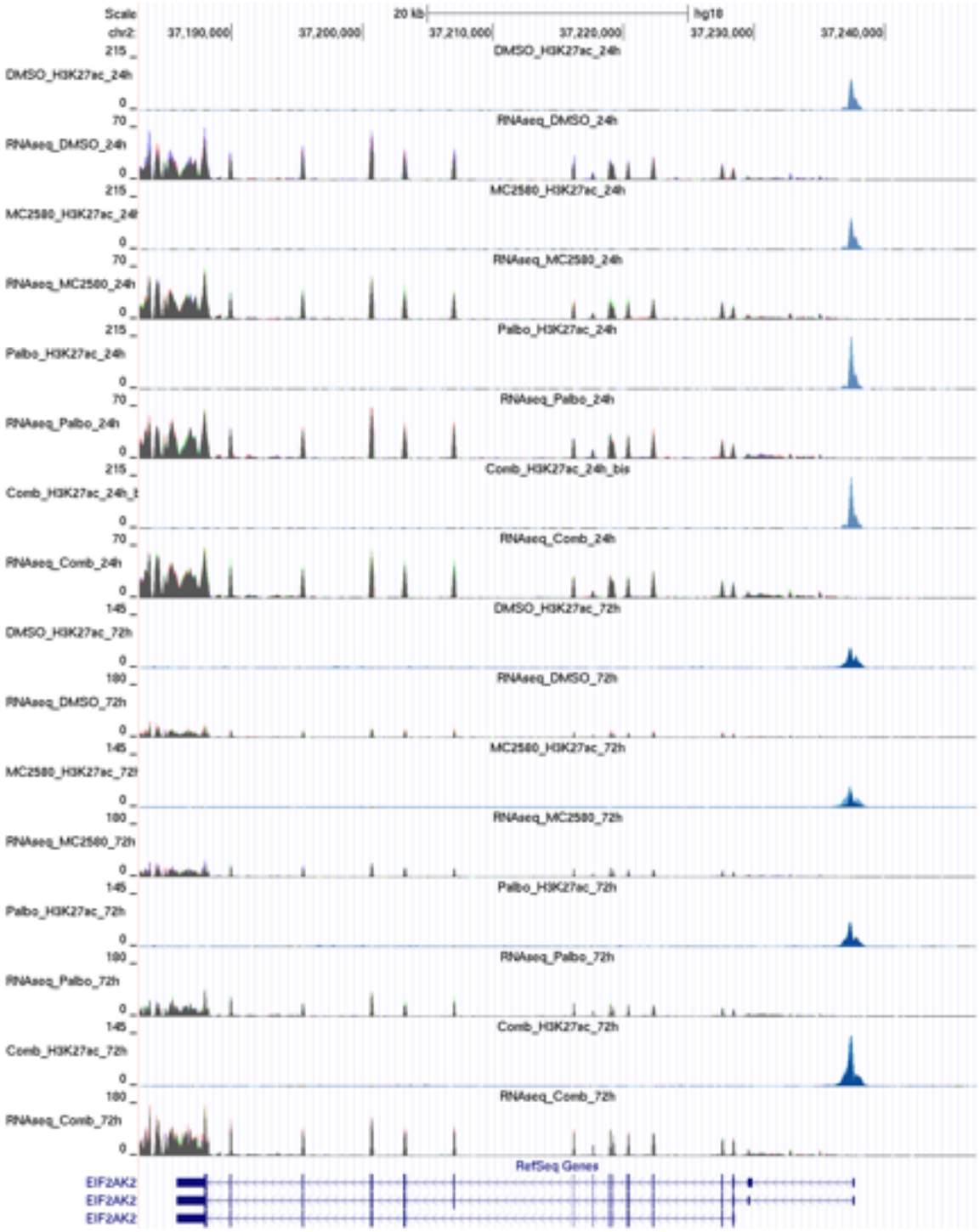

Figure 63. ***Increased epigenetic and genetic regulation of PKR transcription upon LSD1 inhibition in G1-extended NB4 cells****. Snapshot of the EIF2AK2 (AKA PKR) genomic locus, representing H3K27ac and RNA levels in NB4 cells treated with vehicle (DMSO) or 2µM MC2580 or 50nM Palbociclib or combination of 2µM MC2580 + 50nM Palbociclib, 24- and 72-hours post LSD1 inhibition. Each track is annotated at the top, mentioning the treatment, time point, and correspondence to H3K27ac or RNA. Tracks are scaled equally for each experiment and time-point. The order from top to bottom is H3K27ac-24hrs followed by RNA-seq track-24hrs for DMSO, MC2580, Palbociclib, and MC2580+Palbociclib; then H3K27ac-72hrs followed by RNA-seq track-72hrs for DMSO, MC2580, Palbociclib, and MC2580+Palbociclib.*

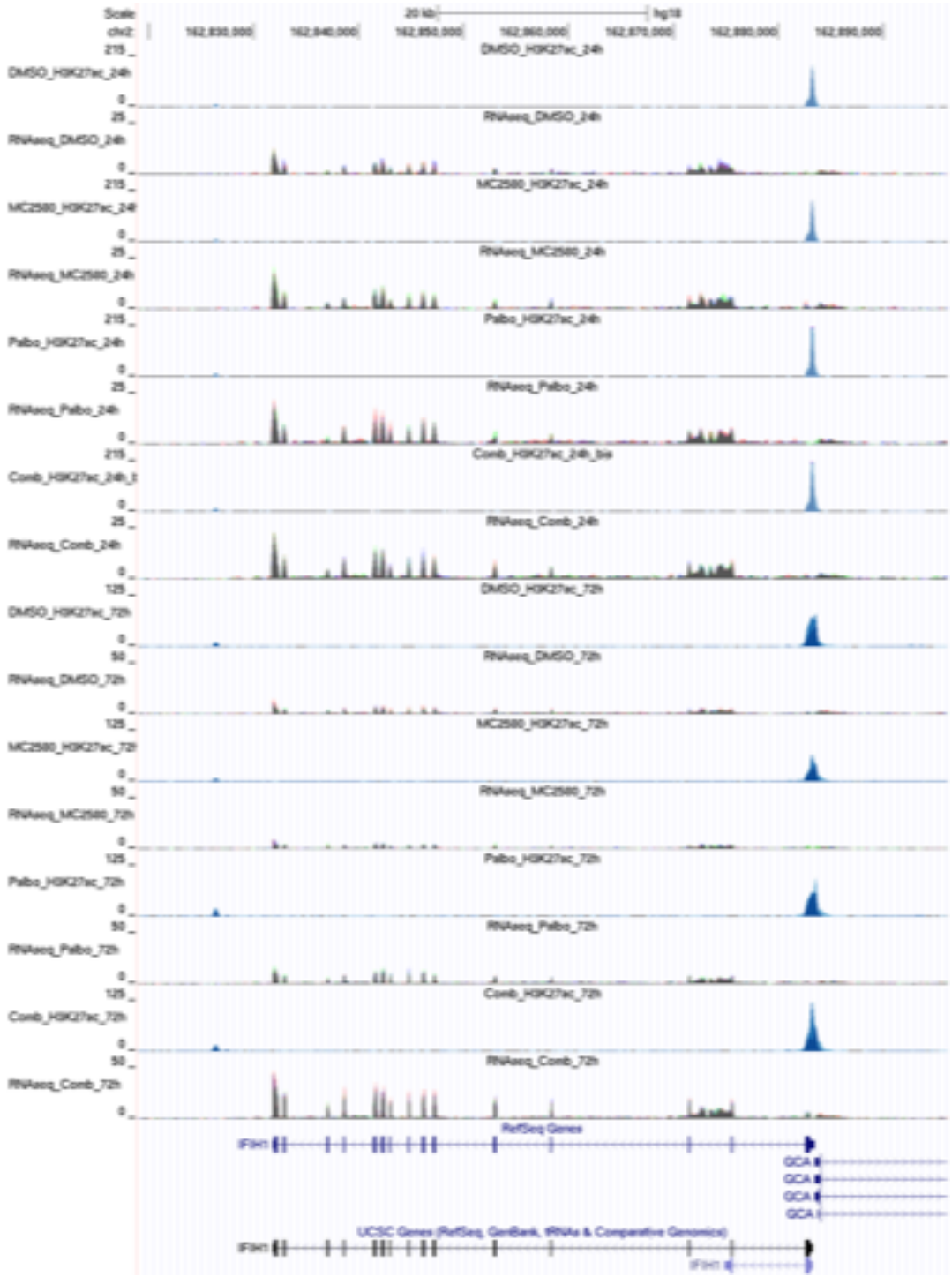

Figure 64. ***Increased epigenetic and genetic regulation of MDA5 transcription upon LSD1 inhibition in G1-extended NB4 cells****. Snapshot of the IFIH1 (AKA MDA5) genomic locus, representing H3K27ac and RNA levels in NB4 cells treated with vehicle (DMSO) or 2µM MC2580 or 50nM Palbociclib or combination of 2µM MC2580 + 50nM Palbociclib, 24- and 72-hours post LSD1 inhibition. Each track is annotated at the top, mentioning the treatment, time point, and correspondence to H3K27ac or RNA. Tracks are scaled equally for each experiment and time-point. The order from top to bottom is H3K27ac-24hrs followed by RNA-seq track-24hrs for DMSO, MC2580, Palbociclib, and MC2580+Palbociclib; then H3K27ac-72hrs followed by RNA-seq track-72hrs for DMSO, MC2580, Palbociclib, and MC2580+Palbociclib.*

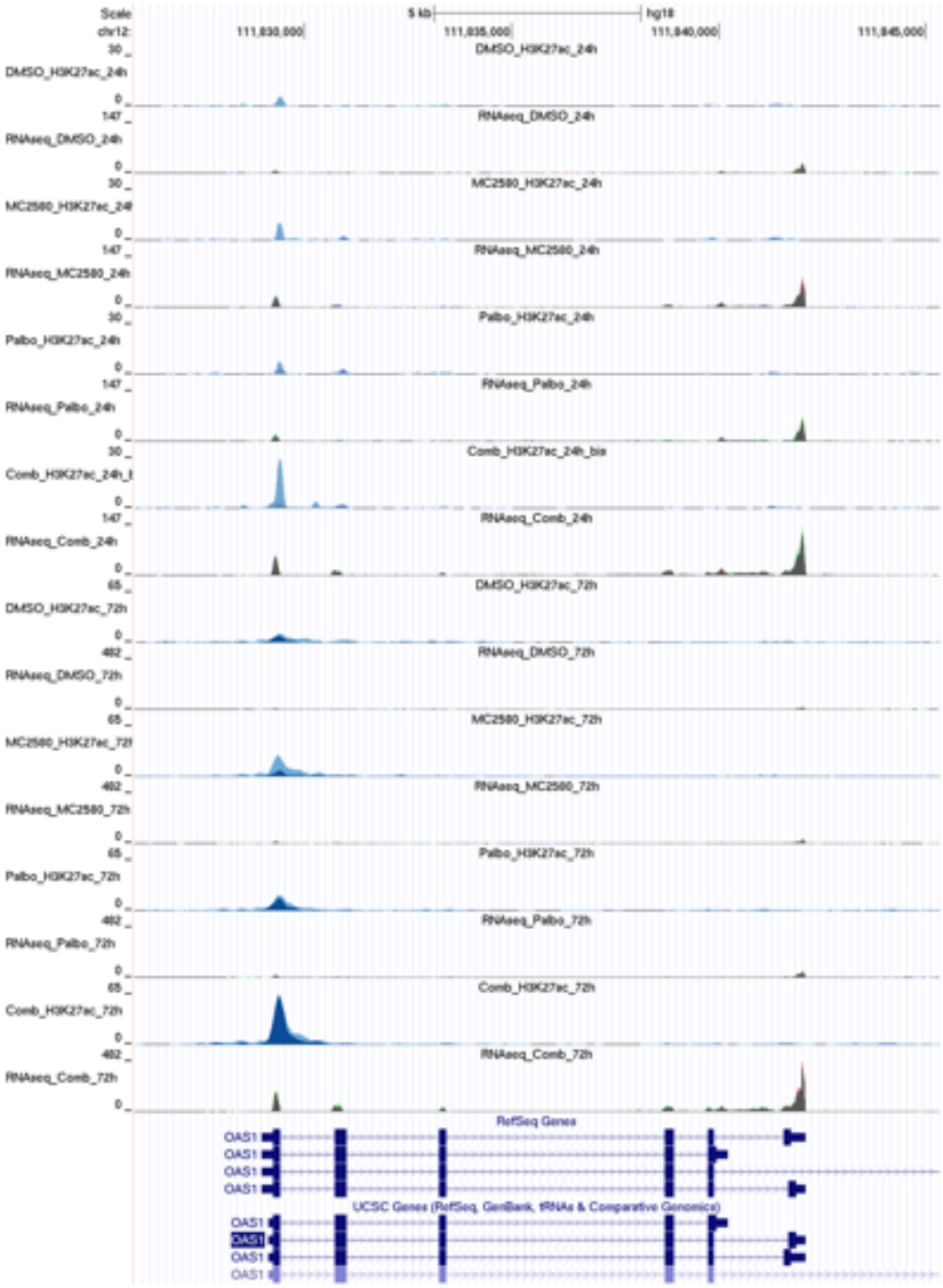

Figure 65. ***Increased epigenetic and genetic regulation of OAS1 transcription upon LSD1 inhibition in G1-extended NB4 cells****. Snapshot of the OAS1 genomic locus, representing H3K27ac and RNA levels in NB4 cells treated with vehicle (DMSO) or 2µM MC2580 or 50nM Palbociclib or combination of 2µM MC2580 + 50nM Palbociclib, 24- and 72-hours post LSD1 inhibition. Each track is annotated at the top, mentioning the treatment, time point, and correspondence to H3K27ac or RNA. Tracks are scaled equally for each experiment and time-point. The order from top to bottom is H3K27ac-24hrs followed by RNA-seq track-24hrs for DMSO, MC2580, Palbociclib, and MC2580+Palbociclib; then H3K27ac-72hrs followed by RNA-seq track-72hrs for DMSO, MC2580, Palbociclib, and MC2580+Palbociclib.*

Figure 66. ***Increased epigenetic and genetic regulation of OAS2 transcription upon LSD1 inhibition in G1-extended NB4 cells****. Snapshot of the OAS2 genomic locus, representing H3K27ac and RNA levels in NB4 cells treated with vehicle (DMSO) or 2µM MC2580 or 50nM Palbociclib or combination of 2µM MC2580 + 50nM Palbociclib, 24- and 72-hours post LSD1 inhibition. Each track is annotated at the top, mentioning the treatment, time point, and correspondence to H3K27ac or RNA. Tracks are scaled equally for each experiment and time-point. The order from top to bottom is H3K27ac-24hrs followed by RNA-seq track-24hrs for DMSO, MC2580, Palbociclib, and MC2580+Palbociclib; then H3K27ac-72hrs followed by RNA-seq track-72hrs for DMSO, MC2580, Palbociclib, and MC2580+Palbociclib.*

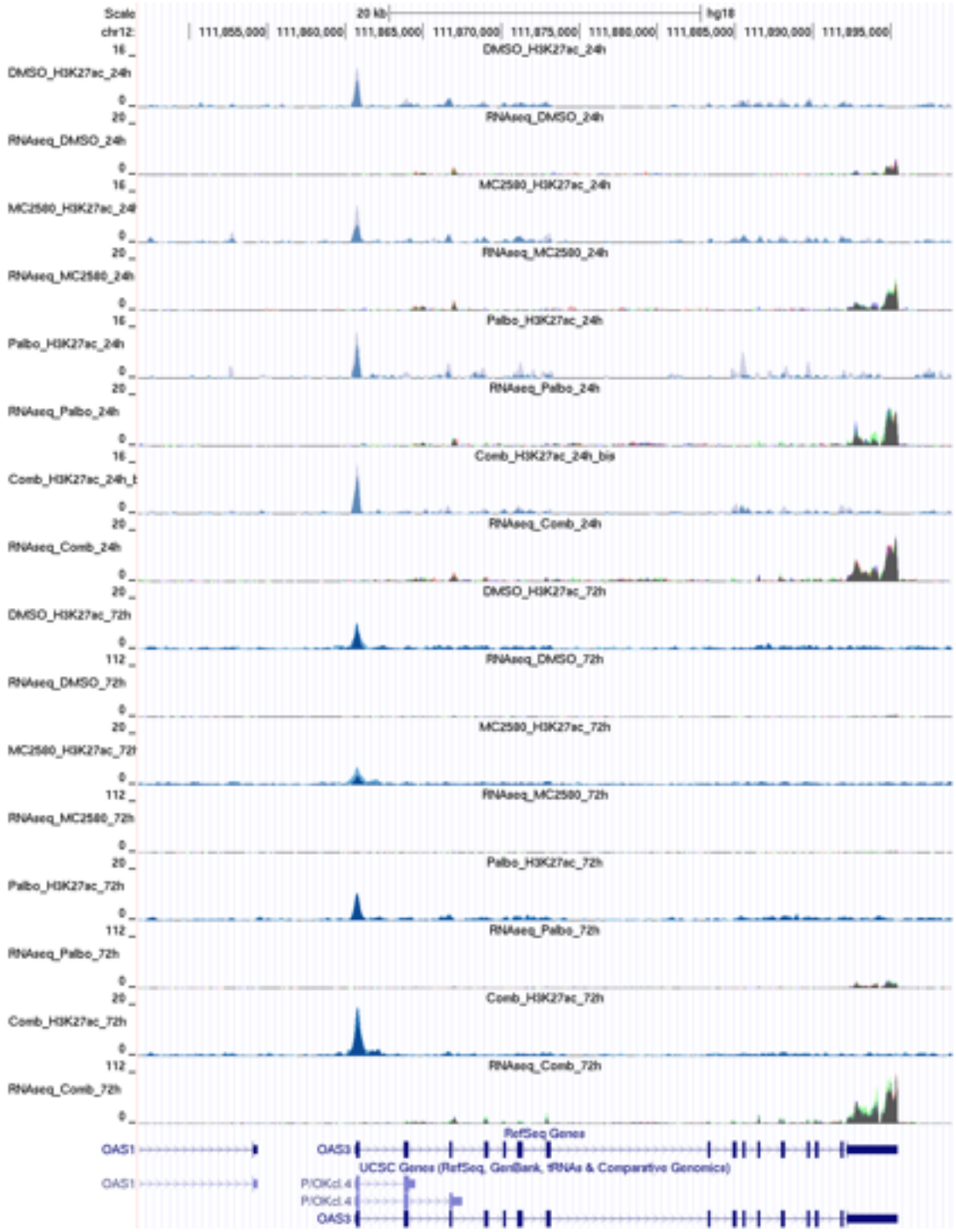

Figure 67. ***Increased epigenetic and genetic regulation of OAS3 transcription upon LSD1 inhibition in G1-extended NB4 cells****. Snapshot of the OAS3 genomic locus, representing H3K27ac and RNA levels in NB4 cells treated with vehicle (DMSO) or 2µM MC2580 or 50nM Palbociclib or combination of 2µM MC2580 + 50nM Palbociclib, 24- and 72-hours post LSD1 inhibition. Each track is annotated at the top, mentioning the treatment, time point, and correspondence to H3K27ac or RNA. Tracks are scaled equally for each experiment and time-point. The order from top to bottom is H3K27ac-24hrs followed by RNA-seq track-24hrs for DMSO, MC2580, Palbociclib, and MC2580+Palbociclib; then H3K27ac-72hrs followed by RNA-seq track-72hrs for DMSO, MC2580, Palbociclib, and MC2580+Palbociclib.*

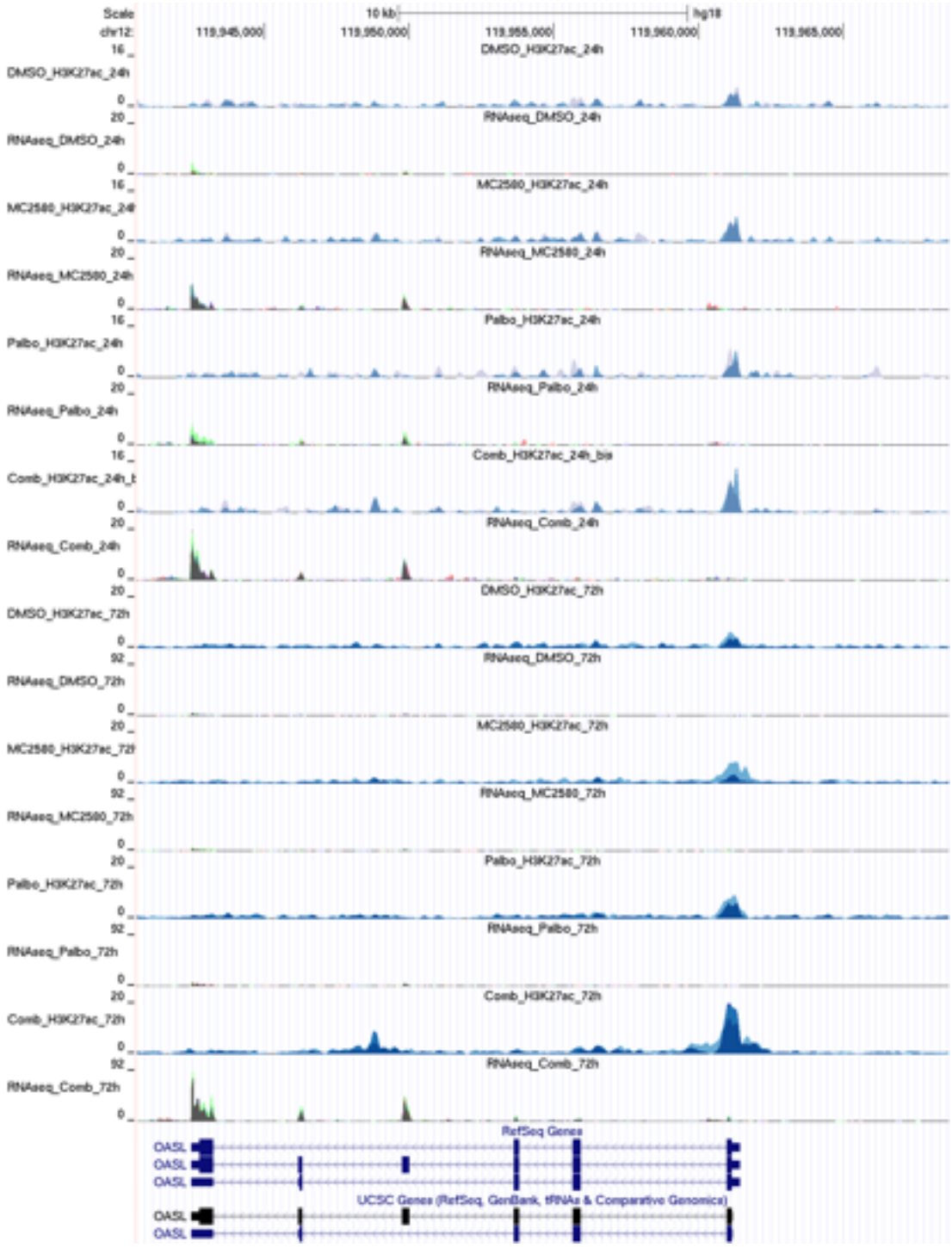

Figure 68. ***Increased epigenetic and genetic regulation of OASL transcription upon LSD1 inhibition in G1-extended NB4 cells****. Snapshot of the OASL genomic locus, representing H3K27ac and RNA levels in NB4 cells treated with vehicle (DMSO) or 2µM MC2580 or 50nM Palbociclib or combination of 2µM MC2580 + 50nM Palbociclib, 24- and 72-hours post LSD1 inhibition. Each track is annotated at the top, mentioning the treatment, time point, and correspondence to H3K27ac or RNA. Tracks are scaled equally for each experiment and time-point. The order from top to bottom is H3K27ac-24hrs followed by RNA-seq track-24hrs for DMSO, MC2580, Palbociclib, and MC2580+Palbociclib; then H3K27ac-72hrs followed by RNA-seq track-72hrs for DMSO, MC2580, Palbociclib, and MC2580+Palbociclib.*

Discussion

Genetic and epigenetic factors contributing to AML initiation, maintenance, and relapse have been subjects of research for various groups throughout decades. Many of these factors have been well identified in detail at molecular levels. Nonetheless, AML continues to have the lowest five-year relative survival rates among leukemias, with the frequent failure of novel emerging drugs in the relevant clinical settings (Hayatigolkhatmi *et al.*, manuscript in preparation; Papaemmanuil *et al.*, 2016; Siegel *et al.*, 2022). This clinical conundrum largely results from the interconnected and extremely complicated networks blocking myeloid differentiation and governing AML leukemogenesis. These networks simultaneously function in the foreground of the repeatedly mutated genomic landscape of AML cells. In such circumstances targeted therapies have decreased chances of overcoming these multilayered obstacles (Hayatigolkhatmi *et al.*, manuscript in preparation; Perl, 2017; Cai and Levine, 2019; Canaani, 2019). Hence, it is crucial to conceptualize AML, like many other cancers, as the complex cellular and molecular system that it is and intend to tackle the entire system down. Importantly, **this entire system is both influenced by and influences the epigenome in a dynamic manner**. This epigenomic plasticity, central to the leukemogenic network, offers in our view a valuable point for medical interventions, which needs to be better exploited with novel combination strategies (Hayatigolkhatmi *et al.*, manuscript in preparation; Papaemmanuil *et al.*, 2016; Liu, 2021; Majchrzak-Celinska, Warych and Szoszkiewicz, 2021; Ueda and Steidl, 2021).

The high proportion of epigenetic factors found to be mutated or showing abnormal expression patterns among AML patients, encouraged researchers to test them as therapeutic targets. Such an approach had hypothetically a wide spectrum of advantages in the clinics. Epidrugs can target a specific epigenetic enzyme, which a leukemic blast relies

heavily on, while the catalytic function of that enzyme is expected to be easily and usually compromised by other enzymes in normal cells. Furthermore, they promise even less toxicity to healthy cells since the impact of epidrugs typically depends on the continuous presence of the drug in the biological system and can be reverted shortly after the treatment is finished. Such therapies can break the commonly observed resistance to targeted therapies through epigenetic modulation and hence are good candidates for effective combinatorial therapies. Epidrugs have a very broad range of effect, such as triggering immune response, and targeting LSCs who can resist conventional therapies and are held responsible for MRD and relapse. Furthermore they are able to cover a wide range of AML subtypes by targeting mutually malfunctioning epigenetic regulators among different AMLs (Hayatigolkhatmi *et al.*, manuscript in preparation; Mehdipour, Santoro and Minucci, 2015; Gambacorta *et al.*, 2019; Jones *et al.*, 2019; Majchrzak-Celinska, Warych and Szoszkiewicz, 2021; Ueda and Steidl, 2021). LSD1 inhibition has been one of the most intriguing epigenetic therapy approaches for AML patients as well as other malignancies. In the context of APL, we have found that interfering with LSD1's non-enzymatic role in its interaction with GFI1 is crucial for inducing differentiation in synergism with ATRA (Ravasio *et al.*, 2020). This finding added more depth to understanding how an epidrug can work effectively in AML patients. Learning the therapeutic potential of LSD1 inhibitors in APL, we intended to further explore its potential independent of ATRA and in a wider range of AML subtypes. Hence, in this study we planned to investigate a novel combinatorial approach and in models beyond APL.

In the first step, we discovered that the CDK inhibitor p21 (*CDKN1A*) has a determining effect on the response to LSD1 inhibition. The differential expression of p21 in UF-1 and NB4 cells, both of which carrying the t(15;17)(q24;q21) translocation and showing a very similar transcriptomic profile, correlates with their contrasting sensitivities to LSD1

inhibition. This is particularly intriguing given that both cell lines have comparable basal levels of LSD1 and show similar global genomic enrichment of H3K4me2 (LSD1's main target hPTM for demethylation), and upregulation of *GFI1B*, and *CD86* (LSD1's target genes) upon LSD1 inhibition. However, LSD1 inhibitors can halt the proliferation of UF-1 cells and initiate myeloid differentiation, whilst NB4 cells show no response to the same interventions (Figure 17 and Figure 18). RNA interference approach knocking down p21 in UF-1, and exogenous mild overexpression of p21 in NB4 cells, completely reverted the natural response of both cell lines to LSD1 inhibition (Figure 23 and Figure 24). Our study further illuminated the role of p21 in cell cycle regulation, specifically in the G1 to S transition, as a critical determinant of LSD1 sensitivity. The use of point mutations in p21 that prevent its interaction with either CDKs or PCNA provided firm evidence that the CDK interaction is crucial for sensitizing cells to LSD1 inhibition (Figure 26). This observation aligns well with the established role of p21 in cell cycle regulation and its interaction with CDKs, thereby providing a possible mechanistic explanation for the observed differential sensitivity to LSD1 inhibition. **These findings suggested that the differential response is not simply a consequence of variable LSD1 expression but is tightly tied to the cell cycle regulation mediated by p21**. Nevertheless, the aim of this project was to be translated to an effective and tolerable therapeutic strategy for a wide range of AML patients. Hence, we examined a novel therapeutic strategy that involves pharmacological manipulation of the cell cycle to sensitize AML cells to LSD1 inhibition. The use of **suboptimal doses of Palbociclib**, a CDK4/6 inhibitor, **effectively mimicked the role of p21 in prolonging the G1 phase without inducing cell cycle arrest**, thereby **sensitizing the cells to LSD1 inhibition** regardless of p21 expression levels (Figure 30). This approach could be particularly beneficial for fast-cycling AML subtypes that are naturally resistant to LSD1 inhibition. **The use of other CDK inhibitors like PF-06873600 and Milciclib further substantiates the concept that targeting**

the G1 to S transition could be a universal strategy to overcome resistance to LSD1 inhibition. We could confirm the same pattern of response to LSD1 inhibitors anticorrelating to the cell cycle speed in non-APL (Kasumi-1) and PML-RARα-free APL (PL-21) cell lines (Kubonishi *et al.*, 1984; Asou *et al.*, 1991). Very interestingly p21-KD in the slow-cycling Kasumi-1 and CDK4/6 inhibition in PL-21 resulted in loss and gain of sensitivity to LSD1 inhibition, respectively (Figure 25 and Figure 32). Such reproducible observation in AML, trigerred a curosity to assess such phenomenon in different tumor types. Hence, we conducted additional experiments using human primary melanoma cells. Six different primary melanoma samples were utilized, selected based on their expression levels of p21 (Figure 69). Consistent with the findings in AML cell lines, primary melanoma cells with high levels of p21 and slower growth rates exhibited greater sensitivity to MC2580 compared to rapidly growing cells with low levels of p21 (Figure 69). Subsequently, we performed p21-KD in the two primary samples that were sensitive to MC2580. The KD of p21 resulted in the rescue of cells from the growth inhibition induced by MC2580 treatment (Figure 69). In summary, these results indicate that the inhibitory impact of the LSD1 inhibitor is compromised by p21 KD, in melanoma models as well as AML. Thus, the translational potential of our findings is significant. The identification of p21 as a potential biomarker for LSD1 sensitivity could guide patient selection in clinical trials.

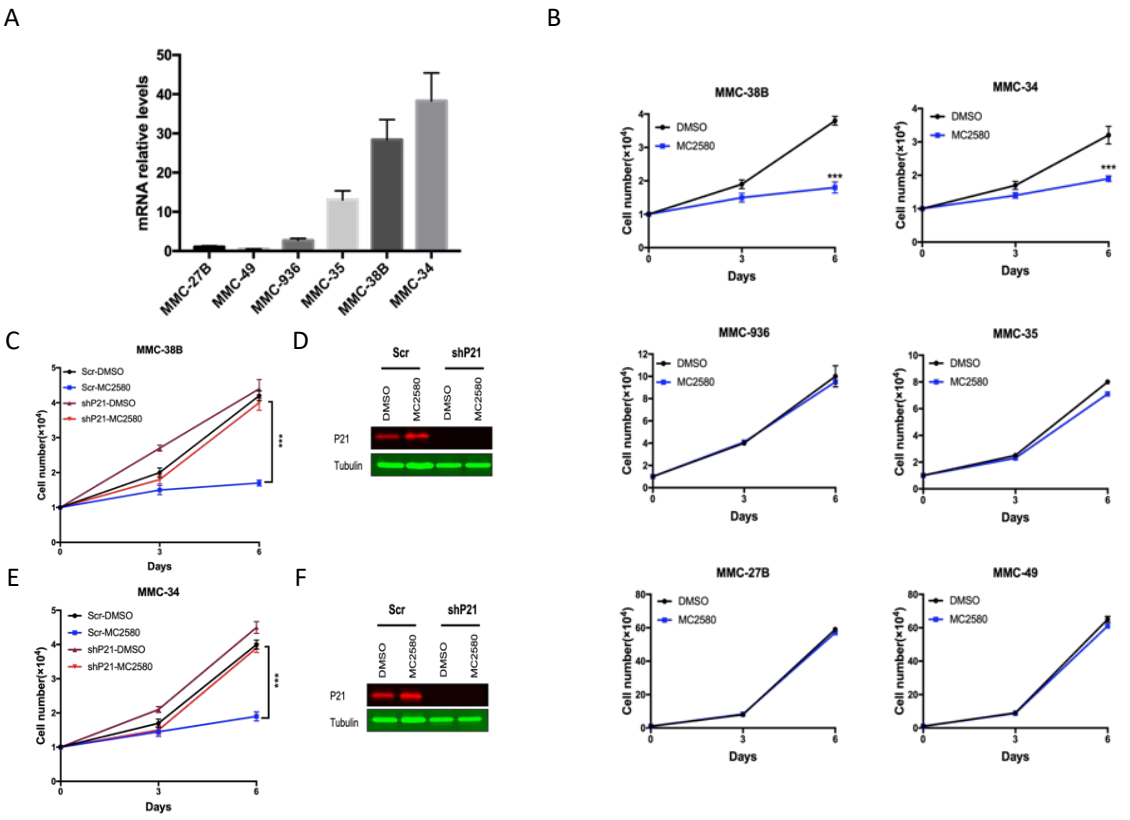

Figure 69. ***Assessment of LSD1 inhibition impact on human primary melanoma samples****. (A) Evaluation of relative p21 mRNA levels in human primary melanoma cells, with normalization against GAPDH. (B) Growth curves for human primary melanoma cells treated with either the vehicle (DMSO) or MC2580, presented as the mean of triplicates ± SD. (C) Growth curves for MMC-38B cells that were stably transduced with the indicated vectors, followed by treatment with either the vehicle (DMSO) or MC2580, presented as the mean of triplicates ± SD. (D) Western blot analysis of p21 protein in cell lysates from MMC-38B cells as described in (C), with tubulin serving as a loading control. (E) Growth curves for MMC-34 cells stably transduced with the indicated vectors, followed by treatment with either the vehicle (DMSO) or MC2580, presented as the mean of triplicates ± SD. (F) Western blot analysis of p21 protein in cell lysates from MMC-34 cells as described in (E), with tubulin as a loading control. Statistical analysis was performed using Bonferroni two-way ANOVA, with significance indicated by P values: < 0.05 (✱), < 0.01 (✱ ✱), and < 0.001 (✱ ✱ ✱).*

Moreover, the combination therapy involving CDK inhibitors and LSD1 inhibitors could be a promising approach for overcoming drug resistance in AML. However, it would be crucial to evaluate the long-term effects and potential toxicities, associated with this combination therapy in pre-clinical models (such as acute mortality due to LSD1 inhibition) before advancing to clinical trials (Wang *et al.*, 2018). In this regard, currently we are devising

therapeutic schedules with the least possible toxicities, while maintaining the therapeutic advantages. These modifications include lowering the administrative doses of the LSD1 inhibitors and minimizing the exposure times to LSD1 inhibitors (Figure 70). The first phase of our study shows that **given the complexity and heterogeneity of AML, a multi-pronged approach that integrates epigenetic therapy with cell cycle regulation could be the key to improving therapeutic outcomes and achieving sustainable disease-free survival rates**.

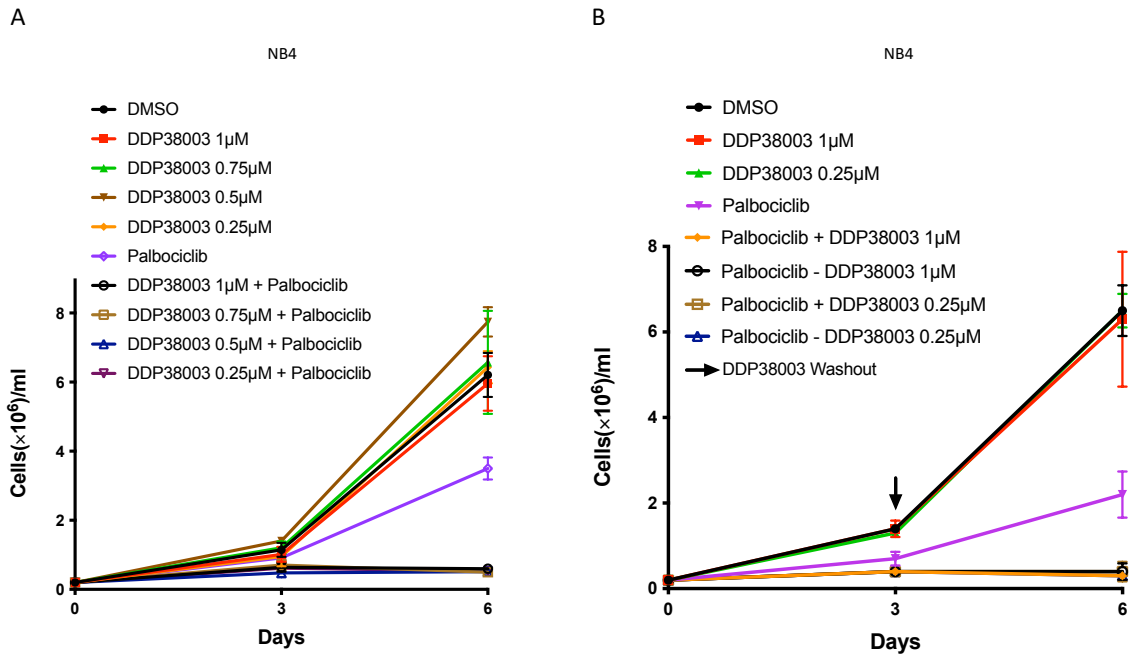

Figure 70. ***In-vitro setups show lower LSD1 inhibitor doses and their periodic removal to successfully maintain the therapeutic advantage in G1-extended NB4 cells****. (A) Growth curves of co-treatments of 75nM Palbociclib with various doses of DDP38003 as indicated in the legend and (B) with washout of DDP38003 at the third day of the co-treatment. Data are presented as mean of triplicates ± SD.*

The second part of our study deciphered the epigenetic implications of G1 phase elongation in AML cells. Our ATAC-seq data reveal that extending the G1 phase significantly alters chromatin accessibility (Figure 33 and Figure 34). This is a critical observation, as chromatin state is a key determinant in the regulation of gene expression and, by extension, cellular differentiation. The fact that Palbociclib treatment alone could induce such changes

underscores the potential of cell cycle manipulation as a strategy for epigenetic modulation. This aligns well with our initial hypothesis that **cells with a longer G1 phase may be more poised for differentiation, possibly due to a more accessible chromatin state that allows for the binding of hematopoiesis-regulating TFs**. Our ChIP-seq data on H3K27ac enrichment further confirms the idea that G1 phase elongation can induce significant changes in the enhancer and SE landscape of AML cells (Figure 35 and Figure 36). Given the role of SEs in regulating gene expression crucial for differentiation, this finding has profound implications (Hnisz *et al.*, 2013; Yamamoto *et al.*, 2018; Jia, Chng and Zhou, 2019). It suggests that **G1 phase elongation could potentially facilitate enhancer-promoter interactions necessary for the activation of differentiation-inducing genes, thereby enhancing the efficacy of LSD1 inhibitors**. The MS data on hPTMs' quantities provide a comprehensive view of the epigenetic landscape changes upon G1 phase elongation. Interestingly, these changes are not confined to the G1 phase but are stable across all cell cycle phases (Figure 38 and Figure 41). Perhaps one of the most striking findings is the epigenetic convergence of fast-cycling NB4 cells with their slow-cycling counterparts, UF-1 and Kasumi-1, upon G1 phase elongation (Figure 40 and Figure 41). These observations are specifically noteworthy as it provides a mechanistic basis for the gain of sensitivity of these fast-cycling cells to LSD1 inhibition post G1-phase elongation. It also opens up the possibility of using epigenetic profiling as a predictive marker for responsiveness to LSD1 inhibitors. **This suggests that the epigenetic remodeling induced by G1 phase elongation is a global alteration that could have far-reaching implications in the cellular response to LSD1 inhibition**. The second phase of our study provides robust evidence that the **G1 phase of the cell cycle serves as a critical window for epigenetic remodeling in AML cells, thereby influencing their responsiveness to LSD1 inhibitors**. *The golden remaining question* here is the precise cascade of events, in which the longer G1 contributes to the altered epigenetic

landscape. One possibility is the direct regulation of epigenetic enzymes by kinase activities of the affected CDKs, which we intend to further investigate as a future plan (Dalton, 2013; Michowski *et al.*, 2020).

The third part of our results uncovers the mechanistic underpinnings of how G1 phase elongation contributes to differentiation induction in AML cells. Our ATAC-seq data reveal that G1-extended cells show increased chromatin accessibility at the binding sites of key hematopoietic TFs such as SPI1, GFI1B, C/EBP family of TFs, and RUNX1 (Figure 44). This observation is particularly significant as these TFs are known to be central in hematopoietic differentiation. The enhanced accessibility to these TFs in the G1-extended cells suggests that the chromatin is in a 'primed' state, ready for the binding of these TFs, thereby facilitating the initiation of the differentiation process. In addition to increased accessibility, our ChIP-seq data indicate that G1-extended cells also experience a reduction or no change in H3K27me3, a key repressive mark, at the binding sites of these hematopoietic TFs, while LSD1 inhibition alone results in increased enrichment of this mark at the same sites (Figure 46). This is an important observation as it suggests that **the chromatin not only becomes more accessible but also less repressed, thereby creating a more conducive environment for the binding of differentiation-inducing TFs**. The disappearance of these repressive domains upon combination treatment with Palbociclib and MC2580 further underscores the synergistic effect of cell cycle manipulation and LSD1 inhibition in promoting differentiation (Figure 46). Taken together, our ATAC-seq and H3K27me3 ChIP-seq data provide compelling evidence that **G1 phase elongation induces an epigenomic remodeling that primes the chromatin for differentiation. This 'primed' state is characterized by increased accessibility and decreased repression at the binding sites of key hematopoietic TFs, thereby creating a chromatin landscape that is more amenable to differentiation induction by LSD1 inhibition**. The second and third phases of our study offer a rational basis

for the design of combination therapies aimed at overcoming resistance to LSD1 inhibitors and possibly other epidrugs in AML. *To assess the actual recruitment of these discovered TFs on the chromatin*, we plan to perform ChIP-seq experiments, locating their exact binding status upon G1 elongation and the subsequent LSD1 inhibition.

The fourth and final segment of our results focuses on the transcriptional changes that occur in AML cells with extended G1-phase upon LSD1 inhibition, particularly focusing on the *early events that precede morphological differentiation*. Our RNA-seq data confirm that LSD1 inhibition, especially when combined with G1 phase elongation, induces a transcriptional shift towards differentiation. This is evident from the increased enrichment of gene sets associated with normal hematopoietic function (Figure 47). These findings support our hypothesis that **differentiation in AML is a complex process involving a cascade of epigenetic and genetic changes**. Interestingly, our data reveal a significant upregulation of immune response genes upon LSD1 inhibition. This includes genes involved in microbial infection sensing, immune signaling, and subsequent immune response (Figure 51-Figure 53). The activation of these pathways suggests that **LSD1 inhibition may be triggering an innate immune response, which could be a critical factor in initiating differentiation**. Our PCA analysis based on the top 50 significant DEGs upon differentiation inducing therapies in three different AML subtypes, reveals that **fast-cycling AML cells with extended G1 phase have a transcriptional profile that closely resembles that of naturally slow-cycling AML cells** (Figure 55). This finding is in line with our earlier observations on the epigenetic similarities between these two cell types and further strengthens the argument for using G1 phase elongation as a strategy for enhancing the efficacy of LSD1 inhibitors in AML treatment. Interestingly, assessing the determinant genes in these similar transcriptomic profiles, shows their main contribution to the same viral mimicry and immune response pathways observed earlier (Figure 56). This is a novel finding that adds

another layer of complexity to our understanding of how LSD1 inhibition induces differentiation in AML cells. We followed this trace and uncovered a fascinating aspect of LSD1 inhibition in AML differentiation: **the activation of TEs, particularly ERVs** (Figure 60). This activation seems to be more pronounced upon G1 lengthening, suggesting a synergistic effect between cell cycle manipulation and LSD1 inhibition (Figure 61). **The activation of TEs could be the underlying mechanism triggering the innate immune response, as evidenced by the increased expression of dsRNA sensors like RIG-I, PKR, and MDA5** (Figure 62-Figure 68). This discovery can redefine our understanding of how epigenetic therapies like LSD1 inhibition work in AML. **Our study has provided a comprehensive insight into the multi-layered mechanisms through which LSD1 inhibition induces differentiation in AML cells. We have shown that this process involves a complex interplay of transcriptional and epigenetic changes. The activation of immune response genes and TEs adds a new dimension to this complexity and opens up exciting avenues for future research**. To find the *relevance of TEs' activation in the context of AML differentiation*, we are performing functional validations through direct targeting of these elements and subsequent phenotypic validation in response to the treatment regimen.

Our study provides a multi-dimensional understanding of how LSD1 inhibition functions in AML, revealing a complex synergy between the cell cycle control, epigenetic shifts, and transcriptional changes to induce **differentiation**. The study highlights the value of extending the **G1 phase of the cell cycle** as a strategy to make AML cells more responsive to **LSD1 inhibition**. This approach not only sets the stage for differentiation at the chromatin level by providing accessible binding sites for hematopoietic TFs, but also activates a series of transcriptional changes, including the upregulation of **immune response genes**. Notably, we identify the activation of TEs, especially elements of **HERVs**, as a new mechanism potentially driving these immune responses. The implications of these findings are

extensive for the future of AML research and treatment. They illuminate the way for the development of more effective, multi-targeted therapeutic approaches that can navigate the complexities of AML towards differentiation. Moreover, the discovery of new mechanistic layers, such as TEs, opens fresh gates for research, potentially revolutionizing our understanding of how epigenetic therapies work in hematological malignancies.

Materials and Methods

Cellular biology procedures

Cell lines and growth conditions

Cell lines were cultured in accordance with ATCC guidelines, under humidified conditions at 37°C and 5% CO_2. Comprehensive details pertaining to the leukemic cell lines utilized, including their AML FAB classification, cytogenetic profiles, and molecular characteristics, as well as their respective growth media, are cataloged in Table 1.

NB4 cells, originally established by Lanotte *et al.*, 1991, from an APL patient, exhibit phenotypic attributes akin to APL blasts (FAB M3). These cells were cultured in RPMI medium supplemented with 10% North American FBS, 100 U/mL penicillin, 1000 mg/mL streptomycin, and 2 mM L-glutamine.

UF-1 cells, characterized by Kizaki *et al.*, 1996, are phenotypically and clinically identical to NB4 cells, representing APL (FAB M3). These cells were cultured in RPMI medium supplemented with 20% South American FBS, 100 U/mL penicillin, 1000 mg/mL streptomycin, and 2 mM L-glutamine.

Kasumi-1 cells, established by Asou *et al.*, 1991, harbor (8;21)(q22;q22) translocation and represent FAB M2 phenotype of AML. These cells were cultured in RPMI medium supplemented with 10% North American FBS, 100 U/mL penicillin, 1000 mg/mL streptomycin, and 2 mM L-glutamine.

PL-21 cells, characterized by Kubonishi *et al.*, 1984, are also driven from an APL patient with similar properties to NB4 and UF-1 cells. These cells were cultured in RPMI medium

supplemented with 20% South American FBS, 100 U/mL penicillin, 1000 mg/mL streptomycin, and 2 mM L-glutamine.

HEK293T cells were designated for lentiviral vector production, owing to their superior transfection efficacy. These cells were similarly cultured in DMEM supplemented with 10% South American FBS, 100 U/mL penicillin, 1000 mg/mL streptomycin, and 2 mM L-glutamine.

Designation	Source	Subtype and molecular characterization	Medium
NB4	AML (APL)	M3; PML-RARα	90% RPMI 1640+10% FBS (North America) + 2mM L-Glutamine
KASUMI-1	AML	M2; AML1-ETO, KIT mut	90% RPMI 1640+10% FBS (North America) + 2mM L-Glutamine
PL-21	AML (APL)	M3; FLT3 ITD. NO PML-RARα	80% RPMI 1640+20% FBS (South America) + 2mM L-Glutamine
UF-1	AML (APL)	M3; PML-RARα	80% RPMI 1640+20% FBS (South America) + 2mM L-Glutamine

Table 9. AML cell lines used in this study.

Growth conditions for human primary melanoma cells

For the primary melanoma cells, we utilized RPMI-1640 medium supplemented with 10% FBS, 2mM glutamine, and 1% Penicillin/Streptomycin. Cells were cultured in a humidified tissue culture incubator set at 37°C under a 5% CO_2 atmosphere.

Proliferative and morphologic studies of the cells

Proliferation assessment

Approximately 4 x 10^5 cells for UF-1 and Kasumi-1, and 2 x 10^5 cells for the NB4 and PL-21 cell lines, were seeded, followed by treatment initiation with the indicated compounds at

time point D0. For *in vitro* assays, cells were subjected to treatment regimens involving 2 µM MC2580, 50 nM Palbociclib, 50nM PF-06873600, 500nM Milciclib and 1 µM DDP38003. Cell counting was conducted on triplicate independent suspensions. Each sample was assayed through an average of three separate counts. To ascertain cell viability, suspensions were stained with Trypan Blue (Sigma) in a 1:1 ratio and analyzed either via a Bio-Rad TC20™ automated cell counter or hemocytometer.

Data were normalized against vehicle-treated controls and are presented as proliferative indices.

Morphologic studies

Cells harvested from culture dishes were subjected to Cytospin deposition onto glass slides utilizing a Cytospin™ 4 Cytocentrifuge. Subsequently, these slides were stained through a May-Grünwald-Giemsa protocol. Cells were initially exposed to an 8-minute incubation in May-Grünwald stain (Sigma Aldrich). The slides then underwent a series of six washes in deionized water, followed by a 30-minute incubation in Giemsa stain diluted with a 19:1 volume ratio of distilled water. Post-incubation, slides were subjected to an additional tripartite wash in distilled water before being air-dried.

For long-term preservation, slides were secured with coverslips using Eukitt® mounting medium, a versatile adhesive and specimen preservative compatible with both manual and automated cover slipping systems.

Flow cytometry

The designated cell populations were subjected to cell cycle and analyses via Fluorescence-Activated Cell Sorting (FACS), employing 4',6-diamidino-2-phenylindole (DAPI) for DNA intercalation and mCherry or mVenus fluorescence for FUCCI(CA)2 examination.

Approximately 1 x 10^6 FUCCI(CA)2-expressing cells were harvested into 1.5 mL Eppendorf tubes and centrifuged at 3000 rpm for 5 minutes. The cell pellet was washed once with 1 mL of 1% BSA in PBS and subsequently centrifuged at 3000 rpm for 10 minutes. The pellet was then resuspended in 250 µL of cold PBS, to which 250 µL of PBS containing a final concentration of 2% formaldehyde was added. Following a 20-minute incubation on ice, cells were centrifuged at 3000 rpm for 10 minutes and washed in 1 mL of 1% BSA in PBS. The cells were pelleted again at 3000 rpm for 5 minutes and resuspended in 250 µL of PBS. A volume of 750 µL of pure ethanol was added dropwise to the cells while vortexing, followed by a minimum of 30-minute incubation on ice. Fixed cells could be stored at 4°C for an extended period. For staining, a cell density of 1 x 10^6 per sample was used, and cells were washed once in 1 mL of 1% BSA in PBS. Post-centrifugation at 3000 rpm for 5 minutes, the pellet was resuspended in 500 µL of DAPI diluted in PBS (5 µg/mL) and incubated overnight at 4°C. The cells and a not-DAPI stained sample (negative control) were subjected to flow cytometric analysis using a BD FACSCalibur instrument (BD Biosciences, Oxford, UK).

Viral vector production

Oligonucleotide Cloning into Vectors

Oligonucleotides of interest were subcloned into suitable vectors. Vectors contained either a puromycin resistance, or GFP gene (for KD or expression purposes, respectively). Digestion was executed at 37°C for 1 hour as per the following specifications:

- Plasmid: 3-10 µg
- 10X Digestion Buffer: 5 µL
- Restriction Enzymes: 5U

- Deionized water: Up to 50 µL

Subsequent to digestion, the plasmid was dephosphorylated using 1 µL of Antarctic Phosphatase (New England Biolabs, Ipswich, MA) and its corresponding 10X buffer. This incubation was performed at 37°C for 30 minutes and terminated by inactivating the enzyme at 70°C for 5 minutes. To isolate the digested DNA, the sample was subjected to 1% agarose gel electrophoresis in 1X TAE buffer. DNA bands were excised and purified using the QIAquick Gel Extraction Kit (QIAGEN, Venlo, NL) as per the manufacturer's guidelines.

Ligation of synthetic oligonucleotide expression construct (refer to the “Materials” section) was performed with the relevant vector at a molar ratio of 1:6. The ligation mix included 1 µL of T4 DNA Ligase (New England Biolabs) and was incubated at room temperature for 15 minutes. Alternatively synthetic oligonucleotide expression construct was ligated into the relevant vector at a molar ratio of 1:3. The ligation mix included 1 µL of Quick Ligase (New England Biolabs) and was incubated at room temperature for 10 minutes. The ligation mix components for both methods were as follows:

- Dephosphorylated vector: 10-100 ng
- Synthetic oligonucleotides: 1:6/1:3 insert:vector
- 10X T4 Ligase Buffer/2X Quick Ligation Reaction Buffer: 2 µL/10 µL
- T4 DNA Ligase/Quick Ligase: 1 µL
- Deionized water: Up to 20 µL

Finally, 10 µL of the ligation mixture was used to transform E. coli competent cells according to established transformation procedures detailed in the next section.

Transformation Protocol

Ten microliters of the ligation product, as prepared according to the subcloning into protocols, were introduced into E. coli competent cells (strain STBL3). Following the addition of the ligation product, the cells were kept on ice for 30 minutes. A heat shock step

was then conducted at 42°C for 30 seconds, subsequently followed by an additional 10 minutes incubation on ice. A post-heat shock recovery phase was carried out by incubating the cells at 37°C for 30 minutes in Luria-Bertani (LB) medium.

Transformed cells were then plated on LB agar plates containing 50 µg/µL of ampicillin and incubated at 37°C overnight. Colonies demonstrating ampicillin resistance were selected (5-10 colonies) and each was inoculated into 5 mL of LB medium supplemented with 100 µg/mL ampicillin (500X concentrated). Overnight culturing was conducted at 37°C.

Plasmid DNA was extracted from the bacterial cultures using the QIAprep Miniprep or Maxiprep kit (QIAGEN, Venlo, NL) following the manufacturer's standard protocols. To ascertain the presence of the targeted DNA fragment, an enzymatic digestion assay or Sanger sequencing was carried out.

Plasmid Preparation and Cell Expansion

HEK293T cells were expanded 1:5 in 100-mm plates, starting with five initial plates. Cells were transferred to medium-sized flasks and distributed evenly among 25 plates with 3-4 x 10^6 cells per plate. No trypsinization was required, as these cells detached upon pipetting. The cells were cultured in DMEM supplemented with 1% penicillin-streptomycin and 10% FBS (South America) at 37°C for 24 hours.

Transfection Preparations

The master mix was prepared, accounting for overages and omitting 2X HBS. A mixture of Dr 8.2 (8.0 µg), VSVG (5.0 µg), and target DNA (10 µg) was formulated with 62.5 µL $CaCl_2$ and enough water, adjusted to reach a volume of 500 µl. Upon the addition of 500 µl of 2X Hepes-buffered solution (HBS, composed of 250mM Hepes pH7, 250mM NaCl and 150mM Na_2PO_4), bubbles were created in the master mix, and the mixture was left at room temperature for 10 minutes. A volume of 1 ml of the master mix was then gently added to

each 100-mm plate from the previous day, ensuring even distribution over the cell monolayer. The plates were then transferred to a biosafety level 2 (BSL-2) environment.

Harvesting Lentivirus

The media were replaced 24 hours post-transfection, taking care not to disturb the attached cells. Lentiviral supernatants were harvested using a syringe fitted with a PVDF 0.45 µm Millipore filter. The harvested volume was supplemented with 10 ml of cold polyethylene glycol (PEG), thoroughly mixed, and stored at 4°C overnight.

Virus Concentration and Storage

The supernatant-PEG mix was centrifuged at 1500 xg for 1 hour at 4°C, and the supernatant was discarded. The viral pellet was resuspended in an appropriate volume of cold PBS for 100X concentration. Aliquots were prepared based on experimental needs and stored at -80°C until further use.

PEG Preparation

For PEG preparation, 200 ml of MilliQ water was mixed with 120g of PEG and 2.7g of NaCl. The mixture was stirred until completely dissolved, followed by filtration under a BSL-1 hood. The protocol could be paused after the addition of PEG to the harvested supernatants, allowing for storage at 4°C for two days.

Lentiviral shRNA Constructs

shRNA-encoding lentiviral constructs were engineered through the ligation of synthetic oligonucleotides targeting the specified mRNA transcripts into a custom pLKO vector, where the puromycin resistance cassette was substituted with an eGFP reporter gene. These oligonucleotides, designed with overhangs conducive to hairpin formation, were integrated into an AgeI- and EcoRI-digested pLKO vector using T4 DNA ligase (Invitrogen). The specific shRNA sequences utilized are mentioned in “Table of Oligos”.

P21-WT, P21-PCNAm, P21-CDKm Expression Plasmid

Expression vectors for WT p21, PCNA mutants, and CDK mutants were generously provided by Prof. Pelicci. In the p21-CDK mutant, residues W49, F51, and D52 were mutated to R49, S51, and A52, respectively; in the p21-PCNA mutant, residues M147, D149, and F150 were altered to A147, A149, and A150, respectively. All constructs underwent sequencing to confirm the intended mutational changes without any other mutations. Each plasmid incorporated a GFP reporter gene, and GFP-positive cells were isolated using a FACSAria cell sorter (BD Biosciences, Oxford, UK).

FUCCI(CA)2 Expression Plasmid

Expression vectors for FUCCI(CA)2 system were provided by RIKEN BRC. Each plasmid incorporated both mCHerry and mVenus reporter genes, and mCherry/mVenus-positive cells were isolated using a FACSAria cell sorter (BD Biosciences, Oxford, UK).

Infection of the cells

Cells were seeded in 24-well plates at a density of 5 x 10^5 cells in 500 µL of culture medium per well. Viral particles were either freshly diluted in RPMI supplemented with 10% serum and antibiotics or frozen at -80°C 100X concentrated in PBS, allowing for the addition of either 500 µL or 30 µL, respectively, to each well. Two or three rounds of transduction (based on the efficiency) were performed utilizing 5 µg/mL of polybrene (Sigma) as a transduction enhancer. Subsequently, the plate was subjected to centrifugation at 2500 rpm for 1 hour at room temperature and then incubated overnight at 37°C. Transduced cells featured either antibiotic resistance or fluorescence emission as selection markers. The populations expressing the selection marker were isolated via specific antibiotic treatment or fluorescence-activated cell sorting (FACSAria/FACSMelody™, BD Biosciences, Oxford, UK), respectively.

Fluorescence-activated cell sorting (FACS) of live cells

For sorting procedures, a minimum of 5 x 10^5 cells was deemed necessary. Cells were counted and resuspended in sorting solution, comprised of PBS supplemented with 2% FBS, 1% penicillin/streptomycin, 0.3% v/v Gentamicin (from a 50 mg/mL stock solution), and a final concentration of 1X Amphotericin B. A cell density of 5 x 10^6/mL to 1 x 10^7/mL was achieved prior to filtration through a 70-µm filter to eliminate cell aggregates. Sorting was executed on both infected cells and an uninfected control. Specialized tubes for cell transfer were obtained from the designated supplier based on the FACS system. Collection media were prepared, consisting of medium with 33% FBS, 3% penicillin/streptomycin, and 0.3% Gentamicin. Post-sorting, cells were maintained in standard medium supplemented with 1X Amphotericin B until subsequent freezing or utilization. The sorting was performed on either FACSAria™ cell sorter (BD Biosciences, Oxford, UK) or FACSMelody™ (BD Biosciences, Oxford, UK).

Live-cell imaging

In triplicates, approximately 250,000 Kasumi-1 and NB4 cells were seeded in individual wells of Tethis SBS 12-well plates at time point D0 (Krol *et al.*, 2021). Cells were covered with pre-diluted concentrations of Palbociclib 2nM, 10nM, 50nM, 250nM, and 1250nM, each administered in 3ml of a mix of 80ml MethoCult™ H4230 RPMI-1640 plus 20ml Roswell Park Memorial Institute (RPMI) 1640 medium with final concentrations of 10% FBS, 2mM glutamine and 1% Penicillin/Streptomycin.

Image acquisitions were performed by the imaging unit of IEO, Milan, Italy. However, in brief they were performed utilizing a Leica Thunder Imager outfitted with a Lumencor Spectra X Light Engine for fluorescence excitation, a motorized stage, and a Leica DFC9000 GTC camera. LAS X software (version 3.7.5.24914) was employed in conjunction with a 20X/0.75NA air objective, and a 2x2 binning was implemented to enhance the signal-to-noise ratio. Fluorescent signals from mCherry and mVenus were captured using excitation filters spanning 540-580 nm and 460-500 nm, respectively, along with 585 and 505 nm dichroic mirrors and 592-668 nm and 512-542 nm emission filters. A brightfield channel was concurrently recorded for contextual representation. Between 20 to 25 fields of view per well were imaged, with focal points manually calibrated for each position. Focus stability throughout time-lapse imaging was ensured by adaptive focus control. A total time-lapse duration of 72 hours was set for AML cells, and images were captured at one-hour intervals to minimize phototoxic effects.

Cell cycle quantification

Quantifications of live-cell imaging data were performed by the bioinformatics unit of Prof. Saverio Minucci's group in IEO, Milan, Italy. However, in brief the time-lapse tracking data were imported into R v4.3 for the cell cycle quantification. Cycling cells were identified using an in-house machine learning algorithm developed using tidymodels v1.1.0 and timetk v2.8.3. Cell cycle quantification was performed using tidyverse v.2.0.0.

ATAC-seq

Cell Harvesting

Cells were freshly isolated from *in vitro* culture prior to experimentation. Cells were washed once with 1X PBS and resuspended at a concentration of 5 x 10^4 cells in a 1.5 mL Eppendorf tube. Centrifugation was performed at 500g for 10 minutes at 4°C using a swinging bucket centrifuge.

Cell Lysis

After centrifugation, the supernatant was carefully aspirated without disturbing the cell pellet. The pellet was resuspended in 50 µL of chilled ATAC-Resuspension Buffer (RSB) containing 0.1% NP-40, 0.1% Tween-20, and 0.01% Digitonin. Cells were lysed by pipetting up and down thrice, followed by incubation on ice for 3 minutes. The lysis buffer was washed out using 1 mL of cold ATAC-RSB with 0.1% Tween-20 and no NP-40 or Digitonin, with inversion of the tube three times to mix. Nuclei were pelleted at 500 RCF for 10 minutes at 4°C.

Transposase Reaction (Tagmentation)

All supernatant was aspirated carefully, avoiding the cell pellet. The pellet was resuspended in 50 µL of transposition mixture and subjected to six pipetting cycles for uniform resuspension. The transposition mixture consisted of the following:

- 10 µL 5X Tn5 buffer
- 1 µL Tn5 enzyme
- 16.5 µL 1X PBS
- 0.25 µL 2% Digitonin

- 0.5 µL 10% Tween-20
- 21.75 µL nuclease-free H2O

The samples were briefly spun down to remove bubbles and incubated at 37°C for 30 minutes in a thermomixer set to 600 RPM.

Transposase Reaction Cleanup (TR Cleanup)

After tagmentation, a cleanup step was carried out. To each sample, 20 µL of a stop-mix was added, composed of 10 µL Cleanup buffer, 4 µL 5% SDS, 2 µL Proteinase K (20 mg/mL), and 4 µL nuclease-free H_2O. The samples were incubated at 40°C for 30 minutes, followed by centrifugation.

SPRI Beads Cleanup

SPRI beads were equilibrated at room temperature for 30 minutes and 105 µL were added to each sample. After pipetting 15 times, samples were incubated at room temperature for 5 minutes and placed on a magnet for 5 minutes. The supernatant was discarded, and the beads were washed twice with 100 µL of freshly prepared 80% Ethanol. After vacuum removal of ethanol and air-drying for 30 minutes, samples were resuspended in 22 µL of EB buffer or milliQ water.

Library Preparation and PCR Amplification

Library barcoding occurred during PCR. A master mix was prepared containing KAPA HiFi DNA Polymerase and other reagents (DNA 18 µL, Kapa buffer 5X 8.8 µL, dNTP 10 mM 1.32 µL, Kapa HiFi polymerase 0.88 µL, H2O 11 µL), except primers. Primers i5 and i7 (10 µM, indexed) were added separately 2 µL to each sample. PCR was performed under the following conditions: initial denaturation at 72°C for 5 min and 98°C for 2 min, followed by 15 cycles of 98°C for 20 s, 63°C for 30 s, and 72°C for 1 min.

Size Selection and Primer Cleanup

The protocol for size selection of DNA fragments <500 bp and primer cleanup was executed using 0.65X and 1.8X volumes of SPRI beads, respectively. DNA was eluted in 22 µL of molecular-grade water.

Quality Control

The DNA concentration was measured using a Glomax instrument, with expected concentrations ranging between 2-20 ng/µL. Additionally, libraries were run on a TapeStation to confirm fragment sizes of 180-200 bp for mononucleosome and 310-330 bp for dinucleosome fractions.

Buffers and Reagents:

ATAC-RSB (250ml)	STOCK	FINAL VOLUME
- 10 mM TrisHCl pH 7.4	1M	2.5ml
- 10 mM NaCl	5M	0.5ml
- 3 mM MgCl2	1M	0.75ml

Tn5 5X buffer (50ml)		
- 50 mM TrisHCl pH 8.4	1M	2.5ml
- 25 mM MgCl2	1M	1.25ml

Cleanup buffer (50ml)		
- 900 mM NaCl	5M	9ml
- 30 mM EDTA	0.5M	3ml

EB buffer (50ml)

-	TrisHcl 10 mM pH 8	1M	0.5ml

This methodological approach was validated for a robust and repeatable framework for conducting ATAC assays from cell-lines such as NB4, Kasumi-1, and UF-1, following the protocol provided by Croces and colleagues (Corces *et al.*, 2017).

ChIP-seq

Cross-Linking and Cell Lysis

Cells from AML cell lines were cross-linked using 1% formaldehyde at room temperature for 10 minutes. Cross-linking was terminated by adding glycine to a final concentration of 0.125M and incubating for an additional 5 minutes at room temperature. Cells were then centrifuged at 1,500 RPM for 10 minutes at 4°C. The cell pellet was washed twice with cold phosphate-buffered saline (PBS) and subsequently lysed in 200 µL of SDS buffer containing a protease inhibitor cocktail.

Sonication

The cell lysate was diluted using 100 µL of Triton dilution buffer to reach the desired IP buffer ratio (2 parts SDS buffer + 1 part Triton dilution buffer) and transferred to 1.5 mL Bioruptor® Pico microtubes. Samples were sonicated using the Diagenode Bioruptor® Pico with the following settings: 46 cycles of 30 seconds on and 30 seconds off, ensuring a chromatin fragment size between 100-300 bp.

Chromatin Quantification

For chromatin quantification, a master mix containing 10% SDS, 1M NaHCO3, and water was prepared. Samples were incubated at 65°C for one hour, followed by the addition of RNaseA and incubation at room temperature for 15 minutes. Proteinase K was added, and

samples were incubated at 65°C for another 30 minutes. DNA was purified using the Qiagen PCR purification kit and eluted in 15 µL of elution buffer. Then run on 1% agarose gel (with SYBR Safe) for 40 minutes using 100 V power. The gel was visualized to check the correct 100-300 chromatin fragments size.

Pre-clearing

BSA-blocked Protein A Sepharose beads were washed twice in IP buffer and resuspended in 1 mL of IP buffer containing protease inhibitors. Cell lysates were added to the beads and incubated at 4°C for two hours on a rotator. Following centrifugation at full speed for 10 minutes at 4°C, the supernatant was collected for subsequent steps.

Chromatin Immunoprecipitation

Chromatin samples were divided into at least two technical replicates with 1 mL aliquots for each immunoprecipitation (IP), 1 mL aliquots for mock (IgG) control, and 25 µL aliquots for each input. Primary antibodies were added at concentrations ranging from 0.5-3 µg/IP for hPTMs. Protein G/A magnetic beads were added to each IP, and the samples were incubated overnight at 4°C on a rotating wheel.

Washing and Decrosslinking

After overnight incubation, the beads were separated using a magnetic rack and washed three times with different buffers. Beads were then resuspended in 200 µL of decrosslinking solution and incubated at 65°C in a thermomixer at 1200 RPM. Proteinase K was added to the samples for overnight incubation.

DNA Purification and Quantification

Samples were centrifuged briefly to prevent evaporation, and the supernatant was collected and processed with the Qiagen PCR purification kit according to manufacturer's instructions. Elution was performed in 70 µL of elution buffer, and DNA concentration was measured using a Qubit DNA high sensitivity (HS) assay.

For initial validation and subsequent sequencing, the acquired DNA was subjected to quantitative real-time PCR (qPCR) prior to its use in ChIP-Seq library preparation, as outlined in the Illumina protocol. A quantity of 2ng of immunoprecipitated DNA was employed for the preparation of libraries.

ChIP-qPCR Validation

Validation of specific regions was carried out through ChIP-qPCRs. A dilution of immunoprecipitated DNA was prepared in 9.6 µl of H2O for each reaction and combined with 400 nM of primers to achieve a final volume of 20 µl in SYBR Green. To ensure reproducibility, each ChIP experiment was executed with a minimum of three biological replicates. The primers utilized for these ChIP-qPCRs are mentioned in “Table of Oligos”.

Buffers and Reagents:

SDS buffer

Reagent	Stock concentration	Final concentration	Volume of stock (for 250 ml)
TRIS-Cl pH8.1	1M	50mM	12.5 ml
SDS	10%	0.50%	12.5 ml
NaCl	5M	100mM	5 ml
EDTA pH8.0	0.5M	5mM	2.5 ml
NaN_3	10%	0.02%	500 ul
H_2O			Add to 250 ml

Triton dilution buffer

Reagent	Stock concentration	Final concentration	Volume of stock (for 250 ml)
Triton X-100	20%	5%	62.5 ml
TRIS-Cl pH8.6	10%	100mM	25 ml
NaCl	5M	100mM	5 ml
EDTA pH8.0	0.5M	5mM	2.5 ml
NaN_3	10%	0%	500 ul
H_2O			Add to 250 ml

Add Proteinase inhibitors cocktail immediately prior to use
Complete EDTA free Roche for 50 ml of IP buffer
Mini Complete EDTA free Roche for 15 ml of IP buffer

Mixed Micelle wash buffer

Reagent	Stock concentration	Final concentration	Volume of stock (for 500 ml)
Sucrose	65% (w/v)	5.2%	40 ml
Triton X-100	0.2	1%	25 ml
NaCl	5M	150mM	15 ml
SDS	0.1	0.2%	10 ml
TRIS-Cl pH8.1	1M	20 mM	10 ml
EDTA pH8.0	0.5M	5mM	5 ml
NaN_3	0.1	0.02%	1ml
H_2O			Add to 500 ml

Li/Cl detergent buffer

Reagent	Stock concentration	Final concentration	Volume of stock (for 500 ml)
LiCl	4M	250mM	31.25 ml
Deoxycholic acid (sodium salt)	10%	0.5%	25 ml
NP-40	20%	0.5%	12.5 ml
EDTA pH8.0	0.5M	1mM	1 ml
TRIS-Cl pH8.0	1M	10mM	5 ml
NaN_3	10%	0.02%	1 ml
H_2O			Add to 500 ml

buffer 500

Reagent	Stock concentration	Final concentration	Volume of stock (for 500 ml)
NaCl	5M	500mM	50 ml
Triton X-100	0.2	0.01	25 ml
Hepes ph7.5	1M	50mM	25 ml
Deoxycholic acid (sodium salt)	0.1	0.1%	5 ml
EDTA pH8.0	0.5M	1mM	1 ml
NaN_3	0.1	0.0002	1 ml
H_2O			Add to 500 ml

Decrosslinking solution

Reagent	Stock concentration	Final concentration	Volume of stock (for 10 ml)
$NaHCO_3$	1M	0.1M	1 ml
SDS	10%	1%	1 ml
H_2O			Add to 10 ml

Protein A Blocking

Protein A beads were washed three times in 1 mL of TE buffer and resuspended in TE to a final 50% slurry concentration. Lipid-free BSA was added to a final concentration of 0.5 mg/mL.

This methodological approach was validated for a robust and repeatable framework for conducting ChIP assays with low-input cells from cell-lines such as NB4, Kasumi-1, and UF-1.

Immunoblotting

Cell pellets were lysed with 100µL to 200µL of SDS lysis buffer (containing 2% SDS, 10% glycerol, and 50mM Tris HCL) or 8M urea buffer, supplemented with a protease inhibitor cocktail (Sigma Aldrich, Catalog.No.11836170001). Following a 15 minute centrifugation at 4°C and 13,000 RPM, protein concentration was assessed via Bio-rad Bradford assay. A total of 50-80 µg proteins were denatured for 10 min at 95°C after being combined with Laemmli buffer (comprising b-mercaptoethanol and bromophenol blue). Subsequent SDS-PAGE analysis was carried out by loading the denatured lysates into individual gel lanes. Electrophoretic separation was followed by protein transfer to a nitrocellulose membrane (Whatman) using a 1X transfer buffer with 20% methanol at 100 V for 1 hour at 4°C.

For membrane blocking, a TBS-T solution with 0.1% Tween and 5% non-fat dried milk was utilized. Primary antibodies (refer to the "Table of reagent, antibodies, and supplies), diluted in the same blocking solution, were applied for either one hour at room temperature or overnight at 4°C. After three 10-minute washes in 1% TBS-T, membranes were incubated with appropriate IRDye near-infrared (NIR)-labeled secondary antibodies, diluted in 5% milk, for 30 to 60 minutes at room temperature. After three additional TBS-T washes, fluorescent detection of the bound secondary antibodies was accomplished using the Odyssey system from Licor.

MS on hPTMs

MS studies were handled by our colleagues in Prof. Tiziana Bonaldi's group in IEO, Milan. However, a brief description of the protocol is provided here. Around 4 µg of histone octamers were combined with isotopically labeled histones in equivalent quantities, serving

as an internal standard (Noberini and Bonaldi, 2017). These were then subjected to electrophoretic separation via 17% SDS-PAGE. Subsequent to gel excision of histone bands, propionic anhydride was employed for chemical acylation, followed by in-gel proteolytic digestion using trypsin. The peptides underwent N-terminal derivatization using phenyl isocyanate (PIC) (Noberini *et al.*, 2021). The peptide fractions were then partitioned using reversed-phase chromatography, utilizing a 25-cm EASY-Spray column (Thermo Fisher Scientific) with an inner diameter of 75 µm and PepMap C18, 2 µm particles. This was interfaced in real-time with a Q Exactive Plus mass spectrometer via an EASY-Spray™ Ion Source, as previously delineated (Noberini *et al.*, 2021).

Subsequent data acquisition in RAW format was subjected to computational analysis using EpiProfile 2.0 (Yuan *et al.*, 2018), with manual verification for quality control. Quantitative assessment of histone modifications was performed by calculating the % relative abundance (%RA) for both the sample (light channel - L) and the internal standard (heavy channel - H). This was achieved by normalizing the area under the curve (AUC) for each acetylated peptide against the cumulative AUCs for all observed peptide forms of that type, followed by multiplication by 100. Finally, the Light/Heavy (L/H) ratios of %RA were computed.

RNA extraction and qPCR

For the extraction of total RNA, a 1 mL aliquot of TRIzol (Invitrogen) reagent or relevant volume of lysis buffer was introduced to a cell pellet of 2 to 4 million cells. To achieve complete cell lysis, the cell-TRIzol/lysis buffer blend was subjected to meticulous pipetting. Subsequently, the lysate was transferred to a sterile microcentrifuge tube for RNA

purification, employing the RNeasy Mini Kit (Qiagen) or Zymo Research Quick-RNA Miniprep (in case of no directzol) in accordance with the protocol provided by manufacturers. RNA concentration and purity were ascertained via spectrophotometric analysis using the ND1000 NanoDrop or Qubit DNA HS assay.

Reverse transcription of the isolated RNA to complementary DNA (cDNA) was performed utilizing the OneScript Plus Reverse Transcriptase (abm) or SuperScript II Kit (Invitrogen), following the manufacturers' guidelines.

RNA-seq

RNA-seq was executed in compliance with the Illumina TruSeq Low-Sample Protocol, choosing specifically on polyadenylated RNA species. Initially, total RNA integrity was assessed via capillary electrophoresis using the Agilent Bioanalyzer equipped with a picoRNA Chip. Thereafter, ds-cDNA libraries compatible with next-generation sequencing on the Illumina platform were generated.

For library preparation, we employed the Illumina TruSeq v.2 RNA Sample Preparation Kit, adhering to the manufacturer's provided manual. Input RNA ranged from 0.1 to 1 µg and underwent dual rounds of mRNA enrichment using poly-T oligo-attached magnetic beads under denaturing conditions. Subsequent RNA fragmentation was facilitated via the divalent cations present in the Illumina-specific fragmentation buffer, augmented by elevated thermal conditions.

Reverse transcription of fragmented RNA to first-strand cDNA utilized random hexamers and was catalyzed by SuperScript II Reverse Transcriptase (Invitrogen). The synthesis of second-strand cDNA involved DNA Polymerase I and RNase H enzymatic activities. AMPure

XP beads were deployed for the subsequent cDNA purification, their efficiency being concentration-dependent for the retrieval of differently sized PCR products.

The cDNA library displayed non-uniform overhangs due to the fragmentation process. These were rectified via exonuclease and polymerase activities, followed by 3' adenylation. Illumina-specific adapters were ligated to the modified ends, and the library was enriched through 15 PCR cycles using an Illumina-specific primer mix.

Finally, the integrity and concentration of the prepared libraries were validated using an Agilent Bioanalyzer 2100 instrument equipped with a HS DNA assay.

Data and statistical analyses

Data and statistical analyses of this study were performed by the bioinformatics unit of Prof. Saverio Minucci's group in IEO, Milan, Italy. However, in brief the processes are described below for each experimental purpose:

ChIP-seq Analysis

Raw reads 51bp PE were quality-filtered and aligned to the hg18 reference genome using nf-core/chipseq v2.0.0 pipeline using bowtie as aligner and MACS for peaks calling with default parameters except for: --min_reps_consensus 2, --macs_fdr 0.001, --narrow_peak True for the H3K27ac samples while --macs_fdr 0.00001, --narrow_peak False , --broad_cutoff 0.00001 for the H3K27me3 samples. Black and grey hg18 regions were removed from the analysis.

Super-enhancer (SE) identification was performed as previously described in: https://doi.org/10.1016%2Fj.cell.2013.09.053.

Super-silencer (SI) identification was performer as previously described in: https://doi.org/10.1038/s41467-021-20940-y

Motif discovery analysis was performed using Pscan-ChIP v1.3 online tool using:

- Assembly hg18
- Background NB4
- Descriptors Jaspart 2018 NR.

Genomic region annotation was performed using ChIPseeker v1.32.1 while enrichment heatmaps were performed using deeptools v3.5.1.

ATAC-seq Analysis

Raw reads 51bp PE were quality-filtered and aligned to the hg18 reference genome using nf-core/ atacseq v1.2.1 pipeline using bowtie as aligner and MACS for peakcalling with default parameters except: --macs_fdr 0.001, --min_reps_consensus set as 3 for the 24h samples while 1 for the 72h.

Tidybulk v1.8 was used to assess differential accessibility using edgeR quasi-likelihood method with TMM as scaling method. Differentially accessible regions (DARs) were defined as those showing FDR ≤0.05 and linear fold-change ≥0.5.

Differential footprint analysis was performed using Tobias v0.15.1

Genomic region visualization was performed using deeptools v3.5.1

RNA-seq Data Analysis

Gene quantification:

Raw reads 150bp PE for NB4 and Kasumi samples and 51bp PE for PL-21 samples were quality-filtered and aligned to the hg18 reference genome using nf-core/rnaseq v3.9 pipeline using STAR as aligner and Salmon for quantification with default parameters.

Tidybulk v1.8 was used to assess differential expression using edgeR quasi-likelihood method with TMM as scaling methods. Differentially expressed genes (DEGs) were defined

as those showing FDR ≤0.01 and linear fold-change ≥1.5 for NB4 and Kasumi while linear fold-change ≥1 for PL-21.

Pathway analysis and transcription factor prediction analysis were performed with QIAGEN's Ingenuity Pathway Analysis (IPA, QIAGEN Redwood City, www.qiagen.com/ingenuity).

Gene set enrichment analysis was performed using clusterprofiler v.4.4.4 GSEA function with genesets downloaded from Molecular Signatures Database (MSigDB).

The online tool EnricR-KG was used for assessing the ORA enrichment analysis selecting wikipathways, reactome and KEGG as databases.

The combined bigwig files for UCSC browser visualization of genome profiles were obtained using HOMER.

Transposable Elements quantification:

STAR v2.7.1a was used to align NB4 and Kasumi reads to the hg18 genome reference reads for the analysis of transposable element with the following parameters: --outFilterIntronMotifs, --RemoveNoncanonicalUnannotated, --outFilterScoreMinOverLread 0.3, --outFilterMatchNminOverLread 0.3, --winAnchorMultimapNmax 200, --outFilterMultimapNmax 200. The resulted alignments were used in the TEcount package v.1.0.0 for the transposable element quantification. The differential analysis on the TE was performed with Tidybulk as previous described using FDR ≤0.05 and linear fold-change ≥0.5 as threshold.

Table of sourced reagents, antibodies, and supplies

Material	Title	Source	Purpose	Identifiers
Drug	Palbociclib	Selleckchem	CDK4/6 inhibition	S4482
Drug	Milciclib	NerPharma in Nerviano	CDK1/2/4/6 inhibition	PHA-848125
Drug	PF-06873600	Selleckchem	CDK2/4/6 inhibition	S8816
Drug	MC2580	Binda *et al.*, 2010	LSD1 inhibition	Compound 14e
Drug	DDP38003	Vianello *et al.*, 2016	LSD1 inhibition	Compound 15
Antibody	LSD1 antibody	Abcam	Primary antibody targeting LSD1 for immunoblotting	ab17721
Antibody	H3K4me2 antibody	Abcam	Primary antibody targeting di-methylation on lysin 4 of H3 for immunoblotting	ab32356
Antibody	H3K27ac antibody	Abcam	Primary antibody targeting acetylation on lysin 27 of H3 for ChIP	ab4729
Antibody	H3K27me3 antibody	Cell Signaling	Primary antibody targeting tri-methylation on lysin 27 of H3 for ChIP	C36B11
Antibody	Total H3 antibody	Abcam	Primary antibody targeting H3 for immunoblotting	ab1791

Antibody	P21 antibody	Cell Signaling	Primary antibody targeting p21 for immunoblotting	2947S
Antibody	alpha-Tubulin antibody	Santa Cruz	Primary antibody targeting alpha-Tubulin for immunoblotting	sc-32293
Enzyme	Tn5 transposase	Gift from Gioacchino Natoli's group in IEO, Milan, Italy	Tagmentation for ATAC-seq	Tn5
Plasmid	tFucci(CA)2/pCSII-EF	RIKEN BRC through the National BioResource Project of the MEXT, Japan (cat. RDB15446); Sakaue-Sawano, et al., Mol. Cell 68 (3): 626-640.e5. 2017.	Cell cycle profiling	RDB15446
Software	LAS X	Leica Microsystems Inc	Microscopy acquisitions	https://www.leica-microsystems.com/products/microscope-software/
Software	FIJI	Schindelin et al., 2012	Picture analyses	https://fiji.sc/
Software	TrackMate	https://doi.org/10.1016/j.ymeth.2016.09.016	Live-cell image cell tracking	https://imagej.net/plugins/trackmate/
Widefield Microscope	Leica Thunder Imager	Leica	Microscopy	https://www.leica-microsystems.com/products/thunder-imaging-systems/
Supply	SBS-Glass bottom multiwell plate	Tethis s.p.a corporation	Immobilized cell culture	P12G-1.5-14-F

Table 10. Table of sourced reagents, antibodies, and supplies used in this study.

Table of oligos

Target of shRNA	Sequence
Human CDKN1A(p21) #1	GTCACTGTCTTGTACCCTTGT
Human CDKN1A(p21) #2	CGCTCTACATCTTCTGCCTTA

Table 11. Sequence of oligonucleotide constructs used for RNA interference in this study.

Primer name	Forward primer (Fw)	Reverse primer (Rv)
GAPDH	GCCTCAAGATCATCAGCAATGC	CCACGATACCAAAGTTGTCATGG
LSD1	AGACGACAGTTCTGGAGGGTA	TCTTGAGAAGTCATCCGGTCA
P21	TCACTGTCTTGTACCCTTGTGC	GGCGTTTGGAGTGGTAGAAA
GFI1b	TCTGGCCTCATGCCCTTA	GGCACTGGTTTGGGAATAGA
CD86	CAAGACGCGGCTTTTATCTT	ATCCAAGGAATGTGGTCTGG

Table 12. Sequence of primers used for qPCR in this study.

Primer name	Forward primer (Fw)	Reverse primer (Rv)
GAPDH	TTCGCTCTCTGCTCCTCCTG	CCTAGCCTCCCGGGTTTCTC
Gene Desert	AGCTATCTGTCGAGCAGCCAAG	CATTCCCCTCTGTTAGTGGAAGG
PI16	AGCCCTCACAGATGAGGAGA	GCCACACTTACCATGTGCAG
SPI1	GAGGGGAAACCCTTCCATT	CAGGGGATCTGACCGACTC

Table 13. Sequence of primers used for ChIP-qPCR in this study.

ChatGPT as a support tool

ChatGPT (OpenAI, https://chat.openai.com) was employed as an aid in literature analysis and text refinement. The system assisted in comparing relevant studies, and highlighting main concepts. All content produced was carefully verified and validated against the original references. Importantly, artificial intelligence tools were not involved in generating, processing, or altering experimental data, and did not substitute the authors' original scientific input.

References

Abbas, T. and Dutta, A. (2009) 'P21 in cancer: Intricate networks and multiple activities', *Nature Reviews Cancer*, 9(6), pp. 400–414. Available at: https://doi.org/10.1038/nrc2657.

Abdel-Aziz, A.K. *et al.* (2020) 'Tuning mTORC1 activity dictates the response to LSD1 inhibition of acute myeloid leukemia', *Haematologica*, 105(8), pp. 2105–2117. Available at: https://doi.org/10.3324/haematol.2019.224501.

Ahuja, A.K. *et al.* (2016) 'A short G1 phase imposes constitutive replication stress and fork remodelling in mouse embryonic stem cells', *Nature Communications*, 7(May 2015). Available at: https://doi.org/10.1038/ncomms10660.

Alberich-Jordà, M. *et al.* (2012) 'C/EBPγ deregulation results in differentiation arrest in acute myeloid leukemia', *The Journal of Clinical Investigation*, 122(12), pp. 4490–4504. Available at: https://doi.org/10.1172/JCI65102.

Arnold, O. *et al.* (2022) 'The Role of DOT1L in Normal and Malignant Hematopoiesis', *Frontiers in Cell and Developmental Biology*, 10. Available at: https://doi.org/10.3389/FCELL.2022.917125.

Asada, S. *et al.* (2019) 'The role of ASXL1 in hematopoiesis and myeloid malignancies', *Cellular and molecular life sciences : CMLS*, 76(13). Available at: https://doi.org/10.1007/S00018-019-03084-7.

Asou, H. *et al.* (1991) 'Establishment of a human acute myeloid leukemia cell line (Kasumi-1) with 8;21 chromosome translocation', *Blood*, 77(9), pp. 2031–2036. Available at: https://doi.org/10.1182/blood.v77.9.2031.2031.

Bansal, I., Pandey, A.K. and Ruwali, M. (2023) 'Small-molecule inhibitors of kinases in breast cancer therapy: recent advances, opportunities, and challenges', *Frontiers in Pharmacology*, 14, p. 1244597. Available at: https://doi.org/10.3389/fphar.2023.1244597.

Beaver, J.A. *et al.* (2015) 'FDA approval: Palbociclib for the treatment of postmenopausal patients with estrogen receptor-positive, HER2-negative metastatic breast cancer', *Clinical Cancer Research*, 21(21), pp. 4760–4766. Available at: https://doi.org/10.1158/1078-0432.CCR-15-1185.

Bennett, J.M. *et al.* (1976) 'Proposals for the classification of the acute leukaemias. French-American-British (FAB) co-operative group', *British Journal of Haematology*, 33(4), pp. 451–458. Available at: https://doi.org/10.1111/j.1365-2141.1976.tb03563.x.

Bentsen, M. *et al.* (2020) 'ATAC-seq footprinting unravels kinetics of transcription factor binding during zygotic genome activation', *Nature Communications*, 11(1), p. 4267. Available at: https://doi.org/10.1038/s41467-020-18035-1.

Besse, B. *et al.* (2018) 'Efficacy of milciclib (PHA-848125AC), a pan-cyclin d-dependent kinase inhibitor, in two phase II studies with thymic carcinoma (TC) and B3 thymoma (B3T) patients.', *Journal of Clinical Oncology*, 36(15_suppl), pp. 8519–8519. Available at: https://doi.org/10.1200/JCO.2018.36.15_suppl.8519.

Bewersdorf, J.P. *et al.* (2019) 'Epigenetic therapy combinations in acute myeloid leukemia: what are the options?', *Therapeutic Advances in Hematology*, 10, pp. 1–19. Available at: https://doi.org/10.1177/2040620718816698.

Binda, C. *et al.* (2010) 'Biochemical, structural, and biological evaluation of tranylcypromine derivatives as inhibitors of histone demethylases LSD1 and LSD2', *Journal of the American Chemical Society*, 132(19), pp. 6827–6833. Available at: https://doi.org/10.1021/ja101557k.

Bird, A. (2007) 'Perceptions of epigenetics', *Nature 2007 447:7143*, 447(7143), pp. 396–398. Available at: https://doi.org/10.1038/nature05913.

Biswas, S. and Rao, C.M. (2018) 'Epigenetic tools (The Writers, The Readers and The Erasers) and their implications in cancer therapy', *European Journal of Pharmacology*, 837, pp. 8–24. Available at: https://doi.org/10.1016/j.ejphar.2018.08.021.

Blagitko-Dorfs, N. *et al.* (2019) 'Combination treatment of acute myeloid leukemia cells with DNMT and HDAC inhibitors: predominant synergistic gene downregulation associated with gene body demethylation', *Leukemia*, 33(4), pp. 945–956. Available at: https://doi.org/10.1038/s41375-018-0293-8.

Braun, T. and Gardin, C. (2017) 'Investigational BET bromodomain protein inhibitors in early stage clinical trials for acute myelogenous leukemia (AML)', *https://doi.org/10.1080/13543784.2017.1335711*, 26(7), pp. 803–811. Available at: https://doi.org/10.1080/13543784.2017.1335711.

Brunetti, L. *et al.* (2018) 'Mutant NPM1 Maintains the Leukemic State through HOX Expression', *Cancer Cell*, 34(3), pp. 499-512.e9. Available at: https://doi.org/10.1016/J.CCELL.2018.08.005.

Bruserud, O. *et al.* (2011) 'Acute myeloid leukemia with the t(8;21) translocation: Clinical consequences and biological implications', *Journal of Biomedicine and Biotechnology*, 2011. Available at: https://doi.org/10.1155/2011/104631.

Cai, S.F. and Levine, R.L. (2019) 'Genetic and epigenetic determinants of AML pathogenesis', *Seminars in Hematology*, 56(2), pp. 84–89. Available at: https://doi.org/10.1053/j.seminhematol.2018.08.001.

Cai, Y. *et al.* (2021) 'H3K27me3-rich genomic regions can function as silencers to repress gene expression via chromatin interactions', *Nature Communications*, 12(1), p. 719. Available at: https://doi.org/10.1038/s41467-021-20940-y.

Canaani, J. (2019) 'Management of AML Beyond "3 + 7" in 2019', *Clinical Hematology International*, 1(1), pp. 10–18. Available at: https://doi.org/10.2991/chi.d.190316.001.

Carnero, A. (2002) 'Targeting the cell cycle for cancer therapy', *British Journal of Cancer*, 87(2), pp. 129–133. Available at: https://doi.org/10.1038/sj.bjc.6600458.

Carnesecchi, J. *et al.* (2017) 'ERRα induces H3K9 demethylation by LSD1 to promote cell invasion', *Proceedings of the National Academy of Sciences*, 114(15), pp. 3909–3914. Available at: https://doi.org/10.1073/pnas.1614664114.

Casey, M.J. *et al.* (2023) 'The scaffolding function of LSD1/KDM1A reinforces a negative feedback loop to repress stem cell gene expression during primitive hematopoiesis', *iScience*, 26(1), p. 105737. Available at: https://doi.org/10.1016/j.isci.2022.105737.

Castex, J. *et al.* (2017) 'Inactivation of Lsd1 triggers senescence in trophoblast stem cells by induction of Sirt4', *Cell Death & Disease*, 8(2), pp. e2631–e2631. Available at: https://doi.org/10.1038/cddis.2017.48.

Cavalli, G. and Heard, E. (2019) 'Advances in epigenetics link genetics to the environment and disease', *Nature 2019 571:7766*, 571(7766), pp. 489–499. Available at: https://doi.org/10.1038/s41586-019-1411-0.

Chakrabarti, A. *et al.* (2015) 'HDAC8: a multifaceted target for therapeutic interventions', *Trends in Pharmacological Sciences*, 36(7), pp. 481–492. Available at: https://doi.org/10.1016/j.tips.2015.04.013.

Chammas, P., Mocavini, I. and Di Croce, L. (2020) 'Engaging chromatin: PRC2 structure meets function', *British Journal of Cancer*, 122(3), pp. 315–328. Available at: https://doi.org/10.1038/s41416-019-0615-2.

Chang, S., Yim, S. and Park, H. (2019) 'The cancer driver genes IDH1/2, JARID1C/ KDM5C, and UTX/ KDM6A: crosstalk between histone demethylation and hypoxic reprogramming in cancer metabolism', *Experimental & Molecular Medicine 2019 51:6*, 51(6), pp. 1–17. Available at: https://doi.org/10.1038/s12276-019-0230-6.

Chaturvedi, A. *et al.* (2016) 'Enantiomer-specific and paracrine leukemogenicity of mutant IDH metabolite 2-hydroxyglutarate', *Leukemia*, 30(8), pp. 1708–1715. Available at: https://doi.org/10.1038/leu.2016.71.

Chen, C. *et al.* (2013) 'Cancer-associated IDH2 mutants drive an acute myeloid leukemia that is susceptible to Brd4 inhibition', *Genes & development*, 27(18), pp. 1974–1985. Available at: https://doi.org/10.1101/GAD.226613.113.

Chen, C. *et al.* (2017) 'LSD1 sustains estrogen-driven endometrial carcinoma cell proliferation through the PI3K/AKT pathway via di-demethylating H3K9 of cyclin D1', *International Journal of Oncology*, 50(3), pp. 942–952. Available at: https://doi.org/10.3892/ijo.2017.3849.

Chen, C.W. and Armstrong, S.A. (2015) 'Targeting DOT1L and HOX gene expression in MLL-rearranged leukemia and beyond', *Experimental Hematology*, 43(8), pp. 673–684. Available at: https://doi.org/10.1016/j.exphem.2015.05.012.

Chen, J., Odenike, O. and Rowley, J.D. (2010) 'Leukemogenesis: More Than Mutant Genes', *Nature reviews. Cancer*, 10(1), pp. 23–36. Available at: https://doi.org/10.1038/nrc2765.

Chen, Z. *et al.* (2006) 'Structural Insights into Histone Demethylation by JMJD2 Family Members', *Cell*, 125(4), pp. 691–702. Available at: https://doi.org/10.1016/j.cell.2006.04.024.

Chera, B.S. *et al.* (2021) 'Phase 1 trial of adavosertib (AZD1775) in combination with concurrent radiation and cisplatin for intermediate-risk and high-risk head and neck

squamous cell carcinoma', *Cancer*, 127(23), pp. 4447–4454. Available at: https://doi.org/10.1002/cncr.33789.

Cheuk, A.T.C. and Guinn, B. (2008) 'Immunotherapy of acute myeloid leukaemia: development of a whole cell vaccine', *Frontiers in Bioscience: A Journal and Virtual Library*, 13, pp. 2022–2029. Available at: https://doi.org/10.2741/2820.

Chiappinelli, K.B. *et al.* (2015) 'Inhibiting DNA Methylation Causes an Interferon Response in Cancer via dsRNA Including Endogenous Retroviruses', *Cell*, 162(5), pp. 974–986. Available at: https://doi.org/10.1016/j.cell.2015.07.011.

Chung, M. *et al.* (2019) 'Transient Hysteresis in CDK4/6 Activity Underlies Passage of the Restriction Point in G1', *Molecular Cell*, 76(4), pp. 562-573.e4. Available at: https://doi.org/10.1016/j.molcel.2019.08.020.

Cimmino, L. *et al.* (2017) 'Restoration of TET2 Function Blocks Aberrant Self-Renewal and Leukemia Progression', *Cell*, 170(6), pp. 1079-1095.e20. Available at: https://doi.org/10.1016/j.cell.2017.07.032.

Corces, M.R. *et al.* (2017) 'An improved ATAC-seq protocol reduces background and enables interrogation of frozen tissues', *Nature Methods*, 14(10), pp. 959–962. Available at: https://doi.org/10.1038/nmeth.4396.

Cornwell, J.A. *et al.* (2023) 'Loss of CDK4/6 activity in S/G2 phase leads to cell cycle reversal', *Nature*, 619(7969), pp. 363–370. Available at: https://doi.org/10.1038/s41586-023-06274-3.

Couture, J.-F. and Trievel, R.C. (2006) 'Histone-modifying enzymes: encrypting an enigmatic epigenetic code', *Current Opinion in Structural Biology*, 16(6), pp. 753–760. Available at: https://doi.org/10.1016/j.sbi.2006.10.002.

Creutzig, U. *et al.* (2012) 'Diagnosis and management of acute myeloid leukemia in children and adolescents: Recommendations from an international expert panel', *Blood*, 120(16), pp. 3167–3205. Available at: https://doi.org/10.1182/blood-2012-03-362608.

Cuartero, S., Innes, A.J. and Merkenschlager, M. (2019) 'Towards a Better Understanding of Cohesin Mutations in AML', *Frontiers in Oncology*, 9, p. 462818. Available at: https://doi.org/10.3389/FONC.2019.00867/BIBTEX.

Cuneo, K.C. *et al.* (2019) 'Dose Escalation Trial of the Wee1 Inhibitor Adavosertib (AZD1775) in Combination With Gemcitabine and Radiation for Patients With Locally Advanced Pancreatic Cancer', *Journal of Clinical Oncology*, 37(29), pp. 2643–2650. Available at: https://doi.org/10.1200/JCO.19.00730.

Cusan, M. *et al.* (2018) 'LSD1 inhibition exerts its antileukemic effect by recommissioning PU.1- and C/EBPα-dependent enhancers in AML', *Blood*, 131(15), pp. 1730–1742. Available at: https://doi.org/10.1182/blood-2017-09-807024.

Dafflon, C. *et al.* (2016) 'Complementary activities of DOT1L and Menin inhibitors in MLL-rearranged leukemia', *Leukemia 2017 31:6*, 31(6), pp. 1269–1277. Available at: https://doi.org/10.1038/leu.2016.327.

Dai, X.-J. *et al.* (2020) 'Tranylcypromine Based Lysine-Specific Demethylase 1 Inhibitor: Summary and Perspective', *Journal of Medicinal Chemistry*, 63(23), pp. 14197–14215. Available at: https://doi.org/10.1021/acs.jmedchem.0c00919.

Dalton, S. (2013) 'G1 compartmentalization and cell fate coordination', *Cell*, 155(1), p. 13. Available at: https://doi.org/10.1016/j.cell.2013.09.015.

Daser, A. and Rabbitts, T.H. (2004) 'Extending the repertoire of the mixed-lineage leukemia gene MLL in leukemogenesis', *Genes and Development*, 18(9), pp. 965–974. Available at: https://doi.org/10.1101/gad.1195504.

Daud, A.I. *et al.* (2015) 'Phase I Dose-Escalation Trial of Checkpoint Kinase 1 Inhibitor MK-8776 As Monotherapy and in Combination With Gemcitabine in Patients With Advanced Solid Tumors', *Journal of Clinical Oncology*, 33(9), pp. 1060–1066. Available at: https://doi.org/10.1200/JCO.2014.57.5027.

Dawson, M.A. *et al.* (2014) 'Recurrent mutations, including NPM1c, activate a BRD4-dependent core transcriptional program in acute myeloid leukemia', *Leukemia*, 28(2), pp. 311–320. Available at: https://doi.org/10.1038/LEU.2013.338.

Deb, G. *et al.* (2019) 'Pre-clinical activity of combined LSD1 and mTORC1 inhibition in MLL-translocated acute myeloid leukaemia', *Leukemia 2019 34:5*, 34(5), pp. 1266–1277. Available at: https://doi.org/10.1038/s41375-019-0659-6.

Delvecchio, M. *et al.* (2013) 'Structure of the p300 catalytic core and implications for chromatin targeting and HAT regulation', *Nature Structural & Molecular Biology*, 20(9), pp. 1040–1046. Available at: https://doi.org/10.1038/nsmb.2642.

Dhall, A. *et al.* (2019) 'Intersection of epigenetic and metabolic regulation of histone modifications in acute myeloid leukemia', *Frontiers in Oncology*, 9(MAY). Available at: https://doi.org/10.3389/fonc.2019.00432.

Di Croce, L. *et al.* (2004) 'Altered epigenetic signals in human disease', *Cancer Biology and Therapy*, 3(9), pp. 831–837. Available at: https://doi.org/10.4161/cbt.3.9.1103.

Di Nardo, C.D. and Cortes, J.E. (2016) 'Mutations in AML: Prognostic and therapeutic implications', *Hematology*, 2016(1), pp. 348–355. Available at: https://doi.org/10.1182/asheducation-2016.1.348.

Ding, J. *et al.* (2013) 'LSD1-mediated epigenetic modification contributes to proliferation and metastasis of colon cancer', *British Journal of Cancer*, 109(4), pp. 994–1003. Available at: https://doi.org/10.1038/bjc.2013.364.

Döhner, H. *et al.* (2010) 'Diagnosis and management of acute myeloid leukemia in adults: Recommendations from an international expert panel, on behalf of the European LeukemiaNet', *Blood*, 115(3), pp. 453–474. Available at: https://doi.org/10.1182/blood-2009-07-235358.

Dombret, H. and Itzykson, R. (2017) 'How and when to decide between epigenetic therapy and chemotherapy in patients with AML', *Hematology*, 2017(1), pp. 45–53. Available at: https://doi.org/10.1182/asheducation-2017.1.45.

Donjerkovic, D. and Scott, D.W. (2000) 'Regulation of the G1 phase of the mammalian cell cycle', *Cell Research*, 10(1), pp. 1–16. Available at: https://doi.org/10.1038/sj.cr.7290031.

Dyda, F., Klein, D.C. and Hickman, A.B. (2000) 'GCN5-Related N-Acetyltransferases: A Structural Overview', *Annual Review of Biophysics and Biomolecular Structure*, 29(1), pp. 81–103. Available at: https://doi.org/10.1146/annurev.biophys.29.1.81.

Dzama, M.M. *et al.* (2020) 'Synergistic targeting of FLT3 mutations in AML via combined menin-MLL and FLT3 inhibition', *Blood*, 136(21), pp. 2442–2456. Available at: https://doi.org/10.1182/BLOOD.2020005037.

Egolf, S. *et al.* (2019) 'LSD1 Inhibition Promotes Epithelial Differentiation through Derepression of Fate-Determining Transcription Factors', *Cell Reports*, 28(8), pp. 1981-1992.e7. Available at: https://doi.org/10.1016/j.celrep.2019.07.058.

Fang, Y. *et al.* (2021) 'Natural products as LSD1 inhibitors for cancer therapy', *Acta Pharmaceutica Sinica B*, 11(3), pp. 621–631. Available at: https://doi.org/10.1016/j.apsb.2020.06.007.

Fang, Y., Liao, G. and Yu, B. (2019) 'LSD1/KDM1A inhibitors in clinical trials: Advances and prospects', *Journal of Hematology and Oncology*, 12(1), pp. 1–14. Available at: https://doi.org/10.1186/s13045-019-0811-9.

Fatemi, M. *et al.* (2002) 'Dnmt3a and Dnmt1 functionally cooperate during de novo methylation of DNA', *European Journal of Biochemistry*, 269(20), pp. 4981–4984. Available at: https://doi.org/10.1046/j.1432-1033.2002.03198.x.

Felsenfeld, G. and Groudine, M. (2003) 'Controlling the double helix', *Nature 2003 421:6921*, 421(6921), pp. 448–453. Available at: https://doi.org/10.1038/nature01411.

Fennell, K.A., Bell, C.C. and Dawson, M.A. (2019) 'Epigenetic therapies in acute myeloid leukemia: Where to from here?', *Blood*, 134(22), pp. 1891–1901. Available at: https://doi.org/10.1182/blood.2019003262.

Fiorentini, A. *et al.* (2020) 'The Time Has Come for Targeted Therapies for AML: Lights and Shadows', *Oncology and therapy*, 8(1), pp. 13–32. Available at: https://doi.org/10.1007/S40487-019-00108-X.

Fiskus, W. *et al.* (2009) 'Combined epigenetic therapy with the histone methyltransferase EZH2 inhibitor 3-deazaneplanocin A and the histone deacetylase inhibitor panobinostat against human AML cells', *Blood*, 114(13), pp. 2733–2743. Available at: https://doi.org/10.1182/BLOOD-2009-03-213496.

Flotho, C., Sommer, S. and Lübbert, M. (2018) 'DNA-hypomethylating agents as epigenetic therapy before and after allogeneic hematopoietic stem cell transplantation in myelodysplastic syndromes and juvenile myelomonocytic leukemia', *Seminars in Cancer Biology*, 51, pp. 68–79. Available at: https://doi.org/10.1016/J.SEMCANCER.2017.10.011.

Ford, D.J. and Dingwall, A.K. (2015) 'The cancer COMPASS: navigating the functions of MLL complexes in cancer', *Cancer Genetics*, 208(5), pp. 178–191. Available at: https://doi.org/10.1016/j.cancergen.2015.01.005.

Freeman-Cook, K.D. *et al.* (2021) 'Discovery of PF-06873600, a CDK2/4/6 Inhibitor for the Treatment of Cancer', *Journal of Medicinal Chemistry*, 64(13), pp. 9056–9077. Available at: https://doi.org/10.1021/acs.jmedchem.1c00159.

Fu, D.-J., Li, J. and Yu, B. (2021) 'Annual review of LSD1/KDM1A inhibitors in 2020', *European Journal of Medicinal Chemistry*, 214, p. 113254. Available at: https://doi.org/10.1016/j.ejmech.2021.113254.

Fujisawa, T. and Filippakopoulos, P. (2017) 'Functions of bromodomain-containing proteins and their roles in homeostasis and cancer', *Nature Reviews Molecular Cell Biology*, 18(4), pp. 246–262. Available at: https://doi.org/10.1038/nrm.2016.143.

Gagliardi, M., Strazzullo, M. and Matarazzo, M.R. (2018) 'DNMT3B Functions: Novel Insights From Human Disease', *Frontiers in Cell and Developmental Biology*, 6. Available at: https://www.frontiersin.org/articles/10.3389/fcell.2018.00140 (Accessed: 14 September 2023).

Gambacorta, V. *et al.* (2019) 'Epigenetic Therapies for Acute Myeloid Leukemia and Their Immune-Related Effects', *Frontiers in Cell and Developmental Biology*, 7(October). Available at: https://doi.org/10.3389/fcell.2019.00207.

Garcia-Bassets, I. *et al.* (2007) 'Histone methylation-dependent mechanisms impose ligand dependency for gene activation by nuclear receptors', *Cell*, 128(3), pp. 505–518. Available at: https://doi.org/10.1016/j.cell.2006.12.038.

Gauthier, N. *et al.* (2012) 'Development of Homogeneous Nonradioactive Methyltransferase and Demethylase Assays Targeting Histone H3 Lysine 4', *Journal of Biomolecular Screening*, 17(1), pp. 49–58. Available at: https://doi.org/10.1177/1087057111416659.

Gillespie, M. *et al.* (2022) 'The reactome pathway knowledgebase 2022', *Nucleic Acids Research*, 50(D1), pp. D687–D692. Available at: https://doi.org/10.1093/nar/gkab1028.

Glass, J.L. *et al.* (2017) 'Epigenetic identity in AML depends on disruption of nonpromoter regulatory elements and is affected by antagonistic effects of mutations in epigenetic modifiers', *Cancer Discovery*, 7(8), pp. 868–883. Available at: https://doi.org/10.1158/2159-8290.CD-16-1032.

Goel, S. *et al.* (2018) 'CDK4/6 Inhibition in Cancer: Beyond Cell Cycle Arrest', *Trends in Cell Biology*, 28(11), pp. 911–925. Available at: https://doi.org/10.1016/j.tcb.2018.07.002.

Göllner, S. *et al.* (2016) 'Loss of the histone methyltransferase EZH2 induces resistance to multiple drugs in acute myeloid leukemia', *Nature Medicine 2016 23:1*, 23(1), pp. 69–78. Available at: https://doi.org/10.1038/nm.4247.

Gough, S.M., Slape, C.I. and Aplan, P.D. (2011) 'NUP98 gene fusions and hematopoietic malignancies: common themes and new biologic insights', *Blood*, 118(24), pp. 6247–6257. Available at: https://doi.org/10.1182/BLOOD-2011-07-328880.

Grossmann, V. *et al.* (2011) 'Whole-exome sequencing identifies somatic mutations of BCOR in acute myeloid leukemia with normal karyotype', *Blood*, 118(23), pp. 6153–6163. Available at: https://doi.org/10.1182/BLOOD-2011-07-365320.

Gruszka, A.M., Valli, D. and Alcalay, M. (2017) 'Understanding the molecular basis of acute myeloid leukemias: where are we now?', *International Journal of Hematologic Oncology*, 6(2), pp. 43–53. Available at: https://doi.org/10.2217/ijh-2017-0002.

Hakimi, M.-A. *et al.* (2003) 'A Candidate X-linked Mental Retardation Gene Is a Component of a New Family of Histone Deacetylase-containing Complexes *', *Journal of Biological Chemistry*, 278(9), pp. 7234–7239. Available at: https://doi.org/10.1074/jbc.M208992200.

Hall, A.B. *et al.* (2014) 'Potentiation of tumor responses to DNA damaging therapy by the selective ATR inhibitor VX-970', *Oncotarget*, 5(14), pp. 5674–5685.

Hall, J.A. and Georgel, P.T. (2007) 'CHD proteins: a diverse family with strong tiesThis paper is one of a selection of papers published in this Special Issue, entitled 28th International West Coast Chromatin and Chromosome Conference, and has undergone the Journal's usual peer review process.', *Biochemistry and Cell Biology*, 85(4), pp. 463–476. Available at: https://doi.org/10.1139/O07-063.

Han, M. *et al.* (2019) 'Epigenetic Enzyme Mutations: Role in Tumorigenesis and Molecular Inhibitors', *Frontiers in Oncology*, 9. Available at: https://www.frontiersin.org/articles/10.3389/fonc.2019.00194 (Accessed: 14 September 2023).

Harbour, J.W. and Dean, D.C. (2000) 'Rb function in cell-cycle regulation and apoptosis', *Nature Cell Biology*, 2(4), pp. E65–E67. Available at: https://doi.org/10.1038/35008695.

Hayakawa, T. and Nakayama, J. (2010) 'Physiological Roles of Class I HDAC Complex and Histone Demethylase', *BioMed Research International*, 2011, p. e129383. Available at: https://doi.org/10.1155/2011/129383.

Hayami, S. *et al.* (2011) 'Overexpression of LSD1 contributes to human carcinogenesis through chromatin regulation in various cancers', *International Journal of Cancer*, 128(3), pp. 574–586. Available at: https://doi.org/10.1002/ijc.25349.

Heenan, P.R. *et al.* (2020) 'Bending and looping of long DNA by Polycomb repressive complex 2 revealed by AFM imaging in liquid', *Nucleic Acids Research*, 48(6), pp. 2969–2981. Available at: https://doi.org/10.1093/nar/gkaa073.

Helin, K. and Dhanak, D. (2013) 'Chromatin proteins and modifications as drug targets', *Nature*, 502(7472), pp. 480–488. Available at: https://doi.org/10.1038/nature12751.

Helin, K. and Minucci, S. (2017) 'The role of chromatin-Associated proteins in cancer', *Annual Review of Cancer Biology*, 1(November 2016), pp. 355–377. Available at: https://doi.org/10.1146/annurev-cancerbio-050216-034422.

Herbst-Gervasoni, C.J. *et al.* (2020) 'Structural Basis for the Selective Inhibition of HDAC10, the Cytosolic Polyamine Deacetylase', *ACS Chemical Biology*, 15(8), pp. 2154–2163. Available at: https://doi.org/10.1021/acschembio.0c00362.

Hess, L. *et al.* (2022) 'A toolbox for class I HDACs reveals isoform specific roles in gene regulation and protein acetylation', *PLOS Genetics*, 18(8), p. e1010376. Available at: https://doi.org/10.1371/journal.pgen.1010376.

Heuser, M. *et al.* (2021) '2021 Update on MRD in acute myeloid leukemia: a consensus document from the European LeukemiaNet MRD Working Party', *Blood*, 138(26), p. 2753. Available at: https://doi.org/10.1182/BLOOD.2021013626.

Hnisz, D. *et al.* (2013) 'XSuper-enhancers in the control of cell identity and disease', *Cell*, 155(4), p. 934. Available at: https://doi.org/10.1016/j.cell.2013.09.053.

Hochegger, H., Takeda, S. and Hunt, T. (2008) 'Cyclin-dependent kinases and cell-cycle transitions: does one fit all?', *Nature Reviews Molecular Cell Biology*, 9(11), pp. 910–916. Available at: https://doi.org/10.1038/nrm2510.

Hoffman, J. and Rosenkrantz, G.S. (1998) 'On the Unity of Compound Things: Living and Non-Living', *Ratio*, 11(3), pp. 289–315. Available at: https://doi.org/10.1111/1467-9329.00072.

Honda, A. *et al.* (2021) 'Loss-of-function mutations in BCOR contribute to chemotherapy resistance in acute myeloid leukemia', *Experimental Hematology*, 101–102, pp. 42-48.e11. Available at: https://doi.org/10.1016/J.EXPHEM.2021.07.005.

Hosseini, A. and Minucci, S. (2017) 'A comprehensive review of lysine-specific demethylase 1 and its roles in cancer', *Epigenomics*, 9(8), pp. 1123–1142. Available at: https://doi.org/10.2217/epi-2017-0022.

Hu, R. *et al.* (2018) 'SKA3 promotes cell proliferation and migration in cervical cancer by activating the PI3K/Akt signaling pathway', *Cancer Cell International*, 18(1), p. 183. Available at: https://doi.org/10.1186/s12935-018-0670-4.

Huang, Y. *et al.* (2007) 'Inhibition of lysine-specific demethylase 1 by polyamine analogues results in reexpression of aberrantly silenced genes', *Proceedings of the National Academy of Sciences*, 104(19), pp. 8023–8028. Available at: https://doi.org/10.1073/pnas.0700720104.

Huang, Y. *et al.* (2009) 'Polyamine analogues targeting epigenetic gene regulation', *Essays in Biochemistry*. Edited by H.M. Wallace, 46, pp. 95–110. Available at: https://doi.org/10.1042/bse0460007.

Hume, S., Dianov, G.L. and Ramadan, K. (2020) 'A unified model for the G1/S cell cycle transition', *Nucleic Acids Research*, 48(22), pp. 12483–12501. Available at: https://doi.org/10.1093/nar/gkaa1002.

Hustedt, N. and Durocher, D. (2017) 'The control of DNA repair by the cell cycle', *Nature Cell Biology*, 19(1), pp. 1–9. Available at: https://doi.org/10.1038/ncb3452.

Hytti, M. *et al.* (2015) 'Fisetin and luteolin protect human retinal pigment epithelial cells from oxidative stress-induced cell death and regulate inflammation', *Scientific Reports*, 5, p. 17645. Available at: https://doi.org/10.1038/srep17645.

Im, A.P. *et al.* (2014) 'DNMT3A and IDH mutations in acute myeloid leukemia and other myeloid malignancies: associations with prognosis and potential treatment strategies', *Leukemia 2014 28:9*, 28(9), pp. 1774–1783. Available at: https://doi.org/10.1038/leu.2014.124.

Imai, Y. *et al.* (2014) 'Crosstalk between the Rb pathway and AKT signaling forms a quiescence-senescence switch', *Cell Reports*, 7(1), pp. 194–207. Available at: https://doi.org/10.1016/j.celrep.2014.03.006.

Ishikawa, Y. *et al.* (2017) 'Synergistic anti-AML effects of the LSD1 inhibitor T-3775440 and the NEDD8-activating enzyme inhibitor pevonedistat via transdifferentiation and DNA rereplication', *Oncogenesis 2017 6:9*, 6(9), pp. e377–e377. Available at: https://doi.org/10.1038/oncsis.2017.76.

Janardhan, A. *et al.* (2018) 'Prominent role of histone lysine demethylases in cancer epigenetics and therapy', *Oncotarget*, 9(76), pp. 34429–34448. Available at: https://doi.org/10.18632/oncotarget.24319.

Jevtic, Z. *et al.* (2022) 'SMARCA5 interacts with NUP98-NSD1 oncofusion protein and sustains hematopoietic cells transformation', *Journal of Experimental and Clinical Cancer Research*, 41(1), pp. 1–15. Available at: https://doi.org/10.1186/S13046-022-02248-X/FIGURES/5.

Jia, Y., Chng, W.J. and Zhou, J. (2019) 'Super-enhancers: Critical roles and therapeutic targets in hematologic malignancies', *Journal of Hematology and Oncology*, 12(1), pp. 1–17. Available at: https://doi.org/10.1186/s13045-019-0757-y.

Jones, P.A. *et al.* (2019) 'Epigenetic therapy in immune-oncology', *Nature Reviews Cancer*, 19(3), pp. 151–161. Available at: https://doi.org/10.1038/s41568-019-0109-9.

Jordan, M.A., Thrower, D. and Wilson, L. (1991) 'Mechanism of Inhibition of Cell Proliferation by Vinca Alkaloids1', *Cancer Research*, 51(8), pp. 2212–2222.

Kakosaiou, K. *et al.* (2018) 'ASXL1 mutations in AML are associated with specific clinical and cytogenetic characteristics', *Leukemia & lymphoma*, 59(10), pp. 2439–2446. Available at: https://doi.org/10.1080/10428194.2018.1433298.

Kalin, B. *et al.* (2020) 'Panobinostat and decitabine prior to donor lymphocyte infusion in allogeneic stem cell transplantation', *Blood Advances*, 4(18), pp. 4430–4437. Available at: https://doi.org/10.1182/BLOODADVANCES.2020002074.

Kalkhoven, E. (2004) 'CBP and p300: HATs for different occasions', *Biochemical Pharmacology*, 68(6), pp. 1145–1155. Available at: https://doi.org/10.1016/j.bcp.2004.03.045.

Kauffman, E.C. *et al.* (2011) 'Role of androgen receptor and associated lysine-demethylase coregulators, LSD1 and JMJD2A, in localized and advanced human bladder cancer', *Molecular Carcinogenesis*, 50(12), pp. 931–944. Available at: https://doi.org/10.1002/mc.20758.

Kerenyi, M.A. *et al.* (2013) 'Histone demethylase Lsd1 represses hematopoietic stem and progenitor cell signatures during blood cell maturation', *eLife*. Edited by S.J. Morrison, 2, p. e00633. Available at: https://doi.org/10.7554/eLife.00633.

Kim, K.H. and Roberts, C.W.M. (2016) 'Targeting EZH2 in cancer', *Nature Medicine*, 22(2), pp. 128–134. Available at: https://doi.org/10.1038/nm.4036.

Kim, S.A. *et al.* (2020) 'Crystal Structure of the LSD1/CoREST Histone Demethylase Bound to Its Nucleosome Substrate', *Molecular Cell*, 78(5), pp. 903-914.e4. Available at: https://doi.org/10.1016/j.molcel.2020.04.019.

King, C. *et al.* (2015) 'LY2606368 Causes Replication Catastrophe and Antitumor Effects through CHK1-Dependent Mechanisms', *Molecular Cancer Therapeutics*, 14(9), pp. 2004–2013. Available at: https://doi.org/10.1158/1535-7163.MCT-14-1037.

Kizaki, M. *et al.* (1996) 'Establishment and characterization of a novel acute promyelocytic leukemia cell line (UF-1) with retinoic acid-resistant features', *Blood*, 88(5), pp. 1824–1833. Available at: https://doi.org/10.1182/blood.v88.5.1824.1824.

Kocpinar, E.F. *et al.* (2023) 'Depletion of Tip60/Kat5 affects the hepatic antioxidant system in mice', *Journal of Cellular Biochemistry*, 124(1), pp. 103–117. Available at: https://doi.org/10.1002/jcb.30348.

Krause, D.S. and Etten, R.A.V. (2007) 'Right on target: eradicating leukemic stem cells', *Trends in Molecular Medicine*, 13(11), pp. 470–481. Available at: https://doi.org/10.1016/j.molmed.2007.09.003.

Krol, I. *et al.* (2021) 'Detection of clustered circulating tumour cells in early breast cancer', *British Journal of Cancer*, 125(1), pp. 23–27. Available at: https://doi.org/10.1038/s41416-021-01327-8.

Kubonishi, I. *et al.* (1984) 'Establishment of a new peroxidase-positive human myeloid cell line, PL- 21', *Blood*, 63(2), pp. 254–259. Available at: https://doi.org/10.1182/blood.V63.2.254.254.

Kunadis, E. *et al.* (2021) 'Targeting post-translational histone modifying enzymes in glioblastoma', *Pharmacology & Therapeutics*, 220, p. 107721. Available at: https://doi.org/10.1016/j.pharmthera.2020.107721.

Lamouille, S., Xu, J. and Derynck, R. (2014) 'Molecular mechanisms of epithelial-mesenchymal transition', *Nature Reviews. Molecular Cell Biology*, 15(3), pp. 178–196. Available at: https://doi.org/10.1038/nrm3758.

Lange, C. and Calegari, F. (2010) 'Cdks and cyclins link G1 length and differentiation of embryonic, neural and hematopoietic stem cells', *Cell Cycle*, 9(10), pp. 1893–1900. Available at: https://doi.org/10.4161/cc.9.10.11598.

Lanotte, M. *et al.* (1991) 'NB4, a maturation inducible cell line with t(15;17) marker isolated from a human acute promyelocytic leukemia (M3)', *Blood*, 77(5), pp. 1080–1086. Available at: https://doi.org/10.1182/blood.v77.5.1080.1080.

Larrew, T. *et al.* (2021) 'Molecular Classification and Therapeutic Targets in Ependymoma', *Cancers*, 13(24), p. 6218. Available at: https://doi.org/10.3390/cancers13246218.

Laurent, B. *et al.* (2015) 'A Specific LSD1/KDM1A Isoform Regulates Neuronal Differentiation through H3K9 Demethylation', *Molecular Cell*, 57(6), pp. 957–970. Available at: https://doi.org/10.1016/j.molcel.2015.01.010.

Lee, Y. *et al.* (2021) 'Increased Histone Acetylation and Decreased Expression of Specific Histone Deacetylases in Ultraviolet-Irradiated and Intrinsically Aged Human Skin In Vivo',

International Journal of Molecular Sciences, 22(4), p. 2032. Available at: https://doi.org/10.3390/ijms22042032.

Lengyel, E. (2023) 'Data from Quantitative High-Throughput Screening Using an Organotypic Model Identifies Compounds that Inhibit Ovarian Cancer Metastasis'. Available at: https://doi.org/10.1158/1535-7163.c.6538335.v1.

Lessard, J. and Sauvageau, G. (2003) 'Bmi-1 determines the proliferative capacity of normal and leukaemic stem cells', *Nature*, 423(6937), pp. 255–260. Available at: https://doi.org/10.1038/NATURE01572.

Li, L.M. and Arnosti, D.N. (2010) 'Fine mapping of chromatin structure in Drosophila melanogaster embryos using micrococcal nuclease', *Fly*, 4(3), pp. 213–215. Available at: https://doi.org/10.4161/fly.4.3.12200.

Li, Y. *et al.* (2018) 'Therapeutic potential of GSK-J4, a histone demethylase KDM6B/JMJD3 inhibitor, for acute myeloid leukemia', *Journal of Cancer Research and Clinical Oncology*, 144(6), pp. 1065–1077. Available at: https://doi.org/10.1007/s00432-018-2631-7.

Liang, B. *et al.* (2023) 'Unlocking the potential of targeting histone-modifying enzymes for treating IBD and CRC', *Clinical Epigenetics*, 15, p. 146. Available at: https://doi.org/10.1186/s13148-023-01562-1.

Lin, T. *et al.* (2010) 'Requirement of the histone demethylase LSD1 in Snai1-mediated transcriptional repression during epithelial-mesenchymal transition', *Oncogene*, 29(35), pp. 4896–4904. Available at: https://doi.org/10.1038/onc.2010.234.

Lin, Y. *et al.* (2010) 'The SNAG domain of Snail1 functions as a molecular hook for recruiting lysine-specific demethylase 1', *The EMBO journal*, 29(11), pp. 1803–1816. Available at: https://doi.org/10.1038/emboj.2010.63.

Liu, H. (2021) 'Emerging agents and regimens for AML', *Journal of Hematology & Oncology*, 14(1), p. 49. Available at: https://doi.org/10.1186/s13045-021-01062-w.

Liu, R. *et al.* (2019) 'Differential localizations of protein phosphatase 1 isoforms determine their physiological function in the heart', *Acta Biochimica et Biophysica Sinica*, 51(3), pp. 323–330. Available at: https://doi.org/10.1093/abbs/gmy171.

Liu, S.-S. *et al.* (2020) 'HDAC11: a rising star in epigenetics', *Biomedicine & Pharmacotherapy*, 131, p. 110607. Available at: https://doi.org/10.1016/j.biopha.2020.110607.

Liu, W. *et al.* (2014) 'DOT1L Inhibition Sensitizes MLL-Rearranged AML to Chemotherapy', *PLOS ONE*, 9(5), p. e98270. Available at: https://doi.org/10.1371/JOURNAL.PONE.0098270.

Lonetti, A. *et al.* (2020) 'Inhibition of Methyltransferase DOT1L Sensitizes to Sorafenib Treatment AML Cells Irrespective of MLL-Rearrangements: A Novel Therapeutic Strategy for Pediatric AML', *Cancers 2020, Vol. 12, Page 1972*, 12(7), p. 1972. Available at: https://doi.org/10.3390/CANCERS12071972.

Lv, T. *et al.* (2012) 'Over-Expression of LSD1 Promotes Proliferation, Migration and Invasion in Non-Small Cell Lung Cancer', *PLOS ONE*, 7(4), p. e35065. Available at: https://doi.org/10.1371/journal.pone.0035065.

Lynch, J.T. *et al.* (2013) 'CD86 expression as a surrogate cellular biomarker for pharmacological inhibition of the histone demethylase lysine-specific demethylase 1', *Analytical biochemistry*, 442(1), pp. 104–106. Available at: https://doi.org/10.1016/J.AB.2013.07.032.

Lynch, J.T., Harris, W.J. and Somervaille, T.C.P. (2012) 'LSD1 inhibition: a therapeutic strategy in cancer?', *Expert Opinion on Therapeutic Targets*, 16(12), pp. 1239–1249. Available at: https://doi.org/10.1517/14728222.2012.722206.

Madan, V. and Koeffler, H.P. (2021) 'Differentiation therapy of myeloid leukemia: Four decades of development', *Haematologica*, 106(1), pp. 26–38. Available at: https://doi.org/10.3324/haematol.2020.262121.

Majchrzak-Celinska, A., Warych, A. and Szoszkiewicz, M. (2021) 'Novel approaches to epigenetic therapies: From drug combinations to epigenetic editing', *Genes*, 12(2), pp. 1–21. Available at: https://doi.org/10.3390/genes12020208.

Mak, T.W. and Saunders, M.E. (2006) 'Hematopoietic Cancers', *The Immune Response*, pp. 1025–1063. Available at: https://doi.org/10.1016/B978-012088451-3.50032-6.

Malumbres, M. (2014) 'Cyclin-dependent kinases', *Genome Biology*, 15(6), p. 122. Available at: https://doi.org/10.1186/gb4184.

Marasca, F. *et al.* (2022) 'LINE1 are spliced in non-canonical transcript variants to regulate T cell quiescence and exhaustion', *Nature Genetics*, 54(2), pp. 180–193. Available at: https://doi.org/10.1038/s41588-021-00989-7.

Matharu, N. and Ahituv, N. (2015) 'Minor Loops in Major Folds: Enhancer–Promoter Looping, Chromatin Restructuring, and Their Association with Transcriptional Regulation and Disease', *PLOS Genetics*, 11(12), p. e1005640. Available at: https://doi.org/10.1371/JOURNAL.PGEN.1005640.

Matthews, H.K., Bertoli, C. and de Bruin, R.A.M. (2022) 'Cell cycle control in cancer', *Nature Reviews Molecular Cell Biology*, 23(1), pp. 74–88. Available at: https://doi.org/10.1038/s41580-021-00404-3.

McGrogan, B.T. *et al.* (2008) 'Taxanes, microtubules and chemoresistant breast cancer', *Biochimica et Biophysica Acta (BBA) - Reviews on Cancer*, 1785(2), pp. 96–132. Available at: https://doi.org/10.1016/j.bbcan.2007.10.004.

Mehdipour, P., Santoro, F. and Minucci, S. (2015) 'Epigenetic alterations in acute myeloid leukemias', *FEBS Journal*, 282(9), pp. 1786–1800. Available at: https://doi.org/10.1111/febs.13142.

Michowski, W. *et al.* (2020) 'Cdk1 Controls Global Epigenetic Landscape in Embryonic Stem Cells', *Molecular Cell*, 78(3), pp. 459-476.e13. Available at: https://doi.org/10.1016/j.molcel.2020.03.010.

Mills, A.A. (2017) 'The Chromodomain Helicase DNA-Binding Chromatin Remodelers: Family Traits that Protect from and Promote Cancer', *Cold Spring Harbor Perspectives in Medicine*, 7(4), p. a026450. Available at: https://doi.org/10.1101/cshperspect.a026450.

Molica, M. *et al.* (2019) 'Maintenance therapy in AML: The past, the present and the future', *American Journal of Hematology*, 94(11), pp. 1254–1265. Available at: https://doi.org/10.1002/ajh.25620.

Montesinos, P. *et al.* (2022) 'Ivosidenib and Azacitidine in IDH1-Mutated Acute Myeloid Leukemia', *The New England journal of medicine*, 386(16), pp. 1519–1531. Available at: https://doi.org/10.1056/NEJMOA2117344.

Mortlock, A.A. *et al.* (2007) 'Discovery, Synthesis, and in Vivo Activity of a New Class of Pyrazoloquinazolines as Selective Inhibitors of Aurora B Kinase', *Journal of Medicinal Chemistry*, 50(9), pp. 2213–2224. Available at: https://doi.org/10.1021/jm061335f.

Nagasaka, M. *et al.* (2022) 'Insights into Regulators of p53 Acetylation', *Cells*, 11(23), p. 3825. Available at: https://doi.org/10.3390/cells11233825.

Nair, V.D. *et al.* (2012) 'Involvement of Histone Demethylase LSD1 in Short-Time-Scale Gene Expression Changes during Cell Cycle Progression in Embryonic Stem Cells', *Molecular and Cellular Biology*, 32(23), pp. 4861–4876. Available at: https://doi.org/10.1128/MCB.00816-12.

Naoe, T. and Kiyoi, H. (2013) 'Gene mutations of acute myeloid leukemia in the genome era', *International Journal of Hematology*, 97(2), pp. 165–174. Available at: https://doi.org/10.1007/s12185-013-1257-4.

Narasimha, A.M. *et al.* (2014) 'Cyclin D activates the Rb tumor suppressor by mono-phosphorylation', *eLife*, 3, p. e02872. Available at: https://doi.org/10.7554/eLife.02872.

Ngai, L.L. *et al.* (2021) 'MRD Tailored Therapy in AML: What We Have Learned So Far', *Frontiers in Oncology*, 10. Available at: https://doi.org/10.3389/fonc.2020.603636.

Nicosia, L. *et al.* (2022) 'Pharmacological inhibition of LSD1 triggers myeloid differentiation by targeting GSE1 oncogenic functions in AML', *Oncogene*, 41(6), pp. 878–894. Available at: https://doi.org/10.1038/s41388-021-02123-7.

Noberini, R. *et al.* (2020) 'Enrichment of histones from patient samples for mass spectrometry-based analysis of post-translational modifications', *Methods*, 184(June), pp. 19–28. Available at: https://doi.org/10.1016/j.ymeth.2019.10.001.

Noberini, R. *et al.* (2021) 'Spatial epi-proteomics enabled by histone post-translational modification analysis from low-abundance clinical samples', *Clinical Epigenetics*, 13(1), p. 145. Available at: https://doi.org/10.1186/s13148-021-01120-7.

Noberini, R. and Bonaldi, T. (2017) 'A Super-SILAC Strategy for the Accurate and Multiplexed Profiling of Histone Posttranslational Modifications', *Methods in Enzymology*, 586, pp. 311–332. Available at: https://doi.org/10.1016/bs.mie.2016.09.036.

Noce, B. *et al.* (2023) 'LSD1 inhibitors for cancer treatment: Focus on multi-target agents and compounds in clinical trials', *Frontiers in Pharmacology*, 14, p. 1120911. Available at: https://doi.org/10.3389/fphar.2023.1120911.

Oka, M. *et al.* (2019) 'Chromatin-bound CRM1 recruits SET-Nup214 and NPM1c onto HOX clusters causing aberrant HOX expression in leukemia cells', *eLife*, 8. Available at: https://doi.org/10.7554/ELIFE.46667.

Oshita, T. (2022) 'Chromatin Remodeling: Fundamental Process', *Epigenetics Research: Open Access*, 4(4), pp. 1–1. Available at: https://doi.org/10.35248/EROA.22.4.123.

Oyama, K. *et al.* (2014) 'Epigenetic regulation of cardiac myocyte differentiation†', *Frontiers in Genetics*, 5, p. 375. Available at: https://doi.org/10.3389/fgene.2014.00375.

Oza, A.M. *et al.* (2020) 'A Biomarker-enriched, Randomized Phase II Trial of Adavosertib (AZD1775) Plus Paclitaxel and Carboplatin for Women with Platinum-sensitive TP53-mutant Ovarian Cancer', *Clinical Cancer Research*, 26(18), pp. 4767–4776. Available at: https://doi.org/10.1158/1078-0432.CCR-20-0219.

Pallavi, R., Mazzarella, L. and Pelicci, P.G. (2019) 'Advances in precision epigenetic treatment for acute promyelocytic leukemia.', *Expert Review of Precision Medicine and Drug Development*, 4(3), pp. 163–178. Available at: https://doi.org/10.1080/23808993.2019.1612238.

Pandey, M.R. and Wang, E.S. (2019) 'What potential is there for LSD1 inhibitors to reach approval for AML?', *Expert opinion on emerging drugs*, 24(4), pp. 205–212. Available at: https://doi.org/10.1080/14728214.2019.1694001.

Papaemmanuil, E. *et al.* (2016) 'Genomic Classification and Prognosis in Acute Myeloid Leukemia', *New England Journal of Medicine*, 374(23), pp. 2209–2221. Available at: https://doi.org/10.1056/NEJMoa1516192.

Parra, M. (2015) 'Class IIa HDACs – new insights into their functions in physiology and pathology', *The FEBS Journal*, 282(9), pp. 1736–1744. Available at: https://doi.org/10.1111/febs.13061.

Pauklin, S. and Vallier, L. (2013) 'The cell-cycle state of stem cells determines cell fate propensity', *Cell*, 155(1), p. 135. Available at: https://doi.org/10.1016/j.cell.2013.08.031.

Pelengaris, S. and Khan, M. (eds) (2013) *The Molecular Biology of Cancer: A Bridge from Bench to Bedside*. 2nd edition. Wiley-Blackwell.

Perl, A.E. (2017) 'The role of targeted therapy in the management of patients with AML', *Blood Advances*, 1(24), pp. 2281–2294. Available at: https://doi.org/10.1182/BLOODADVANCES.2017009829.

Pfister, S.X. and Ashworth, A. (2017) 'Marked for death: Targeting epigenetic changes in cancer', *Nature Reviews Drug Discovery*, 16(4), pp. 241–263. Available at: https://doi.org/10.1038/nrd.2016.256.

Planques, A. *et al.* (2020) 'DNA methylation during development and regeneration of the annelid Platynereis dumerilii'. bioRxiv, p. 2020.11.13.381673. Available at: https://doi.org/10.1101/2020.11.13.381673.

Przespolewski, A. and Wang, E.S. (2016) 'Inhibitors of LSD1 as a potential therapy for acute myeloid leukemia', *Expert Opinion on Investigational Drugs*, 25(7), pp. 771–780. Available at: https://doi.org/10.1080/13543784.2016.1175432.

Puig-Kröger, A. *et al.* (2003) 'RUNX/AML and C/EBP factors regulate CD11a integrin expression in myeloid cells through overlapping regulatory elements', *Blood*, 102(9), pp. 3252–3261. Available at: https://doi.org/10.1182/blood-2003-02-0618.

Quessada, J. *et al.* (2021) 'Cytogenetics of Pediatric Acute Myeloid Leukemia: A Review of the Current Knowledge', *Genes*, 12(6), p. 924. Available at: https://doi.org/10.3390/genes12060924.

Rao, R.C. and Dou, Y. (2015) 'Hijacked in cancer: the KMT2 (MLL) family of methyltransferases', *Nature Reviews Cancer*, 15(6), pp. 334–346. Available at: https://doi.org/10.1038/nrc3929.

Ravasio, R. *et al.* (2020) 'Targeting the scaffolding role of LSD1 (KDM1A) poises acute myeloid leukemia cells for retinoic acid-induced differentiation', *Science Advances*, 6(15), p. eaax2746. Available at: https://doi.org/10.1126/sciadv.aax2746.

Rizo, A. *et al.* (2009) 'Repression of BMI1 in normal and leukemic human CD34+ cells impairs self-renewal and induces apoptosis', *Blood*, 114(8), pp. 1498–1505. Available at: https://doi.org/10.1182/BLOOD-2009-03-209734.

Ronco, C. *et al.* (2017) 'ATM, ATR, CHK1, CHK2 and WEE1 inhibitors in cancer and cancer stem cells', *MedChemComm*, 8(2), pp. 295–319. Available at: https://doi.org/10.1039/C6MD00439C.

Roussel, M.J.S. and Lanotte, M. (2001) 'Maturation sensitive and resistant t(15;17) NB4 cell lines as tools for APL physiopathology: Nomenclature of cells and repertory of their known genetic alterations and phenotypes', *Oncogene*, 20(49), pp. 7287–7291. Available at: https://doi.org/10.1038/sj.onc.1204863.

Rozman, M. *et al.* (2004) 'Type I MOZ/CBP (MYST3/CREBBP) is the most common chimeric transcript in acute myeloid leukemia with t(8;16)(p11;p13) translocation', *Genes, Chromosomes and Cancer*, 40(2), pp. 140–145. Available at: https://doi.org/10.1002/GCC.20022.

Rubin, S.M., Sage, J. and Skotheim, J.M. (2020) 'Integrating Old and New Paradigms of G1/S Control', *Molecular Cell*, 80(2), pp. 183–192. Available at: https://doi.org/10.1016/j.molcel.2020.08.020.

Russler-Germain, D.A. *et al.* (2014) 'The R882H DNMT3A Mutation Associated with AML Dominantly Inhibits Wild-Type DNMT3A by Blocking Its Ability to Form Active Tetramers', *Cancer Cell*, 25(4), pp. 442–454. Available at: https://doi.org/10.1016/j.ccr.2014.02.010.

Sacilotto, N. *et al.* (2021) 'Comprehensive in Vitro Characterization of the LSD1 Small Molecule Inhibitor Class in Oncology', *ACS Pharmacology & Translational Science*, 4(6), pp. 1818–1834. Available at: https://doi.org/10.1021/acsptsci.1c00223.

Sakaue-Sawano, A. *et al.* (2017) 'Genetically Encoded Tools for Optical Dissection of the Mammalian Cell Cycle', *Molecular Cell*, 68(3), pp. 626-640.e5. Available at: https://doi.org/10.1016/j.molcel.2017.10.001.

Saleque, S. *et al.* (2007) 'Epigenetic regulation of hematopoietic differentiation by Gfi-1 and Gfi-1b is mediated by the cofactors CoREST and LSD1', *Molecular Cell*, 27(4), pp. 562–572. Available at: https://doi.org/10.1016/j.molcel.2007.06.039.

Sanborn, A.L. *et al.* (2015) 'Chromatin extrusion explains key features of loop and domain formation in wild-type and engineered genomes', *Proceedings of the National Academy of Sciences of the United States of America*, 112(47), pp. E6456–E6465. Available at: https://doi.org/10.1073/PNAS.1518552112/SUPPL_FILE/PNAS.1518552112.ST01.XLSX.

Sapountzi, V., Logan, I.R. and Robson, C.N. (2006) 'Cellular functions of TIP60', *The International Journal of Biochemistry & Cell Biology*, 38(9), pp. 1496–1509. Available at: https://doi.org/10.1016/j.biocel.2006.03.003.

Sauer, P.V. *et al.* (2018) 'Mechanistic insights into histone deposition and nucleosome assembly by the chromatin assembly factor-1', *Nucleic Acids Research*, 46(19), pp. 9907–9917. Available at: https://doi.org/10.1093/nar/gky823.

Sava, G.P. *et al.* (2020) 'ABC-transporter upregulation mediates resistance to the CDK7 inhibitors THZ1 and ICEC0942', *Oncogene*, 39(3), pp. 651–663. Available at: https://doi.org/10.1038/s41388-019-1008-y.

Schenk, T. *et al.* (2012) 'Inhibition of the LSD1 (KDM1A) demethylase reactivates the all-trans-retinoic acid differentiation pathway in acute myeloid leukemia', *Nature Medicine*, 18(4), pp. 605–611. Available at: https://doi.org/10.1038/nm.2661.

Schiltz, R.L. and Nakatani, Y. (2000) 'The PCAF acetylase complex as a potential tumor suppressor', *Biochimica et Biophysica Acta (BBA) - Reviews on Cancer*, 1470(2), pp. M37–M53. Available at: https://doi.org/10.1016/S0304-419X(99)00037-2.

Schober, M. *et al.* (2019) 'Chiral synthesis of LSD1 inhibitor GSK2879552 enabled by directed evolution of an imine reductase', *Nature Catalysis*, 2(10), pp. 909–915. Available at: https://doi.org/10.1038/s41929-019-0341-4.

Schoelz, J.M. and Riddle, N.C. (2022) 'Functions of HP1 proteins in transcriptional regulation', *Epigenetics & Chromatin*, 15(1), p. 14. Available at: https://doi.org/10.1186/s13072-022-00453-8.

Sela, D. *et al.* (2012) 'Endoplasmic Reticulum Stress-responsive Transcription Factor ATF6α Directs Recruitment of the Mediator of RNA Polymerase II Transcription and Multiple Histone Acetyltransferase Complexes * ♦', *Journal of Biological Chemistry*, 287(27), pp. 23035–23045. Available at: https://doi.org/10.1074/jbc.M112.369504.

Shen, D.-D. *et al.* (2022) 'LSD1 deletion decreases exosomal PD-L1 and restores T-cell response in gastric cancer', *Molecular Cancer*, 21(1), p. 75. Available at: https://doi.org/10.1186/s12943-022-01557-1.

Sheng, W. *et al.* (2018) 'LSD1 Ablation Stimulates Anti-tumor Immunity and Enables Checkpoint Blockade', *Cell*, 174(3), pp. 549-563.e19. Available at: https://doi.org/10.1016/J.CELL.2018.05.052.

Short, N.J., Rytting, M.E. and Cortes, J.E. (2018) 'Acute myeloid leukaemia', *The Lancet*, 392(10147), pp. 593–606. Available at: https://doi.org/10.1016/S0140-6736(18)31041-9.

Shukla, S. *et al.* (2021) 'Small-molecule inhibitors targeting Polycomb repressive complex 1 RING domain', *Nature Chemical Biology 2021 17:7*, 17(7), pp. 784–793. Available at: https://doi.org/10.1038/s41589-021-00815-5.

Siegel, R.L. *et al.* (2022) 'Cancer statistics, 2022', *CA: A Cancer Journal for Clinicians*, 72(1), pp. 7–33. Available at: https://doi.org/10.3322/CAAC.21708.

Silva, P. *et al.* (2017) 'Acute myeloid leukemia in the elderly is characterized by a distinct genetic and epigenetic landscape', *Leukemia*, 31(7), pp. 1640–1644. Available at: https://doi.org/10.1038/leu.2017.109.

Singh, A.M. *et al.* (2013) 'Cell-cycle control of developmentally regulated transcription factors accounts for heterogeneity in human pluripotent cells', *Stem Cell Reports*, 1(6), pp. 532–544. Available at: https://doi.org/10.1016/j.stemcr.2013.10.009.

Singh, A.M. *et al.* (2015) 'Cell-Cycle Control of Bivalent Epigenetic Domains Regulates the Exit from Pluripotency', *Stem Cell Reports*, 5(3), pp. 323–336. Available at: https://doi.org/10.1016/j.stemcr.2015.07.005.

Somasundaram, S. *et al.* (2018) 'The DNMT1-associated lincRNA DACOR1 reprograms genome-wide DNA methylation in colon cancer', *Clinical Epigenetics*, 10, p. 127. Available at: https://doi.org/10.1186/s13148-018-0555-3.

Speranzini, V. *et al.* (2016) 'Polymyxins and quinazolines are LSD1/KDM1A inhibitors with unusual structural features', *Science Advances*, 2(9). Available at: https://doi.org/10.1126/SCIADV.1601017.

Sprüssel, A. *et al.* (2012) 'Lysine-specific demethylase 1 restricts hematopoietic progenitor proliferation and is essential for terminal differentiation', *Leukemia*, 26(9), pp. 2039–2051. Available at: https://doi.org/10.1038/leu.2012.157.

Stallaert, W. *et al.* (2022) 'The structure of the human cell cycle', *Cell Systems*, 13(3), pp. 230-240.e3. Available at: https://doi.org/10.1016/j.cels.2021.10.007.

Stavropoulos, P., Blobel, G. and Hoelz, A. (2006) 'Crystal structure and mechanism of human lysine-specific demethylase-1', *Nature Structural & Molecular Biology*, 13(7), pp. 626–632. Available at: https://doi.org/10.1038/nsmb1113.

Stomper, J. *et al.* (2021) 'Hypomethylating agents (HMA) for the treatment of acute myeloid leukemia and myelodysplastic syndromes: mechanisms of resistance and novel HMA-based therapies', *Leukemia*, 35(7), p. 1873. Available at: https://doi.org/10.1038/S41375-021-01218-0.

Stubbins, R.J. and Karsan, A. (2021) 'Differentiation therapy for myeloid malignancies: beyond cytotoxicity', *Blood Cancer Journal*, 11(12). Available at: https://doi.org/10.1038/s41408-021-00584-3.

Study Record | ClinicalTrials.gov (no date a). Available at: https://clinicaltrials.gov/study/NCT02177812?cond=AML&intr=LSD1&rank=3 (Accessed: 14 August 2023).

Study Record | ClinicalTrials.gov (no date b). Available at: https://clinicaltrials.gov/study/NCT02842827?cond=AML&intr=LSD1&rank=6 (Accessed: 14 August 2023).

Sugeedha, J., Gautam, J. and Tyagi, S. (2021) 'SET1/MLL family of proteins: functions beyond histone methylation', *Epigenetics*, 16(5), pp. 469–487. Available at: https://doi.org/10.1080/15592294.2020.1809873.

Sun, Y., Chen, B.R. and Deshpande, A. (2018) 'Epigenetic regulators in the development, maintenance, and therapeutic targeting of acute myeloid leukemia', *Frontiers in Oncology*, 8(FEB), p. 320797. Available at: https://doi.org/10.3389/FONC.2018.00041/BIBTEX.

Svedružić, Ž.M. (2011) 'Chapter 6 - Dnmt1: Structure and Function', in X. Cheng and R.M. Blumenthal (eds) *Progress in Molecular Biology and Translational Science*. Academic Press (Modifications of Nuclear DNA and its Regulatory Proteins), pp. 221–254. Available at: https://doi.org/10.1016/B978-0-12-387685-0.00006-8.

Swerdlow, S.H. *et al.* (2017) *WHO Classification of Tumours of Haematopoietic and Lymphoid Tissues: Vol. 2*. 4° edizione. Lyon: World Health Organization.

Tamaoki, J. *et al.* (2023) 'LSD1 promotes the egress of hematopoietic stem and progenitor cells into the bloodstream during the endothelial-to-hematopoietic transition', *Developmental Biology*, 501, pp. 92–103. Available at: https://doi.org/10.1016/j.ydbio.2023.06.012.

Tan, A.Y. and Manley, J.L. (2009) 'The TET Family of Proteins: Functions and Roles in Disease', *Journal of Molecular Cell Biology*, 1(2), pp. 82–92. Available at: https://doi.org/10.1093/jmcb/mjp025.

Tenen, D.G. (2001) 'Abnormalities of the CEBP alpha transcription factor: a major target in acute myeloid leukemia', *Leukemia*, 15(4), pp. 688–689. Available at: https://doi.org/10.1038/sj.leu.2402088.

Terzi, M.Y., Izmirli, M. and Gogebakan, B. (2016) 'The cell fate: senescence or quiescence', *Molecular Biology Reports*, 43(11), pp. 1213–1220. Available at: https://doi.org/10.1007/s11033-016-4065-0.

Thambyrajah, R. *et al.* (2016) 'GFI1 proteins orchestrate the emergence of haematopoietic stem cells through recruitment of LSD1', *Nature Cell Biology*, 18(1), pp. 21–32. Available at: https://doi.org/10.1038/ncb3276.

Thol, F. *et al.* (2012) 'Analysis of NUP98/NSD1 translocations in adult AML and MDS patients', *Leukemia 2013 27:3*, 27(3), pp. 750–754. Available at: https://doi.org/10.1038/leu.2012.249.

Tsukada, Y. *et al.* (2006) 'Histone demethylation by a family of JmjC domain-containing proteins', *Nature*, 439(7078), pp. 811–816. Available at: https://doi.org/10.1038/nature04433.

Ueda, K. and Steidl, U. (2021) 'Epigenetic Achilles' heel of AML', *Nature Cancer*, 2(5), pp. 481–483. Available at: https://doi.org/10.1038/s43018-021-00212-w.

Verdin, E., Dequiedt, F. and Kasler, H.G. (2003) 'Class II histone deacetylases: versatile regulators', *Trends in Genetics*, 19(5), pp. 286–293. Available at: https://doi.org/10.1016/S0168-9525(03)00073-8.

Vianello, P. *et al.* (2016) 'Discovery of a Novel Inhibitor of Histone Lysine-Specific Demethylase 1A (KDM1A/LSD1) as Orally Active Antitumor Agent', *Journal of Medicinal Chemistry*, 59(4), pp. 1501–1517. Available at: https://doi.org/10.1021/acs.jmedchem.5b01209.

Vicioso-Mantis, M., Aguirre, S. and Martínez-Balbás, M.A. (2022) 'JmjC Family of Histone Demethylases Form Nuclear Condensates', *International Journal of Molecular Sciences*, 23(14), p. 7664. Available at: https://doi.org/10.3390/ijms23147664.

Villagra, A. *et al.* (2009) 'The histone deacetylase HDAC11 regulates the expression of interleukin 10 and immune tolerance', *Nature Immunology*, 10(1), pp. 92–100. Available at: https://doi.org/10.1038/ni.1673.

Viner, C. *et al.* (2016) 'Modeling methyl-sensitive transcription factor motifs with an expanded epigenetic alphabet'. bioRxiv, p. 043794. Available at: https://doi.org/10.1101/043794.

Wada, T. *et al.* (2015) 'Overexpression of the shortest isoform of histone demethylase LSD1 primes hematopoietic stem cells for malignant transformation', *Blood*, 125(24), pp. 3731–3746. Available at: https://doi.org/10.1182/blood-2014-11-610907.

Wade, P.A., Pruss, D. and Wolffe, A.P. (1997) 'Histone acetylation: chromatin in action', *Trends in Biochemical Sciences*, 22(4), pp. 128–132. Available at: https://doi.org/10.1016/S0968-0004(97)01016-5.

Waga, S. *et al.* (1994) 'The p21 inhibitor of cyclin-dependent kinases controls DNA replication by interaction with PCNA', *Nature*, 369(6481), pp. 574–578. Available at: https://doi.org/10.1038/369574a0.

Wagener, C., Stocking, C. and Müller, O. (2017) *Cancer Signaling: From Molecular Biology to Targeted Therapy*. 1st edition. Wiley-VCH.

Walter, R.B. *et al.* (2013) 'Significance of FAB subclassification of "acute myeloid leukemia, NOS" in the 2008 WHO classification: analysis of 5848 newly diagnosed patients', *Blood*, 121(13), pp. 2424–2431. Available at: https://doi.org/10.1182/blood-2012-10-462440.

Wang, J. *et al.* (2007) 'Opposing LSD1 complexes function in developmental gene activation and repression programmes', *Nature*, 446(7138), pp. 882–887. Available at: https://doi.org/10.1038/nature05671.

Wang, J. *et al.* (2018) 'Histone demethylase LSD1 regulates hematopoietic stem cells homeostasis and protects from death by endotoxic shock', *Proceedings of the National Academy of Sciences*, 115(2), pp. E244–E252. Available at: https://doi.org/10.1073/pnas.1718759114.

Wang, Y. *et al.* (2009) 'LSD1 Is a Subunit of the NuRD Complex and Targets the Metastasis Programs in Breast Cancer', *Cell*, 138(4), pp. 660–672. Available at: https://doi.org/10.1016/j.cell.2009.05.050.

Watts, J.M. *et al.* (2023) 'Olutasidenib alone or with azacitidine in IDH1-mutated acute myeloid leukaemia and myelodysplastic syndrome: phase 1 results of a phase 1/2 trial', *The Lancet. Haematology*, 10(1). Available at: https://doi.org/10.1016/S2352-3026(22)00292-7.

Weber, M. *et al.* (2013) 'Incoming RNA Virus Nucleocapsids Containing a 5'-Triphosphorylated Genome Activate RIG-I and Antiviral Signaling', *Cell Host & Microbe*, 13(3), pp. 336–346. Available at: https://doi.org/10.1016/j.chom.2013.01.012.

Whyte, W.A. *et al.* (2012) 'Enhancer decommissioning by LSD1 during embryonic stem cell differentiation', *Nature*, 482(7384), pp. 221–225. Available at: https://doi.org/10.1038/nature10805.

Williams, G.H. and Stoeber, K. (2012) 'The cell cycle and cancer', *The Journal of Pathology*, 226(2), pp. 352–364. Available at: https://doi.org/10.1002/path.3022.

Wishart, D.S. *et al.* (2018) 'DrugBank 5.0: a major update to the DrugBank database for 2018', *Nucleic Acids Research*, 46(D1), pp. D1074–D1082. Available at: https://doi.org/10.1093/nar/gkx1037.

Wissmann, M. *et al.* (2007) 'Cooperative demethylation by JMJD2C and LSD1 promotes androgen receptor-dependent gene expression', *Nature Cell Biology*, 9(3), pp. 347–353. Available at: https://doi.org/10.1038/ncb1546.

Wu, Q.-J. *et al.* (2022) 'The sirtuin family in health and disease', *Signal Transduction and Targeted Therapy*, 7(1), pp. 1–74. Available at: https://doi.org/10.1038/s41392-022-01257-8.

Wu, Y. *et al.* (2013) 'The Deubiquitinase USP28 Stabilizes LSD1 and Confers Stem-Cell-like Traits to Breast Cancer Cells', *Cell Reports*, 5(1), pp. 224–236. Available at: https://doi.org/10.1016/j.celrep.2013.08.030.

Xie, Y. *et al.* (2022) 'The role and mechanism of histone lactylation in health and diseases', *Frontiers in Genetics*, 13, p. 949252. Available at: https://doi.org/10.3389/FGENE.2022.949252/BIBTEX.

Yamamoto, R. *et al.* (2018) 'Selective dissociation between LSD1 and GFI1B by a LSD1 inhibitor NCD38 induces the activation of ERG super-enhancer in erythroleukemia cells', *Oncotarget*, 9(30), pp. 21007–21021. Available at: https://doi.org/10.18632/oncotarget.24774.

Yan, Y. *et al.* (2022) 'Epigenetic maintenance strategies after allogeneic stem cell transplantation in acute myeloid leukemia', *Experimental Hematology*, 109, pp. 1-10.e1. Available at: https://doi.org/10.1016/J.EXPHEM.2022.03.003.

Yang, C. *et al.* (2022) 'Targeting EZH2 Promotes Chemosensitivity of BCL-2 Inhibitor through Suppressing PI3K and c-KIT Signaling in Acute Myeloid Leukemia', *International Journal of Molecular Sciences*, 23(19), p. 11393. Available at: https://doi.org/10.3390/IJMS231911393/S1.

Yang, J. *et al.* (2021) 'Insights Into the Function and Clinical Application of HDAC5 in Cancer Management', *Frontiers in Oncology*, 11, p. 661620. Available at: https://doi.org/10.3389/fonc.2021.661620.

Yang, L., Rau, R. and Goodell, M.A. (2015) 'DNMT3A in haematological malignancies', *Nature Reviews Cancer*, 15(3), pp. 152–165. Available at: https://doi.org/10.1038/nrc3895.

Yang, M. *et al.* (2006) 'Structural Basis for CoREST-Dependent Demethylation of Nucleosomes by the Human LSD1 Histone Demethylase', *Molecular Cell*, 23(3), pp. 377–387. Available at: https://doi.org/10.1016/j.molcel.2006.07.012.

Yang, M. *et al.* (2007) 'Structural basis of histone demethylation by LSD1 revealed by suicide inactivation', *Nature Structural & Molecular Biology*, 14(6), pp. 535–539. Available at: https://doi.org/10.1038/nsmb1255.

Yuan, Z.-F. *et al.* (2018) 'EpiProfile 2.0: A Computational Platform for Processing Epi-Proteomics Mass Spectrometry Data', *Journal of Proteome Research*, 17(7), pp. 2533–2541. Available at: https://doi.org/10.1021/acs.jproteome.8b00133.

Zhang, D. *et al.* (2019) 'Metabolic regulation of gene expression by histone lactylation', *Nature 2019 574:7779*, 574(7779), pp. 575–580. Available at: https://doi.org/10.1038/s41586-019-1678-1.

Zhang, G. and Pradhan, S. (2014) 'Mammalian epigenetic mechanisms', *IUBMB Life*, 66(4), pp. 240–256. Available at: https://doi.org/10.1002/iub.1264.

Zhang, L. *et al.* (2012) 'Inhibition of Histone Deacetylases Preserves Myocardial Performance and Prevents Cardiac Remodeling through Stimulation of Endogenous Angiomyogenesis', *The Journal of Pharmacology and Experimental Therapeutics*, 341(1), pp. 285–293. Available at: https://doi.org/10.1124/jpet.111.189910.

Zhang, S. *et al.* (2021) 'Targeting LSD1 for acute myeloid leukemia (AML) treatment', *Pharmacological Research*, 164(November 2020), p. 105335. Available at: https://doi.org/10.1016/j.phrs.2020.105335.

Zhang, X. *et al.* (2013) 'Pluripotent stem cell protein Sox2 confers sensitivity to LSD1 inhibition in cancer cells', *Cell Reports*, 5(2), pp. 445–457. Available at: https://doi.org/10.1016/j.celrep.2013.09.018.

Zheng, H. and Xie, W. (2019) 'The role of 3D genome organization in development and cell differentiation', *Nature Reviews Molecular Cell Biology 2019 20:9*, 20(9), pp. 535–550. Available at: https://doi.org/10.1038/s41580-019-0132-4.

Zheng, L. *et al.* (2018) 'Utx loss causes myeloid transformation', *Leukemia 2018 32:6*, 32(6), pp. 1458–1465. Available at: https://doi.org/10.1038/s41375-018-0011-6.

Zheng, Y.-C., Shen, D.-D., *et al.* (2016) 'Baicalin, a natural LSD1 inhibitor', *Bioorganic Chemistry*, 69, pp. 129–131. Available at: https://doi.org/10.1016/j.bioorg.2016.10.004.

Zheng, Y.-C., Yu, B., *et al.* (2016) 'TCPs: privileged scaffolds for identifying potent LSD1 inhibitors for cancer therapy', *Epigenomics*, 8(5), pp. 651–666. Available at: https://doi.org/10.2217/epi-2015-0002.

Zhou, S., Tang, X. and Chen, H.-Z. (2018) 'Sirtuins and Insulin Resistance', *Frontiers in Endocrinology*, 9. Available at: https://doi.org/10.3389/fendo.2018.00748.

Zhou, Y. and Hu, Z. (2016) 'Epigenetic DNA Demethylation Causes Inner Ear Stem Cell Differentiation into Hair Cell-Like Cells', *Frontiers in Cellular Neuroscience*, 10, p. 185. Available at: https://doi.org/10.3389/fncel.2016.00185.

Zou, P. *et al.* (2011) 'p57(Kip2) and p27(Kip1) cooperate to maintain hematopoietic stem cell quiescence through interactions with Hsc70', *Cell Stem Cell*, 9(3), pp. 247–261. Available at: https://doi.org/10.1016/j.stem.2011.07.003.